Towards the clinical translation of Extracellular Vesicles – Surface engineering and optimized vesicle-storage

Dissertation zur Erlangung des Grades des Doktors der Naturwissenschaften der Naturwissenschaftlich-Technischen Fakultät der Universität des Saarlandes

Von Maximilian Richter

Saarbrücken 2021

Tag des Kolloqiums: 26.04.2021

Dekan: Prof. Dr. Jörn Erik Walter

Berichterstatter: Jun.-Prof. Dr. Gregor Fuhrmann

Prof. Dr. Anna K.H. Hirsch

Vorsitz: Prof. Dr. Marc Schneider

Akad. Mitarbeiter: Dr. Michael Ring

"We don't notice things change. We know that things change, we've been told since childhood that things change, we've witnessed things change ourselves many a time, and yet we're still utterly incapable of noticing the moment that change comes--or we search for change in all the wrong places."

Arkady and Boris Strugatsky, *Roadside Picnic*

Table of contents

Brief summary

Extracellular vesicles (EVs) are membrane-bound nanoparticles produced by cells. Their main function is the intercellular transport of information. Their natural biological activity and ability to interact with target cells drives the effort for their evaluation as therapeutic agents and their clinical translation. Thus, the present work aimed at evaluating two important topics for the development of EV-therapeutics, engineering the surface of bacterial EVs to introduce targeting moieties and optimizing the lyophilisation of mammalian EVs.

Different methods for the surface engineering of bacterial EVs were tested. While cholesterol insertion and activated esters were not successful in our setup, diazotransfer to install azide groups on the EV surface followed by click-chemistry demonstrated high efficiency with low impact on vesicle-integrity. Based on these results modular linker-molecules to tether targeting moieties to the vesicle surface were synthesized and evaluated in proof-of-concept experiments that afforded important insights for future optimization of their design.

Initial studies on the lyophilisation and storage of mammalian EVs revealed the high stress of freezing and dehydration. Thus, optimized protocols for the lyophilisation of EVs were developed and successfully produced formulations with long-term stability.

Taken together, effective surface engineering by diazotransfer and optimized lyophilisation of EVs were achieved.

Kurzzusammenfassung

Extrazelluläre Vesikel (EVs) sind von Zellen produzierte Nanopartikel, deren Hauptaufgabe der interzelluläre Transport von Informationen ist. Ihre natürliche biologische Aktivität und ihre Fähigkeit mit Zielzellen zu interagieren, waren Auslöser für die Untersuchung von EVs als Therapeutika mit dem Ziel ihrer klinischen Translation. Ziel der vorliegenden Arbeit war die Evaluierung zweier wichtiger Faktoren für die Entwicklung von EV-Therapeutika, die Oberflächenmodifikation bakterieller EVs mit Molekülen für aktives Targeting und die Lyophilisation von aus Säuger-EVs.

Verschiedene Methoden zur Oberflächenmodifikation von bakteriellen EVs wurden getestet. Während Cholesterol-Insertion und aktivierte Ester wenig erfolgreich waren, zeigte Diazotransfer zur Einführung von Azid-Gruppen gefolgt von Click-Chemie-Reaktionen eine hohe Effektivität mit geringem Einfluss auf die EV-Stabilität. Zur Einführung von Targeting-Molekülen wurden verschiedene modulare Linker-Moleküle synthetisiert und in Machbarkeitsstudien evaluiert, diese lieferten wichtige Erkenntnisse für ihre zukünftige Optimierung.

Erste Untersuchungen der Lyophilisation und Lagerung von Säuger-EVs zeigten eine hohe Beanspruchung der Vesikel durch Einfrieren und Trocknung. Daher wurden die Protokolle für die EV-Lyophilisation optimiert und EV-Formulierungen mit Langzeitstabilität erfolgreich hergestellt.

Insgesamt wurden sowohl bei der Oberflächenmodifikation als auch Lyophilisation von EVs wichtige Fortschritte erzielt.

Abbreviations

Acinetobacter baumannii	*A. baumannii*	Major histocompatibility complex	MHC
ADP-ribosylation factor 6	ARF6	Mesenchymal stem cells	MSC
ALG-2 interacting protein X	ALIX	Minimal information for studies of extracellular vesicles	MISEV
Asymmetric flow-field-flow-fractionation	AF4	Multivesicular endosome	MVE
Azide-labeled OMVs	AzideOMVs	Nanoparticle tracking analysis	NTA
Bicinchoninic acid assay	BCA assay	Nuclear magnetic resonance	NMR
Braun's lipoprotein	Lpp	Optical density	OD
Copper-catalyzed alkyne-azide cycloaddition	CuAAC	Outer membrane vesicle	OMV
1-[1-(Cyano-2-ethoxy-2-oxoethylideneaminooxy)-dimethylamino-morpholino]-uronium hexafluorophosphate	COMU	Peptidoglycan	PG
Dibenzocyclooctyne	DBCO	Phosphate buffered saline	PBS
Dimethyl formamide	DMF	Poloxamer 188	P188
Dimethyl sulfoxide	DMSO	Polyethylene glycol	PEG
N,N-Diisopropylethylamine	DIPEA	Polyvinylpyrrolidone	PVP
Endosomal sorting complex required for transport	ESCRT	preparative high performance liquid chromatography	prepHPLC
Epithelial growth-factor receptor	EGFR	*Pseudomonas aeruginosa*	*P. aeruginosa*
Escherichia coli	*E. coli*	Rabies viral glycoprotein	RVG
Extracellular vesicle	EV	Radioimmunoprecipitation assay	RIPA
Flow cytometry	FACS	Size exclusion chromatography	SEC
Fluorenylmethyloxycarbonyl	Fmoc	small interfering RNA	siRNA
Fluorescein isothiocyanate	FITC	Soluble N-ethylmaleimide-sensitive-factor attachment receptor	SNARE
Förster resonance energy transfer	FRET	Standard deviation	SD
High resolution mass spectrometry	HRMS	*Staphylococcus aureus*	*S. aureus*
High-density lipoprotein	HDL	Strain-promoted alkyne-azide cycloaddition	SPAAC
Human umbilical cord endothelial cell	HUVEC	Tangential flow filtration	TFF
Imidazole-1-sulfonyl azide	ISA	*tert*-Butyloxycarbonyl	Boc
Inductively coupled plasma mass spectrometry	ICP-MS	Transcyclooctene	TCO
Intercellular adhesion molecule 1	ICAM1	Transmission electron microscopy	TEM
Intraluminal vesicle	ILV	Tris(3-hydroxypropyltriazolylmethyl)amine	THPTA
Inverse electron-demand Diels-Alder	IEDDA	Tunable resistive pulse sensing	TRPS
Lipopolysaccharides	LPS	Ultracentrifugation	UC
Liquid chromatography-coupled mass spectrometry	LC/MS	Very low-density lipoprotein	VLDL

1. Introduction

Extracellular vesicles (EVs) are biogenic nanoparticles that are produced by cells and shed into the surrounding medium. They were initially discovered in the 1950s and 60s in algae (1), mammalian cells (2) and gram-negative bacteria (3, 4) and long thought of as just a way for cells to get rid of misfolded proteins and other waste-material (5). Today it is known that they are produced by cells from all parts of the phylogenetic tree, including gram-positive bacteria (6), higher plants (7), mycobacteria (8), archaea (9) and fungi (10). It has been discovered that EVs are an important part of the cellular secretome (11) and their main function is the transfer of information between cells (12, 13). Through active sorting mechanisms during EV-production, cargoes can be packaged in high concentrations and in synergistic combination with other compounds to convey a specific effect (14). Together with mechanisms for selective targeting and uptake of the vesicles (see 1.2 and 1.3), this leads to a more efficient distribution of effector-molecules than simple secretion into the surrounding medium (15). The vesicle-membrane moreover protects sensible cargo-molecules, such as RNA, from degradation in the extracellular milieu (16).

> Throughout this work, the term **extracellular vesicle** or **EV** is used to refer to extracellular vesicles in general regardless of their production organism.
>
> Explicit reference to EVs produced by mammalian cells is denoted by the term **mammalian extracellular vesicle** or **mammalian EV**.
>
> EVs derived from gram-negative bacteria are referred to as **outer membrane vesicles** or **OMVs**.

Box 1: EV-nomenclature

Especially the field of mammalian cell derived EVs got a lot of traction in recent years, when the vital role of EVs in many physiological as well as pathological processes was discovered (13, 17). Today, mammalian EVs as well as EVs derived from gram-negative bacteria – called outer membrane vesicles (OMVs), as they are derived from the bacterial outer membrane (18) – are intensely investigated in pharmaceutical applications, for example as therapeutic nanoparticles (see 1.5) and drug delivery vehicles (see 1.5.1).

1.1. Aims of this work

The overall focus of this work was continuing the development of therapeutics based on EVs derived from both bacteria and mammalian cells. The first two parts of this work was aimed at increasing the potential of bacterial EVs for drug-delivery, the third part was concerned with improving the storage stability of EV-based therapeutics (Box 2).

---

1) Development of an efficient method for the surface modification of myxobacterial OMVs based on physical or chemical modification.

2) Based on this method, introduction of targeting moieties to OMVs that increase their bacterial binding using a modular approach.

3) Evaluation of the effect of different storage conditions on the stability of EVs and development and optimization of protocols for their lyophilisation, to obtain EV-formulations with long-term stability.

Box 2: Aims of this work.
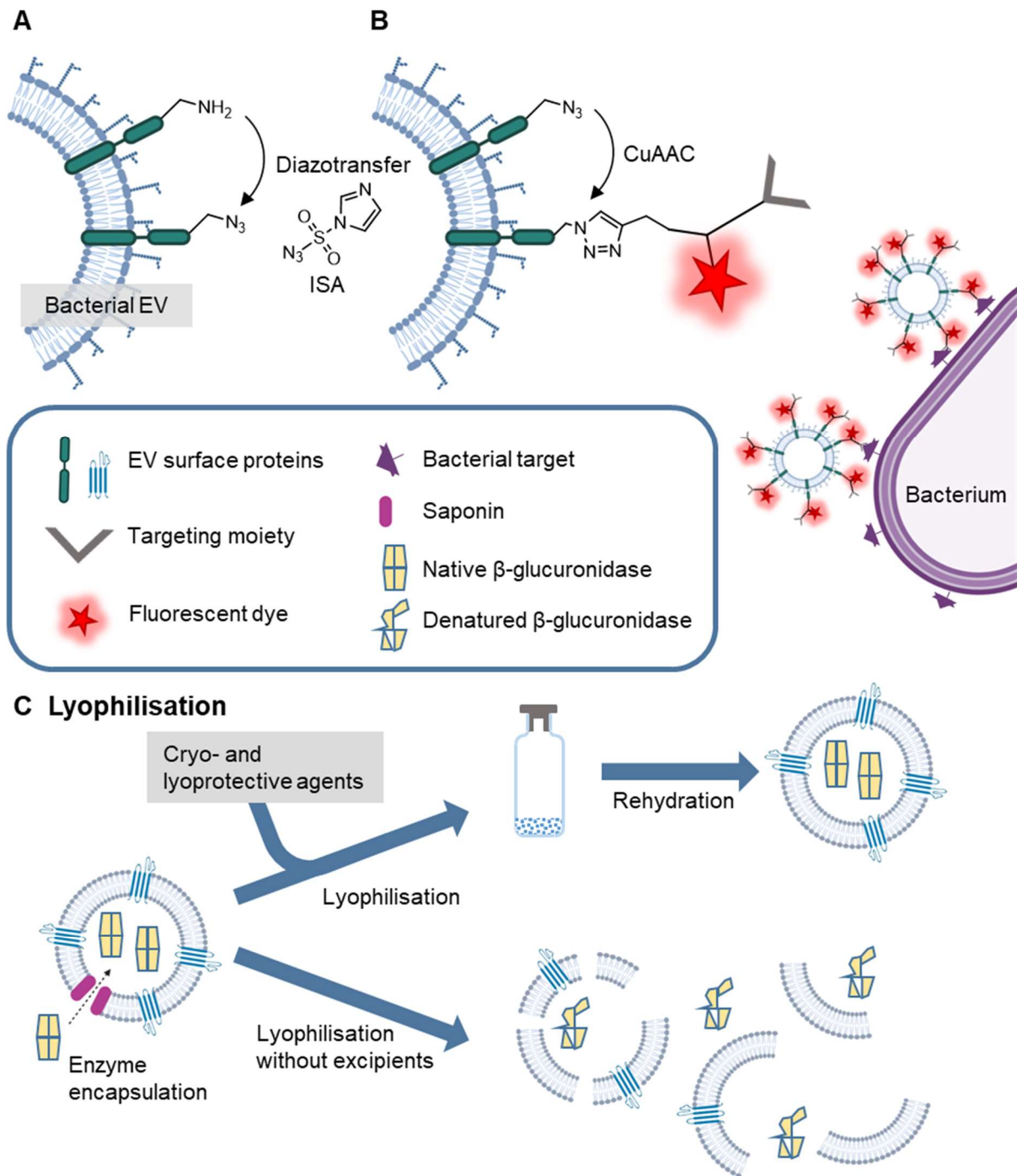
Figure 1: Aims of this work. A: Development of a method to introduce azide groups to the surface of bacterial EVs e.g. based on diazotransfer with imidazole-1-sulfonyl azide (ISA) B: Simultaneous introduction of a bacteria-specific targeting moiety and a fluorescent dye to the surface of azide-labeled OMVs to promote targeting of bacteria e.g. using copper-catalyzed alkyne-azide cycloaddition (CuAAC). C: Optimization of EV-lyophilisation to generate formulations that protect the integrity of lyophilized vesicles using exogenously encapsulated β-glucuronidase as a surrogate for native EV-cargos. The figure was partially prepared using Biorender.

There is a discovery void of new antibiotic agents (19), while the prevalence of bacterial resistance is steadily rising (20). Thus, new antibiotic agents and ways to increase the effectiveness of current antibiotics are highly sought after. OMVs derived from myxobacteria are evaluated in our group as antibacterial agents and drug-delivery vehicles for antibiotics, with promising early results (21, 22). To further amend these results, the vesicles could be equipped with targeting moieties on their surface to increase their interaction with pathogenic bacteria at the site of infection.

The surface modification of OMVs in general and specifically myxobacterial OMVs has not seen much evaluation yet. Thus, an effective method for the surface engineering of OMVs based on physical or chemical modification needed to be developed first (Figure 1 A). Once established, this method would be employed to attain the second goal, introducing bacteria-specific targeting moieties to the vesicle-surface (Figure 1 B). To broaden the scope of this endeavor beyond just one type of targeting moiety or vesicle, a modular linker molecule would be employed to connect vesicles and targeting moieties.

Beyond the properties of myxobacterial vesicles for anti-infective applications, the second main part of this work focused on a more overarching issue for the clinical translation of extracellular vesicles - their storage. A sufficient storage stability is a crucial requirement for the viability of EV-based drugs. Thus, we aimed at gaining further insights into the effect of storage on EV-stability and evaluated lyophilisation of EVs as an alternative to frozen storage to obtain EV-formulations with long-term stability (Figure 1 C).

1.2. Extracellular vesicles derived from mammals and other animals

Eukaryotic cells produce vesicular nanoparticles of various subtypes. During programmed cell-death apoptotic bodies are formed that contain organelles and other remnants from the dying cell (23). These vesicles are distinct from the vesicles produced by cells during their lifetime (24). Here two main groups are described, that are the focus of current research in the field, microvesicles and exosomes (Figure 2). Microvesicles are produced by blebbing from the cell membrane and are mostly sized between 100 and 1000 nm. Exosomes are derived from multivesicular endosomes (MVEs) that can fuse with the plasma membrane to release their intraluminal vesicles (ILVs). They generally differ in size from 30-200 nm. Other subtypes of EVs have emerged, but their physiological roles have not been evaluated in detail yet (25, 26). EVs have been identified as effectors in various physiological processes (13). There is clear evidence that EVs are able to transfer functional cargos over long distances (27-29) and some examples suggest that this transfer at least in part is specific for certain target cells (30-32).

There are multiple pathways for their biogenesis, cargo loading and uptake into recipient cells that vary between cell types and are not comprehensively understood yet (29, 33, 34).
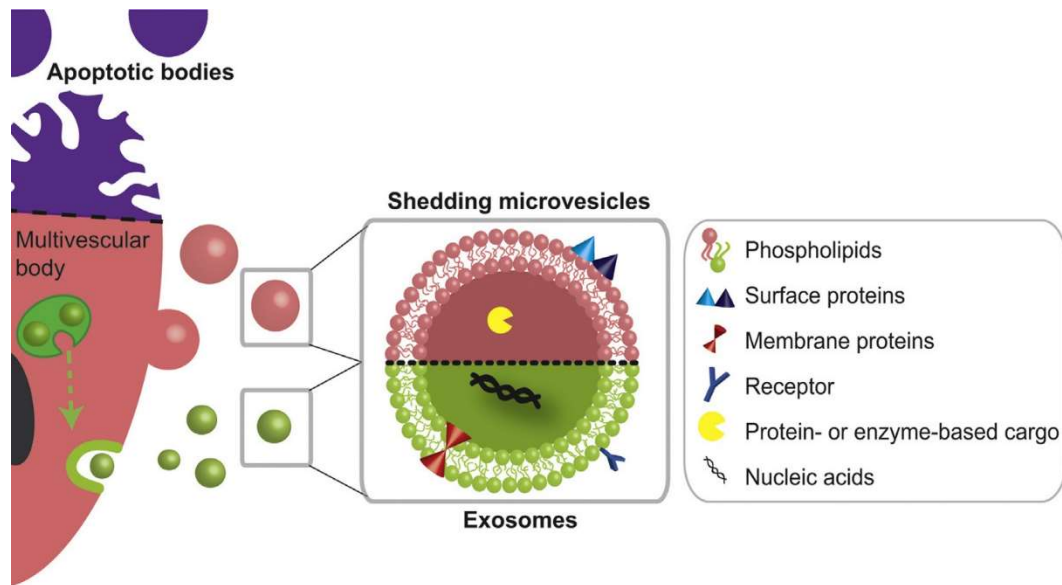
Figure 2: Microvesicles bud directly from the cell membrane, while exosomes are generated in multivesicular endosomes that then fuse with the cell membrane. Apoptotic bodies are derived from cells undergoing apoptosis. In their lumen, exosomes and microvesicles contain cargos such as nucleic acids and proteins, while their surfaces can be decorated with surface- and transmembrane-proteins and receptors. Adapted from Fuhrmann, G., et al. (2015, "Cell-derived vesicles for drug therapy and diagnostics: Opportunities and challenges", Nano Today 10(3): 397-409. With permission from Elsevier.

Research into the biogenesis of EVs has been hampered by the inability of current vesicle-isolation methods to cleanly separate microvesicles from exosomes (33). Nonetheless, researchers have shed some light on the biogenesis of both exosomes and microvesicles (Figure 3).

The biogenesis of exosomes is complex, with multiple pathways that can lead to the generation of MVEs (34, 35) and the composition of exosomes can change during cell maturation (36). The most extensively researched pathway for the recruitment of cargos and the generation of ILVs is the ESCRT (endosomal sorting complex required for transport) machinery, which consists of four protein complexes, ESCRT-0 to ESCRT-III (37). ESCRT-0 is responsible for binding cargos (38), which are generally ubiquitinylated (39). ESCRT-0 associates with ESCRT-I and –II. These in turn are responsible for the clustering of cargos and the recruitment of ESCRT-III (37), which is the driving factor of the scission of the new-formed vesicle into the endosome lumen (40). The interplay between syndecan, syntenin and ALIX (ALG-2 interacting protein X) has been identified as an important alternative to ESCRT-0-based exosome biogenesis. Syndecan is a transmembrane protein that is found on the cell-surface (41). After endocytosis, syntenin binds to its cytosolic domain (42). Syntenin in turn interacts with ALIX,

5

which is an accessory protein of ESCRT III (37), which is again responsible for the vesicle-formation. ALIX is also used as a marker for EV-detection. MVEs however can also be generated independent from ESCRT, as shown by knockdown of all four ESCRT components (43). One of these ESCRT-independent pathways is governed by the sphingolipid ceramide (44). Ceramide can form lipid-raft microdomains to recruit cargo and through its cone-shape, it can induce the deformation of the endosomal membrane. The usage of ILV-generation pathways can vary by cell-type (37) and cargo, e.g. EGFR was packaged into ILVs in an ESCRT-dependent manner, while proteolipid protein was entirely dependent on ceramide (44).
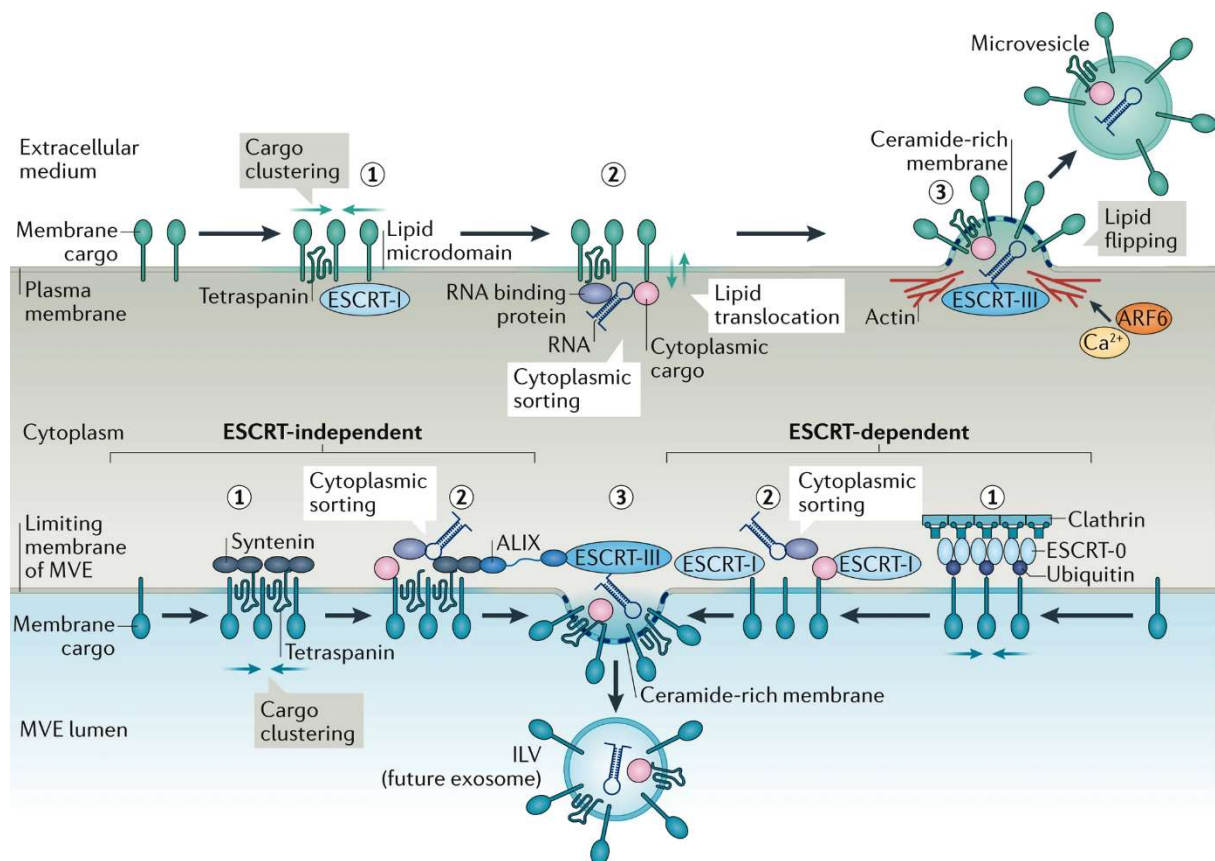
Figure 3: Examples of pathways for cargo recruitment (1), cytoplasmic sorting (2) and budding (3) of microvesicles (upper part) and intraluminal vesicles (ILVs) (lower part). ILVs can be generated either dependent on ESCRT complexes or independent from them e.g. through cross play of syndecan, syntenin and ALIX. ESCRT-0 interacts with typically ubiquitinylated cargos. ESCRT-I and –II are recruited by ESCRT-0, bind further cargoes themselves and recruit ESCRT-III, which drives the scission of ILVs. Alternatively, cargos can be clustered through syndecan, syntenin and tetraspanins, while ALIX recruits ESCRT-III. In case of microvesicles, cargo-clustering and cytoplasmic sorting are dependent on ESCRT-I and –II and tetraspanins. The translocation of lipids, predominantly phosphatidylserine is another factor in microvesicle-production. Budding of the vesicles is effected by ESCRT-III together with the cytoskeleton, where myosin is activated through small GTP-binding proteins such as ARF6 (ADP-ribosylation factor 6). Both for ILVs and microvesicles, the enrichment of ceramide in the budding membrane can also be a driver of vesicle-scission. Adapted with permission by

The biogenesis of microvesicles has not been investigated as extensively yet; however, there is evidence of multiple pathways that might act partially together in the formation of microvesicles (Figure 3). ESCRT-I to –III are instrumental in the budding of vesicles from the plasma membrane (45), ESCRT-0 seems to be absent however (35). Another important factor are cholesterol-rich lipid rafts (34). Membrane vesicles are enriched in this lipid and its depletion from cells reduces their production (46). In *Caenorhabditis elegans*, it has been shown that loss of the lipid-asymmetry of the cell membrane also leads to the budding of vesicles from the cell surface (47). This loss of asymmetry is initiated by lipid-flipping through calcium-dependent flippases (34), which makes the intracellular calcium-concentration another factor in microvesicle production (48). Finally also the small GTP-binding protein ARF6 (ADP-ribosylation factor 6) can, through a cascade of multiple enzymes, lead to activation of myosin, which in interaction with actin can effect the scission of the vesicles (35).

Tetraspanins such as CD9, CD63 and CD81, are used as general markers in the analysis of microvesicles and exosomes (33, 49). They are membrane proteins with four transmembrane domains that play important roles in many physiological processes throughout the body (50). Through association with other tetraspanins and transmembrane proteins, such as syndecan (51), as well as lipids (52) and cytosolic proteins, they can form membrane microdomains. Tetraspanins take part in the sorting of cargos to EVs (53), such as β-catenin (54) or MHC class II (55). They might also directly take part in the formation of ILVs (56).

Besides proteins, EVs also contain nucleic acids, mainly RNA (28, 34). The mechanisms of its encapsulation are however not understood completely yet. Some findings indicate the presence of zip code-like sequences that could lead to its enrichment in EVs (57, 58) and also interactions with ESCRT-II (59) and tetraspanins - through association with RNA-binding proteins - have been identified (60).

While microvesicles are released directly from the cell membrane, MVEs first need to travel through the cytosol and fuse with the phospholipid membrane to set free their ILVs. For endosomes there is a balance between exosome release and degradation through fusion with lysosomes or autophagosomes (34). Accordingly, impairment of lysosome function led to an increase in vesicle-production (61). The fate of MVEs seems to partially depend on the mechanism of their biogenesis, with the syndecan-syntenin-ALIX pathway being associated with exosome release, while the ESCRT-pathway seems to favor degradation (34, 41). Docking to the cell membrane of MVEs destined to release their ILVs as exosomes is mediated by small G-proteins of the Rab family (35). Silencing of Rab-proteins has been associated with reduced exosome-production (62). The final step of fusion between MVE and plasma

membrane is likely mediated by SNARE proteins, which are a key part of membrane-fusion events in cells (63). Different SNARE-complexes have been associated with exosome production in different cell-types (64-66).
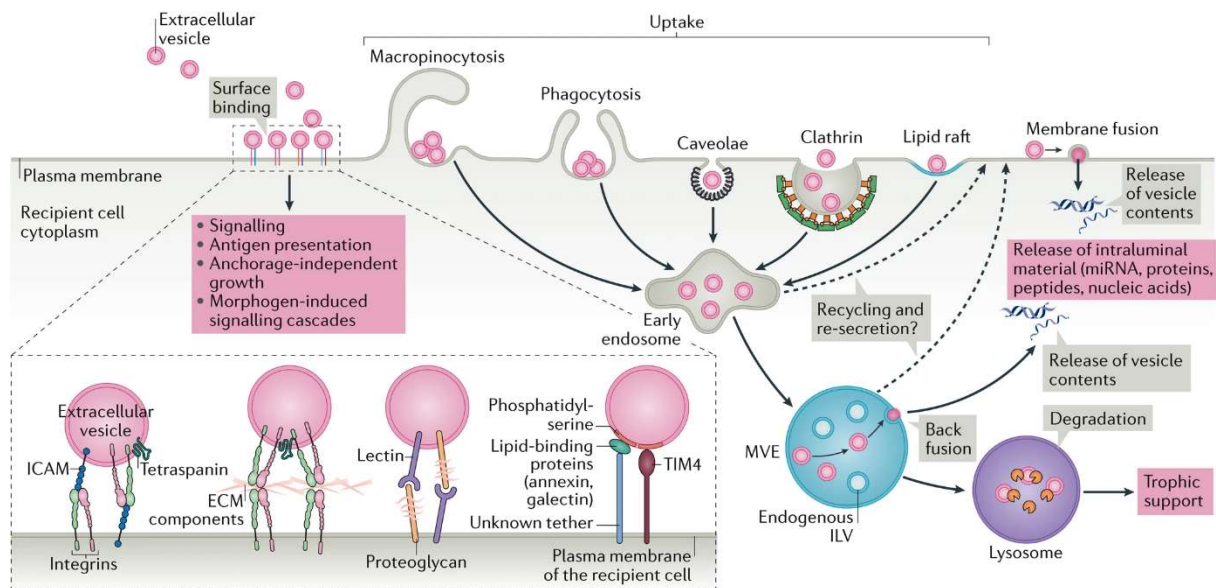
Nature Reviews | Molecular Cell Biology

Figure 4: Uptake of EVs into recipient cells is a multistage process. First vesicles bind to the cell membrane. This can take place through different interactions, for example through integrins on the cell- or vesicle-surface, components of the extracellular matrix (ECM) or the recognition of phosphatidylserine on the surface of microvesicles. Already at this stage, EVs can transfer information to recipient cells through signal cascades or antigen presentation. Endocytosis of EVs depends on the type of EVs and the recipient cells. Once taken up, EVs end up in early endosomes fated for lysosomal degradation. To set free their cargo to the cytosol, EVs can fuse with the endosomal membrane. An alternative to endocytosis is the fusion of EVs with the cell membrane to set free their cargos, endocytosis however seems to be the predominant pathway. Adapted with permission by Springer Nature Customer Service Centre GmbH from van Niel, G., et al. (2018). Nature Reviews Molecular Cell Biology 19(4): 213-228.

After being released from the cells, exosomes and microvesicles travel to recipient cells to convey effects based on their cargos (34). Transfer of information to the recipient cell can either take place already upon binding, e.g. through antigen-presentation (67), or require the uptake of the vesicle and the delivery of its soluble cargo to the lumen of the cell (Figure 4). The initial step of binding to the cell-surface can rely on different interactions (29). For instance it can be based on the interaction of integrins on the vesicles that bind to their cellular counterparts (68), phosphatidylserine exposed on the surface of EVs that can be specifically recognized (69) or through mutual interactions with extracellular matrix components (70).

After binding to the membrane, EVs can fuse with the cell membrane or be taken up by endocytosis (29). However, while some examples of direct fusion with the cell membrane have

been described (71, 72), EVs are mainly taken up by various endocytotic pathways, as indicated by the near abolishment of vesicle-uptake by decreasing temperature to halt energy-dependent processes (29). Uptake can take place by clathrin coated pits (73) or independent from clathrin through interactions with cholesterol-rich lipid-rafts (74) and by phagocytosis (75) or macropinocytosis (30). Once taken up into endosomes, EVs can fuse with the endosomal membrane to set free their cargo into the cytosol, which has been recently demonstrated (76).

EVs are found in all biological fluids of the body and diverse physiological functions have been ascribed to them (13, 77). The procoagulant activity of EVs derived from platelets is well documented (78, 79). Platelet EVs have also shown proangiogenic effects (80). In the immune system, EVs can, among other functions, present antigens on their surface (81) and in breast milk EVs seem to contribute to its immune modulatory properties (82). In the central nervous system EVs are involved in crosstalk between pre and post synapse (83, 84) and glia cells (85). During organ development, EVs mediate crosstalk between epithelial cells and the mesenchyme (86).

In the diseased state EVs can have both beneficial and detrimental effects. In infections, EVs released by neutrophilic granulocytes have demonstrated antibacterial and antifungal effects (87, 88). Moreover EVs can act as decoy-particles for bacterial virulence factors such as the pore-forming toxin of *S. aureus* (89). On the other hand, the packaging of proteins and nucleic acids into EVs has also been highjacked by viruses and EVs derived from infected cells can infect recipient cells (90-92). EVs might also play a role in neurodegenerative diseases (93) and have been implicated with transferring prions between cells (94).

A lot of research is performed into the role of EVs in cancer (95). The information contained in EVs can both prime distant sites in the body for metastasis (96, 97) and transform the phenotype of distant cancer cells (27). EVs derived from cancer cells also contribute to the immune suppressive effects exerted by cancers to promote their survival (98).

Taken together the discovery of EVs and their physiological roles has been the foundation to an ever-expanding field of science that aims at dissecting the intricate workings of EVs in the human body and harnessing them in new therapeutic approaches.

1.3.   Bacterial outer membrane vesicles

OMVs are produced through budding from the outer membrane of gram-negative bacteria. On their surface they retain the features of this membrane in the form of lipopolysaccharides (LPS) and membrane-proteins (Figure 5 A) (99). LPS makes up the outer leaflet of the outer membrane of gram-negative bacteria (Figure 5). It consists of lipid A, the lipophilic portion that forms the membrane, the core oligosaccharide and the o antigen, which is also an

oligosaccharide (Figure 5 B) (100). Its overall structure is well conserved, but there are variations between species and strains (101). The interaction of negatively charged core oligosaccharide and divalent metal cations forms a densely packed hydrophilic structure that effectively prevents the diffusion of small lipophilic compounds while lipid A prevents the passage of hydrophilic compounds thus making gram-negative bacteria impervious to many antibiotics (100, 102). LPS is recognized by the immune system and leads to strong inflammatory effects (103).
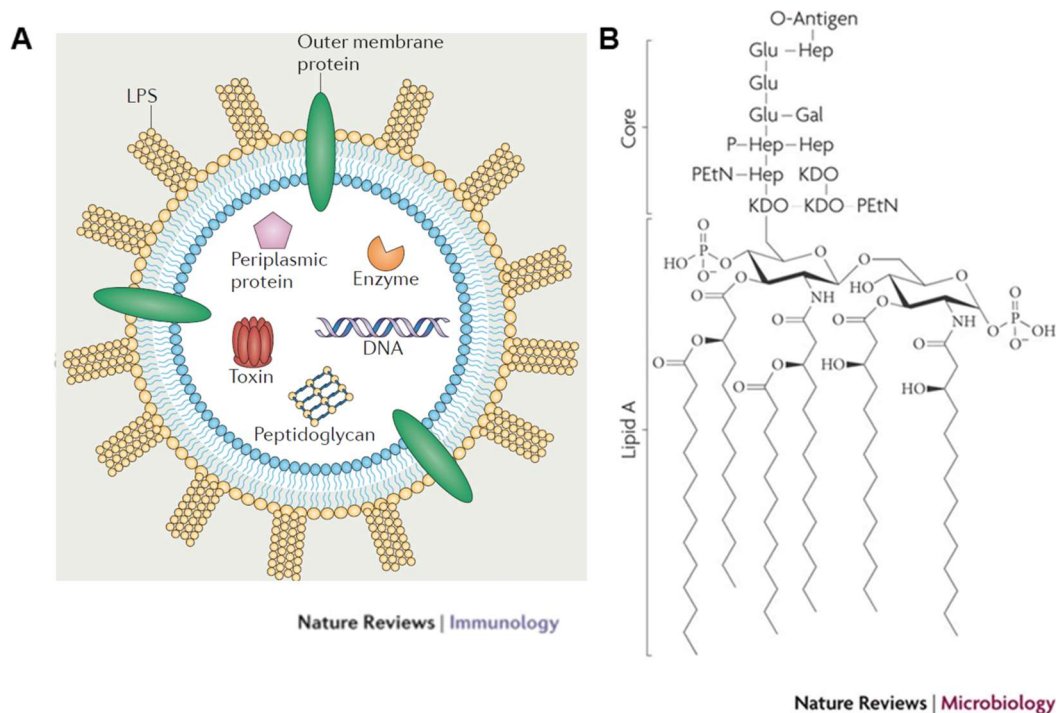
Figure 5: A shows the schematic structure of an OMV. The outer leaflet of their lipid bilayer consists of LPS. Embedded into the bilayer are outer membrane proteins. In their lumen, OMVs can contain various cargos. LPS consists of the lipophilic lipid A and the hydrophilic anionic core oligosaccharide to which the O-antigen is bound, which again is a short oligosaccharide (B). A adapted with permission by Springer Nature Customer Service Centre GmbH from Kaparakis-Liaskos, M. and R. L. Ferrero (2015). "Immune modulation by bacterial outer membrane vesicles", Nat Rev Immunol 15(6): 375-387. (99). B adapted with permission by Springer Nature Customer Service Centre GmbH from Ruiz, N., et al. (2009). "Transport of lipopolysaccharide across the cell envelope: the long road of discovery", Nature Reviews Microbiology 7(9): 677-683.

The production of OMVs is governed by multiple processes (104), which are directly linked to the structure of the gram-negative cell envelope (Figure 6). The stability of bacteria and their complex membrane-structure is dependent on crosslinking of its different components. The outer lipid-bilayer is covalently tethered to the peptidoglycan-layer in the periplasmic space by Braun's lipoprotein (Lpp). In addition to that there are non-covalent interactions through the porin OmpA that also interacts with the peptidoglycan-layer and the Tol-Pal complex that spans from the inner membrane all the way to the outer membrane and plays an important role in

cell-division (105). By regulating the integrity of this network, bacteria are able to shed parts of their outer membrane without destabilizing their whole membrane and putting their viability in jeopardy (Figure 7). The crosslinking through Lpp has a big impact on the amount of OMVs produced, with a lower amount of linkage between the protein and the peptidoglycan-layer correlating with a higher amount of vesiculation (Figure 7 a&b) (106). Areas of lower PG-membrane-crosslinking could also promote the accumulation of misfolded proteins and membrane-components that need to be expelled from the cell (Figure 7 c). These in turn can promote the outward bulging of the membrane to facilitate OMV-production. Finally, similar to mammalian EVs, the presence of lipid-microdomains and the enrichment of e.g. different types of LPS that encourage membrane-curvature could aid OMV-production (Figure 7 d&e). This was first reported for P. aeruginosa, where a charged LPS-subtype is enriched in vesicles (107). Elhenawy et al. saw a similar effect in in *S. typhimurium*, were remodeling of lipid A through deacetylation led to an increase in OMV-production (108). Turnbull et al. discovered that at least in P. aeruginosa there is also another less organized way for vesicle-production, explosive cell lysis (18). In biofilm settings, some bacteria rupture to set free their DNA, which forms an integral part of the biofilm. The remaining membrane fragments then self-organize to form membrane vesicles.
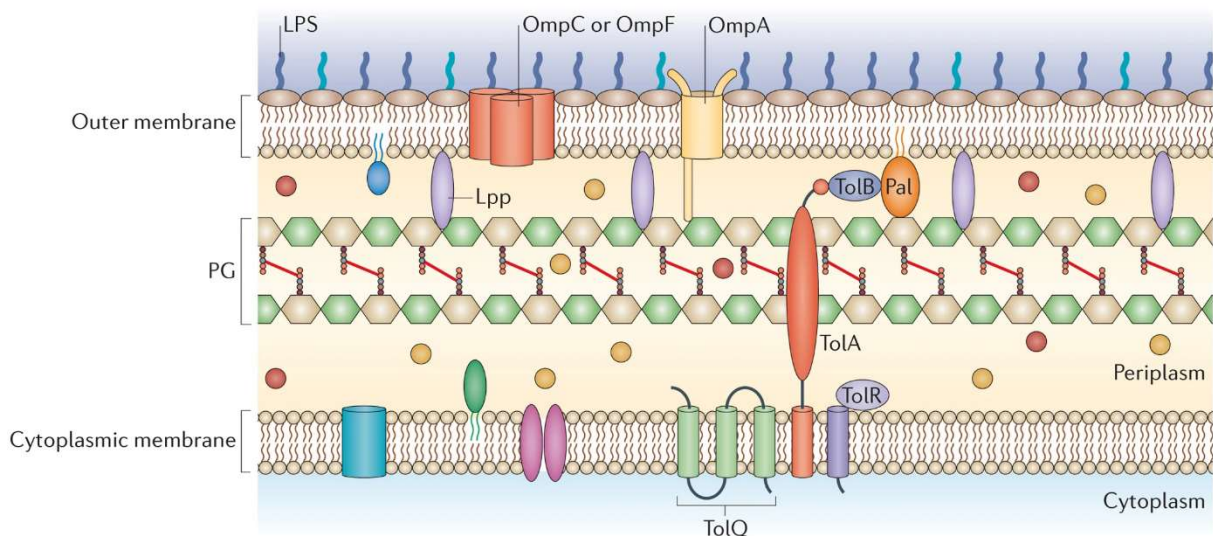
Nature Reviews | Microbiology

Figure 6: The gram-negative cell envelope consists of two lipid membranes, the cytoplasmic and the outer membrane. Between them, there is the periplasmic space that contains a peptidoglycan (PG) layer and soluble proteins. The cytoplasmic membrane consist of phospholipids, while the outer membrane is asymmetric and its outer leaflet consists of LPS. The stability of the bacterial cell-envelope is based on covalent as well as non-covalent interactions between the outer membrane and other membrane components. Lpp forms covalent crosslinks, while the porin OmpA and the Tol-Pal complex mediate non-covalent interactions. Adapted with permission by Springer Nature Customer Service Centre GmbH

The process of cargo-selection for OMVs is still not comprehensively understood. Schwechheimer and Kuehn postulate that the recruitment of cargo or its exclusion might in part be governed by passive processes, in the way that cargo molecules might be more likely to associate with membrane-features that are located in parts of the outer membrane more likely to bud and form an OMV (Figure 7 f). Excluded molecules conversely might preferably interact with components of the periplasm that are usually not part of OMVs, such as Lpp (104).
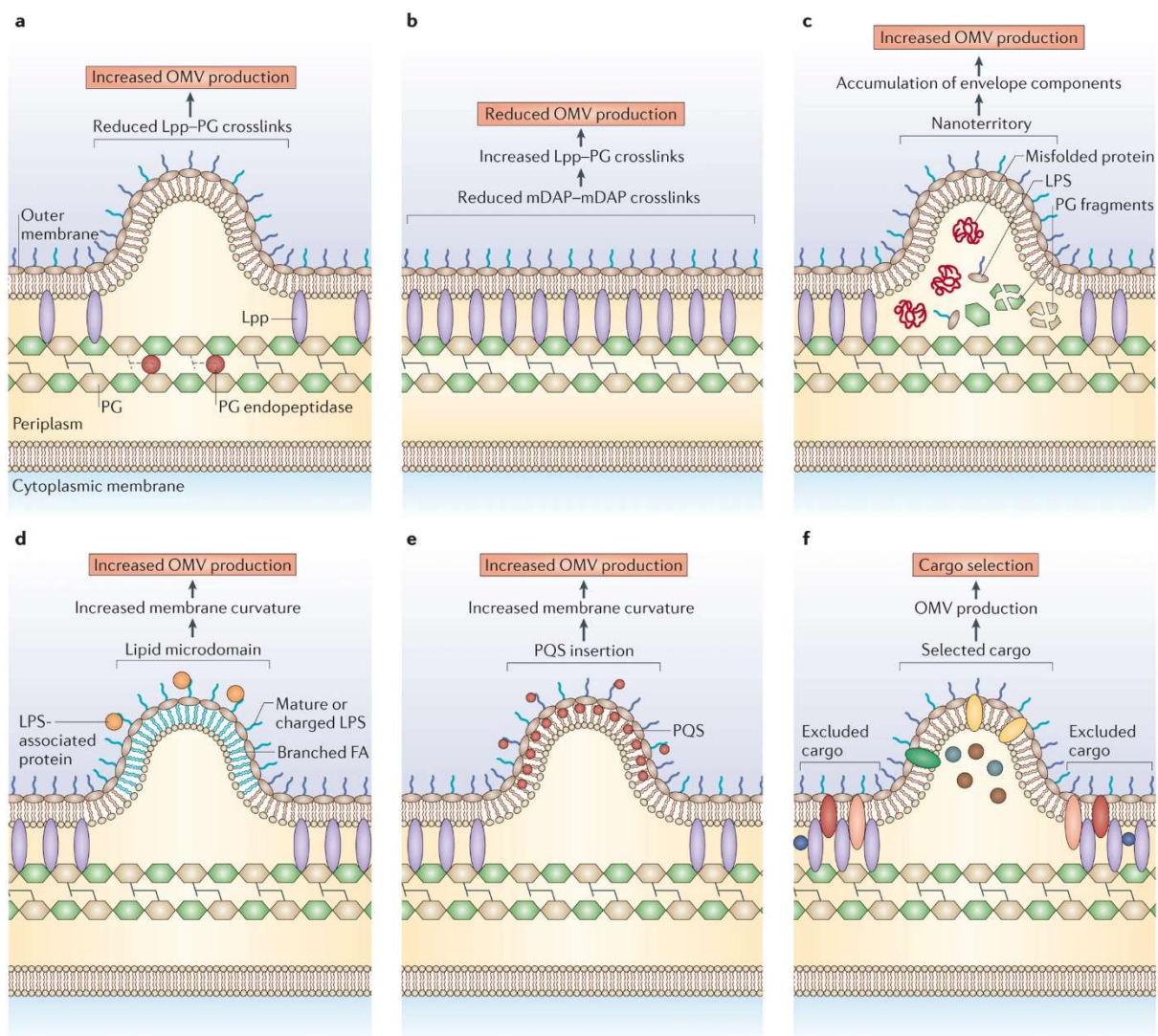
Nature Reviews | Microbiology

Figure 7: Multiple mechanisms are proposed for the formation of OMVs. Areas of reduced covalent crosslinking of PG and Lpp could lead to an increase in OMV-formation (a), while an increase in crosslinking would reduce vesicle-production (b). The accumulation of misfolded proteins and other waste-material could also lead to the outward bulging of the outer membrane and promote OMV-formation (c). Moreover, lipid microdomains containing alternative forms of LPS or other lipophilic molecules such as pseudomonas quinolone signal (PQS) could help vesicle formation (d and e). For cargo-recruitment into OMVs, it is theorized that cargos might preferentially accumulate in areas of the outer membrane more likely to form

After reaching the recipient-bacterium, OMVs can be integrated into the cell-envelope (109), but overall it is not entirely clear if this is the main mechanism of cargo-delivery, which might also be accomplished by the vesicles associating with bacteria and disintegrating to set free their cargos in the direct vicinity of recipient cells (109). Nonetheless, there is a clear indication that OMVs display some degree of selectivity in their interaction with target-bacteria (110).

Regarding OMV-uptake into mammalian cells, there is evidence that all pathways which cells regularly use for the uptake of outside-material can play a role in OMV uptake (see also Figure 3) (111). The primary route of uptake can depend, among other factors, on the OMV-origin, their surface-makers and their size. An often-reported mechanism of entry is the uptake of OMVs through interaction with cholesterol-rich lipid-raft-domains (112-114). O'Donoghue et al. determined that uptake of OMVs through this mechanism likely depends on the presence of the O-antigen on the vesicle-surface (115). The O antigen is the outermost part of LPS and is typically more prevalent in pathogenic bacteria. This insinuates that the pathogenicity of certain bacteria is in some way linked to the efficient uptake of their OMVs by host cells.

In the same way as EVs, OMVs can contain a wide array of cargoes and be important factors under different circumstances. For the producing bacterium itself, formation of OMVs has been proven an important stress-response-mechanism. OMV-production allows for the rapid removal of misfolded proteins and other toxic compounds (116). A reduced OMV production-capability is hence linked to impaired growth and increased sensitivity to external stressors (104). Shedding of OMVs can also help bacteria adapt to changes of their environment, by facilitating rapid alterations of the LPS-layer facing the outside medium (117). In bacterial communities, OMVs can act as common goods that help not only the producing bacterium, but the whole community (104, 118). They improve the acquisition of nutrients through associated degradative enzymes (14, 119) and iron-binding molecules (12, 120). OMVs themselves can also be used as a nutrient-source, e.g. by heterotrophic bacteria (121). The ability of OMVs to carry poorly soluble molecules over great distances, enables the distribution of hydrophobic quorum sensing factors, such as the pseudomonas quinolone signal, which is a key factor for the virulence of *P. aeruginosa* (111).

In host-pathogen interactions, OMVs can have both mutually beneficial effects as well as detrimental effect for the host. Bacteria encapsulate virulence factors in their OMVs that elicit cytotoxic effects in host-cells and increase the severity of the infection. Examples are outer membrane protein A and tissue-degrading enzymes packaged into *Acinetobacter baumannii*

OMVs (114), cytotoxic necrotizing factor type 1 in OMVs from uropathogenic *E. coli* (113) and enterotoxin found in OMVs derived from enterotoxigenic *E. coli* (112). Nevertheless, OMVs can also have beneficial effects and vesicles derived from commensal bacteria have shown anti-inflammatory effects (122-124). These effects are most prominent for OMVs derived from the gut microbiota, highlighting its importance in the prevention of inflammatory diseases (125).

In the context of bacterial infections, OMVs have several functions that help their parent bacteria colonize the host and survive its countermeasures. OMVs that bind antimicrobial peptides and bacteriophages can act as decoy to shield their producers, similar to their mammalian cousins (126-128). Moreover, OMVs can be associated with beta-lactamases to offer further protection against antibiotics (111, 129). OMVs containing DNA can transform other bacteria and lead to the expression of virulence genes, such as shiga toxin (130), and antibiotic resistance genes, which has been studied most extensively for *A. baumannii*. Its OMVs have been implicated in the transfer of antibiotic resistance genes within the species (131, 132) but also across the species-barrier (133). Finally, OMVs can also trigger the formation of biofilms (134, 135) and vesicles contained in these bacterial communities account for a big portion of the LPS found there (136). Their specific role in this setting, apart from their biological roles previously described, however still is not completely understood (137). The lytic enzymes and antibiotic-binding capabilities of OMVs however, are certainly advantageous for shielding biofilm-dwelling bacteria from detrimental outside-influences.

While OMVs can have many beneficial properties in bacterial communities, some bacteria also produce OMVs with antibacterial properties to fight off rivalling species invading their biological niche or to actively attack other bacteria. In several publications, the antibacterial properties of OMVs derived from *P. aeruginosa* and other gram-negative have been analyzed (138-140). However, of greater relevance for the work presented in this thesis and with greater potential for application as antibacterial nanoparticles, are OMVs produced by myxobacteria.

1.3.1. Myxobacterial OMVs

Myxobacteria are a group of gram-negative bacteria that possess many distinct features and abilities that make them a widely studied group of microorganisms (141). Myxobacteria were discovered in the 19th century, mostly due to their ability to form brightly colored fruiting bodies visible to the naked eye (Figure 8) (142). These fruiting bodies consist of endospores, the so-called myxospores. In their vegetative state myxobacteria generally form short or long rods and are encountered in soil, but also grow on the bark of trees and on the feces of rabbits and other herbivores. The latter have also long been used for the isolation of myxobacterial species in the lab, as they form a relatively selective growth-medium, where other bacteria and fungi have difficulty growing, while myxobacteria develop their typical fruiting bodies (143). Many
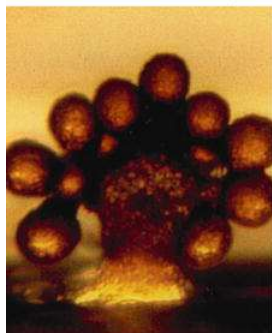
Figure 8: Fruiting bodies from different myxobacterial species. Adapted by permission of Springer Nature Customer Service Centre GmbH from Kaiser, D. (2013). "The Prokaryotes: Prokaryotic Communities and Ecophysiology", Berlin, Heidelberg, Springer Berlin Heidelberg: 511-528.

myxobacteria sustain themselves through hunting and consuming of other bacteria (142). To this end, they have developed a complex cooperative lifestyle, where the bacteria act in unison to engulf and consume their prey, a behavior often compared to a "wolf-pack" (144). To help them lyse and disintegrate other bacteria, myxobacteria produce a wide variety of secondary metabolites with activity against cancer, fungi or bacteria (145). Especially regarding antibiotics, myxobacteria present researchers with a treasure-chest of compounds with novel modes of action to be optimized for their use as new antibiotics (146). One group of new antibiotics discovered in myxobacteria are the cystobactamids that are inhibitors of the bacterial type IIa topoisomerase (147).

It was postulated that as one way of delivering these compounds to their prey, myxobacteria use OMVs, as there was evidence of the packaging of lytic enzymes and antibacterial secondary metabolites into their vesicles (141). Evans et al. were the first to find direct proof of the antibacterial activity of myxobacterial OMVs derived from *Myxococcus xanthus*. They could show that hydrolases packaged into the vesicles effectively killed *E. coli* bacteria (148). Schulz, Goes et al. (21, 22), evaluated OMVs derived from different strains of myxobacteria including strains known to produce cystobactamids (147). Two cystobactamids were found in OMVs derived from *Cystobacter velatus* and *Cystobacter ferrugineus*. Both showed antibacterial activity against planktonic gram-positive and –negative bacteria. Their effect was comparable to free cystobactamid and the established antibiotic gentamicin. Additionally, these vesicles were also taken up by mammalian cells and effectively killed intracellular *S. aureus*. In their effective concentrations myxobacterial OMVs were well tolerated by cells and showed virtually no cytotoxicity, while eliciting only a mild pro-inflammatory response. These findings make myxobacterial OMVs an auspicious target for further research towards their therapeutic use. Thus, one of the aims of this work was to evaluate the surface engineering of OMVs to introduce targeting moieties promoting their selective interaction with bacteria to increase their antibacterial properties.

1.4.   Isolation and characterization of EVs
1.4.1.   EV-isolation

EV-isolation and –purification is concerned with enriching EVs from the complex medium they are released into by their parent-cells. In most cases, this medium is either a bodily fluid such as blood or urine where EVs are found *in vivo* or the culture medium cells are grown in *in vitro*. Both contain many impurities that need to be removed to obtain pure EVs. These impurities can be dissolved in the medium, such as proteins and nutrients or be present in the form of nano- or microparticles, such as the producing cells themselves, their *post-mortem* remnants or other nanoparticles, e.g. viruses, lipoproteins and in case of bacteria flagella (149). These multiform contaminants are challenging to remove and require the use of sophisticated protocols for vesicle-purification (Table 1).

Table 1: Overview of methods for the isolation and purification of EVs and their advantages and disadvantages.

Initial volume	Method	Advantages	Disadvantages
High volume	Ultracentrifugation (UC)	• Produces highly concentrated samples • Complementary to other isolation methods	• Co-isolation of soluble impurities, requires further purification • Pelleting of non-EV-particles • Low recovery rate • Potential damage to EVs due to high forces • High cost of entry • Low scalability
	Tangential flow filtration (TFF)	• Low impact on EV integrity • High scalability	• Potential Co-isolation of soluble impurities • Filter material needs to be optimized
	PEG precipitation	• No specialized equipment • Cheap excipients • Lowimpact on EV integrity • High scalability	• Co-isolation of soluble impurities, requires further purification • Longer processing time than UC and TFF
Low volume	Size exclusion chromatography (SEC)	• Low forces on EVs • Short processing time • Efficient removal of soluble impurities • Relatively cheap equipment	• SEC leads to sample dilution • Co-isolation of particles with the same size as EVs
	Density gradient ultracentrifugation	• Low forces on EVs • Concentration of EVs or EV-subsets • Efficient removal of impurities with different density than EVs	• Co-isolation of particles with the same density as EVs • Long processing time • Components of the density gradient need to be removed • Sucrose gradients might exert osmotic stress • Long processing times

The most widely used method for EV-isolation is differential ultracentrifugation (150). After collection of the conditioned medium, larger particles, such as cells are removed by low-speed centrifugation. The centrifugal force applied in this step depends on the fragility and size of the producing organism. Mammalian cells are sensitive to centrifugal force and comparably large, thus centrifugation is typically carried out in the range of 300 x g (151). For bacterial cultures, higher forces have to be applied due to their smaller size (152). They however also are able to better withstand these forces, without dying (153). After larger particles have been removed, typically another step of centrifugation is carried out at a higher speed to further deplete larger particles, such as cell debris (154). The resulting supernatant is then subjected to ultracentrifugation (UC) at a speed around 100000 x g to pellet EVs (154). The obtained pellet contains concentrated EVs, however these are still contaminated with co-precipitated proteins and residual supernatant. For example, miRNAs derived from medium supplements can be co-isolated and have been wrongly identified as EV-markers (155). Thus, another step of purification is needed. The simplest approach to this, is resuspension in phosphate buffered saline (PBS) and repetition of UC (154). The high forces exerted on EVs during UC can damage the vesicles or lead to their fusion (156). This problem can be somewhat mitigated by employing a cushion of concentrated sucrose on which the vesicles float during UC (157). However, residual sucrose has to be removed from the vesicles by conventional UC or another method.

Due to the disadvantages of UC, alternative methods have found broad application, either alone or as a multistep combination. Besides UC, the method best suited for the large initial volumes encountered in EV-production from cell culture is tangential flow filtration (TFF). Compared to conventional dead-end filtration, TFF circumvents issues such as caking and clogging of pores by maintaining a lateral flow of the feed over the filter membrane (158). This reduces the strain on the vesicles and increases the volume that can be processed (159). TFF is typically performed in two steps. First, a membrane with a pore size large enough to let EVs pass is employed, to filter out any large particulate impurities. The filtered EVs can then be further purified and concentrated by employing a membrane with a molecular weight cutoff that only allows the passage of soluble impurities. While the volume of the EV-containing feed-fluid decreases, soluble impurities, such as proteins from the culture supernatant are filtered out (158). TFF can be used to process large volumes of conditioned medium (160) and compared to an ultracentrifuge the initial cost is much lower while upscaling can be easily implemented by parallelization (161). Thus, TFF is considered one of the most promising methods for future large-scale vesicle production (161, 162). Filtration is also used for the downstream purification of EVs, for example to remove non-incorporated material after surface modification. Here however morphology and size changes due to extrusion through small pores and particle loss due to adsorption to the filter need to be assessed carefully (17, 163).

Another method for the purification of larger volumes of EVs is precipitation of the vesicles using polyethylene glycol (PEG) (164). This simple method has the considerable disadvantage that not only EVs but also soluble proteins from the medium can be co-precipitated, leading to a low purity of isolated vesicles (165). This problem was mitigated by Ludwig et al. by washing the precipitated EVs using UC (166). They also adapted the protocol to make it applicable for the purification of up to 10 L of conditioned medium at once (166).

Small volumes of EV-containing samples, for example from patient plasma or resuspended pellets after UC, can be purified by multiple different methods. The relatively defined size spectrum of EVs is utilized in their isolation by size exclusion chromatography (SEC) and the abovementioned filtration approaches. In SEC, the porous column material separates EVs from soluble impurities ranging from medium constituents to soluble proteins and small nanoparticles. EV are too large to diffuse into the pores of the stationary phase and thus elute with the void volume, while smaller impurities can interact with the column material and elute later (167). SEC is very effective at removing soluble impurities from EVs and the column-size can be scaled to the sample volume. Its main disadvantage is that it leads to the dilution of the samples (17). SEC is also used in a commercial kit for EV-isolation (168).

Very high purity vesicles can be obtained using gradient UC (165). Here a gradient of sucrose or iodixanol is employed that leads to the flotation of EVs and other contaminants according to their buoyancy during UC. Sucrose is the cheaper alternative, but the hyper-osmolarity of concentrated sucrose solutions might damage the vesicles. Iodixanol forms iso osmolar solutions at all concentrations and thus potentially better preserves EV-integrity (165). After gradient UC a second step of purification is needed to remove residual sucrose or iodixanol (169). Gradient UC also separates EV-populations with different densities, which makes it ideally suited for in depth analysis of different vesicle populations. The need for an ultracentrifuge and the long centrifugation time of 16 to 18 h required for gradient UC are the main disadvantages compared to other EV-processing methods.

Particularly difficult samples that contain impurities in both the same size- and density-range as EVs can benefit from the combination of multiple purification steps. For plasma that contained both very low-density lipoprotein (VLDL) overlapping with EVs in size and high-density lipoprotein (HDL) overlapping with EVs in density, Karimi et al. designed a two-step process combining gradient UC with SEC (170). Gradient UC effectively removed VLDL and enriched EVs and HDL. HDL was then efficiently removed from EVs by SEC due to its much smaller size.

New and emerging techniques for EV-purification include enrichment of EVs through binding of specific surface markers (171, 172), a plethora of methods based on microfluidics (173-175) and asymmetric flow-field-flow-fractionation (AF4) (25, 176).

1.4.2. EV-characterization

EVs can be characterized regarding their physicochemical properties and regarding their composition and cargo. Guidelines to a comprehensive analysis of mammalian EVs are collected in the "Minimal information for studies of extracellular vesicles" (MISEV) document published by the international society for extracellular vesicles (33). According to these guidelines, typical protein markers, EV-size and appearance need to be analyzed and vesicles should be quantified, ideally combining different measurements, such protein content, particle number or lipid content (33).

Physicochemical parameters can be measured using the techniques that are the standard for nanoparticle-characterization (177), with the caveats that EVs are generally less uniform than synthetic nanoparticles and that EV-samples are frequently of comparably low concentration. Thus, for example dynamic light scattering is of limited applicability for vesicle characterization, as it over represents larger particles and cannot adequately display the multimodality of EV-samples (178).
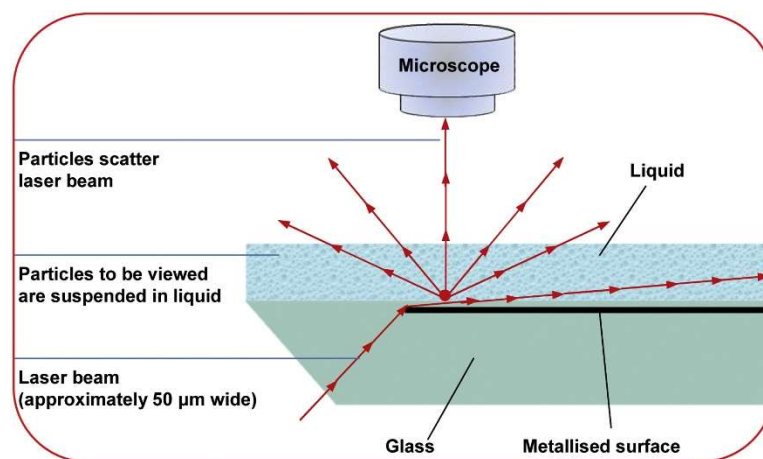
Figure 9: In nanoparticle-tracking-analysis (NTA) measurements, a laser beam travels through a chamber containing suspended particles. Scattered light from particles that travel into the laser's light-path is collected by a microscope-assembly. A camera connected to the microscope captures videos of the moving particles that can be analyzed regarding particle-number and size using software. Adapted from Dragovic, R. A., et al. (2011). Nanomedicine: Nanotechnology, Biology and Medicine 7(6): 780-788. Used under the Creative Commons CC-BY 4.0 license.

The most widely used technique to reliably assess both the size and the particle-concentration of EVs is nanoparticle-tracking-analysis (NTA) (179). Here particle suspensions are illuminated

with a laser, which is scattered when it hits a particle (Figure 9). The scattered light is collected by a microscope assembly set orthogonal to the light path of the laser and a camera captures videos of the moving particles. Through the movement per frame of the illuminated particles and the viscosity of the medium, the size of particles can be determined using the velocity of their Brownian motion. At the same time, the amount of trackable particles in the field of view can be used to extrapolate the particle concentration. After staining the vesicles e.g. through the binding of a fluorescently labeled antibody, NTA can also be employed to discriminate between different EV-populations by fluorescence (180).

While light scattering based methods can measure the size-distribution and concentration of nanoparticles, their identity as vesicles is best determined by electron microscopy (181). In transmission electron microscopy (TEM) the membrane and lumen of EVs is visible and thus they can be discriminated from other particulates in the medium. While regular TEM with negative staining of EVs using heavy metal ions is relatively easily realized, only cryo TEM can show the vesicles in their native state, as here no staining or drying are necessary to visualize the vesicles. In cryo TEM, thin films of EV-containing samples are vitrified by flash-freezing and then imaged using a special cooled sample holder (182). Scanning electron microscopy has also been employed for the visualization of EVs. Here the vesicles are visible as small spheres. The drying of the sample during sample preparation however often leads to the formation of aggregates (183). Electron microscopy of EVs can be combined with immunogold labeling to also obtain information about surface markers of EVs (181).

Physical characterization of EVs can also be performed by atomic force microscopy, which offers information about their mechanical properties (184), and tunable resistive pulse sensing that measures particle size and concentration (185) and can also be used for the evaluation of the zeta potential of nanoparticles (186). However both techniques are less widely used than NTA and TEM (181).

The protein content of EVs can be assessed on the bulk level, using typical assays such as BCA- and Bradford-assay. A caveat is that these assays usually can only reliably assess proteins on the surface of the vesicles. To measure proteins present in the lumen of EVs, they first need to be lysed. This can be done using Radioimmunoprecipitation assay (RIPA) buffer (187), however compatibility problems with the protein-quantification assay of choice may arise. Even without lysis, the protein-content of EV samples combined with their particle number can be used for an easy assessment of their purity for the comparison of different EV-isolation protocols (187). Specific proteins can be assessed using western blotting or LC/MS, the latter is also used to analyze the lipid-content of EVs. Another technique that is popular for assessing EV-markers is flow cytometry (FACS).

Compared with Western blotting, where EVs can be processed in the same way as cells (188), FACS-based analysis of EVs is considerably more complex than the analysis of mammalian cells. The small size of EVs is near or below the resolution limit of most conventional flow cytometers (189). Thus, the cytometer settings need to be optimized to reliably detect single EVs and distinguish EVs from similar background events (190, 191). A more sensitive detection of EVs can be realized by employing imaging flow cytometry (189). Here, scattered light is captured by a microscope and measured by a camera with much higher resolutions than conventional photodiodes or photomultiplier tubes. This allows for the direct visual detection of single EVs (189). Specialized flow cytometers for EV-detection are not ubiquitously available and if a semi-quantitative assessment of the presence or absence of e.g. a tetraspanin on the vesicle surface is the sole concern of the measurement, EVs can also be chemically linked to beads sized in the range of few micrometers (192). These beads give similar signals to cells and can thus be measured with standard flow cytometers.

1.5.   EVs in biomedical applications

EVs are currently evaluated in many therapeutic and diagnostic applications and there are 233 clinical trials that focus among other aims on the use of EVs as biomarkers and therapeutics (ClinicalTrials.gov was searched for "exosome OR (extracellular vesicle)", last visited 09.10.2020 at 13:19).

In EV-based diagnostics, researchers utilize the specific effects diseases can have on the composition of EVs and their easy availability from all bodily fluids. EVs are being developed as biomarkers for, among others, the detection and monitoring of various cancers such as lung cancer (193), prostate cancer (194) or breast cancer (195), Parkinson's disease (196) and liver diseases (197). To this end, liquid biopsies containing EVs carrying the relevant information have been obtained from blood (195-197), synovial fluid (198), urine (194, 199), saliva (200) and tears (201). The latter three can be obtained without any invasive procedures, thus minimizing risks and unpleasantness for the patient.

For therapeutic use, EVs exhibit some general advantages that prompted researchers to further evaluate them. Their intrinsic pharmacological activity, the selective enrichment of active cargoes, their ability to cross biological barriers and transfer sensitive cargoes over long distances (see 1.2 and 1.3 for a closer evaluation) and their good safety profile (21, 124, 202, 203) all contribute to the potential of EVs in therapeutic applications. Moreover, methods have been developed to engineer EVs to encapsulate the cargoes of choice (see 1.5.1) and introduce new moieties to their surface (see 1.7).

In therapeutic approaches, EVs can either themselves act as the therapeutic agent or be utilized as drug delivery vehicles. The main fields of therapeutic application of native mammalian EVs are tissue regeneration and wound healing (204, 205), where especially EVs derived from mesenchymal stem cells have shown broad activity (206, 207). These results however have been put under suspicion by the recent finding that a large portion of the observed activity might be caused by co-purified soluble proteins instead of EVs (208). Another source for EVs with regenerative activity are cardiosphere-derived cells, whose EVs improve the healing of myocardial injuries (209).

One more important application aimed at the native activity of EVs and especially OMVs, is vaccination (210). Bacterial vesicles carry antigens on their surface and as their cargo that can elicit a specific immune response (211). Additionally the immunogenic LPS found on OMVs can act as an adjuvant (212, 213). The potentially excessive toxicity of LPS however (103), can require the modification of this membrane component to produce OMVs with an acceptable safety profile (see 1.8.1). One OMV-containing vaccine against *Neisseria meningitidis* serogroup B has been authorized in 2013 and 2015 in the EU and US respectively and today is in use for all age groups (214). An OMV-based vaccine against *Shigella sonnei* is currently in development and has completed phase 1 clinical trials (215).

Despite the promising results of EVs as therapeutics and drug delivery vehicles, their broad clinical translation has not been realized yet, due to a multitude of hindrances that still need to be addressed (see 1.6).

1.5.1. EVs as drug delivery vehicles

In the context of this work, the applicability of EVs as drug delivery vehicles is of special concern, as the surface-engineering techniques presented herein are mainly aimed at developing a method for the efficient decoration of EVs with targeting moieties to facilitate EV-based drug delivery.

The first step to successful drug delivery using nanoparticles is the encapsulation of drugs. Here the endogenous loading of EVs with therapeutically active compounds by the parent cells and the exogenous encapsulation of drugs after EV-isolation can be differentiated.

Endogenous loading is carried out either naturally by the parent cells themselves (see 1.2 and 1.3) or by genetic engineering. Loading through genetic engineering has been achieved, by the overexpression of the cargo-molecules of choice, as exemplified by Mizrak et al., who produced EVs loaded with enzymes and the corresponding mRNA that once transferred to target cells made them susceptible to treatment with 5-fluorocytosin (216). Overexpression however can lead to overall changes in gene-expression that might also influence EV-

production and –components (217). Thus, more specific ways methods to target cargoes to EVs have been developed. Cells have been engineered to express fusion-proteins consisting of an EV-enriched membrane protein and an RNA-binding domain that selectively binds the cargo-RNA resulting in effective RNA-enrichment into EVs (218, 219). It has also been discovered that certain RNA-sequences can convey loading into EVs by the cellular machinery (57, 58), which could be utilized to encapsulate therapeutic RNAs. Drugs can also be encapsulated into EVs by adding them to the growth-medium of their parent cells. This way, gentamicin loaded OMVs (220) and mammalian EVs loaded with paclitaxel have been obtained (221).

For exogenous encapsulation after EV-isolation, the approach depends on the structure of the prospective cargo. Hydrophobic drugs are easily encapsulated, as they embed themselves into the phospholipid bilayer, as demonstrated for hydrophobic porphyrins and curcumin (222, 223). Encapsulation into the EV-membrane increased the bioavailability of curcumin in vivo and protected mice from septic shock induced by LPS-injection (222).

While the lipid membrane of EVs helps them protect sensitive molecules in their lumen, it also forms a natural barrier for the encapsulation of hydrophilic drugs. Multiple techniques have been evaluated for the encapsulation of hydrophilic molecules in EVs.

Haney et al. compared sonication, freeze-thaw cycles, saponin incubation and incubation at RT for the loading of mammalian EVs with the enzyme catalase (224). They found that sonication, extrusion and saponin-treatment led to the highest encapsulation of active enzyme. However, sonication and extrusion, as well as freeze-thaw cycles, also affected the size and shape of EVs of the vesicles and might affect their therapeutic efficiency (224). Nonetheless, both EVs loaded by saponin-incubation and sonication showed antioxidant and neuroprotective effects in mice. Saponin incubation was also evaluated for the encapsulation of hydrophilic porphyrins into EVs by Fuhrmann et al., who tested it alongside hypotonic dialysis, extrusion and electroporation (223). They found that both dialysis and saponin-incubation led to a significant improved loading efficacy, however dialysis compromised the ability of EVs to transfer their cargo into cells. Electroporation, which was not effective for the hydrophilic model-porphyrin, significantly enhanced loading with a porphyrin of intermediate hydrophilicity (223). Indeed, electroporation seems to be a suitable method for small molecules such as doxorubicin (225), for larger and more complex molecules however, encapsulation by electroporation has been associated with problems, regarding OMV-stability (226) and the precipitation of RNA-cargos (227). Nevertheless, electroporation remains a popular method for exogenous drug-loading of EVs (217). An alternative to encapsulating cargos in the lumen of EVs is anchoring them on their surface (228-230), which is discussed in more detail in 1.9.1.2.

Successful examples of EV-based drug delivery include the abovementioned catalase-loaded EVs to convey neuroprotection in Parkinson-models (224), the loading of EVs with a photosensitizer by incubation of their parent cells leading to loaded vesicles that significantly outperformed liposomes in drug delivery to tumor organoids (231) and the delivery of siRNA to the brain of mice using EVs engineered with brain specific viral protein on their surface (232). The last study is also an example for the introduction of targeting moieties to the EV surface. EV surface engineering and its objectives are evaluated in more detail in 1.7, 1.8 and 1.9.

1.6.   Challenges towards clinical translation of EVs

To reach the market, potential EV-based therapeutics need to successfully pass through pre-clinical and clinical evaluation and gain approval from the respective governing body. In context of the rules and regulations that apply to EVs, they are best categorized as biological medicinal products (233, 234).
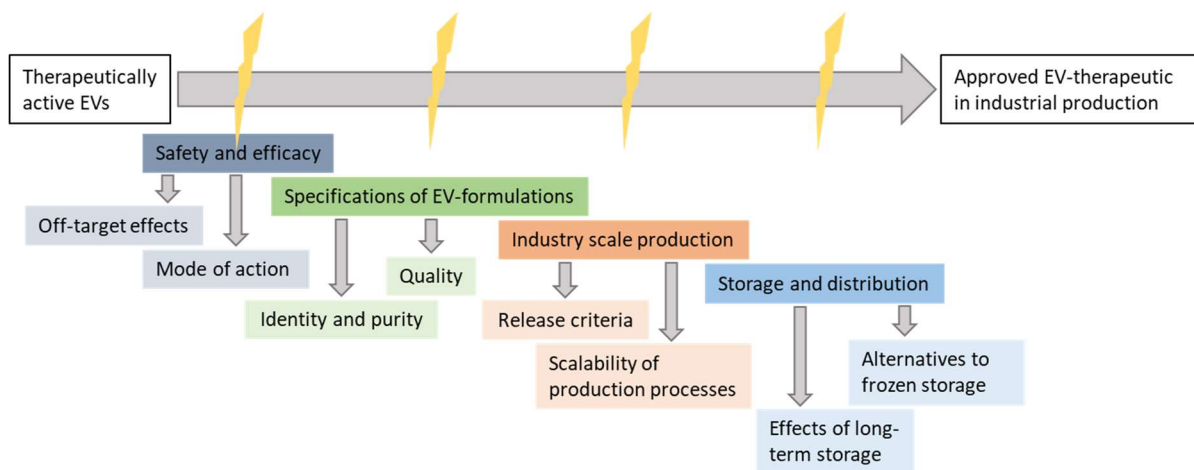
Figure 10: Multiple hurdles currently hinder the transition from therapeutically active EVs to approved EV-therapeutics. The safety and efficacy of EVs need further evaluation to determine unwanted off-target effects and the mode of action of the vesicles. The identity and purity as well as other quality criteria of EVs still need to be defined also in light of the limitations of current methods for EV-isolation and characterization. Quality criteria of EVs are also important to derive from them release criteria for the industrial production of EVs. Here moreover, the scalability of EV-production processes needs to be assessed. Finally, the storage stability of EV-formulations needs to be evaluated with the aim of establishing alternatives to frozen storage of EVs to make the storage and distribution of EV-formulations more feasible.

Besides the positive example of OMVs as part of a clinically approved meningococcal vaccine (214), clinical translation of EV-based therapeutics has not been realized yet. The journey of EVs from bench to bedside is still held back by challenges during the translation-process (162).

The most difficult of these hurdles mainly relate to the safety and efficacy of EVs, the specifications of EV formulations and their industrial scale production (Figure 10).

Regarding safety, the cargos of EVs and their pleiotropic effects in the body are under investigation. The possible pro-metastatic and tumorigenic effects of EVs derived from cancer cell lines are already discussed (95-97), but also the procoagulant or proangiogenic activity of some EVs could prove problematic (78-80). Additionally, the heterogeneous populations of EVs produced by cells make it difficult to anticipate possible unwanted off-target effects (235). The heterogeneity is also problematic for assessing the efficacy of EV formulations and determining a mode of action (236), knowledge of which is required as part for the documentation required for the initiation of clinical trials (237). Due to the presence of multiple active molecules in EVs evaluation of their pharmacodynamics is complicated (238).

Regarding the specifications of EV formulations, the main question is how to define identity and purity of EVs (162). The methods for EV purification are limited and the higher throughput required for their upscaled production further limits applicable methods (see 1.4.1). While the differentiation between different subsets of EVs cannot be realized with current methods (33), they also always carry over some non-EV components of the cellular secretome (162). Thus instead of defining the final product as "exosomes" or "EVs", Gimona et al. proposed to rather define the formulations as vesicle enriched secretome fractions (162). Fortuitously the inherent heterogeneity of biological products is also acknowledged in the ICH guidelines concerning biological medicinal product (239), making this a viable approach.

To define the quality of EV formulations, also a higher degree of standardization in their production and evaluation is needed, as seemingly small changes in culture- and isolation-conditions can have a big impact on their functionality, affecting the comparability of different studies. For EVs derived from mesenchymal stem cells, the number of passages in culture altered their pharmaceutical activity (240) and different isolation methods might not only affect the purity of isolated EVs but also their activity (241). Another important aspect in this regard are the cells used for EV-production. As in other human-derived medicinal products, inclusion criteria for donors must be defined (233), as diseases and other parameters can affect the safety and activity of EVs. In a recent study, the influence of donor-age on vesicle-activity was demonstrated (242). Some cell-types, such as mesenchymal stem cells can also be isolated from different tissues such as the umbilical cord, bone marrow or adipose tissue (236). Studies have shown that there are differences in the composition and pharmaceutical activity of MSC-EVs based on the tissue of origin (243, 244). The international society for extracellular vesicles is thus focusing on generating universal guidelines for the production, evaluation and application of EVs. Examples of the fruits of these efforts are the MISEV guidelines discussed above (33), MIFlowCyt-EV (245), which deals with the reporting of FACS-experiments and the

recently published comprehensive discussion of reference materials for EV-measurements (246).

As the purification process has great influence on the final EV-product, as it is the case for most biologicals (247), another important aspect of the EV production process is its scalability. Increasing the production volume without changing the process, could greatly speed up the transition from laboratory scale production of EVs to the larger batches needed for preclinical evaluation and clinical trails to the potentially even larger batches after successful approval (162). For OMVs the GMP-conform production has already been realized (248), for mammalian cells only the isolation of the complete secretome without EV-enrichment has been demonstrated (249).

The quality of EV formulations, i.e. identity, purity, potency and quantity also need throughout evaluation to derive from it robust parameters for release criteria for industrial production (239). Here especially *in vitro* potency assays are needed (234). An assay for the evaluation of MSC-derived EVs are currently investigated (250)

The final hurdle in EV translation refers to the storage stability of EV-based products and their distribution, which is discussed in detail in the following chapter.

In conclusion, a lot of work is still needed to generate the knowledge required for the clinical translation of EV-based therapeutics. Nevertheless, especially for MSC-EVs, substantial progress has already been made and the knowledge gained from this endeavor will be the basis for the future translation of EVs derived from other cell-types.

1.6.1.   EV storage

The complexity of EV-samples makes it important to very thoroughly monitor their storage stability. Especially for the large-scale industrial production, EV-containing therapeutics need to be stable over longer periods of time and during distribution to the patients. However, also EV-containing patient samples for biomarker determination and EVs isolated in laboratory settings for basic research often need to be stored before their analysis without being compromised. Thus, methods for the optimal storage of EVs are under investigation. EV-samples can be stored either in liquid form, frozen or in dried form after lyophilisation or spray-drying.

For storage in liquid form at 4 °C, there is evidence that at least for a short period of a few days EVs derived from various biological fluids and cell culture were sufficiently stable (251, 252). For longer term storage however, there was generally a decline in vesicle-stability for liquid storage of EVs (251). These findings have important implications especially for EV isolation

and characterization, as the time required for some steps can make it impractical to carry out all steps in one day without overnight storage. In this context also another parameter important for EV-storage and -processing needs to be considered, the choice of the vials the samples are stored in. Some materials might lead to the unspecific and irreversible adsorption of EVs (233). Thus, the effect of the vials should be evaluated (253).

Freezing EVs at -80 °C is currently considered as the gold standard for their storage (162). Even after 30 years of storage at this temperature intact vesicles showing typical markers could be obtained from seminal fluid, however a lowered acetylcholine esterase activity and a decreased inhibition of HIV-1 were found in stored samples (254). -80 °C was shown to be better at stabilizing EVs than storage at 4 °C or -20 °C (252). It was also demonstrated that EV-samples benefit from the addition of cryoprotectants in the same way as other complex biological samples, such as proteins (255). Cryoprotecting agents are generally hydrophilic molecules that can promote the formation of amorphous rather than crystalline ice, thus reducing potential damage to EVs through ice crystals. Moreover, through the formation of hydrogen-bonds to macromolecules they can help stabilize their structure (256). Typical molecules employed in this role are amino acids, polymers, non-reducing sugars, sugar-alcohols and di-saccharides such as sucrose and trehalose (257). Trehalose was employed by Bosch et al. and greatly reduced the aggregation of EVs during frozen storage (255).

The main disadvantage of EV-storage at -80 °C are the expense of the required freezers and upholding the cold-chain. Especially the latter would be an important factor once EVs see broad use as therapeutics and EV-containing proprietary medicinal products become available. Thus, another storage-method would be desirable that can successfully preserve EVs at RT or 4 °C. For therapeutic proteins, the method of choice to stabilize them is storing them in the dry state (257). This can be achieved by lyophilisation or spray drying. While spray-drying of EVs has been proposed (256) and tested with OMVs for the production of vaccines (258), it has not been applied widely yet and the influence the spraying process has on the vesicles and their cargo needs to be evaluated. For lyophilisation on the other hand, there are already multiple examples that explored its applicability in EV-preservation.
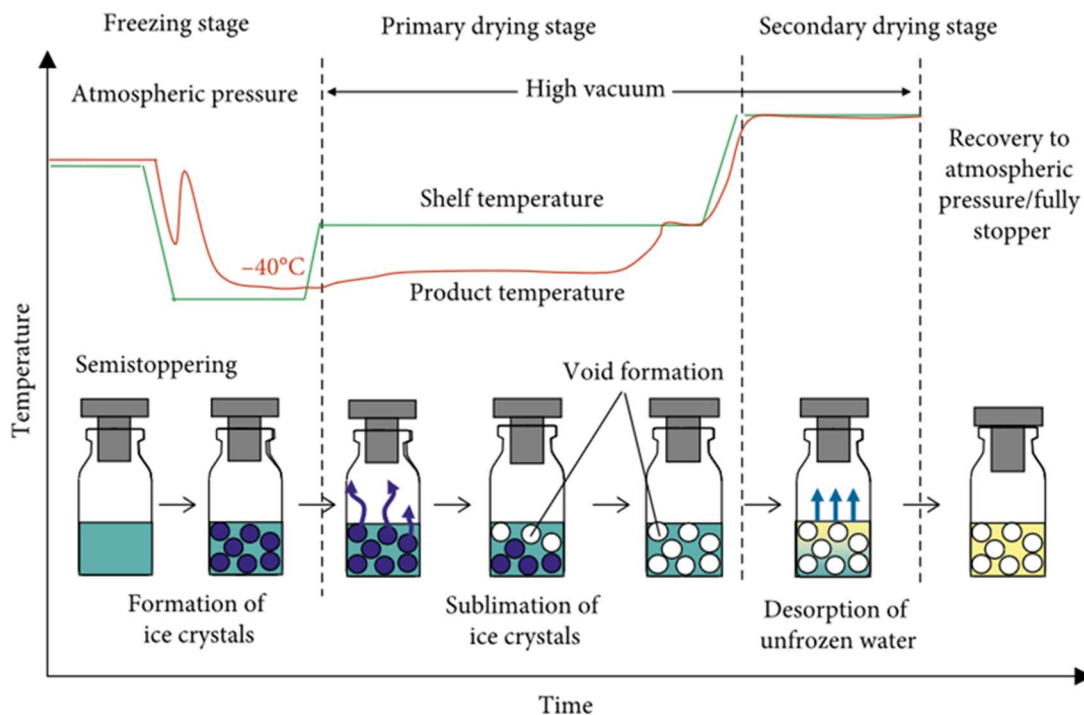
Figure 11: The process of lyophilisation has two main steps. First samples are frozen at low temperature at atmospheric pressure. Then, samples are dried under high vacuum. In the primary drying stage, samples are maintained at a low temperature while the ice sublimates. Then the shelf temperature is increased in the secondary drying stage to promote the desorption of water bound to the lyophilizates. Adapted from Kawasaki, H., et al. (2019). Journal of Chemistry 2019: 9502856. Used under the Creative Commons CC-BY 4.0 license.

In the process of lyophilisation or freeze-drying, samples are frozen and under low pressure the water contained in the sample is sublimated, leaving a dry solid (Figure 11) (257). The lyophilisation process can generally be divided into three parts, the freezing of the sample, the primary drying step that leads to the sublimation of ice and the secondary drying step, where the desorption of bound water takes place (259). As the removal of their hydration shell puts great strain on the conformation of biomolecules, excipients, so-called lyoprotectants, are needed to maintain the native structure of the dried molecules during and after lyophilisation (260). The most important lyoprotectants in practical application are the two disaccharides trehalose and sucrose, which also show cryoprotective properties (260). There are two main hypotheses that try to explain the effect of lyoprotectants during lyophilisation (261). One explanation is that lyoprotective agents can, through their multiple hydroxyl groups, replace the hydrogen bonds that would be lost by the removal of water. This keeps the native conformation of biomolecules as the thermodynamically more favorable state and thus prevents conformation-changes. The other hypothesis depends on the ability of lyoprotectants to form an amorphous solid that forms a rigid matrix for lyophilized biomolecules, which prevents their unfolding and other degradation processes that depend on molecular mobility.

It seems likely that both hypotheses play a role in the stability of lyophilized formulations, but further evaluations are needed to completely understand these processes (262).

El Baradie et al. and Charoenviriyakul et al. determined that EVs could indeed be lyophilized and stabilized by the addition of lyoprotectants such as trehalose and PVP (263, 264). A comprehensive assessment of different buffers, lyoprotectants and lyophilisation-conditions has not been performed so far and the long-term stability of lyophilized EVs has not been measured. Thus, one of the objectives of this study was optimizing the freeze-drying of EVs from various sources for their future application as therapeutics.

1.7. EV surface engineering and targeting

Decoration of the surface of EVs with new moieties is employed to achieve different goals (Figure 12). The most basic of which is fluorescent labeling of EVs to make it possible to follow their fate *in vitro* and *in vivo*. Covalent labeling of EVs by chemical or genetic means can circumvent some disadvantages of lipophilic dyes that are widely employed (265, 266). These lipophilic dyes penetrate into the lipid-membrane of the vesicles and are retained there. Their corresponding low solubility in aqueous media can however also lead to the formation of particles that are difficult to remove (267). Moreover, high concentrations of lipophilic dyes in EV-membranes can lead to quenching of fluorescence and thus the overestimation of EV-uptake into cells, once the dye is diluted in the recipient cell membrane and the fluorescent read-out increases (268). Finally lipophilic dyes can be transferred to other plasma membranes, where they may lead to false assumptions about EV-uptake and –distribution (269).

As mentioned above the structure of LPS on the surface of OMVs can be modified to reduce their toxicity and improve their applicability as vaccines (210). Intervening in the interaction of host cells and EVs is also the aim of PEGylation, which is widely used to increase the circulation time of synthetic nanoparticles by reducing their uptake by the reticulo-endothelial system (270). As EVs, despite their ability to transfer cargoes throughout the body, tend to rapidly accumulate in the liver and spleen after their administration (266), PEGylation could potentially help increase their circulation time. In this case however, the potential adverse effects of PEG also need to be thoroughly evaluated (271).
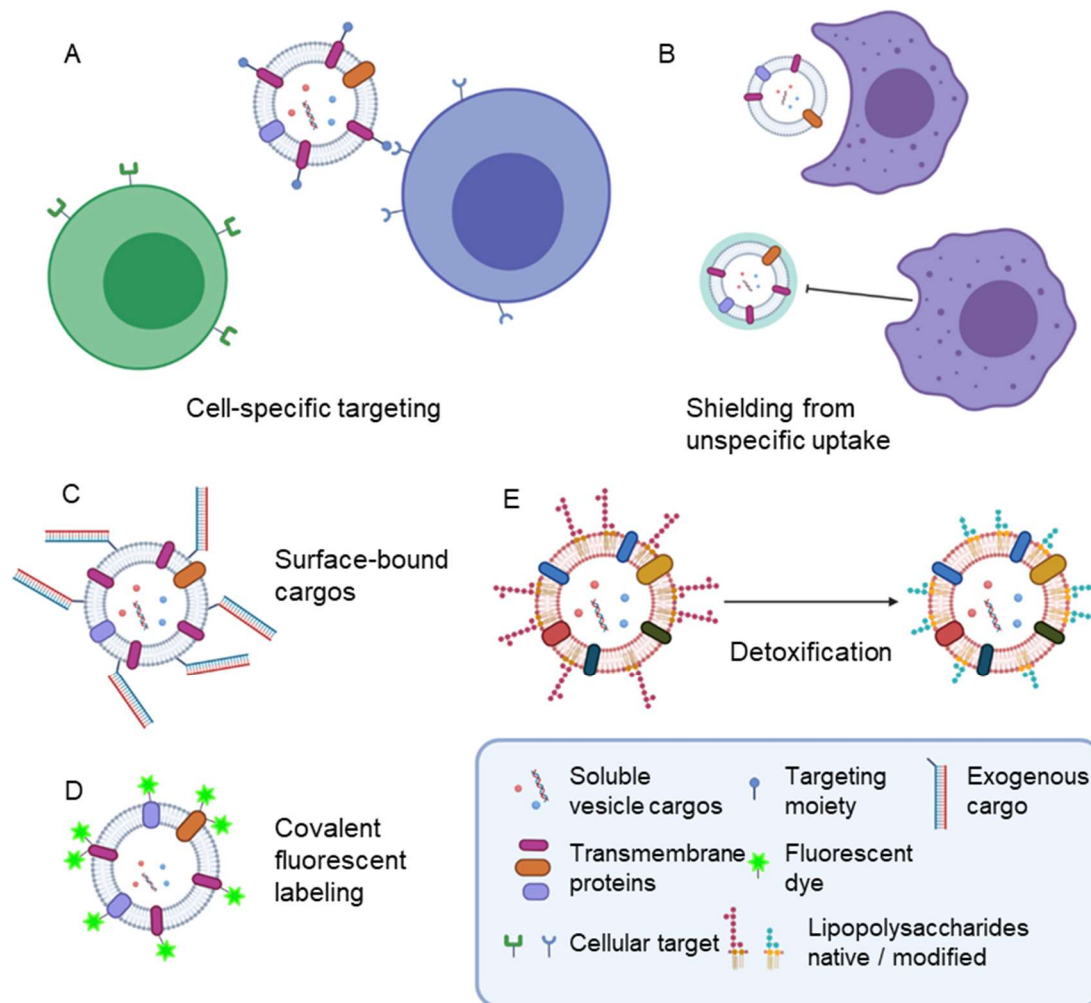
Figure 12: There are multiple aims of EV surface engineering. Cell-specific targeting and uptake can be promoted through surface-bound targeting moieties (A). Meanwhile shielding EVs from unspecific uptake by phagocytic cells could also be achieved through surface modification (B). For OMVs, an important step towards their clinical application is the modification of their lipopolysaccharides to reduce their toxicity (E). Finally, exogenous cargos (C) and fluorescent dyes (D) can be introduced by tethering them to the vesicle surface. This figure was adapted from Richter, Maximilian; Vader, Pieter; Fuhrmann, Gregor (2020). "Approaches to surface engineering of extracellular vesicles". Submitted to Advanced drug delivery reviews. The figure was partially prepared using Biorender.

The main aim of engineering the surface of EVs however is equipping them with targeting moieties to achieve their enrichment in the tissue of choice (272). While some studies have revealed specific tropisms of EVs depending on their origin (96, 266), a deeper understanding of the underlying mechanisms is missing for most EV-types and it is not a given that EVs would exist with natural high affinity to every target of interest. Additionally evidence that EVs would demonstrate any strong tropism after administration *in vivo* is thin, as some researchers reported little to no accumulation at the site of interest for native EVs (273, 274). Thus,

increasing the targeting-capabilities of EVs by introducing new moieties to their surface is of great interest.

1.7.1.   Targeting of pathogenic bacteria

One of the aims of this work is to produce OMVs with enhanced bacterial binding. There are diverse advantages to specifically targeting bacteria using antibacterial nanoparticles, also called nanoantibiotics. By efficiently delivering antibacterial agents to their intended target, higher concentrations can be reached, where they are needed, while off-target sites are less affected. This refers not only to human cells and tissues that would be less affected by adverse reactions such as the nephron- and ototoxic effects of vancomycin and aminoglycosides (275, 276), but also to the human microbiota. By ideally tailoring targeting of the nanoantibiotic selectively to pathogenic bacteria, common side effects that are linked to the unselective killing of bacteria, could be circumvented. While in some cases this can already partially be achieved by using local drug-administration at the site of infection, in many cases there is a natural and beneficial microbiome present that could be affected, e.g. on the skin (277) and in the lung (278). Direct delivery of antibiotics to the bacteria via nanoantibiotics can also help overcome resistance mechanisms by increasing the uptake and saturating efflux pumps (279).

While the field of nanoantibioitcs is expanding with a constant stream of new sophisticated strategies, focused especially on particles composed of various metals, such as gold, silver and copper (280), not much has been published regarding the active targeting of bacteria. This is possibly linked to the increased variability of bacteria compared to the cells of the human body. While research of antibacterial monoclonal antibodies is ongoing, so far there have been few examples of antibody-targeted antibacterial nanoparticles. Al-Sharqi et al. used a two step-method to selectively bind their photoactivatable silver-nanoparticles to *S. aure*us (281). Nanoparticles were decorated with a goat anti-mouse antibody that recognized mouse antibodies against protein A that were adsorbed to the bacterial surface. In another study, Kang et al. addressed intracellular bacteria using gadoliniumoxide-chrome-nanoparticles loaded with tigecyclin and decorated with antibodies against the ICAM1-receptor of endothelial cells (282).

Most approaches for active targeting of bacterial infections however have been conducted using small molecules. These bind to surface-features of bacteria or help the particles reach intracellular bacteria. The most popular example so far has been the glycopeptide antibiotic vancomycin. Its ability to strongly bind to the cell-wall of gram-positive bacteria (283) has been successfully employed in several publications. In a first application, Gu et al. modified gold nanoparticles with vancomycin that, through multivalency, successfully bound vancomycin resistant enterococci and inhibited their growth (284). Surprisingly the same effect was observed for the gram-negative bacterium *E. coli* that is highly resistant to treatment using monovalent vancomycin.
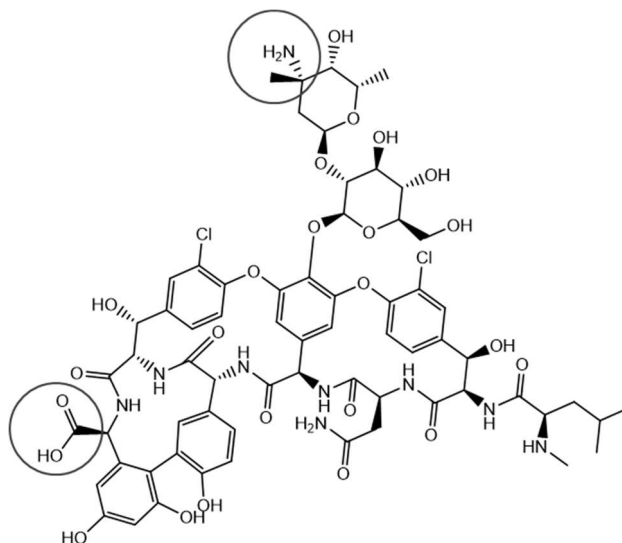
Figure 13: The structure of vancomycin contains a carboxylic acid and amino function (highlighted in circles). Both have been employed for tethering of vancomycin to nanoparticles.

In an interesting approach, Kell et al. modified magnetic nanoparticles with vancomycin and used them for the magnetic isolation of various bacteria from solutions (285). They also evaluated the influence of the architecture of vancomycin on the particles (286). The vancomycin molecule possesses two distinct functional groups that can be easily addressed, and lead to two different conformations of the vancomycin molecules on the nanoparticle surface (Figure 13). The amine can be modified using activated esters and the carboxylic acid can be activated and subsequently coupled to an amine. The latter however holds the caveat that cross-reactivity with the amino groups of other vancomycin molecules is possible. This could lead to the dimerization of vancomycin, which could potentially even increase its binding activity (287, 288) and thus lead to artificially inflated binding of the respective nanoparticles.

In their study, Kell and coworkers found out that linking vancomycin using the carboxylic acid led to a higher capture efficiency compared to the amino group, especially also for gram-negative bacteria, in line with the earlier findings of Gu et al.. They however do not comment on the issues described above and thus it remains unclear, to what extend di- or oligomerization of vancomycin played a role in their results (286).

In more recent publications, vancomycin has acted as the targeting moiety for micelles with lipase-triggered release of ciprofloxacin (289), fluorescent polymeric nanoparticles for in-vivo imaging of infection with *S. aureus* (290) and photoactivatable polypyrrole nanoparticles for the photothermal killing of *S. aureus* (291).

Another class of small molecules that hold great promise for bacterial targeting are short peptides with high binding affinity to bacterial surface epitopes. Through phage-display Hussian et al. developed a cyclic 9-amino acid peptide that, through specific targeting of *S. aureus,* could increase the antibacterial efficacy of their drug-loaded nanoparticles (292).

An alternative approach that is directed at bacteria that persist inside macrophages to escape the immune system and antibiotic therapy is functionalization with mannose. Mannose receptors on the surface of macrophages lead to the uptake of mannosylated particles that thus can reach intracellular bacteria (293). To this end, Xiong and coworkers developed a mannose presenting nanogel that, once taken up, gets degraded by bacteria present in the macrophages to set free its vancomycin-cargo (294). Mannose functionalization has also been realized for EVs to increase uptake into dendritic cells, albeit not with the prospect of antibacterial therapy (295).

Due to the success of vancomycin as a targeting moiety for antibacterial drug delivery and its straightforward chemical modification, it was chosen as a model targeting ligand to be introduced to OMVs by chemical surface engineering.

1.8.   Pre-isolation surface-engineering of EVs

Pre-isolation surface engineering of EVs is performed by manipulation of the parent cell to obtain modified EVs. This can be achieved either by genetic engineering, by metabolic labeling or by directly labeling the membrane of the parent cell (Figure 14 A-C).
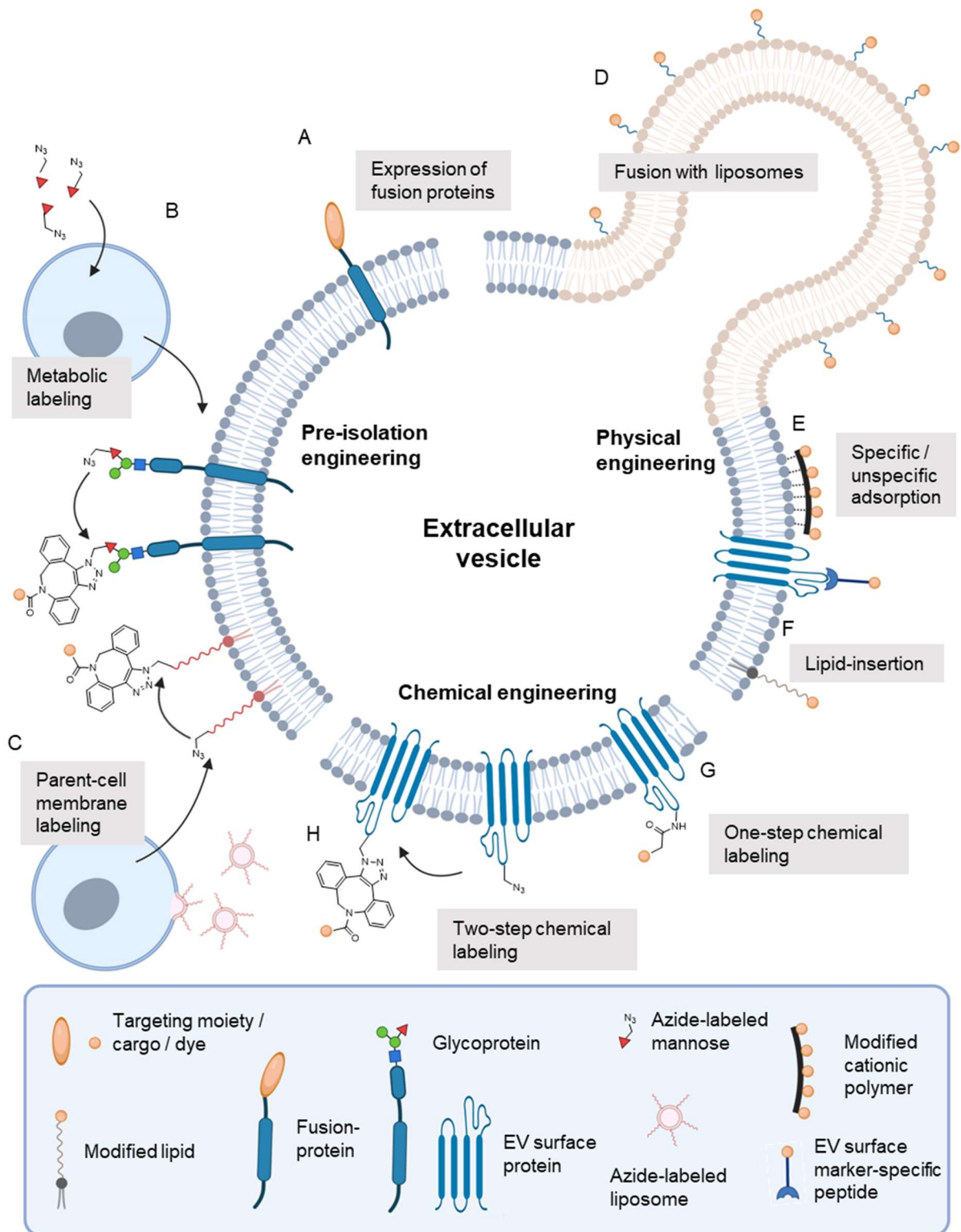
Figure 14: Surface modification of EVs can take place either before or after their isolation. The latter can be achieved by physical or chemical means. The most prominent method for pre-isolation engineering is the expression of fusion proteins of integral EV-surface-proteins and the protein of interest (A). Alternatively, azide-labeled EVs for subsequent chemical labeling can be generated through feeding the parent cells with azide-labeled sugars or amino acids (metabolic labeling, B) or fusing them with azide-labeled liposomes (parent-cell membrane labeling, C). Physical methods for EV surface engineering encompass fusing them with

liposomes D, specifically or unspecifically adsorbing molecules to their surface (E) or inserting modified lipids into their membrane (F). Chemical engineering approaches can take place in one step for simple molecules lacking functional groups with cross-reactivity (G). More complex molecules benefit from a two-step approach, were in the first step azide groups are introduced to the EV-surface, which subsequently are coupled to the molecules of interest in bioorthogonal reactions (F). This figure was adapted from Richter, Maximilian; Vader, Pieter; Fuhrmann, Gregor (2020). "Approaches to surface engineering of extracellular vesicles". Submitted to Advanced drug delivery reviews. The figure was partially prepared using Biorender.

1.8.1. Genetic engineering

The generation of modified EVs through genetic engineering is by far the best-characterized method for EV surface modification. Through the expression of fusion proteins of the transmembrane domains of known EV surface-proteins coupled with the epitope of interest, a wide variety of different targeting moieties have been expressed on the vesicle-surface.

In one of the first examples of endowing EVs with targeting moieties through genetic modification, the rabies viral glycoprotein (RVG) was expressed on the surface of EVs through fusion with Lysosome-associated membrane protein 2 (Lamp2b) derived from immature murine dendritic cells (Figure 15) (232). This protein has previously been shown to mediate the uptake of RVG-modified siRNA into the central nervous system of mice (296). Alvarez et al. encapsulated various siRNAs into the RVG-EVs and could prove that the use of targeted EVs significantly increased gene-silencing in the central nervous system after systemic injection (232). These results could later be replicated by Liu et al. and Yang et al., who used RVG-targeted EVs to convey neuroprotection after stroke (297) and counteract morphine relapse respectively (298). In another example fusion with the tetraspanin CD63 was used to label EVs with green and red fluorescent
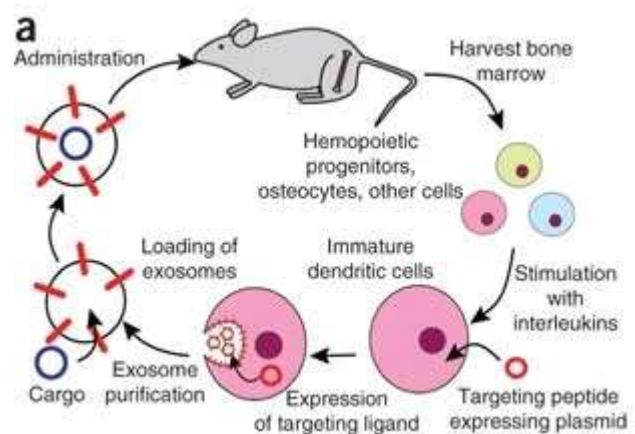
Figure 15: Genetic engineering was used to produce EVs targeted to the brain of mice. Bone marrow was harvested from mice and the cells were differentiated to immature dendritic cells. These cells were transfected with a plasmid expressing a fusion peptide of rabies viral glycoprotein, which promotes targeting, and Lysosome-associated membrane protein 2 (Lamp2b), which mediates transfer to the EV-membrane. After their isolation, vesicles were loaded with a siRNA and administered to mice. Adapted by permission of Springer Nature Customer Service Centre GmbH from Alvarez-Erviti, L., et al. (2011). "Delivery of siRNA to the mouse brain by systemic injection of targeted exosomes", Nat Biotech 29(4): 341-345.

protein (299). The Her2 receptor that is overexpressed in certain types of breast cancer has been the target of a study exploring the delivery of siRNA using OMVs derived from *E. coli* (300). Utilizing these engineered OMVs Gujrati et al. delivered siRNA to xenograft mouse models, effectively reducing tumor-growth. Besides targeting, genetic modification of parent cells can be employed to display antigens on the surface of EVs. For mammalian EVs, fusion with the C1C2 domain of lactadherin was used to generate EVs decorated with tumor-antigens to elicit a tumor-specific immune response (301, 302). Cytolysin A on the surface of E. coli OMVs was also used for antigen-display to protect mice from *A. baumannii* and influenza infections respectively (303, 304).

Instead of displaying new moieties on the vesicle-surface, genetic engineering can also be used to alter the molecules that are naturally present on EVs. This is an important strategy in the development of OMV-based therapeutics, as LPS on the vesicle surface can lead to strong inflammatory responses in parenteral application (103) and the application of OMVs has been hindered by its presence (210). Thus, efforts have been made to remove LPS or reduce its toxicity. In a prove of concept study, Kim et al. generated an E. coli strain that produced LPS of reduced toxicity and expressed a model-peptide on the surface of its OMVs (305). In another study, antigens from *Mycobacterium tuberculosis* and *Chlamydia trachomatis* were successfully expressed on the surface on OMVs derived from *E. coli* and *S. enterica* serovar Typhimurium (306). The native immunogenicity of these detoxified OMVs also makes them useful as adjuvants (210), for example to improve the efficacy of a vaccine against influenza (212).

In general, genetic engineering of parent cells is a very powerful technique, but it completely depends on a good understanding of vesicle surface-proteins. While EVs derived from mammalian cells have been thoroughly evaluated in this regard, knowledge is lacking for EVs of other provenance and in. Thus, especially in case of bacterial vesicles, where the vesicles from only a few species have been characterized well enough to allow for their surface modification by genetic engineering (307-311), more research is needed. Thus, instead of genetic manipulation, the development of a general method to engineer OMVs after their isolation was the central subject of this work.

1.8.2. Other methods for pre-isolation surface engineering

Two very similar methods to obtain already modified EVs from cells are metabolic labeling and the enrichment of modified lipids in the membrane of parent cells.

In metabolic labeling, azide-analogues of natural nutrients such as sugars and amino acids are added to the culture medium. They are taken up by cells and incorporated into

biomolecules. Stochastically some of these molecules will be present on the surface of EVs produced by the cells, where they are accessible to chemical reactions after EV-isolation (see 1.9.2). Lee et al. explored the applicability of different azido-sugar derivatives for fluorescent labeling of EVs and determined that the azide-labeled mannose derivate led to the best surface-availability of azide groups (312). The same azido mannose derivative was also used earlier by Wang et al. (313). They could also show that azido homoalanine can be employed in the same way.

Azide groups can also be introduced to the surface of parent cells by fusing them with fusogenic liposomes that contain azide-labeled phospholipids (314). Shedding of azide-lipids as part of EVs thus works similarly to metabolic labeling and presents the opportunity for downstream chemical modification.

1.9. Post-isolation surface engineering of EVs

Post isolation surface engineering can be achieved either by direct chemical labeling of the vesicle surface or by physical interactions with surface features of EVs or their lipid membrane (Figure 14 D-H).

The main disadvantage of modifying EVs after their isolation, compared to genetic engineering, is the reduced control over the extent and the site of modification. This could affect the efficiency of such approaches and potentially negatively influence vesicle-activity. Moreover, incubation and or reaction conditions might have adverse effects on vesicle integrity and the removal of non-incorporated material requires the use of a suitable method for purification that leaves the vesicles intact while guaranteeing their purity. There are however also advantages that make the exploration of post-isolation surface engineering of EVs a worthwhile pursuit. In contrast to genetic engineering, where researchers are limited to peptides, post-isolation modification allows displaying all kinds of molecules such as fluorescent dyes and small synthetic molecules on the vesicle surface, but also larger molecules such as aptamers (315, 316). As no engineering of the parent cell is required, the methods described in the following chapters can also be employed to engineer autologous EVs derived from a patient's plasma or harvested cells, circumventing possible adverse effects due to the administration of exogenous EVs. Without the requirement of extensive knowledge of surface proteins of the EVs to be modified, post-isolation modification can also be employed in cases where knowledge about suitable targets for the generation of fusion proteins is sparse. This is especially important in the field of OMV-research. The surface proteins of bacterial vesicles can vary by species and strain (317) and proteomic analysis of OMVs derived from the myxobacteria employed in this work has not been carried out yet.

1.9.1. Physical modification of EVs
1.9.1.1. Fusion with liposomes

Liposomes have been extensively studied and their easy and reproducible production and drug loading are big advantages for their use in EV-modification. Moreover, förster resonance energy transfer (FRET) based assays to study the fusion of liposomes are already established (318). These assays are based on the presence of two lipophilic dyes in the liposome membrane that form a FRET-pair (Figure 16). Once the liposome fuses with another phospholipid membrane, its lipids and the lipophilic dye are diluted in the membrane of the newly formed hybrid particle reducing the FRET effect. However, for FRET to give reliable information about the actual full fusion of the particles, hemifusion, i.e. interaction of only the outer leaflet of the lipid bilayers, needs to be precluded, as it does not necessarily lead to full fusion (319, 320). To only assess full fusion, one of the FRET-partners in the outer leaflet can be inactivated by oxidation, to assess only mixing of the inner leaflet, which does not occur by hemifusion (321). Alternatively the mixing of encapsulated contents in the respective particle-populations can be assessed (322). With suitable assays to quantify the fusion of liposomes and EVs, two main questions remain how to achieve the fusion of EVs and liposomes and how to remove non-fused liposomes and ideally EVs from the mixture.

So far, few studies have examined the fusion of EVs with liposomes using different approaches. Sato et al. evaluated the fusion of EVs derived from two cell lines with liposomes of differing compositions (323). To achieve fusion, they subjected mixtures of EVs and liposomes to ten cycles of freeze thawing, however without differentiation of hemifusion and full fusion. The results of Sato et al. regarding cell-uptake of their hybrid EVs are in disagreement to established knowledge, e.g. cationic lipids decreasing uptake instead of increasing it and PEGylation increasing uptake instead of decreasing it. Moreover they did not address the removal of non-fused particles and stress of freezing and thawing of EVs might have a big impact on EV-integrity and thus would better be avoided (224).
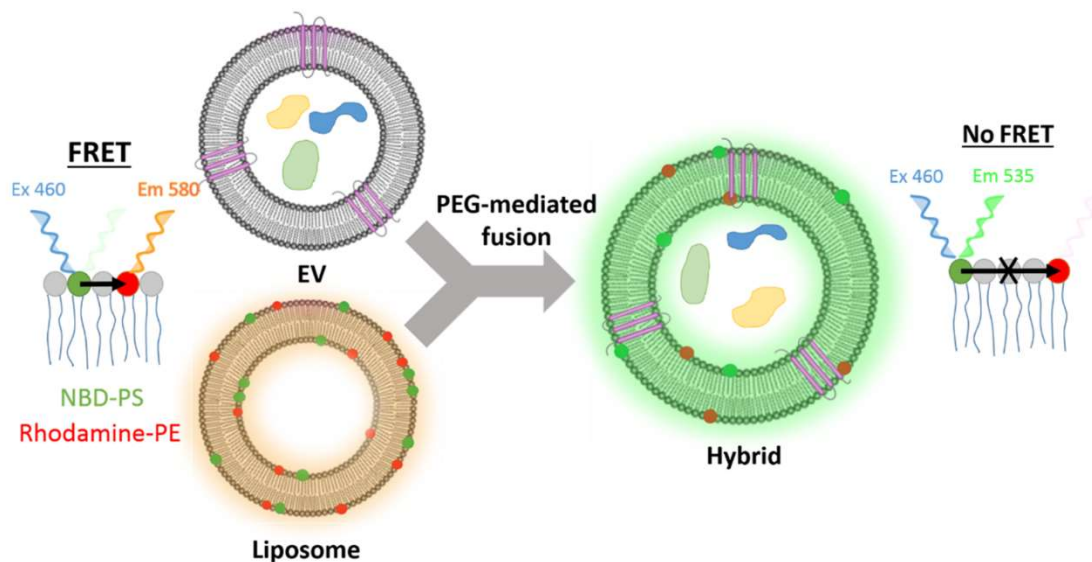
Figure 16: The PEG-mediated fusion of EVs and liposomes can be monitored using FRET. To this end, liposomes were labeled with NBD-PS, which is excited at 460 nm and emits light at 535 nm, and rhodamine-PE, which is excited at 535 nm and emits light at 580 nm. When native liposomes were excited at 460 nm, due to FRET, only the emission of rhodamine at 580 nm was visible. Once liposomes and EVs had fused and the dyes were diluted, the fluorescence of NBD became visible. Adapted with permission from Piffoux, M., et al. (2018). "Modification of Extracellular Vesicles by Fusion with Liposomes for the Design of Personalized Biogenic Drug Delivery Systems", ACS Nano 12(7): 6830-6842. Copyright (2018) American Chemical Society.

Piffoux et al. used another approach to achieve fusion with less implications for EV-integrity and also demonstrated the removal of unfused liposomes (320). Their method was based on the co-incubation of EVs and liposomes with PEG8000, which mediated the formation of hybrid particles (Figure 16). To prove that PEG8000 led to full fusion of EVs and liposomes, they used the oxidation-based method described above. Non-fused liposomes were removed by gradient UC. With their method, they achieved a fusion of up to 62% of added liposomes with EVs and the PEGylated hybrid particles they created showed a greatly decreased uptake into cells. They also assessed the fate of liposome- and EV-cargoes upon fusion and showed that there was no leakage of native EV cargoes, while liposome cargoes were efficiently carried over into the newly formed hybrid particles. Thus, the simultaneous surface modification and drug-loading of EVs could be achieved.

While PEG-mediated fusion with liposomes has great potential for the engineering of mammalian cell derived EVs, it is unclear as of yet, whether this technique would also work with OMVs, as the presence of LPS on the OMV surface might hinder the effect of PEG.

1.9.1.2. Lipid insertion into the EV-membrane

The phospholipid bilayer of EVs also plays an important role in methods based on the insertion of phospholipids or cholesterol into their membrane. Phospholipid- and cholesterol-post-insertion are two established methods for the post-production modification of liposomes (324, 325). In the development of liposomal formulations, these techniques are employed, when the molecule of choice would be sensitive to the organic solvents employed in the conventional production of liposomes. In EV-research, they can be used for the post-isolation surface modification of EVs.

Phospholipid- or cholesterol-labeled hydrophilic molecules can insert into target membranes upon co-incubation, but they differ in the incubation temperature needed to achieve efficient insertion. Phospholipid insertion is typically taking place at 60 °C, while cholesterol insertion already can take place at 17 °C, depending on the inserting molecule (326). While the temperature requirement of the latter variant is more suitable for EV-engineering, both methods have been employed to produce modified vesicles.

Extracellular vesicles
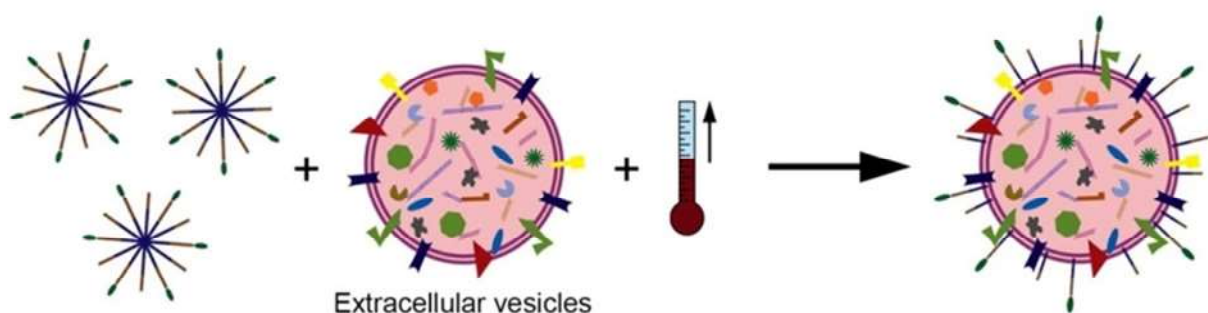
Figure 17: Co-incubation of micelles containing the lipids of choice and EVs under increased temperature leads to the insertion of these lipids into the EV membrane. Adapted with permission from Elsevier from Kooijmans, S. A. A., et al. (2016). "PEGylated and targeted extracellular vesicles display enhanced cell specificity and circulation time", Journal of Controlled Release 224: 77-85.

Phospholipid-post-insertion was employed for the PEGylation and introduction of a targeting moiety to EVs by insertion of lipids modified with PEG and an EGFR-binding nanobody (Figure 17) (327). As expected insertion at 60 °C, while most effective in terms of the amount of inserted molecules, led to damaging of the vesicles reducing their activity in *in vitro* assays. The authors determined that 40 °C was better suited for EVs, balancing insertion efficiency and vesicle-stability. Targeting of EVs with the nanobody was successful *in vitro*, *in vivo* however, only an increased circulation time of EVs was visible with no measurable targeting of EGFR-expressing cells. Choi et al. also used lipid post-insertion to generate mannose-functionalized EVs (295). They incubated their vesicles for 3 h at 37 °C and found that insertion was proportional to the number of phospholipid-PEG-mannose molecules per EV. In *in vivo*

experiments, they could show a higher accumulation of their mannose-targeted EVs in lymph nodes close to the injection site compared to native EVs.

Cholesterol insertion has so far not been used to equip EVs with targeting moieties. Instead, it was employed to load EVs with a cargo of cholesteryl-modified siRNA. Three groups have used this approach to deliver siRNA to silence the cancer-related human antigen R (228), the huntingtin gene (229) and CD45 or eGFP (230). The optimization of cholesterol-post-insertion was exhaustively evaluated by O'Loughlin and coworkers, who got some important insights into the optimization this method. They optimized the incubation-time, -temperature and -volume and determined that 1 h at 37 °C in a volume of 100 µl would lead to the best results. They also looked at the insertion efficiency as a function of the ratio of cholesteryl-siRNA molecules to EVs. A lower ratio led to a higher encapsulation efficiency, while increasing the ratio decreased the percentage of inserted siRNA. The amount of inserted molecules per EV however increased. Thus, the ratio of vesicle and cholesteryl-modified molecule depends on the aim of the study. In case of O'Loughlin and coworkers, the aim was to achieve a high encapsulation efficiency of the expensive modified siRNA, while the natural targeting ability of EVs was used to deliver the molecule to its target, thus they used a very low ratio. A high ratio could be employed, if the foremost aim was achieving the insertion of as many molecules per particle, for example to produce targeted EVs.

Both lipid- and cholesterol-post-insertion have the disadvantage that inserted molecules can potentially leak from the vesicle membrane in the presence of acceptor membranes and serum proteins (326, 328). Especially cholesterol-anchored molecules might easily dissociate from the vesicles, which makes the throughout evaluation of insertion stability a crucial step in developing methods for EV surface engineering by post-insertion techniques. Nonetheless, the simple experimental conditions and molecules employed for cholesterol post-insertion prompted its investigation as a method for the surface engineering of myxobacterial OMVs.

1.9.1.3. Adsorption to the EV-surface

Adsorption to the surface of EVs can either be multivalent and rely on the general negative surface charge of EVs or highly specific and tailored to EV surface markers.

Sawada et al. modified EVs by adsorbing an amphiphilic cationic nanogel to their surface, to increase their uptake in recipient cells (329). In another example, cationized pullulan was adsorbed to EVs , which led to their selective uptake into liver cells both *in vitro* and *in vivo* (330).

Specific interaction with the tetraspanin CD63, which is a typical surface marker of EVs (49), was employed by Gao and coworkers (331). They coupled a morpholino oligomer with activity

against Duchenne muscle dystrophy and a muscle-targeting peptide to a short peptide with high binding affinity to CD63. EVs modified with these molecules displayed efficient muscle targeting and showed activity *in vivo* in a muscle dystrophy mouse model.

1.9.2. Chemical modification of EVs

In general, the approach for the chemical surface-modification of EVs depends on the complexity of the introduced molecules. For simple molecules such as fluorescent dyes or PEG-derivatives (295), without functional groups that could lead to side-reactions, one-step-processes often suffice. Here functional groups present on the EV-surface are targeted. The most accessible of these are amino groups, found in lysine side-chains and N-termini of EV-surface-proteins (332, 333). These amines can be coupled with carboxylic acids to form a stable amide-bond. The most practical variant is using an activated ester such as N-hydroxysuccinimide (NHS) or its sulfonated analogue, as this strategy allows for the preparation of the ligand in advance. Moreover, in many cases NHS esters of dyes and PEG-derivatives are commercially available. However, this approach only works, as long as the molecule to be installed on the EV-surface contains no amines itself. Otherwise side products consisting of di- or oligomers might be formed. This reduces the amount of available molecules for the reaction with EVs and may also lead to vesicles modified with a heterologous mixture of molecules, with potentially reduced activity.

In these cases, a two-step-process is needed. In the first step, a suitable functional group is installed on the EV-surface. This can be done through NHS esters, but also, as described above through metabolic labeling or through physical processes, e.g. lipid-insertion as described by Di et al. (334). Another method to achieve this -using diazotransfer- is one of the subjects of this work. In the second step, this group is then coupled to the molecule to be displayed on the vesicles. To work well in this set-up, the reaction performed in the second step must fulfill certain requirements. It must be orthogonal to the functional groups encountered in both the EVs and the ligand. It should work under tolerable conditions for the vesicle, in the best case under physiological conditions without the addition of organic solvents. Moreover, as EV-concentrations are oftentimes low and the ligands used expensive, the reaction should work well also in diluted solutions. Finally fast kinetics are desirable, to limit the exposure of EVs to potentially detrimental conditions and to streamline the process of EV-modification. All these requirements are satisfied very well by reactions subsumed under the term "click-chemistry" that is discussed in detail in the following chapter.

1.9.2.1. Click-chemistry and bioorthogonal chemistry

The term "click-chemistry" was devised by Sharpless and coworkers in 2001 (335). Per its definition it refers to reactions that can me modularly employed to generate a wide variety of compounds with high yields and fast kinetics from simple starting materials (335). These reactions should ideally work in water or without the addition of solvents and only generate unproblematic byproducts (335). While they describe multiple reaction types in their paper that fulfill click-chemistry-criteria, the term click-chemistry has become almost synonymous with the copper-catalyzed Huisgen-type [2+3] alkyne-azide cycloaddition (CuAAC, Figure 18), published independently by two groups in 2002 (336, 337). The reaction is often referred to as "copper-catalyzed click-chemistry". Indeed, CuAAC is one of the quintessential click-reactions. It works very well in aqueous media, with fast kinetics, stereoselectivity and little unspecific side-reactions. The mechanism of this reaction was elucidated by Worrell et al. who determined that different from earlier assumptions, two chemically equivalent copper-ions take part in the reaction (338). The copper(I)-ions required for CuAAC are typically generated *in situ* through reduction of copper(II) by ascorbic acid. Copper(I) however is unstable and prone to generate reactive oxygen species that can damage biomolecules (339). Thus, it needs to be stabilized by ligands (340). Especially ligands based on tris(triazolmethyl)amine are popular as their solubility can be tuned through the substitution of the triazoles and they increase the reaction rate (332).
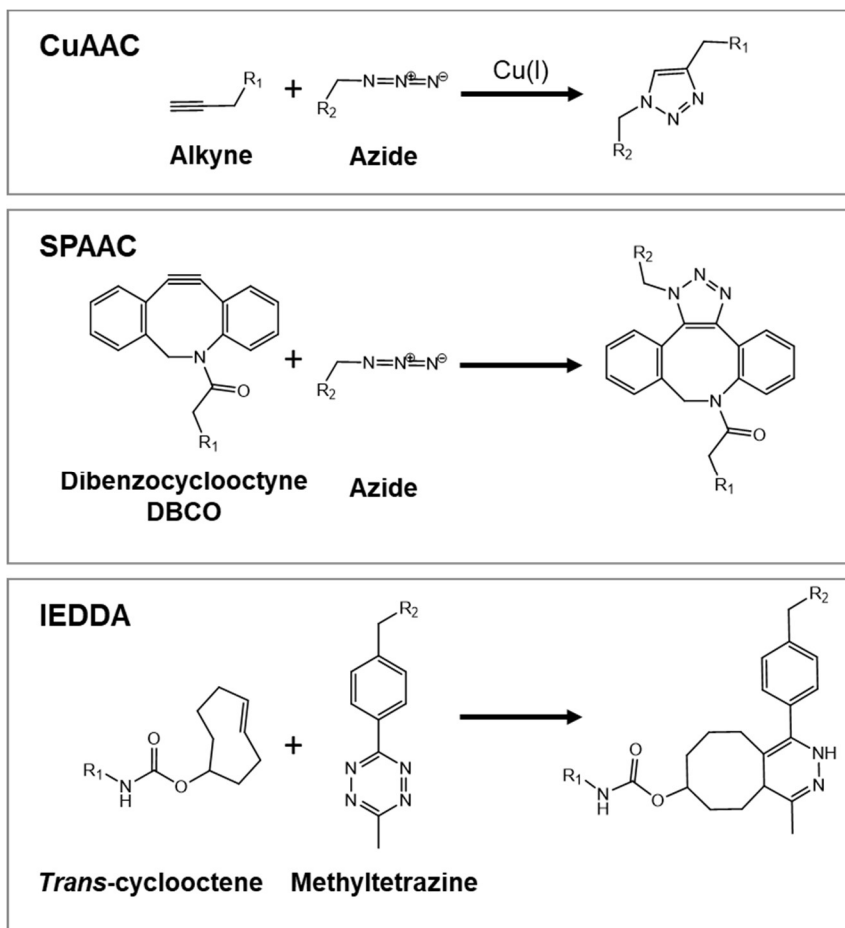
Figure 18: This figure shows examples of the click-chemistry reactions employed in this work. In CuAAC, a terminal alkyne and an azide form a triazole under catalysis by Cu(I). A catalyzer can be omitted in SPAAC, were the alkyne is incorporated into a strained cyclooctane ring, e.g. into dibenzocyclooctyne (DBCO). In inverse electron-demand Diels-Alder reactions (IEDDA), tetrazines, e.g. methyltetrazine, react with suitable dienophiles, such as trans-cyclooctene.

In 2004 Carolyn Bertozzi and coworkers presented a modified version of the [2+3] alkyne-azide cycloaddition that did away with the copper-catalyst by incorporating the alkyne group into a strained cyclooctane ring (341), based on earlier findings of Wittig and Krebs (342). While this strain-promoted alkyne-azide-cycloaddition (SPAAC, Figure 18), loses its stereoselectivity and has slower kinetics than CuAAC, it is still fast and selective and the absence of a toxic catalyst make it more benign for application in biological systems (341). While the initially synthesized cyclooctyne-derivatives had slow reaction kinetics with azide, they were improved by the introduction of electron-withdrawing fluorine atoms next to the alkyne (343) and by increasing the ring-strain through the addition of two aryl rings to the cyclooctyne and the introduction of an endo- or exocyclic amide (344, 345).

Even faster kinetics than in CuAAC can be reached in inverse electron-demand Diels-Alder reactions (IEDDA, Figure 18) between 1,2,4,5-tetrazines and strained alkenes or alkynes. Here the fastest variants approach the rate constant of enzyme-catalyzed reactions (346).

Thalhammer et al. evaluated the reactions of varying dienophiles with tetrazines and in some cases found very fast kinetics, especially for *trans*-cyclooctene (TCO) (347). Blackman et al. later adapted this reaction for the modification of biomolecules in aqueous media (348) and since then IEDDA has been intensely investigated and found wide application (332, 349). Both the tetrazine as well as the dienophile can be tuned in regards to reactivity and stability. The highest reaction rates are reached with TCO-derivatives (350) and monophenyl-substituted tetrazines (351).

Besides organic synthesis, were especially CuAAC is a versatile tool, click-chemistry reactions are quintessential tools of bioorthogonal chemistry (346). Bioorthogonal chemistry strives to achieve the selective labeling of biomolecules by employing reactants that show no cross-reactivity with the functional groups encountered in biological systems (332, 352). With their fast kinetics in aqueous media and the absence of a toxic catalyst, both SPAAC and IEDDA are ideal for the modification of biomolecules. Azide-groups are quite inert *in vivo* and can be introduced to biomolecules both chemically using e.g. activated esters (332) or diazotransfer (see 0) as well as through metabolic labeling (353, 354) and genetic code expansion (355). Using this approach, Chang et al. successfully labeled azido-sugars in living mice with a model peptide (354). SPAAC has however some limitations for *in vivo* application as the strained alkynes employed in these reactions show some reactivity towards nucleophiles encountered in the lumen of cells (356, 357). This issue is not present for IEDDA reactions that exhibit high selectivity in *in vivo* conditions (349). IEDDA has been employed for intracellular fluorescent labeling, for example for super-resolution imaging of actin filaments (358) and its high selectivity and fast reaction rate even at very low concentrations make it ideally suited for pretargeting (349, 359). Pretargeting is mainly utilized in targeted radionuclide-therapy and -imaging. First, a TCO-labeled antibody against a tumor-antigen is injected and allowed to bind, while unbound antibody is eliminated. Then the tetrazine-labeled radionuclide is injected and selectively accumulates at the target site through IEDDA reaction with the antibody. Thus, off-target-labeling and radiotoxicity can be significantly reduced (359). IEDDA and SPAAC or CuAAC can also be employed orthogonally to each other, for example for dual labeling of cells (360). To achieve this however the right cyclooctynes need to be chosen that do not show reactivity towards tetrazines. One such example is the dibenzocyclooctyne derivative (DBCO, Figure 18) developed by Kuzmin et al. (345), which was also employed in this work.

1.9.2.2. Diazotransfer

Besides their use in click-chemistry, azide groups also find application in organic synthesis. They can form protection groups for amines that can be removed under mild conditions, e.g. using the Staudinger reduction (361), they can be used to generate amides and carbamates (362) and they are utilized in pro-drug strategies (363). While azide groups can be introduced to biomolecules through reactions with azide-containing molecules, such as 2-azidoacetic acid, they can be also directly generated from primary amines using diazotransfer (Figure 19 B).

Figure 19: Triflyl azide and imidazole-1-sulfonyl azide (ISA) HCl are the most widely employed diazotransfer agents (A). Diazotransfer can, under basic conditions and with Cu(II) as a catalyzer, transform amino groups into azides (B).

In diazotransfer, the azide is generated by transfer of a diazo group from an azide-containing donor molecule (364). The main advantage of diazotransfer is that unlike approaches employing sodium azide as the nucleophile in a nucleophilic substitution reaction, the stereochemistry of the molecule is retained and no elimination products are formed (365). Pandiakumar and coworkers evaluated the mechanism of the diazotransfer reaction and determined that the amine attacks the terminal nitrogen of the azide group of the donor molecule, which leads to the formation of the azide-containing product and leaves one nitrogen attached to the donor molecule (364).

Diazotransfer was typically performed in organic media using triflyl azide (Figure 19 A) (366). While this method works well and has been widely applied, triflyl azide has several drawbacks. Trifluoromethanesulfonic anhydride is expensive and the triflyl azide has a poor shelf life. It can only be stored in solution and its reported explosiveness make its handling difficult (367). These disadvantages where addressed by Goddard-Borger and Stick, who developed imidazole-1-sulfonyl azide (ISA) HCl as a shelf-stable and cheap alternative to triflyl azide (Figure 19 A) (365). ISA HCl was successfully used to convert various amines into the respective azides and has also been applied by other researchers (365, 368, 369). In later studies it was discovered that ISA HCl was not as inert as initially assumed and the sulfate and mesylate salts of ISA were confirmed to be more stable and less prone to explosive decomposition (370). The discovery of van Dongen et al. that diazotransfer with ISA can also be performed in aqueous media (371), opened up its application in the modification of peptides and other biomolecules (372). Based on these results, diazotransfer with ISA was evaluated in this work as a method to generate azide-labeled OMVs (AzideOMVs) that could be subsequently modified using CuAAC and SPAAC.
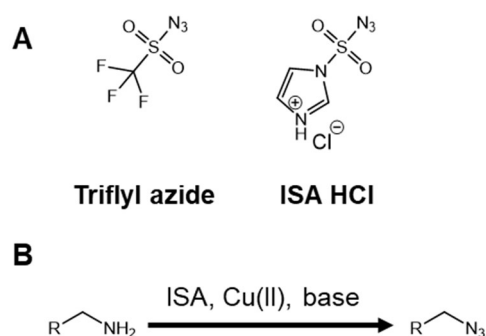
1.9.2.3. Examples of chemical surface modification

So far, only few publications have explored the chemical surface modification of EVs. Choi and coworkers employed a simple one-step process, using an NHS ester to introduce biotin-modified PEG to EVs derived from bovine serum albumin (295). While biotin was successfully introduced to the vesicles, they observed the formation of EV-aggregates, which was absent in their alternative approach, where biotin and mannose were introduced by phospholipid-post-insertion. In another study EVs derived from red blood cells were labeled with AlexaFluor 488 NHS ester to evaluate their association with Neuro2A cells and A431 cells after the introduction of targeting moieties by genetic engineering (373). Di et al. performed a two-step modification, by first introducing maleimide groups through lipid insertion that were subsequently coupled with either a fluorescent dye, magnetic nanoparticles or gold nanoparticles (334).
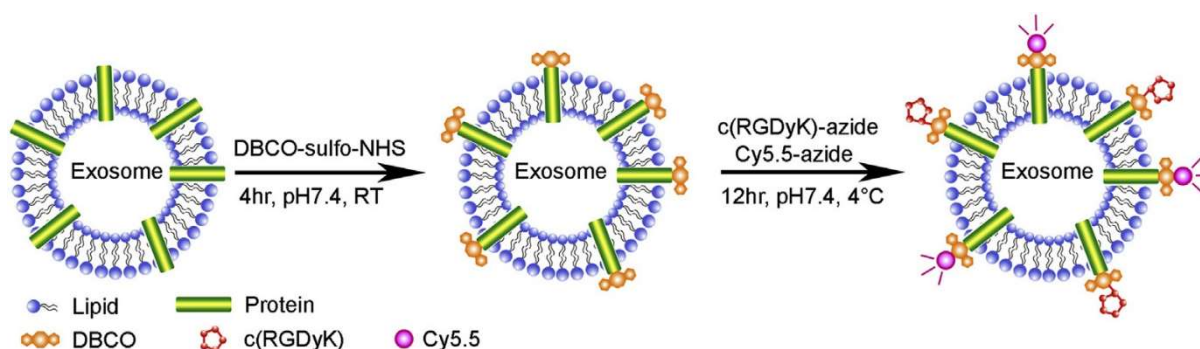
Figure 20: In this figure, a two-step approach to the chemical surface modification of EVs is demonstrated. First DBCO-groups are introduced to the vesicle surface through reaction with DBCO sulfo-NHS ester. These groups subsequently take part in a SPAAC reaction with an azide-modified c(RGDyK)-peptide to obtain targeted EVs. Adapted with permission from Elsevier from Tian, T., et al. (2018). "Surface functionalized exosomes as targeted drug delivery vehicles for cerebral ischemia therapy", Biomaterials 150: 137-149.

A two-step approach based on click-chemistry was first realized by Smyth and coworkers (333). First they introduced an alkyne to the EV-surface using pentinoic acid NHS ester, then using bathophenantroline as the copper-ligand, they introduced an azide-labeled fluorescent dye to the vesicles to track their uptake into cells. In their publication, they show that CuAAC did not have an impact on EV-size, however they do not comment on recovery rate of EVs after modification. SPAAC has been employed for the surface modification of EVs both after metabolic labeling and after reaction with a DBCO NHS ester. As detailed above, different azide-modified sugars and amino acids can be used to generate azide-labeled EVs by metabolic labeling (see 1.8.2). Wang et al. used the azide groups on their EVs to prepare biotinylated EVs by reaction with DBCO coupled biotin (313). These vesicles were subsequently further functionalized with streptavidin-Horseradish peroxidase. This allowed for

the intracellular delivery of this enzyme through EV-uptake by recipient cells. Tian et al. first modified their EVs using the sulfo-NHS ester of DBCO (Figure 20) (225). By using the sulfonated form of NHS, they greatly increased the solubility of the molecule, circumventing the issue of precipitation in aqueous media, caused by the lipophilicity of DBCO. In the next step, they introduced an azide-modified cyclic RGD-peptide to selectively target the EVs to ischemic lesions in the brain of mice. They also analyzed the degree of surface-modification by SPAAC using a fluorescent derivative of their peptide and estimated a modification with approx. 260 molecules per vesicle.

While chemical surface engineering of EVs has great potential for the introduction of targeting moieties to the vesicles, so far it has not been utilized extensively. Especially for myxobacterial OMVs, were surface-proteins suitable for the expression of fusion-proteins have not been identified yet, and for the targeting of bacteria, were typical targeting moieties cannot be easily expressed as proteins (see 1.7.1), chemical surface engineering could prove to be of high utility.

2. Materials

Chemicals

Chemical	Supplier	Chemical	Supplier
1,2 dimyristoyl-sn glycero-3-phospho-choline (DMPC)	Lipoid GmbH, De	Imidazole	Sigma-Aldrich, De
1,2-dipalmitoyl-sn-glycero-3-phospho-choline (DPPC)	Sigma-Aldrich, De	K-phosphate	VWR International, De
4 M HCL in dioxane	Alfa aesar, De	Maltose moonohydrate	MP Biomedicals SARL, FR
Acetonitrile, HPLC grade	Thermo Fisher Scientific, US	Methanol, HPLC grade	Thermo Fisher Scientific, US
Alkyne Af549	Jena Bioscience, De	Methyltetrazine NHS ester	Sigma-Aldrich, De
Azide-PEG$_3$-Cy5-PEG$_4$-amine	Broadpharm, US	Methyltetrazine-PEG$_4$-biotin	Broadpharm, US
Bacto Casitone	Becton, Dickinson, US	MgSO$_4$ (anhydrous)	Merck, De
Bacto Soytone	Becton, Dickinson, US	MgSO$_4$ heptahydrate	Sigma-Aldrich, De
BCA assay kit	Sigma-Aldrich, De	N2-Boc propargylglycine	VWR, De
Bovine serum albumin (BSA)	Sigma-Aldrich, De	Na-Phosphate	Sigma-Aldrich, De
CaCl$_2$ dihydrate	Sigma-Aldrich, De	Piperidine	Merck, De
Carboxylated polystyrene particle standards	CPC100 and CPC1000, Izon Science, UK	Poloxamer 188 (P188)	BASF, De
Cellobiose	MP Biomedicals SARL, FR	Polyvinylpyrrolidone (PVP)	Kollidon® 17 PF, BASF, De
Chloroform	Sigma-Aldrich, De	Potassium hydroxide	Thermo Fisher Scientific, US
Cholesterol PEG 2000 FITC	tebu-bio, De	Saponin	Sigma-Aldrich, De
COMU	Sigma-Aldrich, De	Sat. NaHCO$_3$ in H2O	prepared from NaHCO3 (VWR) and purified water
Copper(II) Sulfate Pentahydrate	Sigma-Aldrich, De	Sephadex G75	Sigma-Aldrich, De
D-(+)-Trehalose dihydrate	Sigma-Aldrich, De	Sepharose Cl-2b	Sigma-Aldrich, De
DBCO AF549	Jena Bioscience, De	Sodium azide	Sigma-Aldrich, De
deuterated chloroform	Sigma-Aldrich, De	Sodium hydroxide	Sigma-Aldrich, De
deuterated DMSO	Sigma-Aldrich, De	Sucrose	Sigma-Aldrich, De
DMSO, anhydrous	VWR, De	Sulfo-cyanine 5 NHS ester	Lumiprobe, De
Dioxane	Merck, De	Sulfo-cyanine 7 COOH	Lumiprobe, De
Disiopropyl ethylamine (DIPEA)	Sigma-Aldrich, De	Sulfo-cyanine 7 NHS ester	Lumiprobe, De
DMSO	Sigma-Aldrich, De	Sulfuryl chloride	Sigma-Aldrich, De
Ethanol	Thermo Fisher Scientific, US	TCO-PEG$_4$-DBCO	Broadpharm, US
Ethyl acetate	Sigma-Aldrich, De	TCO-PEG$_6$-amine	Broadpharm, US
Ethyl acetate, anhydrous	Sigma-Aldrich, De	TCO-PEG$_8$-amine	Broadpharm, US
Fluorescein di-β-D-glucuronide	Thermo Fisher Scientific, US	Triethylamine	Sigma-Aldrich, De
Fmoc propargylglycine	Sigma-Aldrich, De	Tris(3-hydroxypropyl-triazolmethylamine)	Sigma-Aldrich, De

Formic acid	Sigma-Aldrich, De	Triton X-100	Thermo Fisher Scientific, US
Glucose	Sigma-Aldrich, De	Trypsin/EDTA, 0,05%	Thermo Fisher Scientific, US
HEPES	Carl Roth, De	Vancomycin HCl	Sigma-Aldrich, De
Highly purified water	prepared using Milli-Q Reference, Merck, De	β-glucuronidase from *E. coli*	Sigma-Aldrich, De

Bacteria and cell lines

SBCy050 bacteria	Department of Microbial Natural Products, HIPS, Saarbrücken	RO cells (ACC452)	DSMZ, De
A549 (ATCC® CCL-185™)	ATCC, US	HUVEC cells	Lonza Verviers, S.p.r., Be

Cell culture media

EBM-2 medium	Lonza Verviers, S.p.r., Be	2SWC medium	- 0.5% Bacto Casitone - 0.1% Bacto Soytone - 0.2% glucose - 0.1% maltose monohydrate - 0.2% cellobiose - 0.05% CaCl2 dihydrate - 0.1% MgSO4 heptahydrate - 10 mM HEPES - adjusted to pH 7.0 with KOH
EGM-2 bullet kit	Lonza Verviers, S.p.r., Be		
Fetal bovine serum (FBS)	neoLab, De		
RPMI 1640 medium	Thermo Fisher Scientific, US		

Consumables

0.2 µm PES membrane syringe filter	VWR international, De	Igloo rubber stoppers	West pharmaceutical services, De
0.45 µM bottle top filter, polyvinylidene fluoride membrane	Steritop, Merck, De; Neolab De	Microcentrifuge Tubes, Polypropylene	Axygen, US
15 and 50 ml conical flasks	Greiner bio-one GmbH, De	NMR tubes	VWR, De
2R glass vials	Fiolax clear, Schott, De	Nucleopore 200 nm track-etch polycarbonate membranes	GE Healthcare, US
30 kDa regenerated cellulose membrane	Wyatt Technology Europe, De	Plastic pipette tips	Brand, De
Black 96 well plates	Greiner bio-one GmbH, De	Polycarbonate bottles for ultracentrifugation	Beckman Coulter, US
Clear 96 well plates	Greiner bio-one GmbH, De	Serological pipettes	Greiner bio-one GmbH, De
Cuvettes	Sarsted, De	T225 flasks	Corning Incorporated, Corning, US
ELISA Plate Sealers	R&D Systems, US	T75 flasks	Greiner bio-one GmbH, De
Filter support	Avanti Polar Lipids, US	0.2 µm pore size filter	Whatman, mixed cellulose, GE Healthcare, US
Glass pasteur pipettes	VWR, De		

Software

ChemDraw 17.1	PerkinElmer, US	NTA software	Nanosight-software version 3.1, Malvern Pananalytical, UK
Chromeleon 7	Dionex, US	Sigmaplot 14.0	Systat Software GmbH, De
Endnote X9	Clarivate, US	Topspin 4.0.9	Bruker, US
Microsoft Office 2016	Microsoft, US	Zen lite	Carl Zeiss Microscopy GmbH, De

Instruments

-80 °C freezer	Binder Ins., US	HRMS	Dionex Ultimate 3000 RSLC, Thermo Fisher Scientific, De
AF4 Automated fraction collector	Thermo Fisher Scientific, De	HRMS Column	Acquity UPLC® BEH C8, 150 x 2.1 mm, 1.7 µm column, Waters, De
AF4 Buffer filtration	Durapore Membrane filter, PVDF, 0,1 µm, 47 mm, Merck, DE	Incubator bacterial culture	Infors, CH
AF4 Column oven	Hitachi High-Technologies, Jap	Incubator cell culture	Binder Ins., US
AF4 Eclipse dualtec	Wyatt Technology Europe, De	Inductively coupled plasma mass spectrometry	Agilent ICP-MS 7500cx, Agilent, US
AF4 Light scattering detector	DAWN HELEOS II, Wyatt Technology Europe, De	LC/MS	Dionex UltiMate 3000. Thermo Fisher Scientific, De
AF4 PEEK Inline filter holder	Wyatt Technology Europe, De	LC/MS Column	Hypersil GOLD VANQUISh C18 UHPLC column, Thermo Fisher Scientific, De
AF4 Small channel	Wyatt Technology Europe, De	Light microscope	Carl Zeiss Microscopy GmbH, De
AF4 Spacer	350 µm spacer, Wyatt Technology Europe, De	Lyophilizer A549 and HUVEC EVs	ALPHA 2-4 LSC, Christ, De
AF4 Ultimate 3000 Dionex auto sampler	Thermo Fisher Scientific, De	Lyophilizer Ro EVs	FTS LyoStar^{TM} 3, SP Scientific, US
AF4 Ultimate 3000 Dionex isocratic pump	Thermo Fisher Scientific, De	Micropipettes	Brand, De
AF4 Ultimate 3000 Dionex online vacuum degasser	Thermo Fisher Scientific, De	NMR 1	Bruker Ascend II 500, Bruker, US
AF4 UV detector	Thermo Fisher Scientific	NMR 2	Bruker Ascend 700, Bruker, US
ÄKTA start	Cytiva, US	NTA	Nanosight LM14 equipped with a green laser, Malvern Pananalytical, UK
Cell counting	Casy® Model TT, Innovatis, De	Plate reader	Infinite 200Pro, Tecan, CH
Cell density meter	Biochrom, UK	PrepHPLC	Ultimate 3000 UHPLC+ focused, Thermo Fisher Scientific, De
Centrifuges	Rotina 420 R and Universal 320 R, Hettich, De	PrepHPLC Column	C18 column, 5 µm, Macherey-Nagel, De

Cryo-Tem holder	Gatan model 914, Gatan US	SEC columns	Kimble flex columns, Kimble, US
ESI Orbitrap LC-MS/MS system	Q Exactive Focus mass spectrometer, Thermo Fisher Scientific, De	Slide-A-Lyzer^{TM} MINI dialysis device	Thermo Fisher Scientific, De
ESI Quadrupole MS	MSQ Plus, Thermo Fisher Scientific, De	Transmission electron microscope	JEOL JEM-2100 LaB6, Jp
Extruder	Avanti Polar Lipids, US	Tunable resistive pulse sensing	qNano, Izon, UK
Flow adaptors	Kimble, US	Ultracentrifuge	OptimaTM L-90 K, Beckman Coulter, US
Frac30 fraction collector	Cytiva, US	Ultracentrifuge rotors	SW32 Ti and SW40 Ti, Beckman Coulter, US
Gatan cryoplunger model CP3	Gatan, US	Water bath	Typ WNB14, Memmert, De
Hamilton syringes	Hamilton, US		

3. Methods

3.1. Bacterial Culture

3.1.1. Culture of SBCy050 myxobacteria and production of conditioned medium

SBCy050 bacteria were used as a production organism for the isolation of OMVs. To cultivate the bacteria, first a pre-culture was prepared by adding 1ml of a cryostock containing 25% glycerol to 50 ml of 2SWC-medium. After 48 h of growth, the preculture with an OD_{600} of approx. 1.0 was used to inoculate the cultures for OMV-isolation. 150 ml of 2SWC-medium per 500 ml conical culture-flask were inoculated with a starting OD_{600} of 0.04±0.01. After 96 h of cultivation and reaching of the late stationary phase, the vesicle-containing culture-supernatant was harvested.

First bacteria and large debris were pelleted by centrifugation at 9500*g for 10 min. Then the supernatant was either filtered or subjected to another round of centrifugation at 9500*g for 15 min to remove residual bacteria. Filtration was carried out using a 0.45 µm pore-size bottle top filter. The resulting cell-free conditioned medium was then typically directly subjected to ultracentrifugation as described below.

3.2. Cell culture

3.2.1. A549 lung cancer cells

A549 cells were cultured in RPMI 1640 medium supplemented with 10% FBS. T75 flasks were used for maintaining the culture, while T225 flasks were used to generate sufficient amounts of conditioned medium for EV-isolation. After passaging new T75 flasks were seeded with 0.2*10^6 cells in 12 ml medium and T225 flasks with 0.6*10^6 cells in 30 ml of medium. Flasks were maintained for 120 h, with a medium exchange after 48 h. After 120 h, flasks to be used for EV-isolation were washed once with PBS, then RPMI 1640 without FBS was added, while for T75 flaks used for maintaining the culture, the medium was exchanged with FBS-containing medium. After another 48 h, the cells in T75 flasks were trypsinized, counted using a CASY cell counter and seeded into new flasks. The medium from T225 flasks was harvested and centrifuged 4 min at 300*g to pellet detached cells and the supernatant was typically stored at -80 °C for up to three weeks. After thawing and before UC conditioned medium was centrifuged for 15 min at 9500*g.

3.2.2. Human umbilical cord endothelial cells (HUVEC)

HUVEC cells were cultured in EGM-2 medium containing 2% FBS. Passages 5-9 after thawing were used for EV-isolation. During passaging, cells obtained from one T225 flask were split into four new T225 flasks. Cells were cultivated with 25 ml of EGM-2 medium per flask for 120 h, with feeding after 48 h. After 120 h cells were washed once with PBS and cultured for 48 h with serum-free EBM-2 medium. Conditioned medium was harvested and centrifuged at 300*g for 4 min and typically stored at -80 °C for up to three weeks After thawing and before UC conditioned medium was centrifuged for 15 min at 9500*g. Cells from flasks used for passaging were washed twice with PBS, trypsinized and split into four new T225 flasks.

3.2.3. RO cells

RO cells (DSMZ, ACC 452) were cultured by Eilien Heinrich as described previously (374). RPMI medium supplemented with 1% (v/v) insulin-transferrin-selenium-ethanolamine was used to culture the cells. Generally, 0.75×10^6 cells/mL were seeded in 45 ml of medium in a T75 flask. After 3 days, 25 ml of medium were replaced with 50 ml of fresh medium. After 7 days, conditioned medium was harvested. Cells were pelleted at 300*g for 8 min, then the supernatant was centrifuged at 9500*g for 15 min and subsequently filtered through a 0.45 µm pore-size bottle top filter.

3.3. Liposome preparation

Liposomes were prepared using the lipid-film hydration method followed by extrusion (375). To produce lipid films a solution of 2 mM DMPP and 3 mM DPPC in chloroform was prepared and 1 ml aliquots of it air-dried in glass-HPLC vials. Lipid-films were rehydrated with 1 ml of PBS at 42 °C, vortexed and then extruded eleven times through a 200 nm polycarbonate membrane. Liposomes were then directly used in experiments or diluted as necessary.

3.4. EV-isolation
3.4.1. Ultracentrifugation

To obtain concentrated EVs from conditioned medium, particles were pelleted using ultracentrifugation. Typically samples were subjected to 2 h of centrifugation at 100000*g and 4 °C using an SW32 Ti rotor with thick-wall PC-tubes. This allowed for the simultaneous processing of approx. 180 ml conditioned medium.

After UC, the supernatant was decanted. EVs were either resuspended in residual supernatant or PBS was added to the pellet for resuspension. Pellets were typically used directly or stored up to 24 h at 4 °C.

3.4.2.   Size exclusion chromatography

SEC was generally performed using Kimble Flex-columns filled with Sepharose Cl-2b as the stationary phase and filtered PBS as the mobile phase. Purification of samples was conducted using either gravity-driven elution or partially automated using an ÄKTA start chromatography system equipped with a fraction collector. The use of a differing setup is indicated in the respective method section. For SEC-purification using the ÄKTA start instrument, columns were equilibrated to be used with a flow of 1 ml/min. Fractions of either 0.5 or 1 ml were collected. Between runs, columns were cleaned with at least 1.5 column volumes of buffer to ensure the removal of residual contaminants from the previous run.

3.5.   Characterization of extracellular vesicles
3.5.1.   EV-size and concentration

EV-size and concentration were mainly measured by NTA. Moreover, the size of EVs was also assessed using Cryo-TEM.

NTA was performed using Nanosight-instruments in varying setups, due to maintenance and failure of components of the system. Differences in sensitivity of the setups led to different results regarding the apparent particle-concentration of EV-samples. This made the comparison of some of the results, especially for the assessment of bound molecules per particle difficult. This problem however was mitigated, by normalizing results to control or standard samples measured in parallel.

Cryo-TEM measurements were performed by Marcus Koch as previously described (21). 3 µl of EV-pellet or purified EVs were pipetted onto a holey carbon film and after blotting for 2 s, the sample was frozen rapidly by plunging into liquid ethane at 108 K using a cryoplunger. Frozen samples were transferred to a cryo-TEM sample holder and imaged in bright field TEM at a temperature of 100 K.

3.5.2. Protein content

The protein content of EVs and other samples was measured using a bicinchoninic acid assay according to the manufacturer's instructions. A calibration curve was prepared freshly for each experiment and samples were diluted to a protein concentration between 0.5 and 30 µg/ml to conform to the linear range of the kit. Samples were measured using a plate reader.

3.5.3. SBCy050 autofluorescence

The autofluorescence of SBCy050 OMVs was measured with an excitation wavelengths of 410 nm and an emission wavelength of 629 nm, as described in the master thesis of Eilien Heinrich.

3.6. Surface functionalization of EVs
3.6.1. Chemical synthesis and analysis of synthesized compounds

All reagents were obtained from commercial suppliers and used as received. Liquid chromatography-coupled mass spectrometry (LC/MS) analysis was generally performed using a Dionex UltiMate 3000 system equipped with a MSQ Plus ESI Quadropol mass spectrometer. Samples were typically analyzed using a gradient from 5% ACN and 95% H_2O to 100% ACN over the course of 5 min. High-resolution mass spectrometry (HRMS) was performed using a Dionex Ultimate 3000 RSLC equipped with a Q Exactive Focus mass spectrometer and a Acquity UPLC® BEH C8 column. Preparative HPLC (prepHPLC) was generally performed using an Ultimate 3000 UHPLC+ focused system with a C18 column.

NMR spectra were recorded using a Bruker AV 500 or Bruker Ascend 700. Chemical shifts are reported as part per million (ppm). Coupling constants of reported signals are given in Hertz (Hz). Data was reported as chemical shift, multiplicity of the signal (singulet (s), doublet (d), triplet (t), quartet (q), doublet of doublets (dd), doublet of triplets (dt), multiplet (m) and broad (br)), coupling constants and integration.

3.6.2. General approach

The surface of SBCy050 OMVs was modified after their isolation with various methods. Vesicles were generally modified with fluorescent molecules to allow for the assessment of the modification efficiency by measuring the fluorescence.

3.6.3.   Cholesterol insertion

For cholesterol insertion, purified SBCy050 OMVs, A549 EVs or freshly prepared liposomes, diluted to the same concentration range as EVs, were incubated with 1000 molecules per particle of cholesterol PEG 2000 FITC for 1 h at 30 °C and 300 rpm. SBCy050 OMVs and liposomes were incubated with or without the addition of 0.1 mg/ml of saponin.

After the incubation period, samples were purified by gravity-flow-driven SEC using a 10 ml Sephadex G75 column for SBCy050 OMVs and A549 EVs and a 25 ml Sepharose Cl-2b column for liposomes. Collected fractions were analyzed by NTA and regarding their FITC fluorescence (excitation: 490 nm, emission: 525 nm). From this, the number of inserted cholesterol PEG 2000 FITC-molecules per particle was calculated.

3.6.4.   Functionalization with activated esters

SBCy050 UC-pellets were purified by SEC using a 35 ml column before introduction of the activated ester. The protein-content of vesicle-containing fractions was measured by BCA-assay and adjusted to a concentration of 48.8 µg/ml. The sample was then mixed with either sulfo-cyanin-7 NHS ester in different concentrations or with sulfo-cyanin-7 carboxylic acid at 9.8 µM. Both compounds were dissolved in dry DMSO at 8 mg/ml and stored in -80 °C in single-use aliquots. Samples were incubated for 1 h at RT. Then they were purified using a 30 ml SEC column covered with aluminum foil. Fractions were analyzed by NTA and regarding their fluorescence (excitation: 750 nm, emission: 781 nm) and the amount of dye-molecules per particle was calculated.

3.6.5.   Diazotransfer

Diazotransfer was performed by mixing 400 or 1000 µl of the resuspended vesicle-pellet with 0.32 mM CuSO4, 0.81 mM ISA and varying concentrations of NaOH. After incubation for 30 min to 20 h, the sample was purified using the same 35 ml SEC-column that was employed for pellet-purification in NHS ester-experiments. The obtained AzideOMVs were typically directly used in click chemistry-based surface engineering experiments.

3.6.5.1. Synthesis of imidazole-1-sulfonyl azide (ISA) HCl
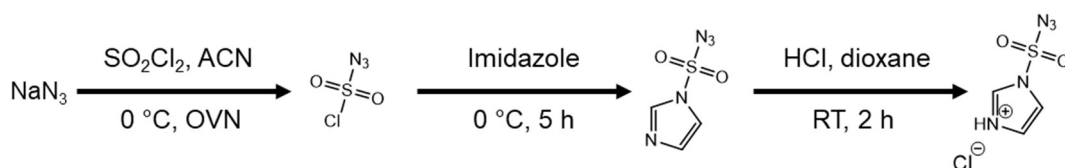
Figure 21: Reaction scheme of the synthesis of ISA HCl.

ISA was synthesized based on the protocol of Goddard-Borger and Stick (365).

500 mg of NaN$_3$ (7.7 mmol) were weighed into a 100 ml two-necked RBF (Figure 21). After the introduction of a nitrogen-atmosphere, NaN$_3$ was suspended in 7.7 ml of dry acetonitrile. The stirred suspension was cooled to 0 °C and 0.63 ml (7.7 mmol) sulfuryl chloride were added dropwise over 10 min. The mixture was allowed to slowly reach RT and stirred overnight. Then, after re-cooling to 0 °C, 1 g of imidazole (14.69 mmol) dissolved in 15 ml of dry acetonitrile was added slowly to the mixture. After stirring for 5 h, approx. 25 ml of ethyl acetate were added to the reaction mix. The organic phase was washed with saturated NaHCO$_3$ and dried over MgSO$_4$. Approx. 4 ml of 4 M HCl in dioxane were added to the organic layer. After 2 h, the HCl-salt of ISA was isolated as colorless crystals. ISA HCl was stored at -20 °C under an argon atmosphere.

3.6.6. Chemical modification of AzideOMVs by SPAAC

Typically, 500 µl of AzideOMVs were mixed with 4.9 µM of DBCO AF594 or SPAAC-based linker and incubated for 20 h at RT and 300 rpm. To this end, DBCO AF594 and the SPAAC-based linker were dissolved in DMSO and aliquoted in 1 µl aliquots containing 2.45 nmol per aliquot, enough to prepare 500 µl of a 4.9 µM solution. Samples were purified by SEC with the same 30 ml SEC-column that that was employed for purification after incubation with activated esters. Fractions were analyzed by NTA and regarding their fluorescence (DBCO AF594: excitation: 590 nm, emission: 627 nm; SPAAC-based linker: excitation: 649 nm, emission: 681 nm).

3.6.6.1. Synthesis of the SPAAC-based linker
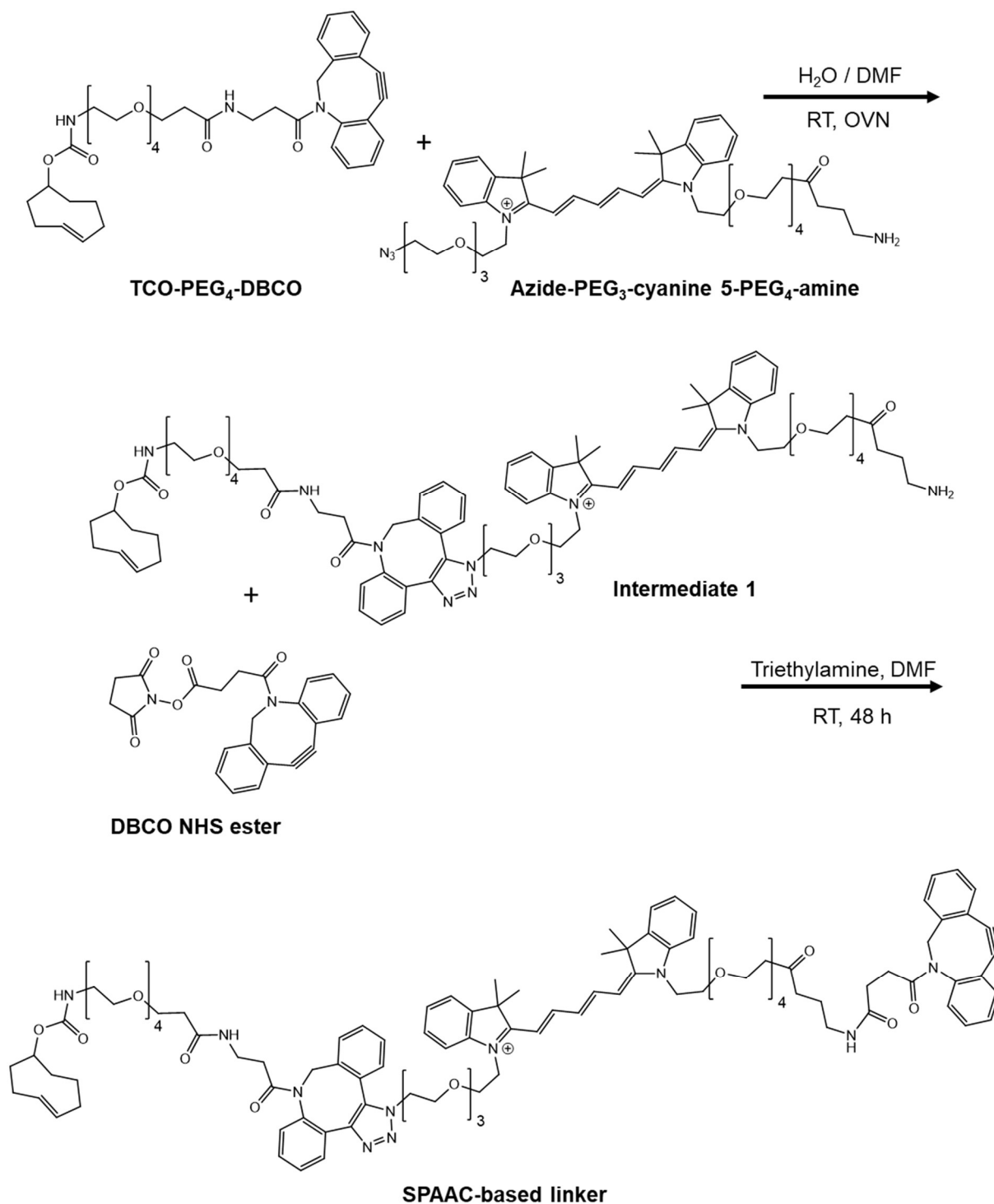
Figure 22: Reaction scheme for the synthesis of the SPAAC-based linker.

2 mg (2.23 µmol) of azide-PEG$_3$-cyanine5-PEG$_4$-amine were dissolved in 250 µl of a mixture of water/DMF 1:1 (v/v) (Figure 22). To this solution 1.66 mg (2.45 µmol) of TCO-PEG$_4$-DBCO dissolved in 250 µl of 1:1 water/DMF were added. The mixture was stirred overnight until

completion of the first reaction-step, as indicated by LC-MS analysis. The mixture was concentrated under a stream of nitrogen and stored at -80 °C.

In the next step, 0.45 mg (2.45 µmol) of DBCO NHS ester were dissolved in 250 µl of dry DMF and added to the intermediate, together with 3.5 µl of trimethylamine diluted 1:10 (v/v) in dry DMF (2.23 µmol). The mixture was stirred for 48 h at RT until the presence of the desired product was confirmed. The reaction mixture was purified by prepHPLC.

3.6.6.2. Synthesis of methyltetrazine vancomycin
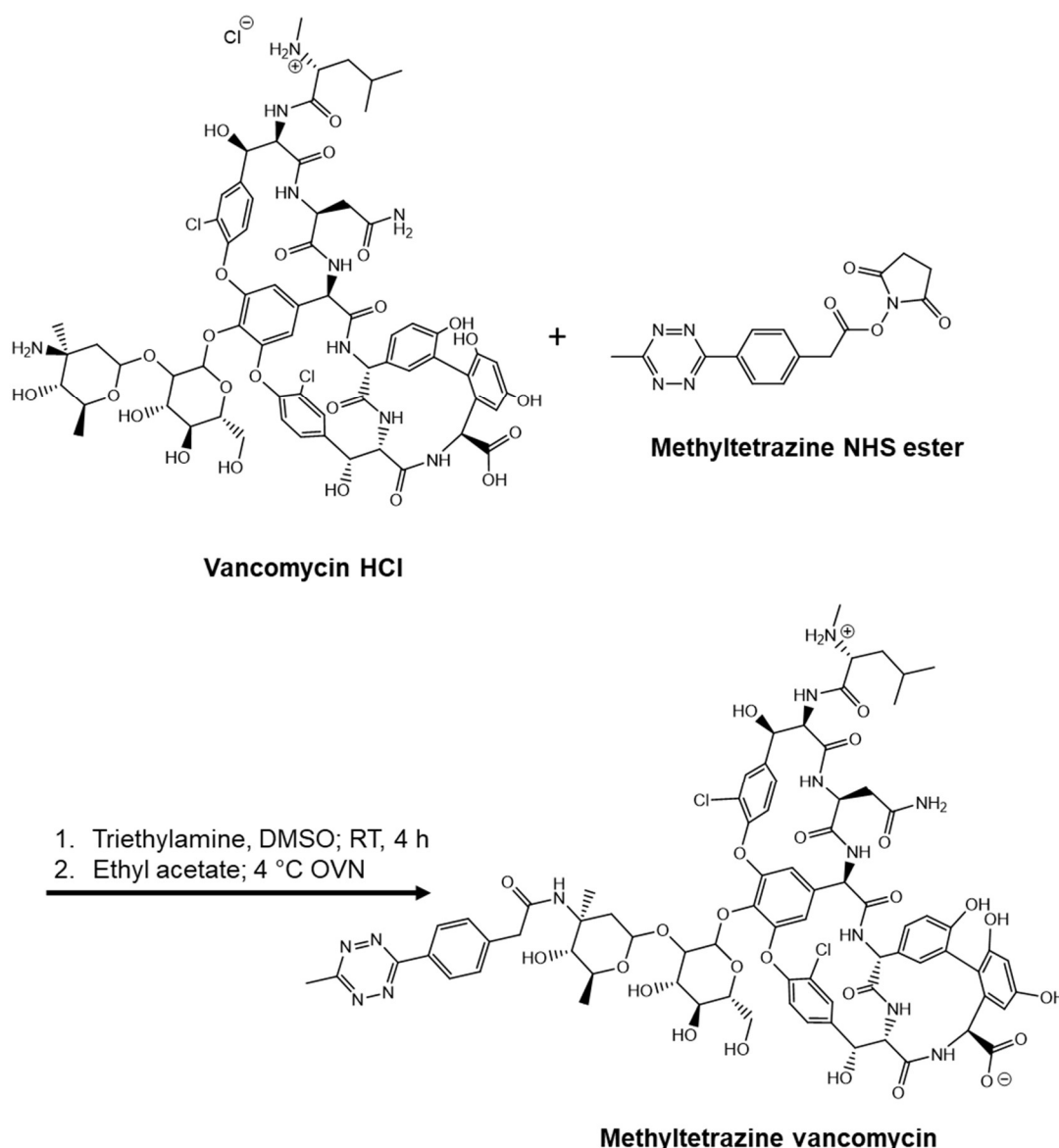
Figure 23: Reaction scheme for the synthesis of methyltetrazine vancomycin.

37.8 mg of vancomycin HCl (25.46 µmol) were dissolved in 4730 µl of dry DMSO and 7.06 µl trimethylamine (50.92 µmol) were added (Figure 23). To this, 10 mg of methyltetrazine NHS ester (30.55 µmol) were added and the mixture was stirred at RT for 4 h until completion as

indicated by LC/MS. Cold ethyl acetate was added to the reaction mixture and the solution was stored overnight at 4 °C. On the next day, a pink precipitate was isolated by filtration and lyophilized. The lyophilized precipitate was further purified by prepHPLC.

3.6.6.3. IEDDA reaction conditions

The respective TCO-group containing molecule (either SPAAC-based linker, TCO-PEG$_4$-DBCO, PEG$_8$ CuAAC-linker or PEG$_6$ CuAAC-linker) was reacted with a methyltetrazine containing molecule (either methyltetrazine vancomycin or methyltetrazine-PEG$_4$-biotin), by mixing equal amounts of both compounds dissolved in DMSO in a volume of 2 to 6 µl. After 1 h incubation at RT, the product was used in OMV modification without further purification.

3.6.7.   Chemical modification of AzideOMVs by CuAAC

To perform CuAAC, Na ascorbate was freshly dissolved in either water or 40 mg/ml NaOH at a concentration of 200 mg/ml. 14.11 µl of this solution were mixed with 20 µl of 10 mg/ml CuSO4 in water. Of this 5.53 µl were added to a mixture of 14.1 µl of 20 mg/ml Tris(3-hydroxypropyltriazolylmethyl)amine (THPTA) and the respective alkyne (either alkyne Af594, the CuAAC-linker or the product of the reaction of a linker and methyltetrazine-vancomycin or methyltetrazine-PEG$_4$-biotin). The resulting solution was quantitatively added to 500 µl of AzideOMVs. After typically 4 h of incubation at RT and 300 rpm, purification using the 30 ml SEC-column was performed as described above. Fractions were analyzed by NTA and regarding their fluorescence (Alkyne AF594: excitation: 590 nm, emission: 627 nm; CuAAC linkers: excitation: 646 nm, emission: 681 nm).

3.6.7.1. Synthesis of the PEG₈ CuAAC-linker
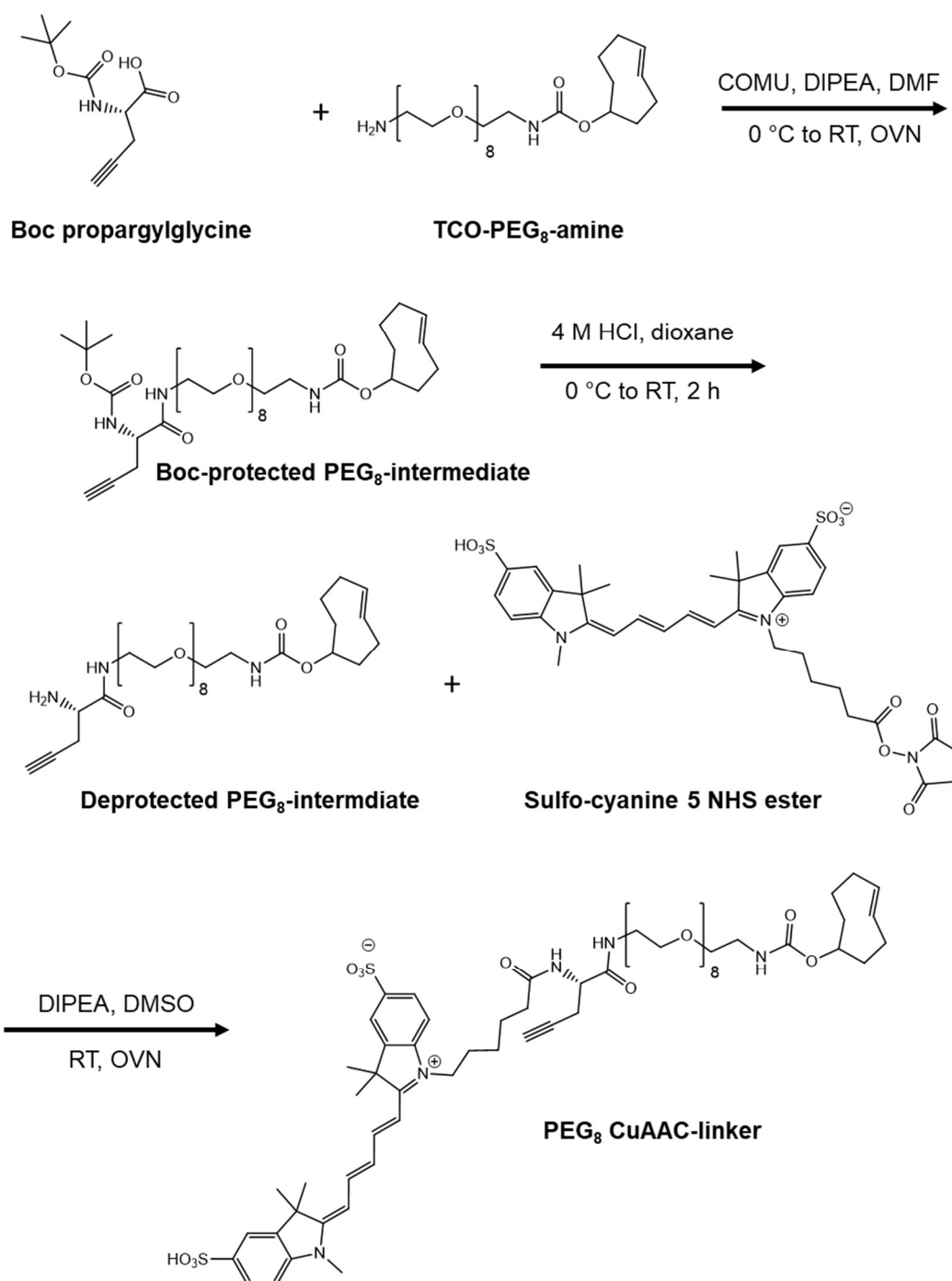
Figure 24: Reaction scheme for the synthesis of the PEG₈ CuAAC-linker.

23.0 mg Boc propargyl glycine (0.108 mmol) were dissolved in 830 µl of dry DMF and solution was cooled to 0 °C on ice. 45.5 mg of COMU (0.106 mmol) and 39.1 µl DIPEA (0.230 mmol) were added (Figure 24). Then 50.0 mg of TCO-PEG₈-amine (0.089 mmol) dissolved in 250 µl of dry DMF were added slowly. The reaction was left to warm up to RT overnight. The product of this reaction was purified by prepHPLC to obtain the Boc-protected intermediate. Boc-deprotection was carried out by dissolving the lyophilized Boc-protected intermediate in

approx. 200 µl of dioxane, cooling it to 0 °C and adding 2 ml of 4 M HCl in dioxane. The mixture was warmed to RT over the course of 2 h. Deprotection of the intermediate was confirmed by LC/MS and HCl, dioxane and the bi-products of the Boc deprotection were removed under vacuum. 26 mg of the deprotected intermediate (0.039 mmol) were dissolved in 100 µl of dry DMSO and 11.2 µl DIPEA (0.066 mmol) were added. To this, 25 mg of sulfo-cyanine 5 NHS ester (0.033 mmol) dissolved in 400 µl of DMSO were added. The reaction was stirred overnight at RT. The product was purified by prepHPLC and lyophilized.

3.6.7.2. Synthesis of the PEG$_6$ CuAAC-linker
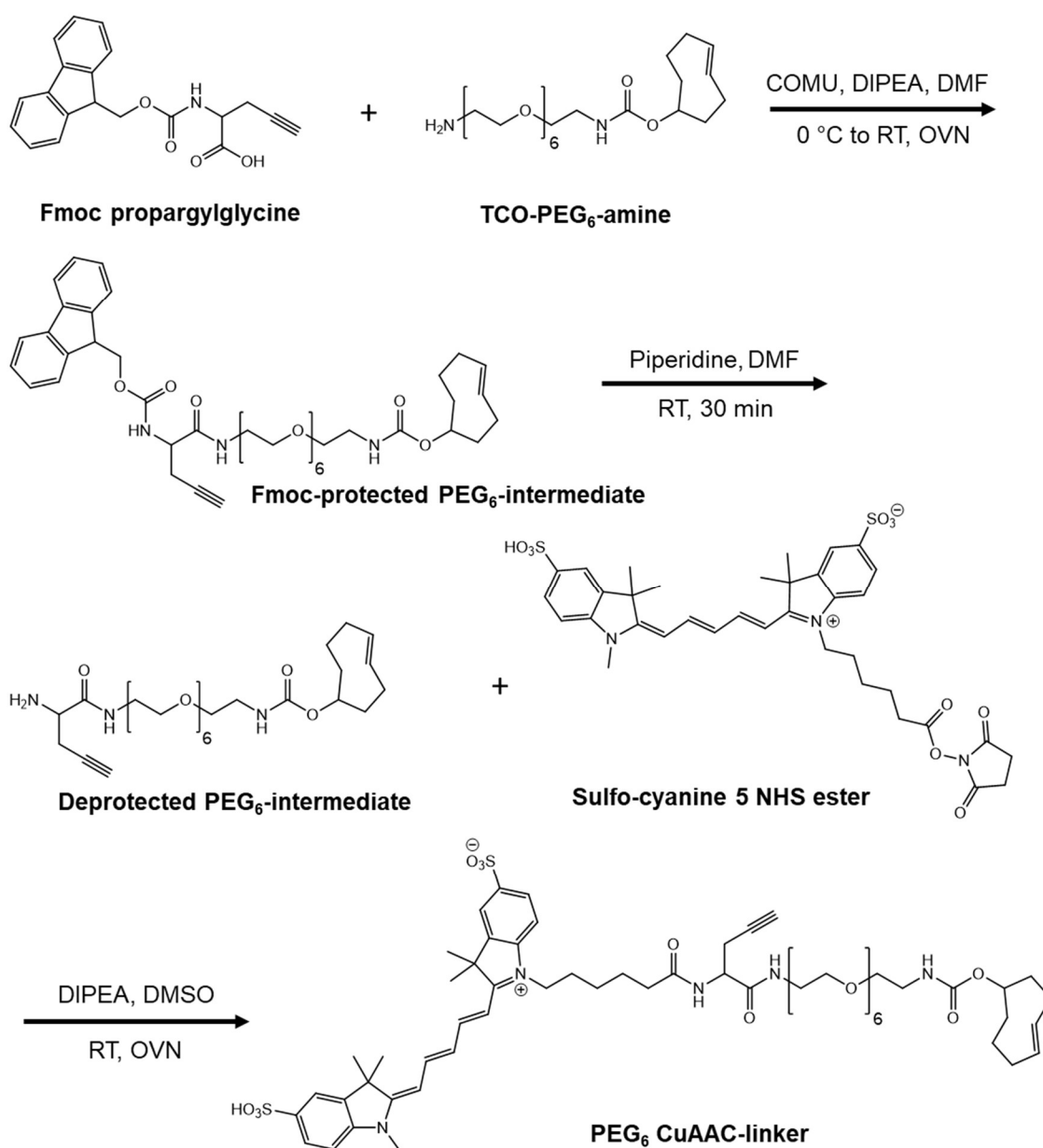
Figure 25: Reaction scheme for the synthesis of the PEG$_6$ CuAAC-linker.

The whole synthesis was executed protected from light as far as possible. 42.9 mg of Fmoc propargyl glycine (0.128 mmol) were dissolved in 830 µl of dry DMF and the solution was cooled to 0 °C on ice. Then 53.9 mg of COMU (0.126 mmol) and 46.0 µl DIPEA (0.273 mmol) were added (Figure 25). Then 50.0 mg of TCO-PEG$_6$-amine (0.105 mmol) dissolved in 250 µl of dry DMF were added slowly. The reaction was left to warm up to RT overnight. The product of this reaction was purified by prepHPLC to obtain the Fmoc-protected intermediate. Fmoc-deprotection was carried out based on the protocol of Hoffmann et al. (376). The purified intermediate was dissolved in 2 ml of 20% piperidine in DMF (v/v) and incubated at RT for 30 min. After confirmation of complete deprotection, DMF and piperidine were removed under high vacuum and the product was purified by prepHPLC. 17 mg of the deprotected intermediate (0.030 mmol) were dissolved in 100 µl of dry DMSO and 9.0 µl DIPEA (0.052 mmol) were added. To this, 22.7 mg of sulfo-cyanine 5 NHS ester (0.030 mmol) dissolved in 400 µl of DMSO were added. The reaction was stirred overnight at RT. The product was purified by prepHPLC and lyophilized.

3.6.8. Assessment of residual copper after diazotransfer and CuAAC

The amount of residual copper in SBCy050 OMVs after diazotransfer and after subsequent CuAAC was assessed using inductively coupled plasma mass spectrometry (ICP-MS). ICP-MS measurements were performed by Ralf Kautenburger and Kristina Brix.

Samples were treated with 0.3% triton X-100 to lyse vesicles, filtered through a 0.2 µM syringe filter and 2 ml per sample were diluted 1 in 5 and measured by ICP-MS. To assess residual copper-content for diazotransfer, 2.5 ml each of OMVs subjected to diazotransfer under optimized conditions, untreated OMVs and a control containing SEC fractions obtained from the injection of pure PBS were used for analysis. CuAAC was assessed using OMVs subjected to CuAAC with alkyne AF594 under optimized conditions, untreated OMVs and a control containing SEC fractions obtained from the injection of pure PBS.

3.6.9. Testing of biotinylated OMVs

500 µl of biotinylated OMVs or controls were incubated with 2.5 µg/ml streptavidin-FITC for 1 h and purified by SEC using a 10 ml sepharose column. Fractions of 0.5 ml were collected and analyzed for streptavidin-FITC by fluorescence measurement (excitation: 480 nm, emission: 516 nm).

3.7. Storage-stability of EVs

3.7.1. General protocol for β-glucuronidase encapsulation

β-glucuronidase was encapsulated in EVs by co-incubation with saponin. EV-pellets after UC were mixed with 0.1 mg/ml saponin and 1.5 mg/ml β-glucuronidase, vortexed briefly and then incubated for 10 min at RT with intermitted mixing by gentle flicking of the tube to limit the generation of foam. Directly after the end of the incubation period, samples were purified by SEC to remove non-encapsulated enzyme, saponin and soluble impurities carried over from UC.

3.7.2. β-glucuronidase assay

The activity of β-glucuronidase encapsulated in EVs was assessed by the enzymatic conversion of non-fluorescent fluorescein di-β-D-glucuronide into fluorescent fluorescein. 125 µl of EVs were mixed with 25 µl of fluorescein di-β-D-glucuronide in a well of a black 96-well plate to obtain a final concentration of 8.3 µg/ml fluorescein di-β-D-glucuronide. The initial fluorescence was measured directly after the sample preparation at an excitation wavelength of 480 nm and an emission wavelength of 516 nm. Then the plate was covered with adhesive film to counteract evaporation and incubated in the dark for 18 h at 37 °C. Then the fluorescence at t18 h was acquired. The enzyme activity was calculated by subtraction of t0 from t18 and subsequent subtraction of the blank consisting of pure buffer.

3.7.3. Initial experiments with A549- and HUVEC-EVs

Storage of A549- and HUVEC-EV-samples was assessed as part of the publications of Frank, Richter et al. (377, 378). EVs were purified by gravity-flow SEC using 15 ml Sepharose Cl-2b in a 1.0 cm diameter column. A sample volume of up to 400 µl was purified in one SEC run and fractions of 1 ml were collected. Vesicle-containing fractions were pooled for storage. Samples were either stored at 4 °C, -80 °C or samples were lyophilized with or without the addition of 4% (w/v) trehalose in a Lyophilizer ALPHA 2-4 LSC. For lyophilisation, samples were frozen at -80 °C for 1 h and then lyophilized with the following parameters. The main-drying step lasted for 46 h at a pressure of 0.180 mbar, with the shelf temperature set to 15 °C. Then pressure was reduced to 0.0035 mbar and the shelf temperature increased to 25 °C for the final drying step lasting two hours. After lyophilisation, samples were stored at 4 °C. Lyophilized samples were re-dispersed in water for 30 min before further analysis.

Purified A549-EVs were stored for 48 h at 4 °C, -80 °C or they were lyophilized without the addition of 4% trehalose and stored at 4 °C. After storage, particle-size and concentration were

assessed by NTA. HUVEC-EVs were initially stored for 14 d at RT, 4 °C, -80 °C or lyophilized without the addition of 4% trehalose and stored at 4 °C. Then particle-size and concentration were assessed by NTA.

In a subsequent experiment, β-glucuronidase was encapsulated into HUVEC-EVs and they were stored for 7 d at 4 °C, -80 °C or lyophilized with the addition of 4% (w/v) trehalose. After storage potentially leaked enzyme was removed using asymmetric flow-field-flow-fractionation (AF4), performed by Kathrin Fuhrmann. EV-purification was carried out using a small channel equipped with a 30 kDa molecular weight cut-off cellulose membrane and a 350 μm spacer. PBS filtered through a 0.1 μm filter was used as the mobile phase. 300 μl of EVs were injected at a rate of 0.2 ml/min and focused for 10 min. Then, the sample was eluted at a rate of 1 ml/min with a cross-flow that decreased from 2 ml/min to 0.1 ml/min in 8 minutes. Elution was continued for another 10 min without cross-flow. Eluting proteins were detected using UV-absorption at 280 nm. Particles were detected by multi-angle light scattering at 658 nm. Fractions of 1 ml of the eluate were collected between 12.5 and 27 min. EV-containing fractions were assessed regarding particle-size and –concentration by NTA and enzyme activity was measured using the β-glucuronidase assay and compared to unstored samples that were treated in the same way.

3.7.4. Long-term storage of optimized RO-EV-formulations

The parameters for EV-lyophilisation were optimized in cooperation with the group of Prof. Wolfgang Frieß, LMU Munich.

After initial freeze-thaw and lyophilisation experiments (Trenkenschuh E., Richter, M. et al. (2020). "Formulation development of lyophilized extracellular vesicles with long-term stability", manuscript submitted to Advanced Healthcare Materials), RO-EVs were subjected to long-term storage in lyophilized form. Eilien Heinrich cultured RO-cells and performed UC. M. Richter encapsulated β-glucuronidase in the vesicles, purified them by SEC and assessed enzyme activity before and after storage and lyophilisation. E. Trenkenschuh prepared the EV-formulations from purified EVs, performed lyophilisation and the analysis of the colloidal stability of EVs.

The buffer of purified RO-EVs with encapsulated β-glucuronidase was exchanged with Na- or K-phosphate using Slide-A-Lyzer MINI dialysis devices (20K MWCO), samples were filtered through a 0.02 μm pore-size filter and four formulations were prepared:

1. 10 mM Na-phosphate with 5% sucrose and 0.02% poloxamer-188 (P188)

2. 10 mM K-phosphate with 5% sucrose and 0.02% P188

3. 10 mM Na-phosphate with 5% sucrose and 0.02% polyvinylpyrrolidone (PVP)

4. 10 mM Na-phosphate with 5% PVP and 0.02% P188

Samples of 190 µl were lyophilized using a LyoStar TM 3 pilot-scale freeze-dryer. Samples were frozen at -50 °C for 2 h, then primary drying was performed at -20 °C and 53 mbar. Final drying was carried out at 20 °C and 53 mbar. Samples were stoppered under nitrogen at 600 mbar. Samples were stored at 2-8, 25 and 40 °C for one month and six months. Enzyme activity and colloidal stability of RO-EVs was assessed before lyophilisation, directly after lyophilisation, after one month and after six months.

Colloidal stability was measured using tunable resistive pulse sensing. EV-recovery was assessed using a NP100 nanopore with a measurement size-range of 50-330 nm. Formation of larger aggregates was assessed using a NP600 nanopore with a measurement size-range of 275-1570 nm.

For the measurement of enzyme activity potentially leaked enzyme was removed by SEC. SEC was performed using a 10 ml volume, 1.0 cm diameter Sepharose Cl-2b column with 10 mM Na-Phosphate as the mobile phase, to match the osmolarity of the buffer of the EV-samples. Fractions of 0.5 ml were collected. Vesicle-containing fractions were assessed using the β-glucuronidase assay.

3.8. Plotting of data and statistical analysis

All data is plotted as mean ± SD if not explicitly stated otherwise. The number of independent experiments is stated in the text. Statistical analysis was performed using Sigmaplot 14.0. Pairwise comparison of samples was performed using one-way analysis of variance (ANOVA) followed by a Tukey post hoc test. Differences between samples were considered significant at $p \leq 0.05$. In graphs, symbols above bars indicate that the respective sample shows significant difference to all other samples bearing the same symbol. Groups of samples that share a significant difference with another sample or group of samples are indicated by a horizontal bar above them.

4. Results

4.1. Characterization of SBCy050 bacteria and OMVs
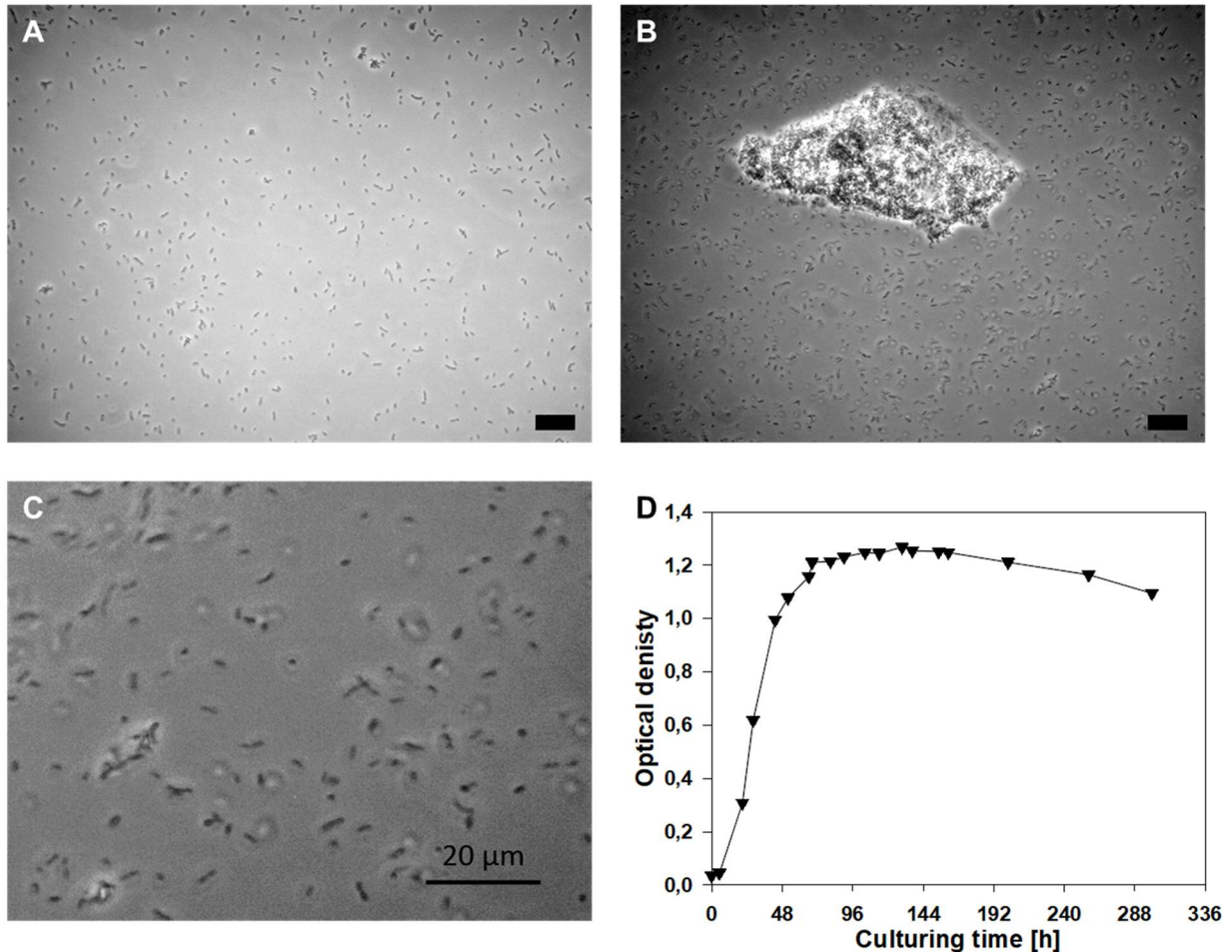
Figure 26: Panels A-C show light microscopy pictures of SBCy050 bacteria after 96 h in culture. Aggregates as seen in B started to appear when the bacteria were close to reaching the stationary phase. As visible in the growth curve (D), SBCy050 reached the stationary after approx. 72 h (mean values of n=3 cultures). Black bars represent 20 µm.

The growth of SBCy050 bacteria was assessed by measuring OD_{600}. It was determined that the stationary phase was reached after approx. 72 h (Figure 26 D). OMVs were harvested after 96 h. Comparing the OD_{600} at isolation over the course of one year a mean OD_{600} of 1.33 ± 0.12 was reached by the bacteria (n=30). Under the microscope, SBCy050 bacteria were rod-shaped and started to form small aggregates once they approached the stationary phase (Figure 26 A&C). After 72-96 hours of culture, red clumps started to appear on the sides of the culture flasks (Figure 26 B). These were also visible in the pellet obtained by centrifuging of bacterial cultures.
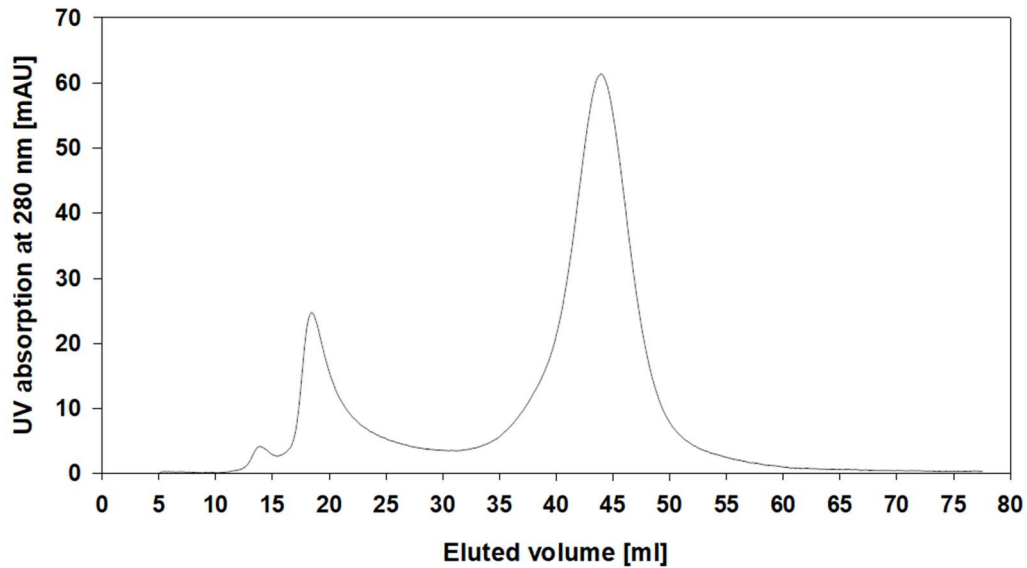
Figure 27: Representative chromatogram of the purification of a SBCy050 pellet using the ÄKTA instrument. OMVs eluted in the first larger peak after around 18 to 20 ml, while soluble impurities and proteins aggregates eluted later around 45 ml. Both peaks were well separated.

After UC, the OMV-pellet appeared dark red. Pellets after UC and OMVs purified by SEC were analyzed by cryo TEM. While the pellet (Figure 28 C) showed more vesicular structures, a lot of non-vesicular material was visible, which was not the case for purified OMVs (Figure 28 D). The removal of soluble impurities was also well visible in the UV-chromatogram of OMVs purified by SEC (Figure 27). OMVs eluted after around 20 ml, while the elution of soluble impurities started at approx. 32 ml. NTA-analysis of purified OMVs showed a reproducible mean size of around 100 nm (Figure 29). OMVs further showed a characteristic autofluorescence at 629 nm, when irradiated at 410 nm (Figure 28 A&B).
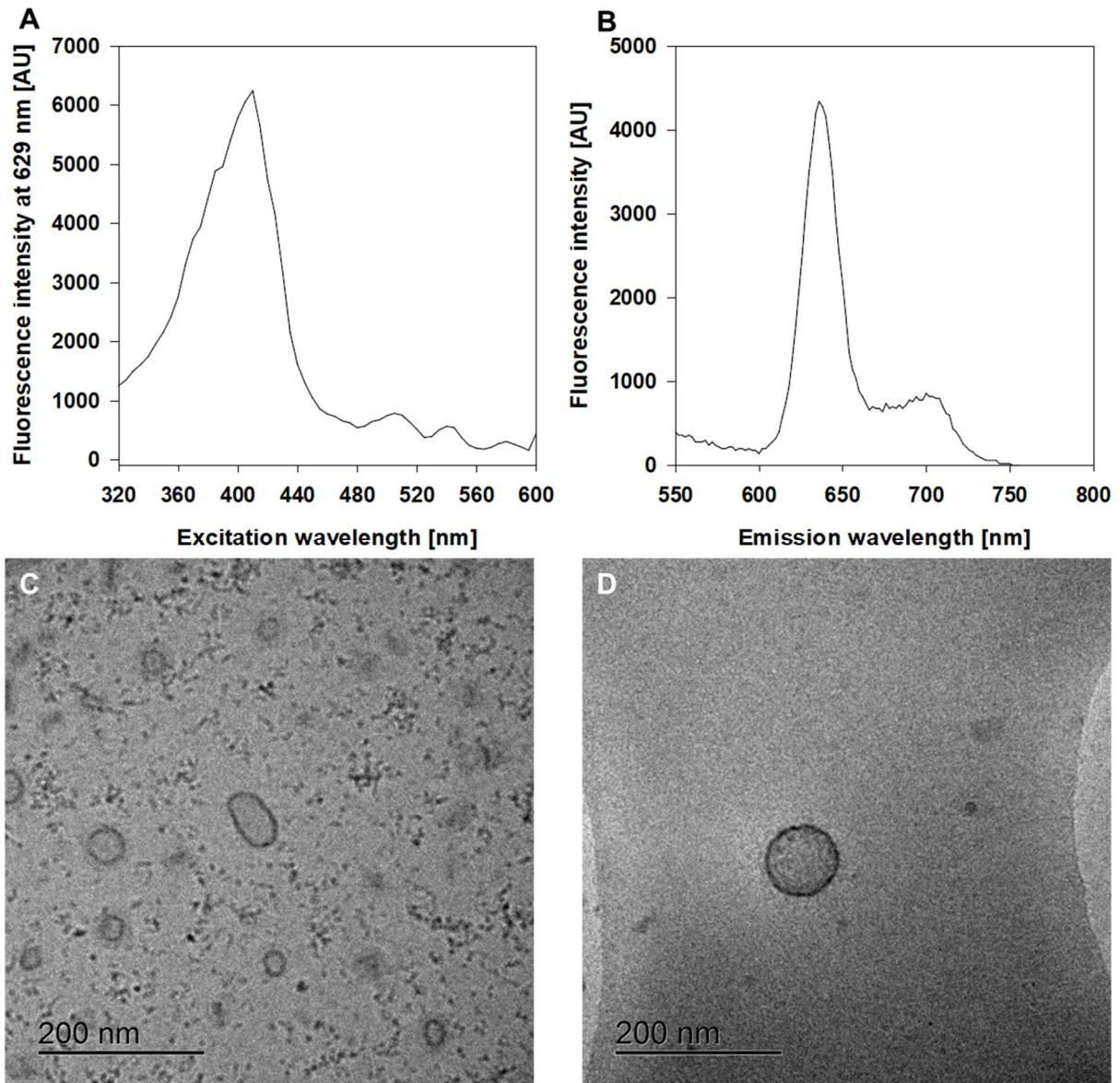
Figure 28: SBCy050 OMVs showed a characteristic autofluorescence. Excitation (A) and emission scans (B) revealed an optimal excitation wavelength of 410 nm with an emission maximum at 629 nm. Panels C and D show cryo TEM pictures of the SBCy050 pellet after UC and purified OMVs after an additional step of SEC. While in the pellet (C) more vesicular structures were visible, it also contained much more non-vesicular material than SEC-purified samples (D).

4.1.1.   Optimization of OMV-purification

600 ml of SBCy050 cultures were pooled and processed by either two-time centrifugation or filtration. After UC and SEC of the samples, the particle-yield, the size-distribution and the protein-content per particle were compared. Filtration using the Merck Steritop filter system led to particle-recovery of 114.1±5.6% (n=3), while the protein content per particle was 96.8% of the filtered OMVs (n=2). The size distributions of the obtained vesicles were very similar (Figure 29). Subsequently the Merck Steritop filter was compared with another model produced

by Neolab with the same membrane material and pore size. Using the Neolab filter, the particle yield was reduced to 33.4% (n=2). Thus, filtration using the Steritop 0.45 µm pore size filter subsequently replaced the second centrifugation step in OMV-isolation.
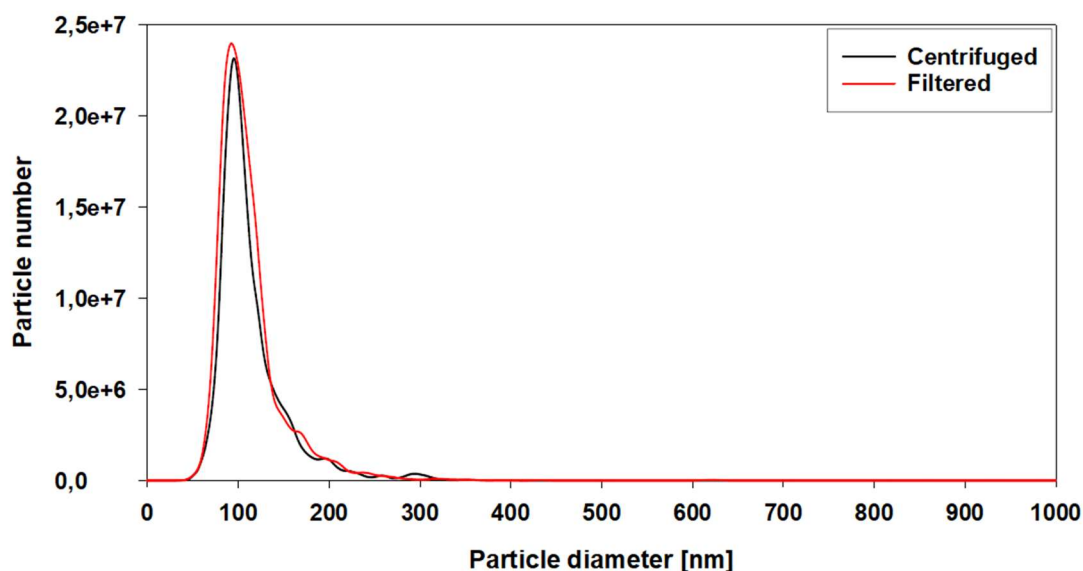
Figure 29: Size distribution after UC and SEC-purification of SBCy050 OMVs, where the bacterial cultures were processed by either two-time centrifugation (black) or centrifugation and filtration through a Steritop 0.45 µm filter (red) (mean values from n=3).

4.2.   Cholesterol insertion

SBCy050 OMVs, liposomes and A549 EVs were subjected to cholesterol insertion (for characterization of A549 cells and EVs and liposomes see Supp. figure 1 & Supp. figure 2). To this end, the particle concentration of the purified vesicles or diluted liposomes was first measured, then they were incubated with 1000 cholesteryl-PEG200-FITC molecules per particle. For OMVs and liposomes, also the addition of 0.1 mg/ml saponin during incubation was tested. After purification the particle concentration and fluorescence intensity were measured (Figure 30). On average 100.9±22.9 molecules inserted into liposomes and 114.5±69.8 molecules inserted into A549 EVs. Only 4.3±1.4 molecules inserted into SBCy050 OMVs. The addition of 0.1 mg/ml saponin during incubation decreased the insertion into liposomes to 48.7±17.3, while increasing the insertion into OMVs to 7.6±8.1 molecules per particle (all cholesterol insertion experiments were performed as n=3). The results described here were obtained using the first, less sensitive nanosight setup, thus they can only be directly compared to the results detailed in 4.3 and not later results.
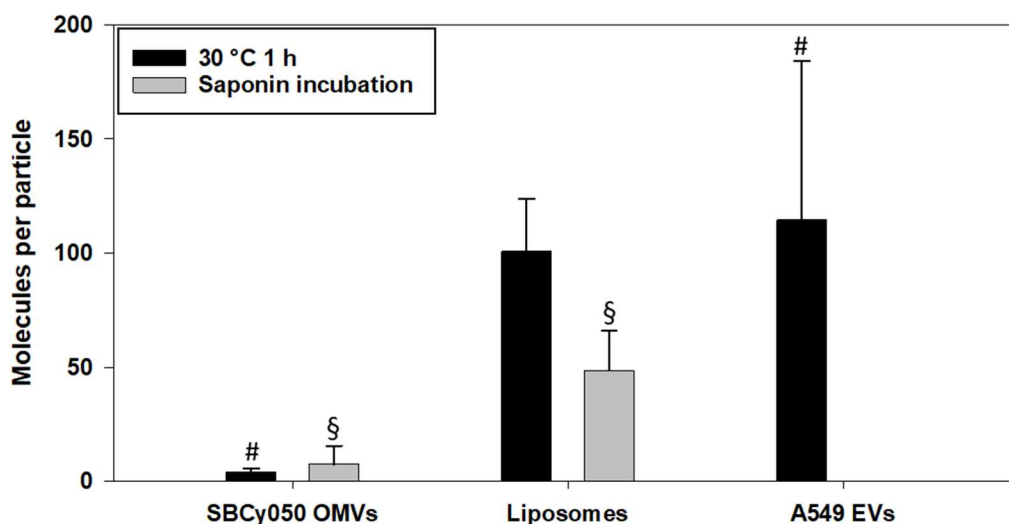
Figure 30: Inserted cholesteryl-PEG2000-FITC molecules per particle for SBCy050 OMVs, liposomes and A549 OMVs. Black bars represent samples modified by 1 h incubation at 30 °C (performed for all three), grey bars represent samples modified by 10 min incubation with 0.1 mg/ml saponin (performed for OMVs and liposomes). 30 °C 1 h: SBCy050 OMVs were significantly different from A549 EVs (p=0.044); Saponin incubation: SBCy050 OMVs were significantly different from Liposomes (p=0.020).

4.3.   OMV surface-modification with activated esters

Purified SBCy050 OMVs were modified with different concentrations of sulfo-cyanine 7 NHS ester (Figure 31). With the addition of 9.80 µM of the NHS ester, 571.7±151.7 dye molecules per particle were found on the OMVs (n=9). 546.8±163.1 dye molecules per particle were found for 4.90 µM (n=8), 470.3±135.9 for 2.45 µM (n=3) and 196.4±35.8 for 0.98 µM (n=3). The negative control containing 9.80 µM of sulfo-cyanine 7 carboxylic acid led to the recovery of 17.8±0.8 dye molecules per particle (n=3). The results described here were obtained using the first, less sensitive nanosight setup, thus they can only be directly compared to the results detailed in 4.2 and not later results.
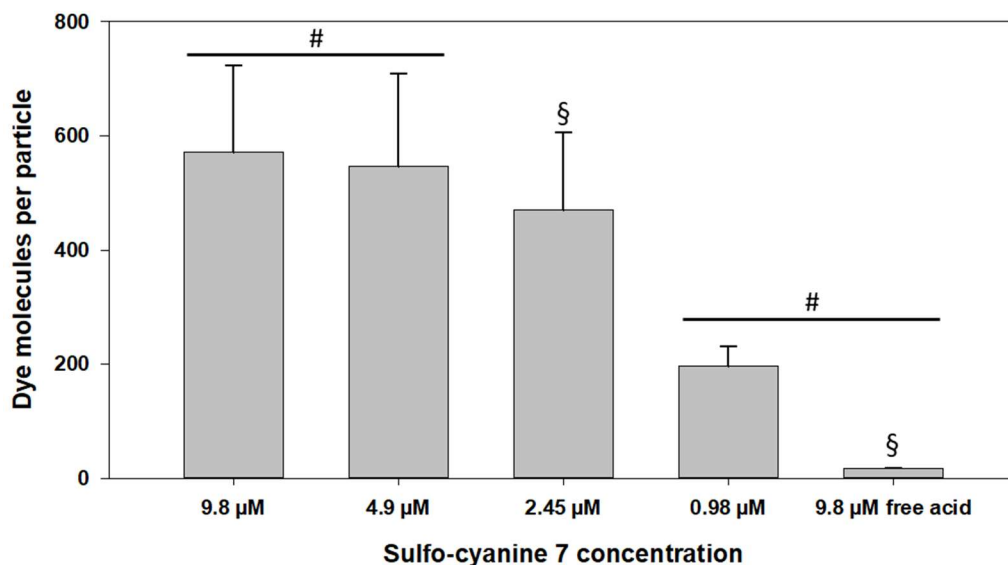
Figure 31: Dye molecules per particle for SBCy050 OMVs modified with differing concentrations of sulfo-cyanine 7 NHS ester, compared to the negative control treated with sulfo-cyanine 7 carboxylic acid (9.8 µM free acid). 9.8 µM and 4.9 µM were significantly different from 0.98 µM and 9.8 µM free acid (p≤0.010); 2.45 µM was significantly different from 9.8 µM free acid (p=0.006).

4.4.   EV surface-modification by diazotransfer

4.4.1.   Preliminary experiments

In preliminary experiments the conditions for aqueous diazotransfer described by van Dongen and coworkers were tested with SBCy050 OMV pellets (371). SBCy050 pellets were incubated with 0.588 mg/ml K_2CO_3 and 0.073 mg/ml $CuSO_4$ for 20 h. After incubation and purification 82.4% of particles were recovered compared to untreated controls (n=2). Microscopic assessment of treated samples revealed the formation of aggregates that were not present in control samples (Figure 32 A&B). Subsequently, it was assessed whether aggregates were caused by soluble proteins in the pellet or magnesium and calcium ions carried over from the 2SWC medium. Thus, either 150 µg/ml BSA, a solution of 0.125 mg/ml $CaCl_2$ and 0.25 mg/ml $MgSO_4$ or a combination of BSA, $CaCl_2$ and $MgSO_4$ were incubated for 20 h with either K_2CO_3 and $CuSO_4$ or the same amount of water. While all negative controls did not contain any aggregates, all samples containing K_2CO_3 and $CuSO_4$ contained small but morphologically similar aggregates to the SBCy050 pellet (Figure 32 C-E). After replacement of K_2CO_3 with NaOH, no formation of aggregates was visible in future experiments.
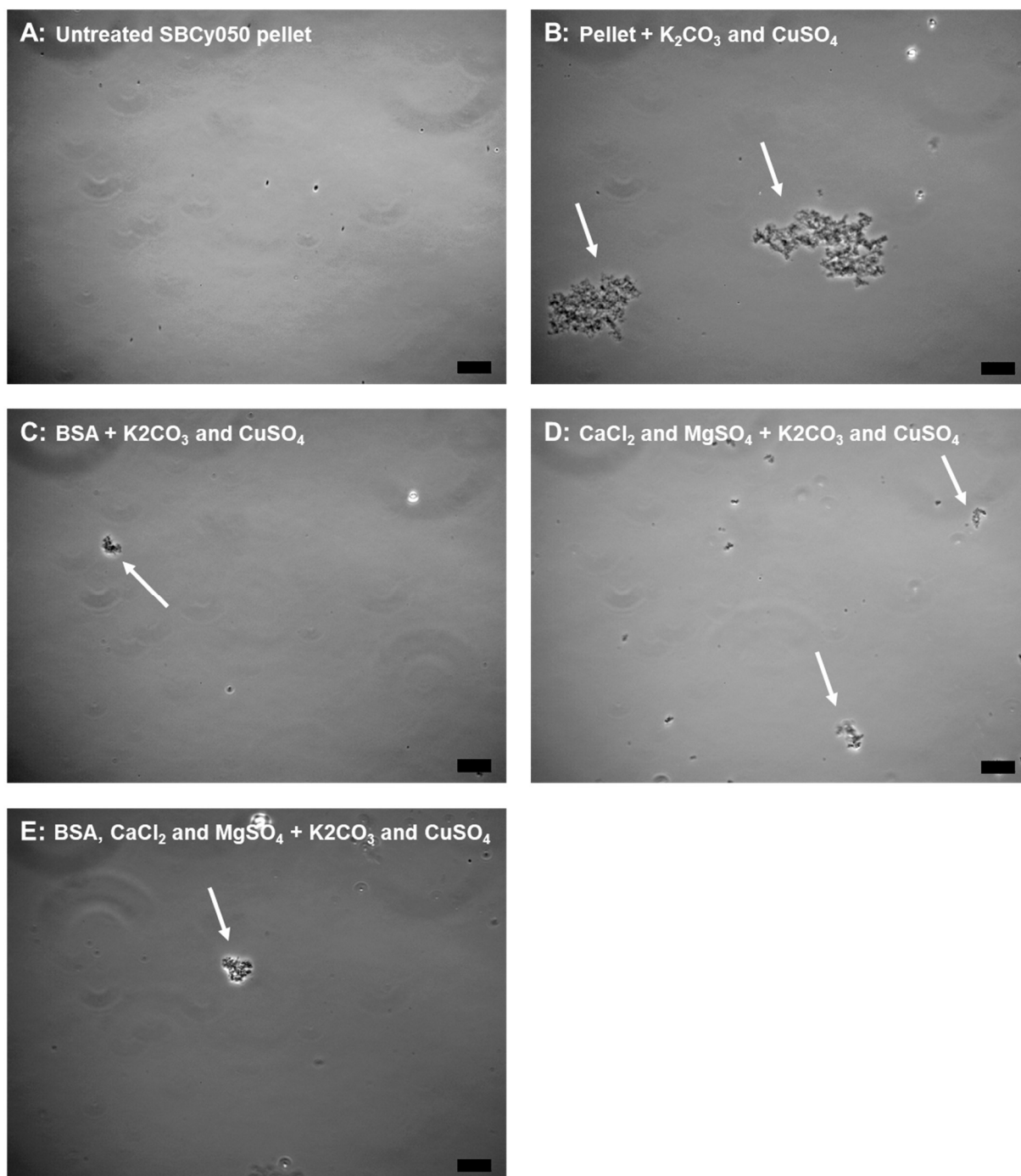
Figure 32: Light microscopy pictures of the untreated SBCy050 pellet (A) and the mixture of pellet, K2CO3 and CuSO4 (B). The aggregates found in B were compared to aggregates formed in samples containing K_2CO_3, $CuSO_4$ and either BSA (C) or $CaCl_2$ and $MgSO_4$ (D) or BSA, $CaCl_2$ and $MgSO_4$ (E). White arrows point at aggregates of similar morphology, black bar represent 20 µM.

4.4.2. Synthesis of ISA HCl

The synthesis was carried out as planned until the ultimate step of ISA-precipitation. With part of the solution precipitation as ISA hydrogen sulfate was attempted according to Potter et al. (379), however, no precipitation was observed. Thus, the remaining solution was precipitated

using 4 M HCl in dioxane and ISA HCl was successfully isolated as clear crystals. In total, 355 mg of ISA HCl were obtained (22.0%). The identity of ISA was confirmed by NMR and FTIR. FTIR revealed a characteristic band for azide at 2125 cm^{-1}. 1H NMR (500 MHz, D2O): 9.17 (s, 1H), 8.06 – 7.92 (m, 1H), 7.57 – 7.51 (m, 1H).

4.4.3. Diazotransfer optimization

Different diazotransfer conditions were evaluated using DBCO AF594 to assess the amount of introduced azide groups. The suitability of DBCO AF594 was tested by injecting the dye dissolved in PBS at 4.9 µM onto the SEC column. No elution of the dye in the fractions usually containing OMVs was measured (Supp. figure 3 A&B). To allow the determination of reacted dye molecules per particle, a calibration curve of DBCO AF594 was created (Supp. figure 4 A).

Preliminary experiments showed an increase in dye-molecules per particle of 140% for increasing the pH from 7.3 to 9.4 (n=3-4) and an increase of 28% for reducing incubation time from 20 h to 4 h (n=2-4). Thus, the effect of pH and incubation time on modification efficiency and OMV stability were systematically evaluated with 30 min incubation time and varying pH and pH 9.5 and varying incubation times respectively.
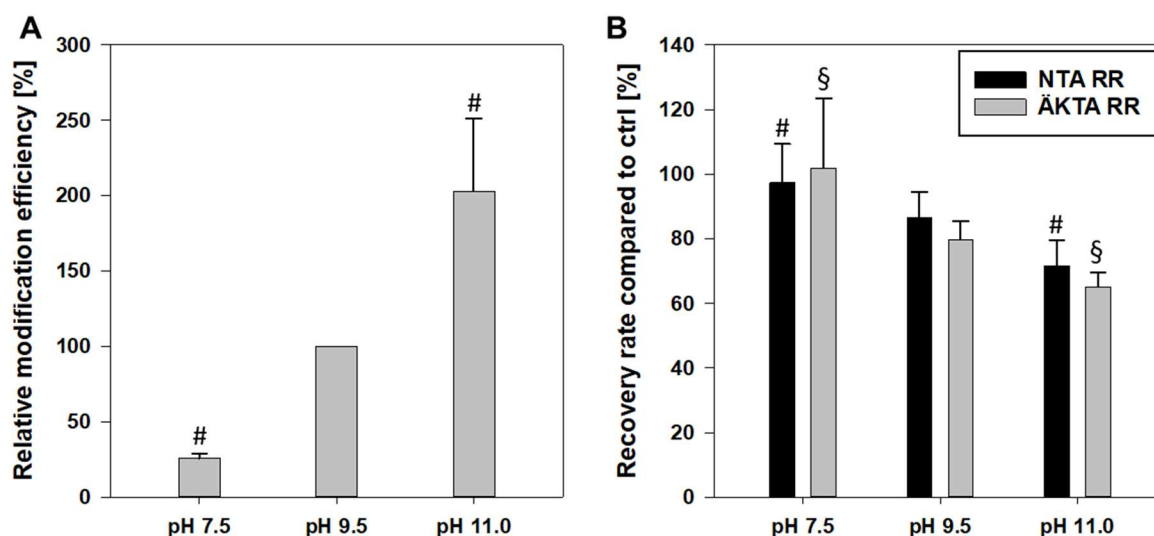
Figure 33: SBCy050 pellets were subjected to diazotransfer for 30 min at different pH values. The modification efficiency was plotted relative to pH9.5 (A) and OMV-stability was evaluated by NTA and ÄKTA AUC and compared to untreated control OMVs (B). A: pH 7.5 was significantly different from pH 11.0 (p<0.001); B: NTA RR: pH 7.5 was significantly different from pH 11.0 (p=0.027); ÄKTA RR: pH 7.5 was significantly different from pH 11.0 (p=0.016).

Increasing of the incubation pH led to a higher modification efficiency (Figure 33). Compared to pH 9.5 (n=4) only 25.7±3.2% of the surface modification was reached at pH 7.5 (n=3), while the modification efficiency was increased to 204.0±46.6% at pH 11.0 (n=3). Regarding OMV

stability, increasing the pH led to a decrease in recovery rates compared to untreated OMVs. At pH 7.5 97.4±11.9% of particles and 100.1±15.5% of the ÄKTA AUC were recovered (n=3). This decreased to 86.7±7.7% particle and 79.8±5.7% AUC recovery at pH 9.5 (n=4) and 71.8±7.8% particle and 65.1±4.4% AUC recovery at pH 11 (n=3).
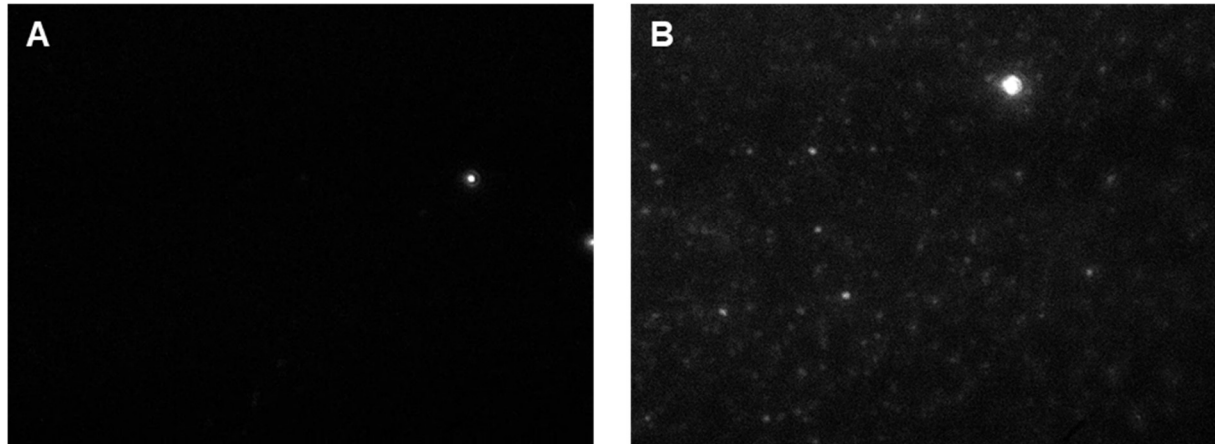
Figure 34: Representative frames from NTA-videos of SBCy050 OMVs treated with diazotransfer at pH 7.5 (A) or pH 9.5 (B) followed by SPAAC with DBCO AF594. Samples were measured in the fluorescence mode of the NTA instrument.

Differences in modification efficiency were also qualitatively visible in the fluorescence mode of the NTA. Figure 34 shows the comparison between representative frames taken from videos captured of diazotransfer followed by SPAAC at either pH 7.5 (A) or pH 9.5 (B). To increase visibility, these measurements were taken using the highest camera level. Injection of the pure AF594 dye dissolved in PBS did not show particles (data not shown).
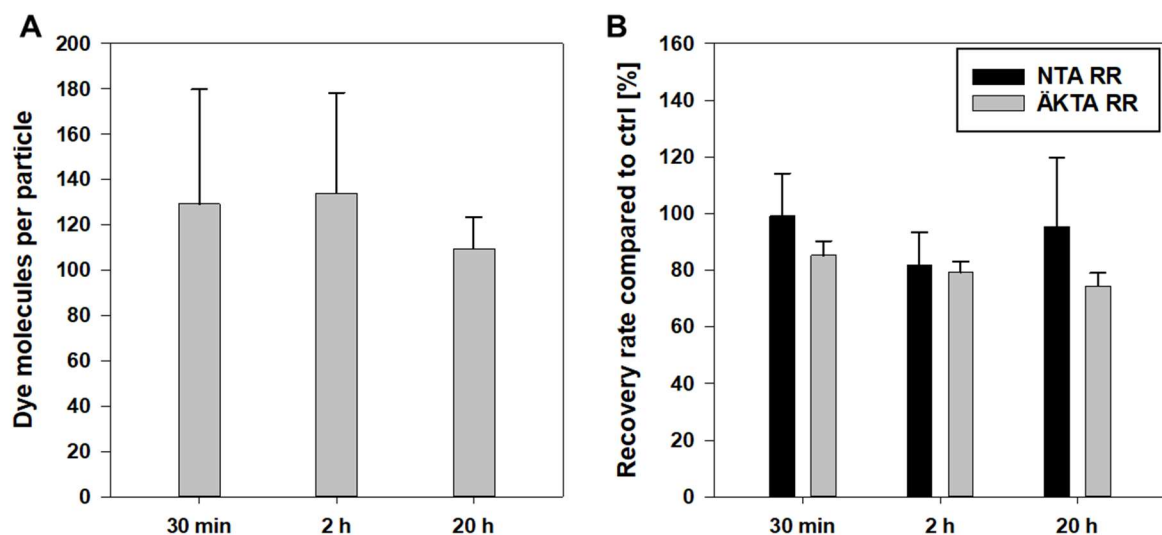
Figure 35: SBCy050 pellets were subjected to diazotransfer at pH 9.5 with differing incubation times. The modification efficiency was compared for 30 min, 2 h and 20 h incubation (A). OMV-stability was evaluated by NTA and ÄKTA AUC relative to untreated control OMVs (B).

Decreasing the incubation time from 20 h to 2 h and to 30 min did not lead to a decrease in modification efficiency and slightly increased recovery rates (Figure 35). At 30 min incubation time 129.2±50.6 dye molecules per particle reacted with OMVs (n=5), 2 h incubation resulted in 134.1±44.2 dye molecules per particle (n=3) and 20 h incubation led to 109.6±13.8 dye molecules per particle (n=3). With 30 min incubation, 99.1±15.1% of particles and 85.3±5.0% of the ÄKTA AUC were recovered compared to untreated control OMVs (n=6). These values decreased to 81.8±11.6% particle and 79.3±3.8% AUC recovery with 2 h incubation time (n=3) and 95.4±24.4% particle and 74.5±4.7% AUC recovery with 20 h incubation time (n=3).
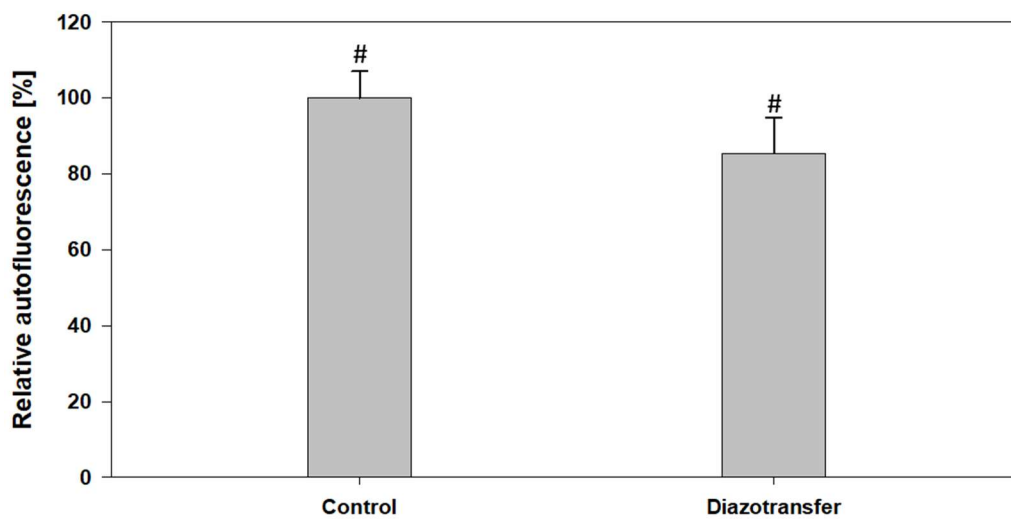
Figure 36: The autofluorescence of SBCy050 OMVs modified by diazotransfer at pH 9.5 for 30 min and purified by SEC was compared to purified untreated control OMVs. Diazotransfer was significantly different from Control (p=0.025).

The effect of diazotransfer conditions was further evaluated by comparing the autofluorescence of OMVs subjected to diazotransfer for 30 min at pH 9.5 with untreated controls (Figure 36). The diazotransfer conditions led to a decrease of the autofluorescence to 85.4±9.4% (n=5).
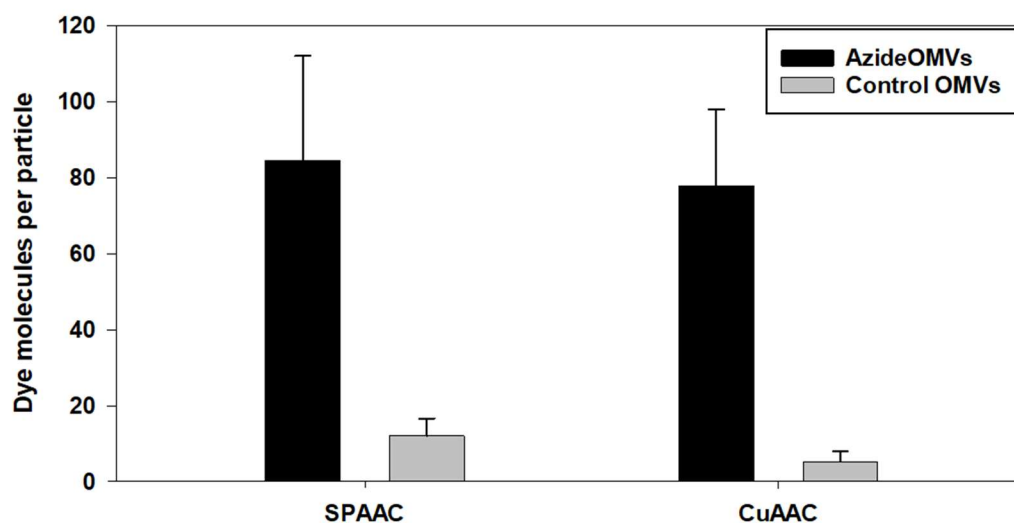
Figure 37: Unspecific binding of DBCO AF594 (SPAAC) and Alkyne AF594 (CuAAC) to control OMVs (grey bars) compared to the reaction with AzideOMVs (black bars). Respective control values were significantly different from AzideOMV samples (p≤0.003).

To rule out that the observed bound dye per particle was solely or to a large degree caused by unspecific interaction of the dye with the vesicles, the labeling of untreated OMVs was compared to azide OMVs (Figure 37). For DBCO AF594 an unspecific labeling of 12.2±4.5 molecules per particle was found (n=3), compared to 84.7±27.4 molecules per particle for AzideOMVs (n=5).

As copper has cytotoxic effects and its divalent cations might be able to intercalate into the LPS of OMVs, the copper-content of OMVs subjected to diazotransfer was measured. OMVs subjected to diazotransfer for 30 min at pH 9.5, untreated OMVs and a control containing SEC fractions obtained from the injection of pure PBS were treated with 0.3% triton X, then filtered through a 0.2 µM filter and the copper content was measured by ICP-MS. The treated sample contained 6.2 ng/ml copper, untreated OMVs contained 3.5 ng/ml and the PBS control contained 2.6 ng/ml. For the calibration curve of the measurement, see Supp. figure 5.
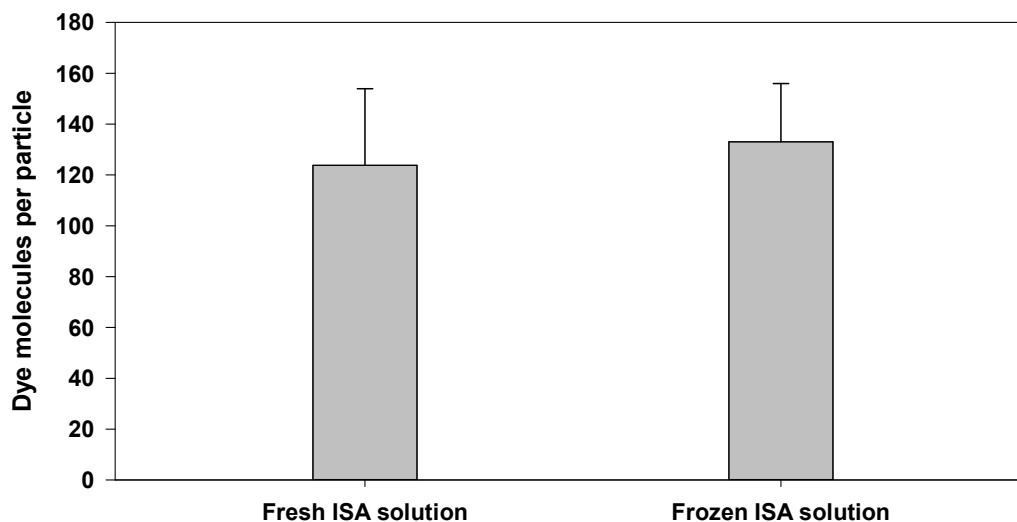
Figure 38: Comparison of the modification efficiency of diazotransfer performed using fresh ISA solution or ISA solution stored at -80 °C for up to 3 months.

Finally, the difference between freshly prepared aqueous solutions of ISA and aliquots that were prepared in advance and stored at -80 °C for up to 3 months was evaluated (Figure 38). Fresh ISA solutions led to 123.8±30.1 dye molecules per particle, while frozen ISA aliquots led to 133.0± 22.2 dye molecules per particle, no significant difference was found between both groups (n=6).

4.4.4.   Comparison of modification with activated ester and diazotransfer

The modification efficiency achieved by diazotransfer and SPAAC was directly compared with surface modification with sulfo-cyanine 7 NHS ester (Figure 39). While treating purified OMVs with 4.9 µM sulfo-cyanine 7 NHS ester led to 206.5±20.2 dye molecules per particle, treating the pellet directly after UC with 4.9 µM sulfo-cyanine 7 NHS ester only led to 40.4±13.3 dye molecules per particle. Increasing the sulfo-cyanine 7 NHS ester concentration to 49 µM increased the surface modification to 103.2±12.2 dye molecules per particle. Diazotransfer and SPAAC led to 142.0±11.2 dye molecules per particle (all experiments n=3).
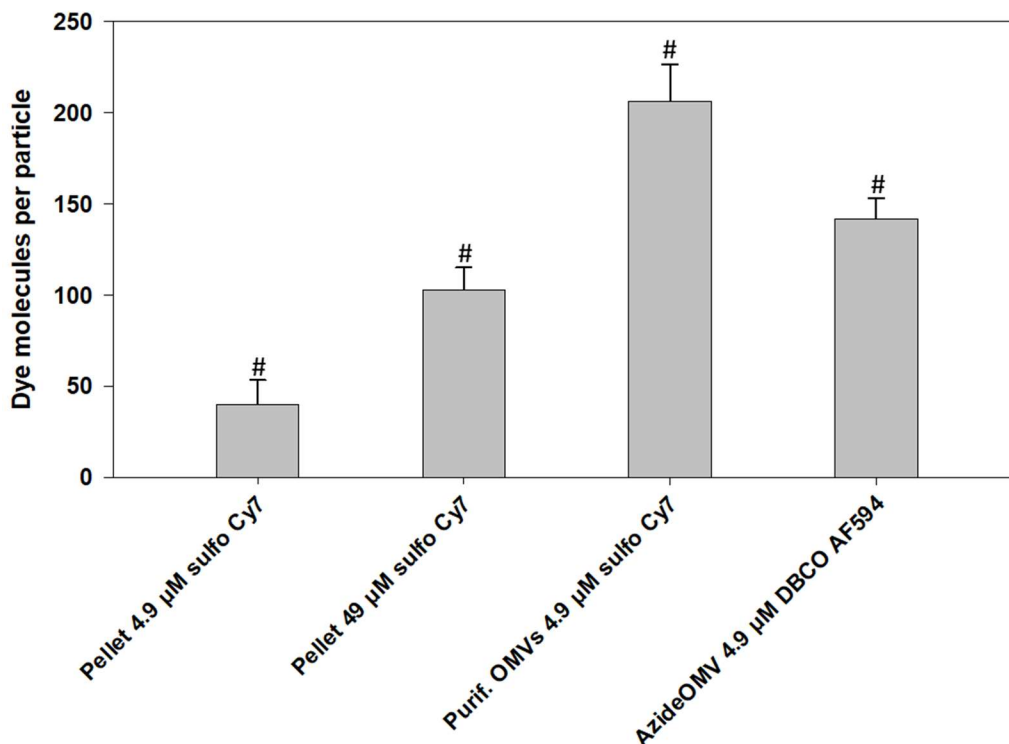
Figure 39: Modification efficiency for the SBCy050 pellet modified with either 4.9 or 49 µM sulfo-cyanine 7 NHS ester, purified OMVs modified with 4.9 µM sulfo-cyanine 7 NHS ester or OMVs treated with diazotransfer and modified by SPAAC. All values showed statistically significant differences from all other values (p≤0.003).

4.5. Introduction of targeting moieties by SPAAC

4.5.1. Synthesis of methyltetrazine vancomycin

The synthesis of methyltetrazine vancomycin was carried out as described in 3.6.6.2. The reaction yielded 2.96 mg of a deeply magenta colored solid (7.0%). During prepHPLC, methyltetrazine vancomycin eluted between 19.7 and 20.9 min corresponding to a concentration of 23-24% ACN. The purified molecule was characterized by LC/MS (Supp. figure 6) and HRMS, dissolved in dry DMSO at 2.45 nmol/µl and aliquoted in 1 µl aliquots. HRMS (ESI) calculated for $C_{77}H_{84}Cl_2N_{13}O_{25}$ [M+H]$^+$: 1660.5073, found: 1660.5072.

4.5.2. Synthesis and implementation of the SPAAC-based linker

The synthesis of the SPAAC-based linker was carried out as described in 0. In the crude product, there were two major peaks with absorption at 646 nm (Supp. figure 7). The peak at 3.69 min was identified as the SPAAC-based linker according to the detected masses of 912.0 and 608.4 m/z that corresponded to the [M+H]$^{2+}$ and [M+2H]$^{3+}$ ions respectively (calculated

from $C_{104}H_{132}N_{11}O_{18}^{+}$). The peak at 3.36 min showed masses of 818.3 and 546.2 m/z corresponding to the $[M+H]^{2+}$ and $[M+2H]^{3+}$ ions of the putative degradation-product without the DBCO-group (calculated from $C_{89}H_{122}N_{10}O_{19}^{+}$) (Figure 40).

SPAAC-based linker

Putative degradation-product
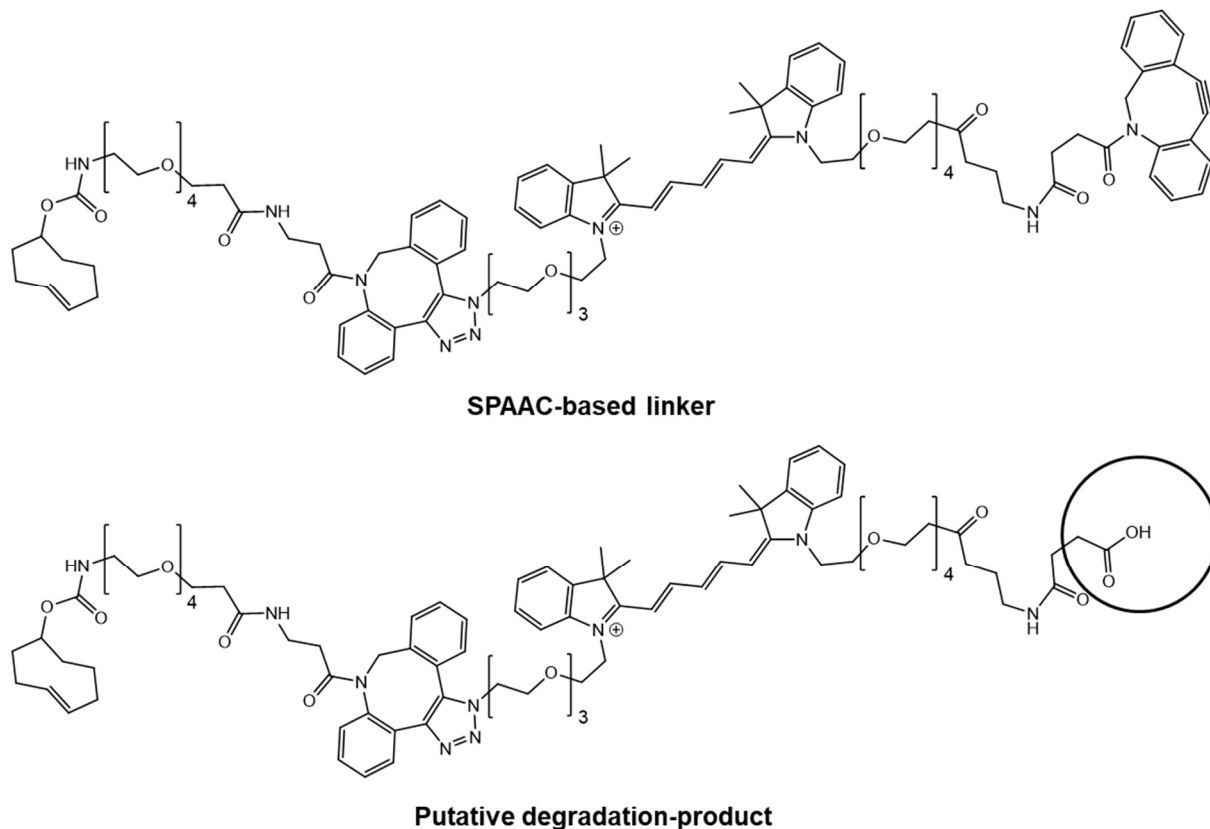
Figure 40: Structure of the SPAAC-based linker and the putative degradation-product lacking the DBCO-group.

The crude mixture was purified by prepHPLC. The SPAAC-based linker eluted between 32 and 34 min corresponding to a concentration of 62-66% ACN. Analysis of the prepHPLC-fractions indicated the presence of this side product in all fractions that contained the linker molecule. Thus, the fractions with the highest ratio of SPAAC-based linker to side-product were collected and lyophilized. A yield of 0.31 mg (7.7%) of the SPAAC-based linker was obtained, LC/MS-analysis however indicated the presence of the beforehand identified side-product in a higher ratio than suggested by the prepHPLC-fractions. To assess the effect LC/MS-analysis had on the molecule, the duration of the LC/MS method was increased to 25 min with proportional adjustment of the solvent-gradient (Supp. figure 8). The longer method led to an increase of the peak-area of the degradation product and the ratio of SPAAC-based linker to degradation product decreased from 0.84 to 0.30. The purified compound was dissolved in at 2.45 nmol/µl and aliquoted in 1 µl aliquots. The SPAAC-based linker was characterized by HRMS. HRMS (ESI): Calculated for $C_{104}H_{132}N_{11}O_{18}^{+}$ $[M]^{+}$: 1822.9747, found: 1822.9750.
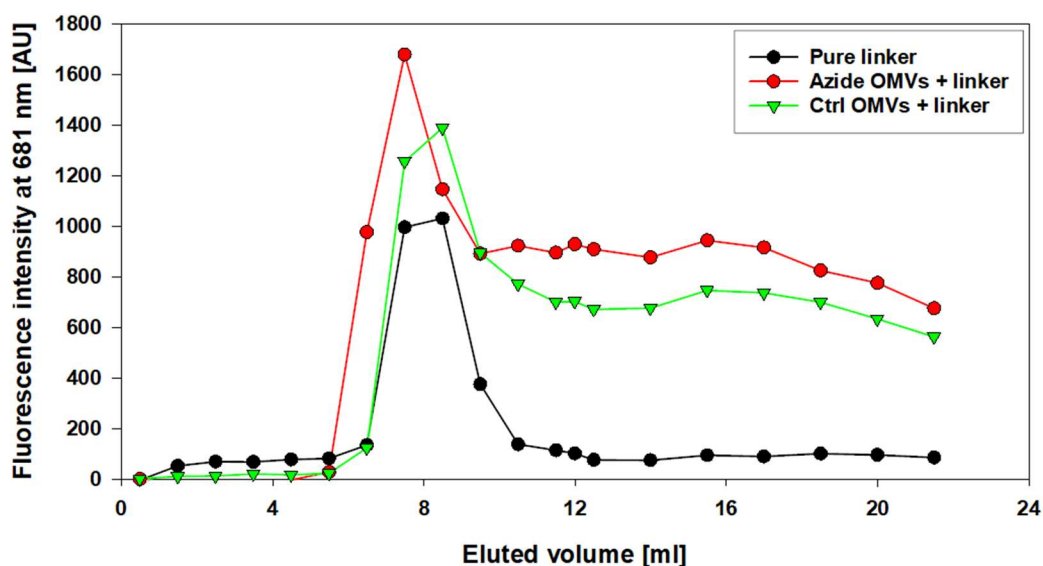
Figure 41: Elution profile of the SPAAC-based linker either dissolved in PBS (black) or mixed with AzideOMVs (red) or control OMVs (green) and incubated for 20 h. The y-axis displays the fluorescence of cyanine 5.

The pure linker molecule was mixed with a final concentration of 4.9 µM with 500 µl of either PBS, AzideOMVs or untreated ctrl OMVs and after 20 h incubation samples were subjected to SEC-purification. As Figure 41 shows, there was a high elution of free linker at the same time as OMVs eluted, thus affecting the determination of bound molecules per particle.

The linker molecule was reacted with methyltetrazine-vancomycin by mixing of one aliquot linker and one aliquot of methyltetrazine vancomycin as described in 3.6.6.3. LC-MS indicated that both the SPAAC-based linker as well as the side-product reacted with methyltetrazine vancomycin and formed two products with 3454.47 da ([M+3H]$^{4+}$ ion identified at 861.3 m/z, calculated from: $C_{181}H_{215}Cl_2N_{22}O_{43}^+$) and 3267.39 da ([M+3H]$^{4+}$ ion identified at 817.8 m/z, calculated from: $C_{166}H_{206}Cl_2N_{21}O_{44}^+$) (Supp. figure 9 & Supp. figure 10). The UV absorption at 649 nm indicated the formation of three peaks per compound with the same mass that were not differentiated in the mass-chromatogram. The IEDDA-product of the linker was confirmed by HRMS. HRMS: Calculated for $C_{181}H_{215}Cl_2N_{22}O_{43}^+$ [M+2H]$^{3+}$: 1152.1610, found: 1152.1586.
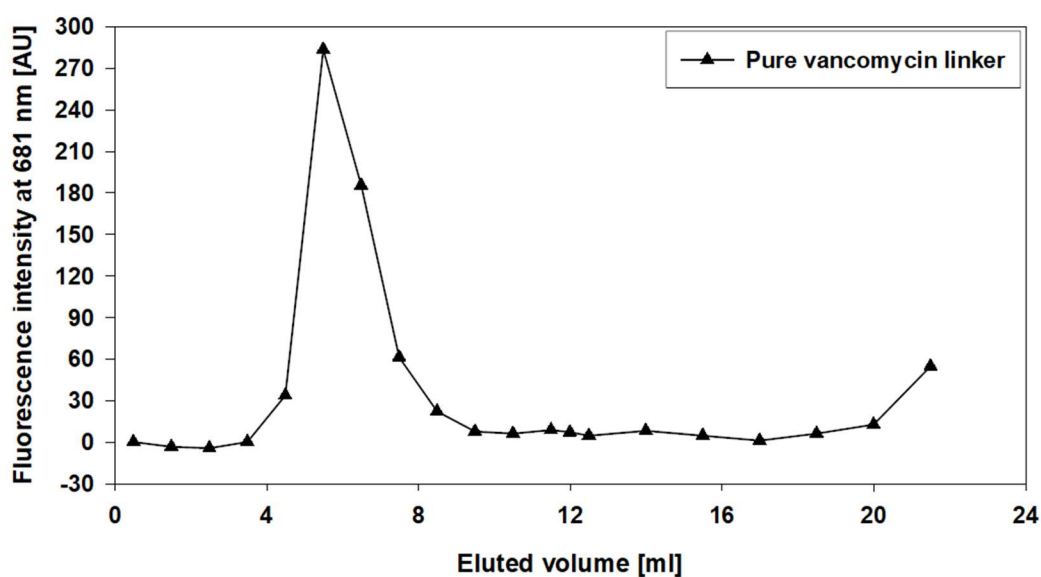
Figure 42: Elution profile of the conjugate of the SPAAC-based linker with methyltetrazine-vancomycin dissolved in PBS. The y-axis displays the fluorescence of cyanine 5.

The effect of the conjugation of vancomycin was tested by dissolving the conjugate at 4.9 µM in PBS and subjecting it to SEC. As Figure 42 shows, there was again an early elution of the linker, indicating its insufficient solubility. Thus, it was decided to develop a new linker molecule based on CuAAC.

4.6. CuAAC with SBCy050 OMVs

To allow the determination of reacted dye molecules per particle, a calibration curve of alkyne AF594 was created (Supp. figure 4 B).

In preliminary experiments, CuAAC was performed according to the protocol of Hong et al. by first mixing CuSO4 with THPTA (340). This was added to a mixture of alkyne AF594 and AzideOMVs and the CuAAC reaction was initiated by addition of sodium ascorbate (340). Using 4.9 µM of alkyne AF594, 11.5% of the modification efficiency of SPAAC with 4.9 µM DBCO AF594 was reached (n=2). Increasing the alkyne Af594 concentration to 19.6 µM increased the modification efficiency to 32.4% (n=2).

In following experiments 19.6 µM of alkyne were used and the protocol was changed to the protocol described in 3.6.7. The suitability of alkyne AF594 for SEC-purification at this concentration was tested by injecting the dye dissolved in PBS at 19.6 µM to the SEC column. No elution of the dye in the fractions usually containing OMVs was measured (Supp. figure 3 C&D). Cu(I) ions were generated by mixing of CuSO4 and sodium ascorbate. This solution was added to the mixture of THPTA and alkyne AF594. The resulting mixture was added to AzideOMVs. Different conditions for CuAAC were tested and compared to SPAAC (Figure 43).

Sodium ascorbate was either dissolved in water or in 40 mg/ml NaOH. In the latter case the incubation time was either 2 h or 4 h. SPAAC led to 84.7±27.4 dye molecules per particle (n=5), 2 h incubation with addition of NaOH to 60.1±13.2 (n=3), 4 h incubation with addition of NaOH to 77.9±20.1 (n=5) and 4 h incubation without NaOH to 41.1±4.9 (n=4). Compared to SPAAC, CuAAC for 2 h with the addition of NaOH led to a particle recovery of 92.8±19.0% (n=3) and an AUC of 98.4% (n=2), 4 h incubation with NaOH-addition led to a particle recovery of 79.1±12.3% (n=4) and an AUC of 90.8±5.1% (n=3). 4 h incubation without the addition of NaOH led to the recovery to 95.4±4.0% of particles (n=4) and an AUC of 99.9±10.9% (n=3). Following these results, CuAAC was performed with 4 h incubation and sodium ascorbate dissolved in 40 mg/ml NaOH.
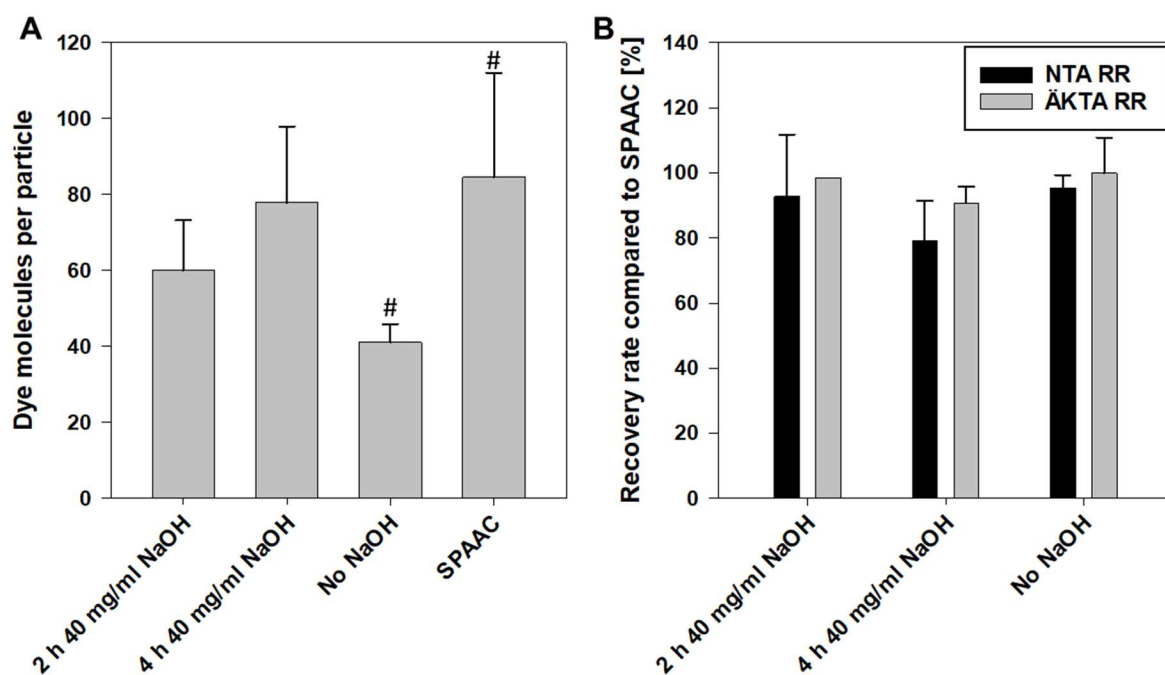
Figure 43: Evaluation of CuAAC-modification of SBCy050 OMVs. In panel A, the modification efficiency of CuAAC performed with ascorbic acid dissolved in 40 mg/ml NaOH (either 2 h or 4 h CuAAC-reaction time) or dissolved in water was compared with SPAAC. In Panel B, the OMV-stability during CuAAC was evaluated relative to SPAAC. A: No NaOH was significantly different from SPAAC (p=0.026).

The copper-content after SEC of OMVs subjected to CuAAC was assessed by ICP-MS. OMVs subjected to CuAAC, untreated OMVs and a control containing SEC fractions obtained from the injection of pure PBS were treated with 0.3% triton X, then filtered through a 0.2 µM filter and the copper content was measured. The treated sample contained 1.6 ng/ml copper, untreated OMVs contained 3.6 ng/ml and the PBS control contained 1.9 ng/ml. For the calibration curve of the measurement, see Supp. figure 5.

The effect of CuAAC on the autofluorescence of SBCy050 OMVs was evaluated by comparing SPAAC to CuAAC with the respective AF594 derivative. CuAAC led to the reduction of the

autofluorescence to 7.8±3.5% of the fluorescence intensity measured for OMVs treated with SPAAC (n=4). Omitting NaOH, as it was later tried for the modification with the IEDDA-product of the PEG$_6$-linker and methyltetrazine-vancomycin, approximately doubled the remaining fluorescence after CuAAC compared to the standard protocol (increase by a factor of 1.9±0.6, n=3).

The unspecific labeling of untreated control OMVs was evaluated in the same manner as for DBCO AF594 (see 4.4.3). An unspecific labeling of control OMVs with 5.3±2.8 molecules per particle was measured (n=3), compared to 77.9±20.1 molecules per particle for AzideOMVs treated in the same way (n=5) (Figure 37).

4.6.1. Synthesis and testing of the PEG$_8$-linker for CuAAC

The synthesis of the PEG$_8$-linker was carried out according to 0. The Boc-protected intermediate was obtained by prepHPLC with a yield of 120.8 mg (89.8%), it eluted between 18.0 and 20.8 min corresponding to a concentration of 63-73% ACN. Its purity was confirmed by LC/MS (Supp. figure 11) and the molecule was characterized by NMR. ^{1}H NMR (500 MHz, DMSO-d_6): 5.72-5.51 (m, 1H), 5.45-5.36 (m, 1H), 4.17 (dd, J=11.73, 5.53, 1H), 4.05 (dt, J=12.49, 5.62, 2H), 3.49-3.44 (m, 28H), 3.41-3.32 (m, 6H), 3.26-3.11 (m, 3H), 3.11-3.01 (m, 2H), 2.77 (t, J=2.25, 1H), 2.48 (dd, J=5.31, 2.54, 1H), 2.38 (ddd, 16.79, 8.46, 2.5, 1H), 2.31-2.16 (m, 3H), 1.92-1.82 (m, 3H), 1.65-1.40 (m, 5H), 1.36 (s, 12H) (Supp. figure 12). ^{13}C NMR (126 MHz DMSO-d_6): 170.8, 156.3, 156.3, 155.5, 135.3, 132.9, 130.0, 129.9, 81.1, 79.6, 78.9, 74.9, 73.1, 70.1, 70.0, 69.9, 69.8, 69.4, 69.1, 53.4, 41.0, 40.3, 38.5, 34.1, 34.0, 32.5, 30.9, 28.4, 25.5, 24.9, 22.3, 22.2 (Supp. figure 13).

Some problems were encountered during Boc-deprotection. While in the test-experiment for the Boc-deprotection only a small amount of a side-product was generated, the deprotection of the main amount of the Boc-protected intermediate led to the generation of significant amounts of a side-product (Supp. figure 14 & Supp. figure 15). In LC/MS-analysis a molecule with a mass of 254.9 eluting at 1.36 min was detected, corresponding with the [M+2H]$^{2+}$ ion of the putative byproduct 1 lacking the TCO group (calculated from $C_{23}H_{45}N_3O_9$) (Figure 44 A). The side product however was only identified later and it was not removed from the deprotected intermediate before the next reaction step.

According to 0, 26 mg of the deprotected intermediate were reacted with 25 mg of sulfo-cyanine 5 NHS ester and LC/MS analysis of the crude product of the reaction with sulfo cyanine 5 NHS ester revealed the presence of multiple compounds with absorbance at 646 nm (Supp. figure 16 & Supp. figure 17). The compound eluting at 2.84 min was identified as the PEG$_8$-linker with a mass of 640.9 corresponding to its [M+ACN-2H]$^{2-}$ ion (calculated from

$C_{62}H_{89}N_5O_{17}S_2$). The compound eluting at 2.13 min showed a mass of 564.7 corresponding to the $[M-2H]^{2-}$ ion of putative byproduct 2.1 (calculated from $C_{55}H_{81}N_5O_{16}S_2$), the compound eluting at 2.49 min showed a mass of 877.0, corresponding to the $[M-2H]^{2-}$ ion of putative byproduct 2.2 (calculated from $C_{87}H_{117}N_7O_{23}S_4$) (Figure 44 B).

The crude product was purified by prepHPLC and eluted between 15 and 19.2 min corresponding to a concentration of 53-68% ACN. Lyophilisation yielded 11.5 mg (26.8%) of a dark blue powder, part of which was dissolved in dry DMSO at 9.78 nmol/μl and aliquoted in 1 μl aliquots. The purified product was characterized by HRMS and NMR and its purity confirmed by LC/MS (Supp. figure 18) The HRMS-measurement of the PEG$_8$-linker was inconclusive and the compound could not be identified. ^{1}H NMR (500 MHz, DMSO-d_6): 8.36 (t, J=13.06, 2H), 8.09-8.03 (m, 2H), 7.81 (s, 2H), 7.63 (ddd, J=8.16, 5.18, 1.53, 2H), 7.31 (dd, J=8.31, 2.60, 2H), 7.04-6.97 (m, 1H), 6.57 (t, J=12.24, 1H), 6.29 (dd, J=24.73, 13.81, 2H), 5.74-5.53 (m, 2H), 4.62-4.52 (m, 1H), 4.39 (dd, J=14.14, 8.08, 1H), 4.07 (t, J=6.56, 2H), 3.75-3.63 (m, 4H), 3.63-3.56 (m, 5H), 3.42-3.30 (m, 30H), 3.27-3.13 (m, 3H), 3.12-3.05 (m, 2H), 2.83 (t, J=2.56, 1H), 2.39 (ddd, J=16.23, 8.00, 2.45, 1H), 2.34-2.23 (m, 1H), 2.21-2.07 (m, 4H), 2.07-1.93 (m, 2H), 1.91-1.73 (m, 3H), 1.69 (s, 12H), 1.64-1.40 (m, 7H), 1.39-1.28 (m, 3H), 1.28-1.19 (m, 5H), 0.90-0.78 (m, 1H) (Supp. figure 19). ^{13}C NMR (126 MHz DMSO-d_6): 173.6, 172.8, 172.0, 170.0, 154.2, 145.3, 145.2, 142.7, 142.0, 140.5, 140.4, 129.6, 129.5, 126.0, 126.0, 125.9, 125.63, 119.95, 119.9, 110.1, 110.0, 103.6, 103.3, 101.3, 94.7, 80.7, 74.4, 73.5, 72.8, 72.3, 70.5, 69.8, 69.6, 69.5, 69.1, 68.8, 66.3, 65.6, 60.2, 51.3, 48.9, 43.6, 43.4, 38.6, 34.8, 33.8, 33.7, 31.2, 29.0, 28.7, 27.1, 26.9, 26.6, 25.6, 25.1, 24.8, 24.6, 22.1, 22.0, 21.9, 21.2, 20.5, 20.0, 14.0 (Supp. figure 20).

A
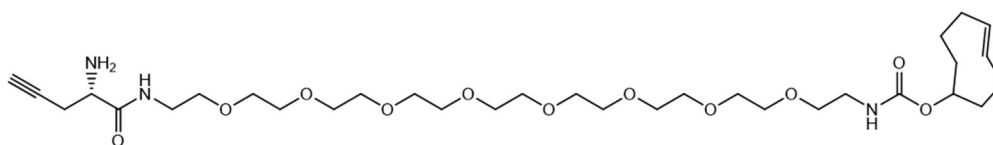
Deprotected intermediate
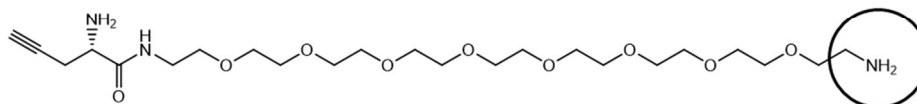
Putative byproduct 1

B
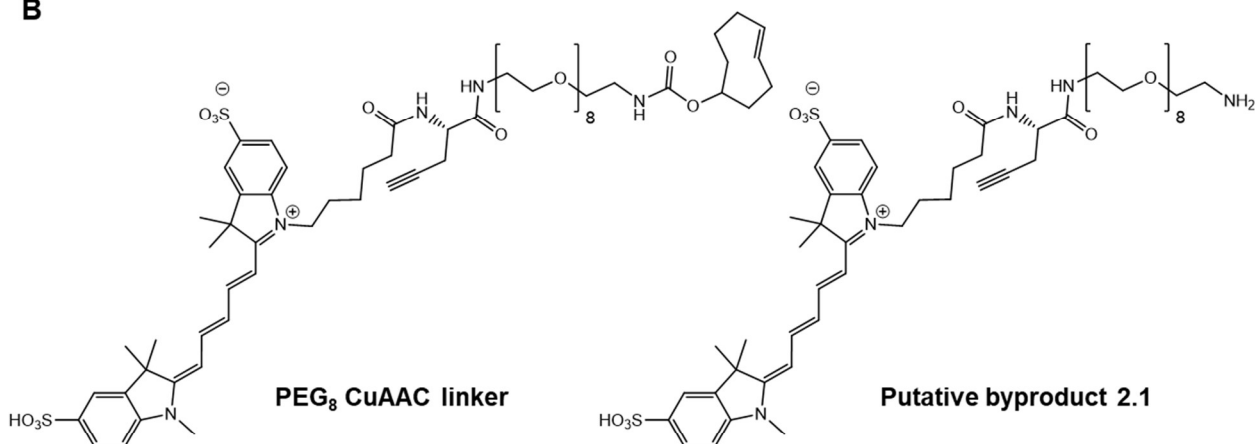
PEG₈ CuAAC linker

Putative byproduct 2.1
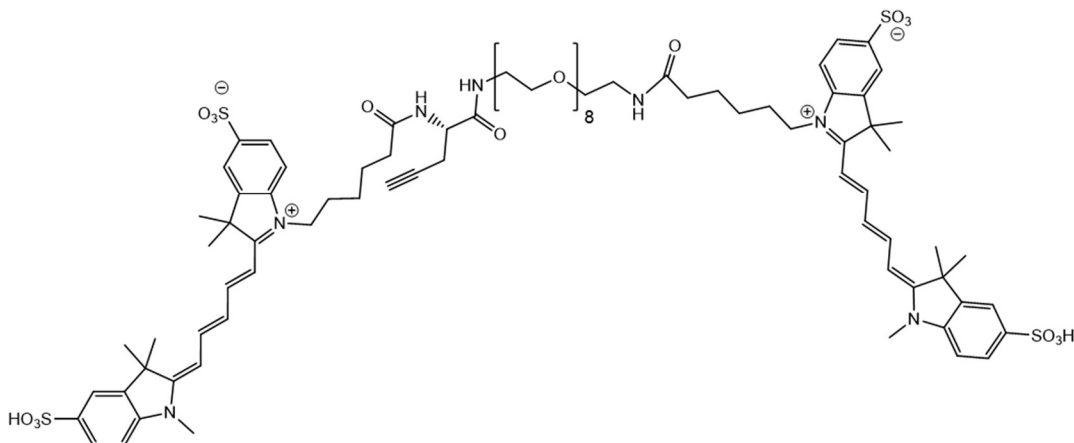
Putative byproduct 2.2

Figure 44: A shows the deprotected intermediate of the PEG₈-linker and the putative byproduct that lost the TCO-group. B displays the finished PEG₈-linker compared to putative byproducts that would result from the reaction of sulfo-cyanine 5 NHS ester with putative byproduct 1.

After the synthesis of the PEG₈ CuAAC linker, its solubility was tested by dissolving the linker at 19.6 µM in PBS and performing an SEC. The solubility of the molecule was deemed sufficient as only little early elution of the PEG₈-linker was visible (Supp. figure 21 A&B).

Next the PEG$_8$-linker was coupled to AzideOMVs by CuAAC. To assess unspecific labeling, control OMVs were treated in the same way. AzideOMVs reacted with 356.0 molecules per particle, while 47.8 molecules did bind unspecifically in control experiments (n=2) (For the calibration curve of the PEG$_8$-linker see Supp. figure 4 C). Due to the inactivity of the PEG$_8$-linker in IEDDA experiments, no further experiments were conducted.
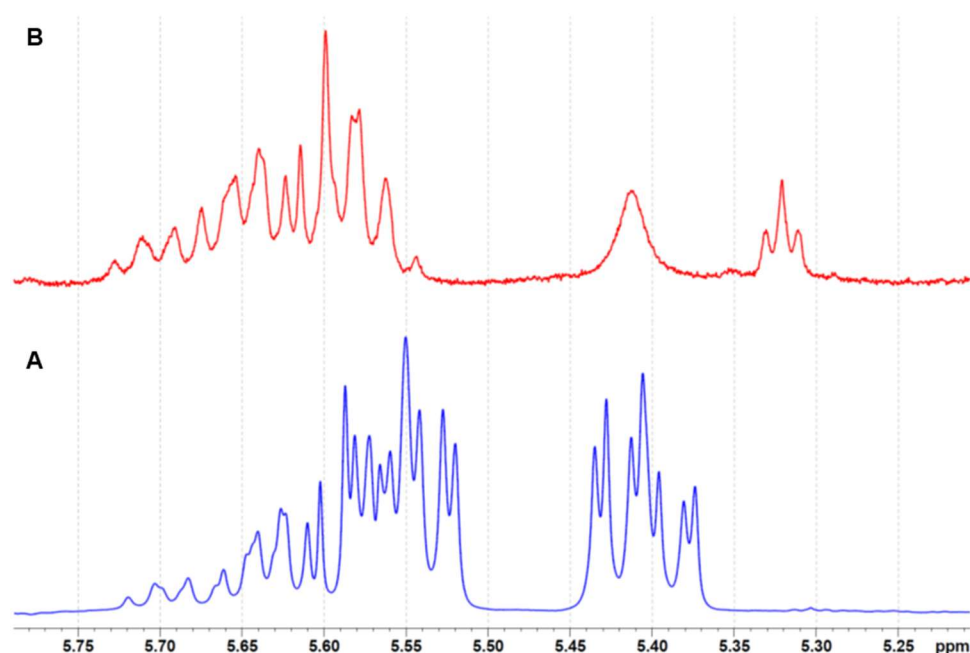
Figure 45: Zoomed view of the ^{1}H-NMR spectra containing the signals of the protons belonging to the alkene-group of cyclooctene. Boc-protected intermediate (A, blue) and the PEG$_8$-linker (B, red).

The PEG$_8$-linker did not show any reactivity towards methyltetrazine-vancomycin, as only the educts were visible, even after leaving both compounds to react overnight (Supp. figure 22). In comparison, the Boc-protected intermediate clearly showed reactivity towards methyltetrazine-vancomycin as indicated by the disappearance of the peak at 2.24 min and the emergence of three new peaks at 2.56, 2.80 and 2.85 min (Supp. figure 23). Comparison of the region of the respective ^{1}H-NMR spectra containing the two alkene-protons revealed a change in the spectra that might coincide with the inactivation of the TCO-group (Figure 45).

Due to these results, it was decided to change the protection group of the amine and employ Fmoc propargyl glycine in the next synthesis attempt.

4.6.2. Synthesis of the PEG$_6$-linker for CuAAC

The synthesis of the PEG$_6$-linker was carried out according to 3.6.7.2. Complete conversion of the starting material to the Fmoc-protected intermediate and its purification were confirmed by LC/MS (Supp. figure 24) and the molecule was characterized by HRMS and NMR. During

prepHPLC-purification, the Fmoc-protected intermediate eluted between 22.1 and 23.9 min corresponding with a concentration of 78-84% ACN. The yield was 62.7 mg (75.3%). HRMS (ESI): Calculated for $C_{43}H_{60}N_3O_{11}$ $[M+H]^+$: 794.4223, found: 794.4219. ^{1}H NMR (700 MHz, CDCl$_3$): 7.75 (d, J=7.56, 2H), 7.58 (d, J=7.07, 2H), 7.38 (t, J=7.46, 2H), 7.30 (dt, J=7.42, 0.91, 2H), 6.86 (br, 1H), 5.82 (br, 1H), 5.62-5.51 (m, 1H), 5.50-5.44 (m, 1H), 5.14 (br, 1H), 4.43 (dd, J=10.65, 7.07, 1H), 4.38-4.28 (m, 3H), 4.21 (t, J=7.00, 1H), 3.65-3.53 (m, 20H), 3.52-3.44 (m, 5H), 3.31 (s, 2H), 2.76 (d, J=15.06, 1H), 2.62 (dd, J=16.11, 4.97, 1H), 2.36-2.26 (m, 3H), 2.15 (t, J=2.52, 1H), 1.99 (d, J=12.21, 1H), 1.94-1.85 (m, 5H), 1.77-1.66 (m, 2H), 1.55-1.47 (m, 1H) (Supp. figure 25). ^{13}C NMR (176 MHz CDCl$_3$): 169.7, 156.3, 155.8, 143.8, 141.3, 134.9, 133.0, 127.8, 127.1, 125.1, 125.1, 120.03, 80.50, 79.4, 77.2, 77.0, 76.9, 72.0, 70.5, 70.4, 70.2, 70.2, 69.7, 67.11, 53.37, 47.1, 41.2, 40.7, 39.6, 38.7, 34.3, 32.5, 31.0, 23.0 (Supp. figure 26).

Fmoc-deprotection and purification of the deprotected intermediate was carried out according to plan and complete deprotection and purification by prepHPLC were confirmed by LC/MS (Supp. figure 27). The molecule was further characterized by HRMS and NMR. During prepHPLC-purification, the deprotected intermediate eluted between 18.8 and 23.3 min corresponding with a concentration of 28-35% ACN. The yield was 20.3 mg (48.8%). HRMS (ESI): Calculated for $C_{28}H_{50}N_3O_9$ $[M+H]^+$: 572.3520, found: 572.3534. ^{1}H NMR (500 MHz, CDCl$_3$): 7.65 (br, 1H), 5.73-5.43 (m, 2H), 5.18 (br, 1H), 4.31 (dd, J=10.1, 6.0, 1H), 3.67-3.57 (m, 20H), 3.56-3.40 (m, 7H), 3.32 (t, J=4.96, 2H). 2.72 (ddd, J=16.86, 4.47, 2.67, 1H), 2.53 (ddd, J=16.86, 7.86, 2.60, 1H), 2.38-2.25 (m, 2H), 2.18-2.06 (m, 1H), 2.05 (t, J=2.60, 1H), 1.99 (d, J=11.82, 1H), 1.95-1.85 (m, 2H), 1.83-1.65 (m, 6H), 1.61-1.46 (m, 2H) (Supp. figure 28). ^{13}C NMR (126 MHz CDCl$_3$): 173.0, 134.9, 133.0, 129.8, 129.7, 80.7, 80.5, 71.1, 70.6, 70.54, 70.52, 70.4, 70.3, 70.2, 69.9, 53.8, 41.2, 40.7, 39.0, 38.7, 34.3, 34.1, 32.6, 31.0, 25.6, 25.3, 24.8, 22.4 (Supp. figure 29).

The deprotected intermediate was reacted with sulfo-cyanine 5 NHS ester. LC/MS-analysis of the crude product revealed that the obtained PEG$_6$-linker consisted of two molecules with the same signal at 597.0 m/z (corresponding to the $[M-2H]^{2-}$ ion of the PEG$_6$-linker, calculated from $C_{60}H_{83}N_5O_{16}S_2$) but slightly different retention times as indicated by the UV-absorption at 254 nm (Supp. figure 31). Reacting a prepHPLC-fraction from a test-purification that contained both compounds with methyltetrazine vancomycin revealed that the peak at 2.77 min preferably reacted, while the second peak at 2.79 min remained (Supp. figure 32). The prepHPLC-method was thus designed to separate both peaks and they were collected separately. The active linker eluted between 34.5 and 36.5 min corresponding to 38-40% ACN. The inactive linker eluted directly afterwards without a clean separation of both peaks. LC/MS-analysis confirmed the purity of the collected fractions containing the active PEG$_6$-linker (Supp. figure 33). However, after lyophilisation, a new peak appeared at 2.09 min and the PEG$_6$-linker peak

showed a shoulder (Supp. figure 34). HRMS analysis of the PEG$_6$-linker was inconclusive with the appearance of multiple unidentified peaks and low detection of the mass corresponding to the linker molecule. In LC/MS the peak of the PEG$_6$-linker showed a signal at 597.0 m/z corresponding to the [M-2H]$^{2-}$ ion (Calculated from $C_{60}H_{83}N_5O_{16}S_2$). The yield of the active PEG$_6$-linker was 12.85 mg (32,8%). The PEG$_6$-linker was dissolved in dry DMSO at 9.78 nmol/µl and aliquoted in 1 µl aliquots. The inactive PEG$_6$-linker isolated from the second peak was lyophilized as well and analyzed by LC/MS and NMR. LC/MS revealed that it indeed contained material exhibiting the same mass as the active linker (Supp. figure 44), however with a slightly later elution. Active PEG$_6$-linker: ^{1}H NMR (500 MHz, DMSO-d_6): 8.36 (t, J=13.14, 2H), 8.07 (d, J=7.20, 2H), 7.82 (s, 2H), 7.63 (dd, J=7.41, 5.61, 2H), 7.31 (dd, J=8.26, 1.71, 2H), 7.03-6.92 (m, 1H), 6.57 (t, J=12.36, 1H), 6.31 (d, J=13.76, 1H), 6.25 (d, J=13.76, 1H), 5.63-5.52 (m, 1H), 5.47-5.37 (m, 1H), 4.38 (dd, J=14.07, 7.76, 1H), 4.19 (dd, J=11.48, 5.25, 1H), 4.07 (t, J=6.88, 2H), 3.59 (s, 3H), 3.49 (s, 21H), 3.39-3.32 (m, 5H), 3.26-3.13 (m, 3H), 3.12-3.01 (m, 2H), 2.97 (dd, J=10.79, 5.36, 1H), 2.83 (s, 1H), 2.39 (dd, J=16.79, 7.80, 1H). 2.31-2.18, (m, 2H), 2.17-2.06 (m, 3H), 1.93-1.79 (m, 3H), 1.69 (s, 12H), 1.60-.146 (m, 5H), 1.40-1.29 (m, 2H), 1.28-1.19 (m, 1H), 0.94-0.80 (m, 1H) (Supp. figure 35). ^{13}C NMR (126 MHz DMSO-d_6): 173.6, 172.9, 172.0, 170.0, 155.8, 154.2, 145.3, 145.2, 142.7, 142.0, 140.5, 140.4, 134.9, 132.5, 126.1, 126.0, 125.7, 120.0, 119.9, 110.13, 110.06, 103.6, 103.4, 80.8, 79.1, 72.8, 69.8, 69.7, 69.66, 69.63, 69.5, 69.2, 68.9, 51.3, 48.9, 40.7, 38.7, 38.2, 34.8, 33.8, 32.2, 30.6, 27.1, 26.9, 26.6, 25.6, 24.9 (Supp. figure 36). COSY (Supp. figure 37), HSQC (Supp. figure 38), HMBC (Supp. figure 39).

Inactive PEG$_6$-linker: ^{1}H NMR (500 MHz, DMSO-d_6): 8.36 (t, J=13.11, 2H), 8.09-8.03 (m, 2H), 7.81 (s, 2H), 7.63 (ddd, J=8.56, 5.30, 1.25, 2H), 7.31 (dd, J=8.28, 2.58, 2H), 7.02-6.92 (m, 1H), 6.57 (t, J=12.19, 2H), 6.31 (d, J=13.82, 1H), 6.25 (d, 13.82, 1H), 5.69-5.54 (m, 2H), 4.55 (m, 1H), 4.39 (dd, J=14.24, 8.13, 1H), 4.07 (t, J=6.96, 2H), 3.59 (s, 3H), 3.49 (s, 20H), 3.40-3.24 (m, 6H), 3.26-3.13 (m, 3H), 3.08 (dd, J=11.79, 5.83, 2H), 2.83 (t, J=2.43, 1H), 2.39 (ddd, 16.68, 8.05, 2.51, 2H), 2.33-2.22 (m, 2H), 2.17 (s, 1H), 2.16-2.07 (m, 4H), 2.06-1.97 (m, 1H), 1.84-1.72 (m, 2H), 1.69 (s, 12H), 1.65-1.58 (m, 1H), 1.58-1.51 (m, 3H), 1.51-1.40 (m, 3H), 1.39-1.29 (m, 3H), 1.28-1.11 (m, 5H), 0.87-0.79 (m, 1H) (Supp. figure 40). ^{13}C NMR (126 MHz DMSO-d_6): 173.6, 172.9, 172.0, 170.0, 155.9, 155.1, 154.2, 145.4, 145.2, 142.7, 142.0, 140.5, 140.4, 129.8, 129.7, 129.5, 126.1, 126.0, 125.6, 120.0, 119.9, 118.2, 110.1, 110.0, 103.6, 103.4, 80.8, 74.4, 72.8, 69.8, 69.7, 69.6, 69.5, 69.1, 68.9, 51.3, 48.9, 38.7, 34.8, 33.8, 33.7, 29.2, 27.1, 26.9, 26.6, 25.6, 25.2, 24.9, 24.6, 22.0, 21.9, 19.5 (Supp. figure 41). COSY (Supp. figure 42), HSQC (Supp. figure 43).
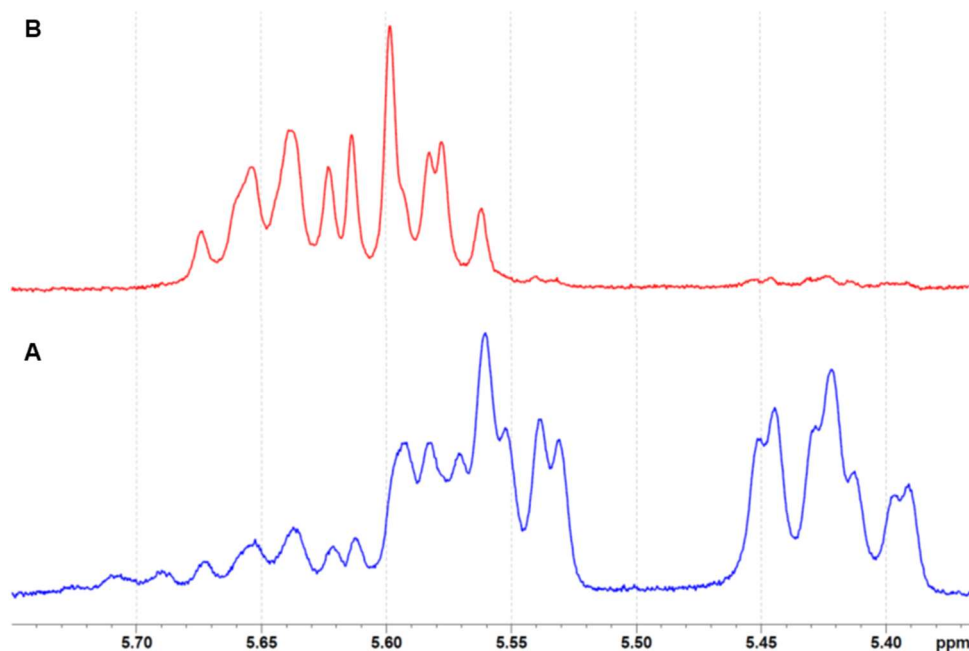
Figure 46: Zoomed view of the ^{1}H-NMR spectra containing the signals of the protons belonging to the alkene-group of cyclooctene. Active PEG$_6$-linker (A) and inactive PEG$_6$-linker (B).

Both active and inactive PEG$_6$-linker were analyzed by NMR to evaluate structural differences between both compounds. To this end, the region of their respective ^{1}H-NMR spectra relevant to the alkene in the TCO-group was compared (Figure 46) and the protons and carbons making up their respective cyclooctene rings were assigned using 2D-NMR (Table 2). Both analyses revealed differences between the compounds.

Table 2: Assignment of the protons and carbons belonging to the cyclooctene ring of the active and inactive PEG$_6$-linker.
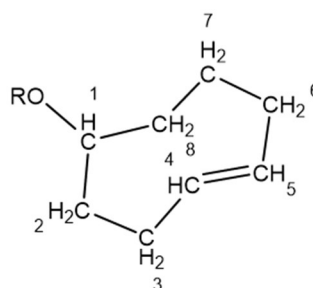
Carbon number	Active PEG$_8$-linker		Inactive PEG$_8$-linker	
	Carbon [ppm]	Proton [ppm]	Carbon [ppm]	Proton [ppm]
1	79.06	4.18	74.44	4.55
2	40.59	1.88	33.73	1.80; 1.48
3	32.14	2.26	21.91	2.27; 2.00
4	134.92	5.56	129.7	5.65
5	132.53	5.43	129.5	5.59
6	33.72	2.26; 1.87	25.14	2.10
7	38.19	1.54	24.57	1.44
8	30.62	1.83; 1.61	33.78	1.62

The purified PEG$_6$-linker was reacted with methyltetrazine-vancomycin and methyltetrazine-PEG$_4$-biotin. LC/MS analysis revealed that the unidentified degradation product did not participate in the reaction and some PEG$_6$-linker remained corresponding to the shoulder found in the starting material (Supp. figure 45 & Supp. figure 46). The correct mass of the IEDDA

product of PEG$_6$-linker and methyltetrazine-vancomycin was found in HRMS. LC/MS revealed three peaks at 2.26, 2.48 and 2.52 min that all showed a signal at 943 m/z corresponding with the [M+3H]$^{3+}$ ion of the reaction product (calculated from C$_{137}$H$_{168}$Cl$_2$N$_6$O$_{41}$S$_2$) (Supp. figure 45) HRMS (ESI): IEDDA PEG$_6$-linker and methyltetrazine-vancomycin: Calculated for C$_{137}$H$_{169}$Cl$_2$N$_6$O$_{41}$S$_2$ [M+H]$^+$: 2828.0444, found: 2828.0442.

Similar results were obtained for the IEDDA reaction with methyltetrazine-PEG$_4$-biotin. The corresponding mass of the product was confirmed by HRMS and again three peaks of the product were visible at 2.41, 2.68 and 2.75 min in LC/MS (Supp. figure 47 & Supp. figure 48). The latter two co-eluting with unreacted methyltetrazine biotin. HRMS (ESI): IEDDA PEG$_6$-linker and methyltetrazine-PEG$_4$-biotin: Calculated for C$_{87}$H$_{125}$N$_{10}$O$_{22}$S$_3$ [M+H]$^+$: 1757.8127, found: 1757.8110.

4.6.3. OMV modification with the PEG$_6$-linker and OMV-biotinylation

The solubility of the PEG$_6$-linker was tested as described before by dissolving it at 19.6 µM in PBS and injecting it on the SEC column (Supp. figure 21 C&D). While the overall picture was the same as for the PEG$_8$-linker, with most of the fluorescence eluting late, the amount of dye that eluted at the same time as OMVs would was notably higher than for the PEG$_6$-linker. Thus, this early elution of PEG$_6$-linker would need to be taken into consideration for the interpretation of surface-modification using this molecule. The product of the IEDDA reaction of the PEG$_6$-linker with methyltetrazine-PEG$_4$-biotin (biotinlinker) was tested in the same way. Here the early elution was in the same range as the PEG$_8$-linker, much lower than for the native PEG$_6$-linker (Supp. figure 21 E&F).

AzideOMVs were reacted with either the PEG$_6$-linker or the biotinlinker and the modification efficiency was measured. The results were compared to CuAAC and SPAAC using the respective AF594 derivatives and the unspecific labeling of the vesicles was assessed using untreated control OMVs (Figure 47). Calibration curves both for the PEG$_6$-linker and the biotinlinker were constructed (Supp. figure 4 D&E). Modification with the PEG$_6$-linker led to the recovery of 269.1±51.4 molecules linked to OMVs (n=6), compared to 46.8±18.7 for the control (n=3). Application of the biotinlinker led to 393.3±52.0 molecules per particle (n=3), compared to 105.3±9.1 for the control (n=3). CuAAC and SPAAC with AF594 led to 87.4±35.7 and 107.8±19.9 molecules per particle respectively (n=3).
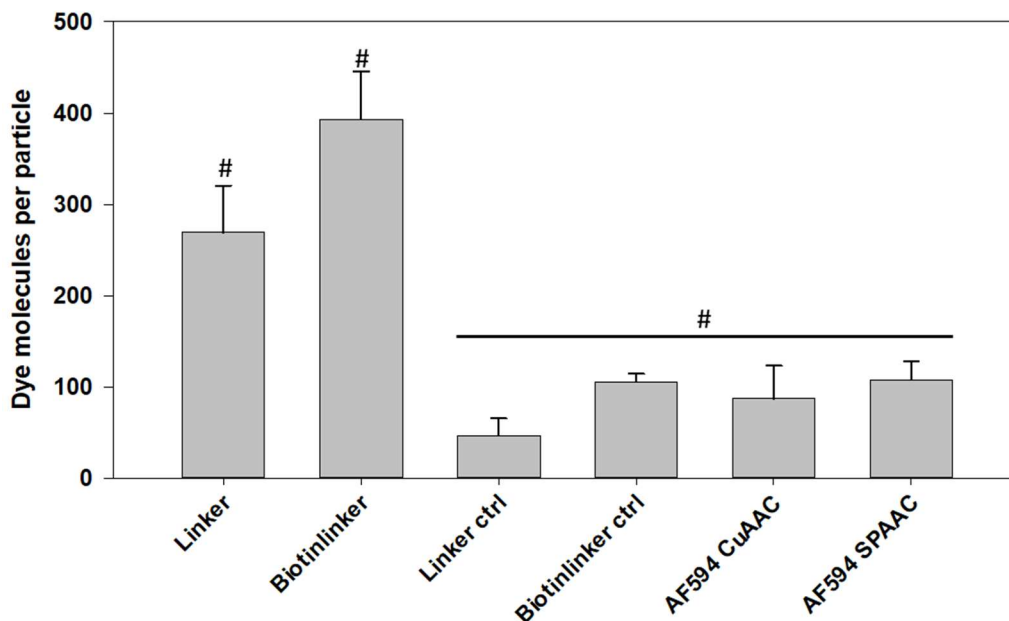
Figure 47: Modification efficiency of the modification of AzideOMVs with the PEG_6-linker, the biotinlinker, alkyne AF594 or DBCO AF594 and unspecific labeling of control OMVs with the PEG_6-linker or the biotinlinker. Linker was significantly different from biotinlinker and both linker and biotinlinker were significantly different from all other samples ($p \leq 0.005$).

The extent of unspecific labeling of OMVs was further evaluated by normalizing the dye molecules per particle of control samples to the results of the modification of AzideOMVs under the same conditions (Figure 48). The highest unspecific labeling was observed for the biotinlinker with 26.8±2.3%. With the PEG_6-linker molecule, an unspecific labeling of 17.4±6.9% was observed. DBCO AF594 led to a similar value of 14.4±5.4%. The lowest unspecific labeling was measured for alkyne AF594 at 6.8±3.6% (all experiments n=3).
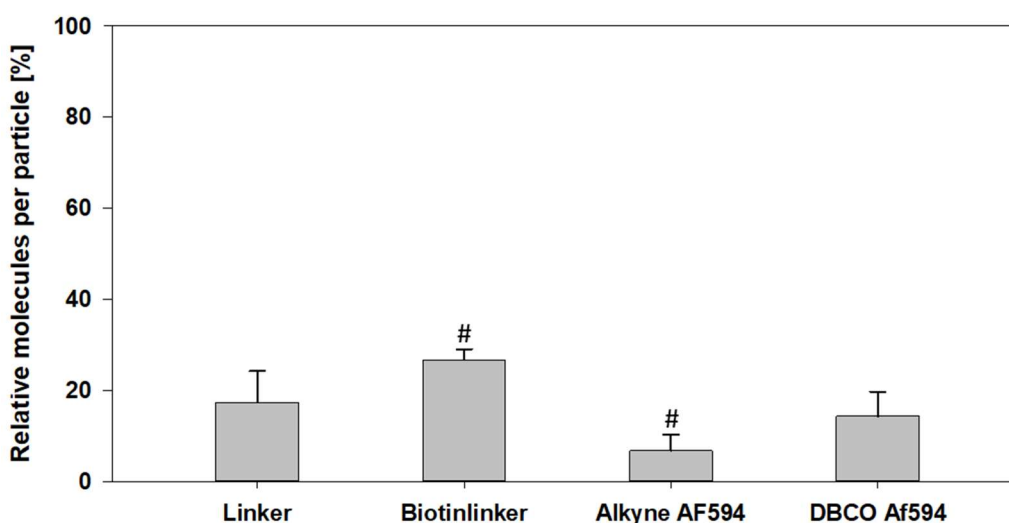
Figure 48: Comparison of the unspecific labeling of control OMVs with the PEG6-linker, biotinlinker, alkyne AF594 or DBCO AF594. Values are relative to the modification efficiency

achieved with AzideOMVs with the same compounds. Biotinlinker was significantly different from Alkyne AF594 (p=0.005).

4.6.4.   Evaluation of biotinylated OMVs

The presence of biotin on the surface of OMVs was evaluated using FITC-labeled streptavidin (Figure 49). To have a further comparison to OMVs biotinylated with the PEG_6-linker, AzideOMVs were also biotinylated using SPAAC with the reaction product of $TCO-PEG_4$-DBCO and methyltetrazine-PEG_4-biotin (SPAAC-biotinlinker). Both types of biotinylated OMVs showed a clear increase above the negative controls. The SPAAC-biotinlinker however, led to by far the highest recovery of streptavidin-FITC in the vesicle-containing fractions and the other results were normalized to reduce the variability introduced by differences in vesicle-concentration between the independent experiments. To confirm that the high degree of labeling was not based on insufficient solubility of the SPAAC-biotinlinker, the pure molecule at 4.9 µM was subjected to SEC and no early elution of the molecule was visible according to the 280 nm UV-cell of the ÄKTA instrument (Supp. figure 49). The control containing only PBS led to a recovery of 1.5±2.0%, the control containing untreated OMVs to 3.2±3.9%. Biotinlinker OMVs led to a recovery of 25.8±8.0%, while control OMVs incubated with the biotinlinker gave a value of 11.7±0.9% and OMVs modified with the PEG_6-linker (linker OMVs) gave a value of 2.4±1.9%. The pure biotinlinker dissolved in PBS at 4.9 nM and the SPAAC-biotinlinker at 4.9 nM led to values of 3.0±1.4% and 1.9±1.0% respectively (all experiments performed as n=3). The IEDDA reaction between $TCO-PEG_4$-DBCO and methyltetrazine-PEG_4-biotin was evaluated by HRMS. HRMS (ESI): Calculated for $C_{65}H_{89}N_8O_{14}S$ $[M+H]^+$: 1237.6213, found: 1237.6212.
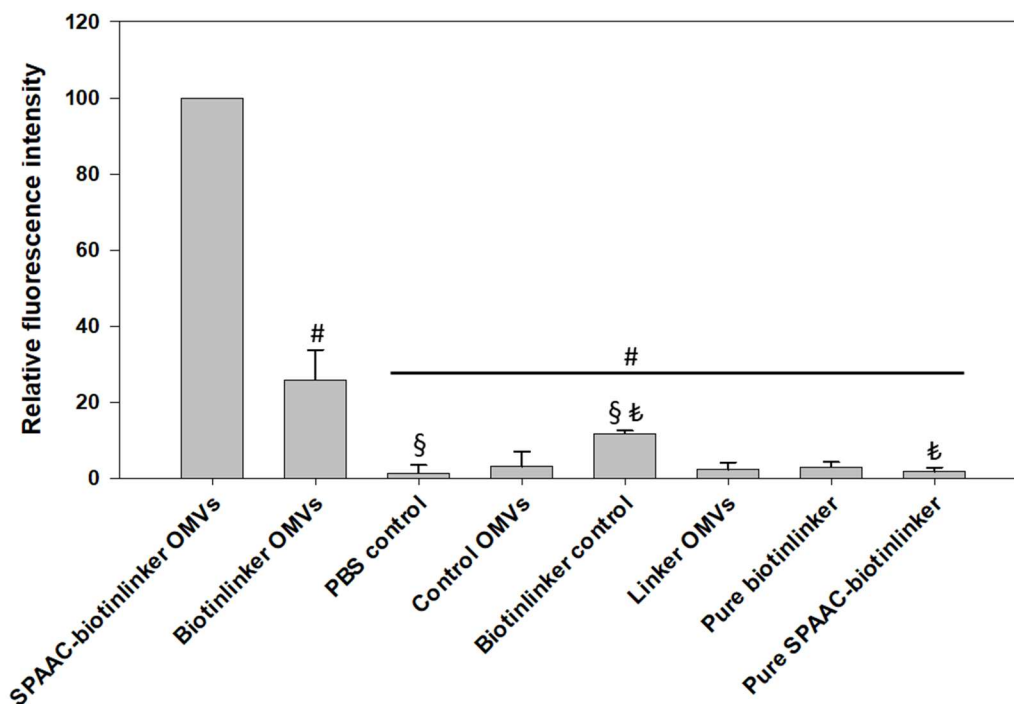
Figure 49: Fluorescence of the OMV-containing fractions after labeling with streptavidin-FITC and SEC-purification. Values are relative to SPAAC-biotinlinker modified OMVs. The "biotinlinker control" refers to untreated OMVs subjected to CuAAC with the biotinlinker. Biotinlinker OMVs were significantly different from all other samples (p≤0.002), Biotinlinker control was significantly different from PBS control (p=0.029) and pure SPAAC-biotinlinker (p=0.039).

4.6.5.   OMV modification with the Vancomycin-linker

Initial experiments indicated that the vancomycin-linker led to an unspecific labeling of control OMVs. This was further evaluated by comparing control OMVs that were either incubated with the vancomycin-linker under standard CuAAC conditions, CuAAC conditions, were sodium ascorbate was dissolved in water instead of NaOH and control OMVs incubated with just the vancomycin-linker and no copper, THPTA and sodium ascorbate (Figure 50). These three conditions were compared to controls that were incubated with the unmodified linker or the biotinlinker (see 4.6.3). The results indicated a significant increase in fluorescent labeling of OMVs in the presence of the excipients used in CuAAC. The controls showed a fluorescence intensity of 741.3±314.3 units (n=6). OMVs incubated with the vancomycin-linker showed an increase to 11893.0±4207.8 units (n=3). This value decreased to 8186.5±5902.9 units for samples incubated without NaOH (n=3) and to 1155.8±118.9 units for samples just incubated with the vancomycin-linker (n=3).
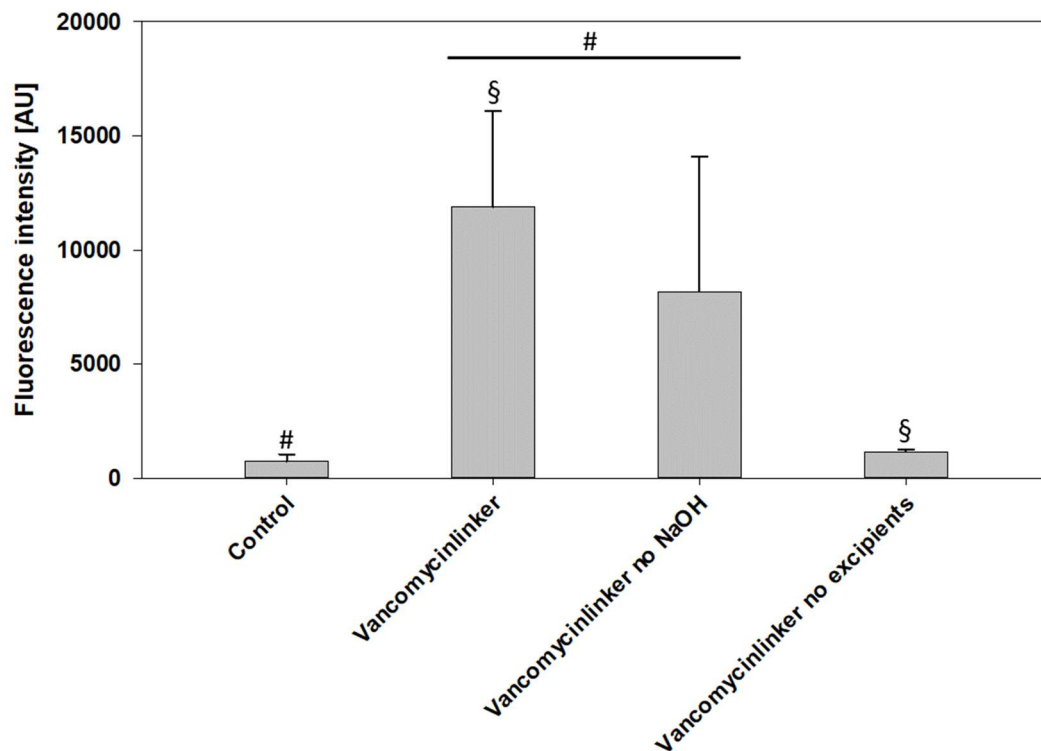
Figure 50: The unspecific labeling of untreated SBCy050 OMVs with the vancomycinlinker under different conditions was compared to the background labeling obtained with the PEG$_6$-linker or the biotinlinker (control). Control OMVs were subjected to CuAAC with the vancomycin-linker either under standard-conditions, without the usage of NaOH to dissolve sodium ascorbate, or by simple co-incubation without addition of CuAAC-excipients. Both vancomycinlinker and vancomycinlinker no NaOH were significantly different from Control (p≤0.026), Vancomycinlinker was significantly different from vancomycinlinker no excipients (p=0.007).

4.7.   EV storage-stability evaluation

4.7.1.   Preliminary short-term storage of A549 EVs

Data presented in this chapter was published as part of Frank, J., et al. (2018). "Extracellular vesicles protect glucuronidase model enzymes during freeze-drying." Scientific Reports 8(1): 12377.

In a preliminary experiment, EVs derived from A549 cells were stored for 2 d at 4 °C, -80 °C or in lyophilized form without the addition of a cryoprotectant (Figure 51). The recovered particle number relative to samples before storage showed a slight increase at 4 °C and -80 °C to 123.2±38.4% and 108.9±16.0% respectively, while the particle recovery was reduced to 65.0±12.0% in lyophilized samples. At the same time, the mean particle size of lyophilized EVs increased to 259.0±20.9 nm compared to 183.9±26.7 nm for samples before storage. Storage at 4 °C and -80 °C did not elicit a change in particle size with mean sizes of 178.6±17.5 nm

and 180.2±14.2 nm respectively. These results are also well visible in the particle size-distribution. While samples before storage and ones stored at 4 or -80 °C show a very similar size distribution, the distribution of lyophilized samples is much broader with a shift to higher diameters (Figure 51 C, for the full size-distribution see Supp. figure 50 A).
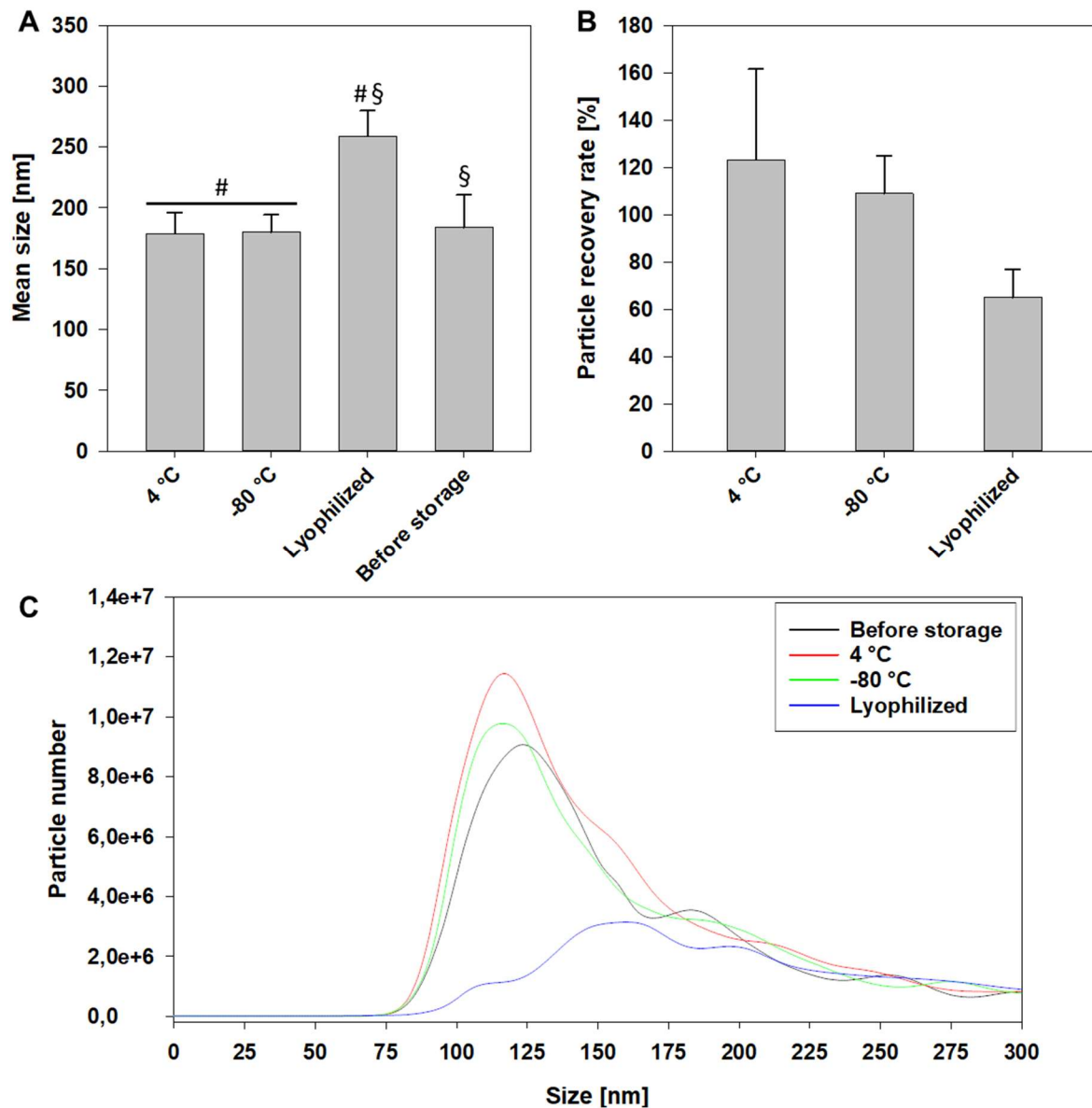
Figure 51: Panel A shows the mean size of A549 EVs stored for 2 d at 4 °C, -80 °C or after lyophilisation compared to samples before storage. In panel B, the particle recovery rate of samples after storage relative to untreated samples is presented. Panel C contains the size distribution of particles in the range from 0 to 300 nm as measured by NTA, mean values from three measurements are plotted. A: The mean size of lyophilized A549 EVs was significantly higher than both the size of EVs before storage (p=0.009) and the size of EVs stored at 4 or -80 °C (p≤0.007).

4.7.2.   Storage stability of HUVEC-EVs

Data presented in this chapter was published as part of Frank, J., Richter, M., et al. (2018). "Extracellular vesicles protect glucuronidase model enzymes during freeze-drying." Scientific Reports 8(1): 12377. Data from the seven day storage experiment was also part of Richter, M., et al. (2019). "Evaluation of the Storage Stability of Extracellular Vesicles." JoVE(147): e59584.

HUVEC cells were cultured until passage 9, for pictures of HUVEC cultures, see Supp. figure 51. In a first evaluation of their storage stability, HUVEC EVs were stored for 14 d at RT, 4 °C, -80 °C and in lyophilized form without the addition of a cryoprotectant (Figure 52). The particle recovery was assessed compared to the particle concentration before storage. At RT 78.1±4.4% of particles were recovered, at 4 °C 66.0±13.0%, at -80 °C 51.7±10.4% and after lyophilized storage 34.7±8.4% of the starting particles were recovered. The particle size increased for all samples during storage. EVs before storage had a mean particle size of 155.3±9.3 nm. After 14 d at RT the mean size was 171.0±4.8 nm, at 4 °C it was 181.3±4.2 nm, at -80 °C it was 193.4±8.5 nm and after lyophilized storage it was 213.5±9.9 (all data n=3). These changes were also observed in the size-distribution of EVs before and after storage, especially in case of -80 °C and lyophilisation (Figure 52 C, for full size-distribution, see Supp. figure 50 B).
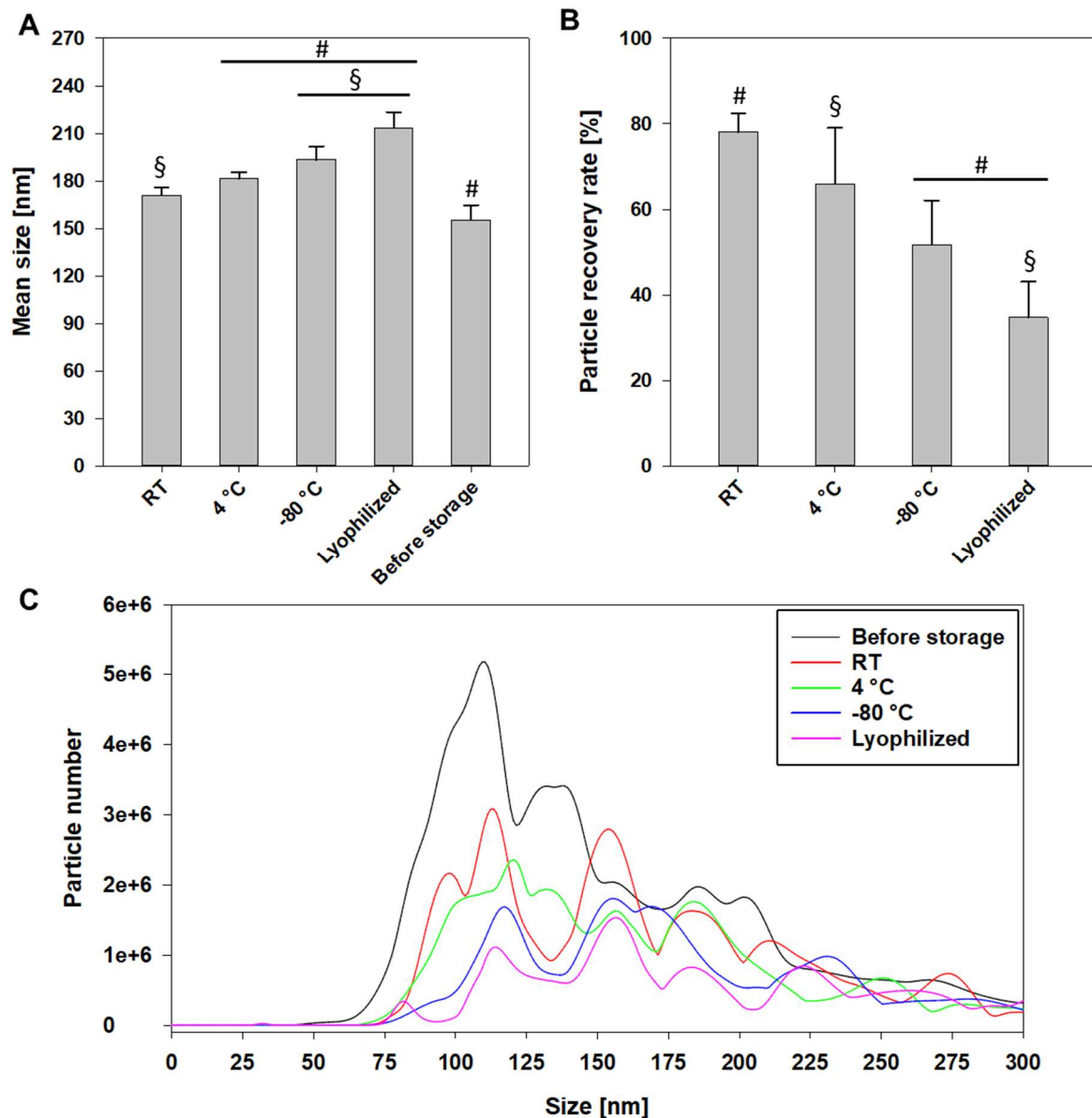
Figure 52: Panel A shows the mean size of HUVEC-EVs after 14 d of storage compared to vesicles before storage. Panel B shows the particle recovery rate of stored samples relative to the initial concentration. Panel C contains the size distribution of particles in the range from 0 to 300 nm as measured by NTA, mean values from three independent experiments are plotted. A: The mean size of EVs stored at 4 °C, -80 °C and lyophilized was significantly higher than before storage (p≤0.014). Both EVs stored at -80 °C and lyophilized were significantly larger than EVs stored at RT (p≤0.033). B: RT led to significantly higher recovery than both -80 °C and lyophilized storage (p≤0.040). Storage at 4 °C led to a significantly higher recovery rate than lyophilized storage (p=0.017).

Next, the effect of trehalose as a cryoprotectant on the stability of HUVEC EVs was tested. As an additional parameter, β-glucuronidase was encapsulated into the vesicles. EVs were subjected to 7 d of storage at 4 °C, -80 °C and in lyophilized form with the addition of 4% (w/v) trehalose (Figure 53). To make sure that no leaked beta glucuronidase would influence the enzyme-activity assessment, samples were subjected to purification by AF4 before the beta

glucuronidase assay was performed. At 4 °C there was no reduction in particle concentration after storage, with a recovery of 103.3±23.7% of the starting concentration. The recovery rate was reduced to 84.9±5.9% at -80 °C and to 57.7±10.2% after lyophilisation. Compared to the previous experiment no changes in particle size were visible. Before storage, the mean particle size of HUVEC EVs was 152.9±25.4 nm. This changed to 142.9±23.7 nm at 4 °C, 154.1±22.7 nm at -80 °C and 149.0±26.6 nm after lyophilisation. The small changes in EV-size were also observed in the size distributions of fresh and stored EVs, where compared to 14 d of storage only small changes were visible (Figure 54, for full size distribution see Supp. figure 50). The recovery of active beta glucuronidase per particle was the highest in lyophilized samples at 58.5±36.8% of the starting material. In samples stored at 4 °C recovery was reduced to 28.6±5.5% and at -80 °C to 10.4±1.1% (all data n=3).
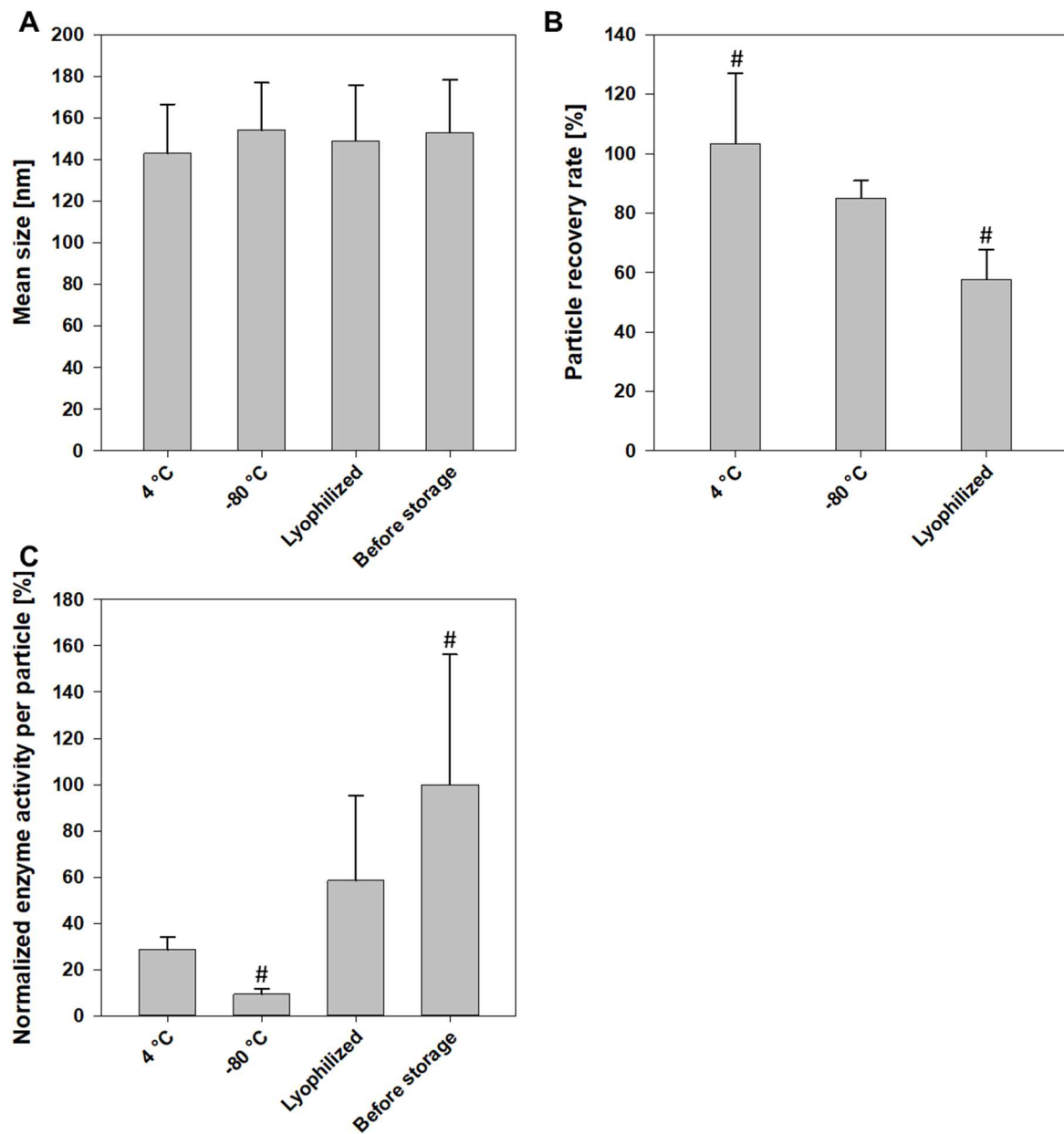
Figure 53: Panel A shows the mean size of HUVEC EVs after 7 d of storage compared to EVs before storage. Panel B shows the particle recovery rate of stored samples relative to the initial concentration. In panel C the enzyme activity per particle, normalized to samples before storage is displayed. B: The particle recovery rate for 4 °C was significantly higher than for lyophilized storage (p=0.025). C: The Enzyme activity per particle in samples stored at -80 °C was significantly lower than before storage (p=0.044).
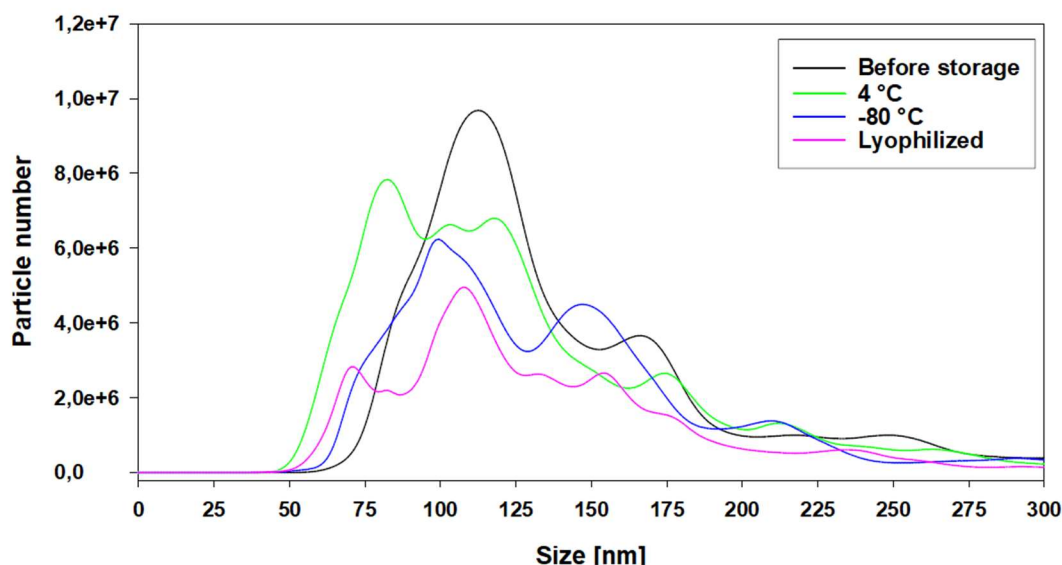
Figure 54: Size distribution of fresh and stored HUVEC EVs in the range from 0 to 300 nm as measured by NTA. Mean values from three independent experiments are plotted.

4.7.3.   Optimization of RO EV storage and long term stability of encapsulated beta glucuronidase

Data presented in this chapter was part of the publication by Trenkenschuh E., Richter, M. et al. (2020). "Formulation development of lyophilized extracellular vesicles with long-term stability", manuscript submitted to Advanced Healthcare Materials.

Four formulations of RO-EVs were evaluated for long-term storage (n=3):

1. 10 mM Na-phosphate with 5% sucrose and 0.02% P188

2. 10 mM K-phosphate with 5% sucrose and 0.02% P188

3. 10 mM Na-phosphate with 5% sucrose and 0.02% PVP

4. 10 mM Na-phosphate with 5% PVP and 0.02% P188

While the evaluation of colloidal stability was carried out by Eduard Trenkenschuh at LMU Munich, the measuring of β-glucuronidase stability was carried out in Saarbrücken by Maximilian Richter. After redispersion, if applicable, samples were purified by SEC and the EV-containing fractions were evaluated regarding their active enzyme content (Figure 55 & Table 3). Before lyophilisation, the PVP-containing samples of conditions 3&4 exhibited almost twice the fluorescence intensity of the conditions 1&2, while no enzyme activity was found in these samples directly after lyophilisation. In samples of conditions 1&2, enzyme activity was reduced to 57.8% and 34.9% respectively directly after lyophilisation.
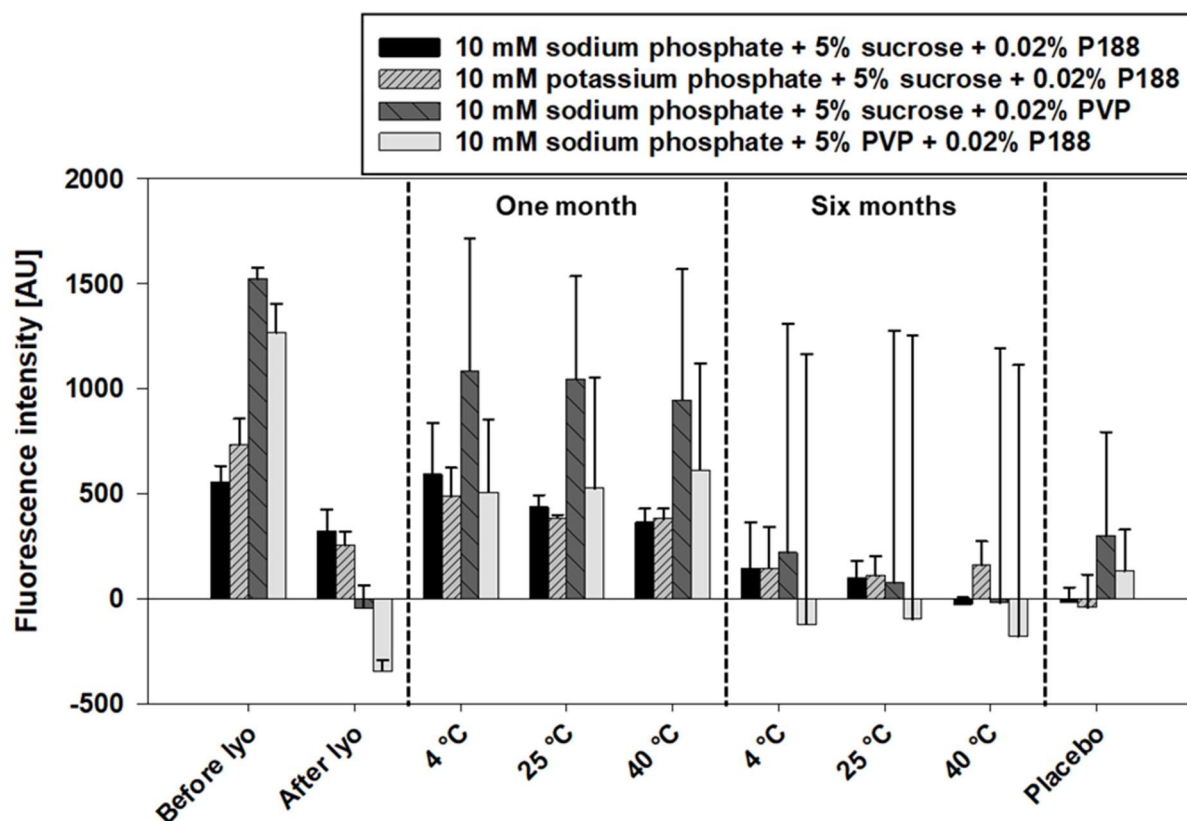
Figure 55: Stability of β-glucuronidase encapsulated in RO EVs stored for 6 months expressed as the fluorescence-intensity of fluorescein generated through the enzymatic conversion of fluorescein-di-β-D-glucuronide. Samples contained either 10 mM sodium or potassium phosphate as a buffer and either 5% sucrose + 0.02% P188, 5% sucrose + 0.02% PVP or 5% PVP + 0.02% P188 as cryo- and lyoprotectants. Placebo samples contained just the respective excipients and no EVs.

After one month of storage enzyme activities generally recovered compared to directly after lyophilisation. For all samples but condition 4, enzyme activity was reduced with higher storage temperature. Condition 1 led to the highest recovery of active enzyme between 106.7 and 65.7%. For condition 2, 66.6 to 52.4% were recovered and 71.2 to 62.1% were recovered for condition 3. Condition 4 exhibited the highest reduction in enzyme activity to 40.1 to 48.5%. After 6 months of storage, enzyme activity was greatly reduced in all samples. Samples containing PVP showed a very high variability in the measured enzyme activity, fluctuating around zero fluorescence. For condition 1, enzyme activity was reduced to 26.3 and 18.2% at 2-8 and 25 °C respectively, while no active enzyme was recovered at 40 °C. Condition 2 led to the recovery of 19.9 to 22.0%. Samples of condition 3 showed a recovery of 14.5 and 5.2% at 2-8 and 25 °C respectively, while no active enzyme was recovered at 40 °C. In condition 4, no active enzyme was recovered at all temperatures. Placebo samples revealed no background fluorescence for conditions 1&2, while conditions 3&4 exhibited a background fluorescence of 19.8 and 10.5% of EVs before lyophilisation respectively.

Table 3: Remaining enzyme activity in lyophilized and stored RO EV samples. Recovered enzyme activity is expressed as the percentage of fluorescein fluorescence found relative to samples before lyophilisation. Placebo samples contained just the respective excipients and no EVs.

Sample	Before lyophilisation	After lyophilisation	1 month			6 month			Placebo
			2-8 °C	25 °C	40 °C	2-8 °C	25 °C	40 °C	
10 mM Na-phosphate, 5% sucrose + 0.02% P188	100±13.8	57.8±19.2	106.7±43.8	78.7±10.2	65.7±11.4	26.3±39.4	18.2±14.6	-4.3±5.7	-2.8±12.9
10 mM K-phosphate, 5% sucrose + 0.02% P188	100±16.9	34.9±8.9	66.6±18.4	52.6±2.0	52.4±6.3	19.9±27.2	15.2±12.5	22.0±15.24	-5.4±21.3
10 mM Na-phosphate, 5% sucrose + 0.02% PVP	100±3.6	-2.8±7.0	71.2±41.5	68.8±32.0	62.1±40.9	14.5±71.4	5.2±76.6	-1.2±79.6	19.8±32.4
10 mM Na-phosphate, 5% PVP + 0.02% P188	100±10.6	-27.1±4.1	40.1±27.3	41.5±41.5	48.5±39.8	-9.6±101.3	-7.4±106.4	-14.0±101.8	10.5±15.5

5. Discussion

5.1. Cultivation of SBCy050 bacteria and Isolation of their OMVs

Compared to other gram-negative bacteria, SBCy050 myxobacteria exhibited a very slow growth. The cultivation conditions for SBCy050 were based on the work Eilien Heinrich performed in her master thesis. As the bacteria did not grow in single colonies once plated on agar, it was not possible to get an assessment of the number of bacteria that gave rise to the OMVs isolated. The data gathered over the course of this project for their OD_{600} at isolation at nonetheless demonstrate the reproducibility of their culture.

While the initial protocol for differential centrifugation was based on centrifuging the bacterial culture twice at 9500 g to pellet bacteria and their debris, the protocol was successfully optimized by replacing the second step of centrifugation with filtration. Analysis of the vesicles obtained with the optimized protocol suggested no changes compared to the original protocol (Figure 29). Filtration not only was faster than the second 15 min centrifugation step, but also led to a higher yield of conditioned medium, as in centrifugation the last 10 ml of supernatant had to be discarded to prevent the disturbance of the bacterial pellet. Thus, for the original protocol the yield of supernatant was only 60%, while the yield approached 100% for the filtration-based protocol. Therefore, despite the increased amount of consumable used, filtration made the process of OMV-production more economical by reducing the consumption of medium, the incubator shelf-space needed for cultivation and the time needed to obtain cell-free conditioned medium. The Steritop filter employed in this protocol was shown to be suitable to filter out bacteria in a recent publication (380). Interestingly, replacing it with another bottle top filter of a competitor that supposedly employed the same material for the filter-membrane greatly reduced the OMV-yield, emphasizing the need for thorough evaluation of every step of vesicle production.

Once conditioned medium has been produced there are multiple methods to obtain purified and concentrated EVs, as discussed above (1.4.1). Since an ultracentrifuge and suitable rotors for the volumes of medium that required processing were available at the institute, UC was the method of choice to concentrate EVs from conditioned medium. With a processing time of approx. 2.5 h to obtain a vesicle-pellet from up to 360 ml of conditioned medium, it was much faster than PEG-precipitation, which requires overnight incubation. On the other hand, TFF, which would reduce the strain on the vesicles during purification and potentially lead to higher yields, would have required a considerable investment into the required instruments and the running costs of the required filter cassettes. Additionally, the early stages of the optimization of OMV surface engineering required many replicates with relatively low volume of conditioned

medium, which for TFF would result in the use of a high amount of consumables. Thus, with the investments into an ultracentrifuge and rotors already done, UC was the more economical variant. Still, a later scale-up of EV-production to larger batches might benefit from TFF as opposed to UC.

The main drawback of the co-isolation of many impurities derived from the conditioned medium was addressed by an additional step of purification using the pellet obtained by UC. Here the choice was between SEC and density gradient UC. While the latter would allow for the isolation of highly purified subsets of EVs and not dilute the samples, as it occurs in SEC, its requirement for long ultracentrifugation steps made it considerably less useful in the present setting. As multiple people depended on the availability of the ultracentrifuge for EV-purification, wide use of density gradient UC would slow down progress for the whole group. Additionally, the main draw of this method, the potential isolation of EV-subsets based on their density was of little importance for the optimization of OMV surface engineering and the evaluation of EV storage stability that were the main subjects of this work. Thus, SEC using cheap self-prepared columns was the method of choice. Especially after partial automation using the ÄKTA start, SEC presented an easy and highly reproducible method that was moreover ideally suited to remove soluble impurities carried over from UC. Its main drawback, the dilution of purified samples, however necessitated the evaluation of methods for EV surface engineering based on the number of purification-steps they would require, favoring methods that could already be used with the pellet after UC.

5.2.   Surface functionalization of EVs

The first of the main objectives of this work was the development of an efficient method for the surface modification of myxobacterial OMVs (Box 2). As described in the introduction, there are three general pathways to EV surface modification: genetic engineering, physical modification and chemical functionalization. As the aim of this project was the introduction of small molecules as targeting moieties against bacteria and they were to be installed on the surface of myxobacterial OMVs, genetic engineering was not a suitable method. Neither could molecules such as vancomycin be expressed easily, nor have the proteomics of SBCy050 OMVs been investigated to determine surface-proteins suitable for the expression of fusion proteins. Thus, only physical and chemical engineering remained.

As described above, the isolation-protocol for OMVs employed in this work influenced the applicability of methods for OMV surface functionalization. SEC excels at removing soluble impurities from the particles, which makes it particularly well suited for the modification of EVs with soluble molecules. Thus, it is favorable for post-insertion, adsorption and chemical modification. On the other hand, SEC is unable to separate particles that are in a similar size-

range, which would be required for approaches based on the fusion of OMVs with liposomes, where unfused liposomes would require removal. Moreover the PEG-based fusion with liposomes had not been published yet at the start of the project (320) and the freeze-thaw based fusion of EVs and liposomes (323) was questionable due to potential negative effects of freezing and thawing on EV-integrity (224) and the lack of removal of unfused particles.

In regards to physical modification, especially lipid-insertion based methods seemed attractive as they combined a relatively straightforward synthesis-task with an easily implemented protocol that would allow for the one-step introduction of targeting moieties to OMVs, potentially even directly after UC. Thus, lipid-insertion was chosen to be investigated first.

To facilitate the quantification of EV-labeling and the optimization of the protocol a fluorescent cholesteryl-PEG-derivative was used. The same was also done in the later labeling-approaches. Based on the fluorescence readout, calibration curves and the particle-concentration as measured by NTA, the amount of dye molecules per particle could be approximated. Due to a change in the NTA-hardware during the course of this project, the sensitivity of particle-detection changed. Thus, the early experiments conducted for cholesterol insertion and NHS ester modification underestimated the amount of particles, which resulted in an overestimation of the modification efficiency compared to later experiments and a direct comparison of absolute values cannot be made.

5.2.1.   Cholesterol insertion

Compared to phospholipid-insertion, the insertion of cholesterol-modified molecules seems to be better suited for the modification of EVs due to the lower incubation temperatures required for optimal insertion (0). Additionally, while it was clear from the start that the different membrane structure of OMVs could be problematic for cholesterol post-insertion, some findings made it seem probable that cholesterol insertion in particular might work with OMVs. Hopanoids, bacterial sterols, are membrane components of the outer membrane of various gram-negative bacteria and they were also identified in myxobacteria (381). Moreover, cholesterol was found to interact with lipid A and sphingomyelin in the same way as its bacterial analogue diplopterol (382). The results of the conducted experiments however clearly indicated that cholesterol insertion does not work with SBCy050 OMVs (4.2). The attempt of transiently disrupting the membrane-integrity with saponin to promote the insertion also was unsuccessful and even led to a decrease in the insertion into liposomes (Figure 30), which were used as a positive control alongside A549 cell derived mammalian EVs. The results were either caused by a badly optimized protocol or the differences in membrane structure between mammalian EVs and OMVs

The protocol was based on the findings of O'Loughlin et al., who determined that a high ratio of cholesterol-modified molecules to EV led to a higher per particle insertion (228). Thus, a ratio of 1000 cholesteryl-PEG-FITC molecules per particle was employed. The insertion of around 100 molecules per particle is well in line with their findings of approx. 165 siRNA molecules per particle for a ratio of 1500:1. Taking this into consideration, it seems unlikely that optimization of the protocol alone could mitigate the low insertion efficiency into SBCy050 OMVs compared to A549 EVs or liposomes.

Looking closer at the structure of the outer membrane the high density of negatively charged LPS becomes apparent (383). The repulsive force of these negative charges is bridged by divalent cations that lead to a tightly knit supramolecular structure that is important for the stability of the gram-negative cell-envelope (383). This structure could be the critical hindrance for the insertion of cholesterol into the membrane. While chelating agents such as EDTA can be used to destabilize the supramolecular structure of LPS, doing so can lead to the overall disintegration of OMVs (384). Thus, cholesterol post-insertion was not pursued further. Interestingly, in a recent publication Jiang et al. reported the post-insertion of a PEGylated phospholipid into OMVs derived from a *Salmonella enterica serovar* Typhimurium strain, which was modified by the deletion of a gene important for the generation of native LPS (385). It seems plausible that such modified OMVs might be more susceptible to post-insertion than native OMVs. However, as the post-insertion method used in their paper was omitted from it, further evaluation in relation to the work presented in this thesis is not possible.

5.2.2. Surface functionalization using Sulfo Cy-7 NHS ester

Compared to post-insertion, a one-step modification is more elusive for chemical functionalization of EVs. As explained in chapter 1.9.2, chemical surface modification with complex molecules is best carried out in two steps, as the functional groups naturally available for coupling on the EV-surface are likely present in the targeting moiety as well and would lead to undesired cross-reactivity.

Amino groups are abundant on the vesicle surface, easily addressable and have already been successfully used for the introduction of groups for bioorthogonal chemistry to mammalian EVs (225, 333). Thus, the modification of OMVs was tested using sulfo-cyanine 7 NHS ester, a water-soluble fluorescent dye.

Amino groups are however also present in the co-pelleted impurities and residual medium encountered in the pellet after UC. Thus, OMVs were first purified by SEC and then modified, followed by another step of SEC. While this method was very successful for OMV-modification, with low unspecific labeling, it already required two steps of SEC. Thus, the actual introduction

of a targeting moiety after NHS ester modification would increase this to three steps of SEC and a roughly 1 in 1000 dilution of OMVs. This could be circumvented by either performing NHS ester modification in the pellet or by finding a suitable protection strategy for amino groups of the targeting moiety, which would allow performing the surface modification in one step.

As it was anticipated that using the pellet instead of purified OMVs would greatly increase the amount of NHS ester needed to achieve the same degree of modification, which was later confirmed (Figure 39), a suitable amine-protection group was sought. With its mild deprotection through Staudinger reduction, the azide group was reckoned as the best-suited variant (386). The overall plan was to protect amino groups of the targeting moiety through diazotransfer and regenerate the amines *in situ* after installation on the vesicles. When literature research into diazotransfer revealed that it could also be performed in aqueous media (371), the question was raised, whether diazotransfer could also be used on the vesicles to generate AzideOMVs and replace NHS ester modification.

5.2.3.   Diazotransfer

The aim of diazotransfer-modification of OMVs was to introduce a new method for the introduction of azide groups to the surface of OMVs that would be insensitive to co-isolated impurities and more economical than using expensive NHS esters. While the synthesis of ISA used in aqueous diazotransfer is straightforward, as with many low molecular weight azide-compounds (387), there are some safety concerns for this molecule. While ISA HCl was originally considered insensitive to impact and friction (365), reports of its explosive behavior prompted a further investigation. Fischer et al. studied the sensitivities of different salts of ISA and determined that the hydrochloride was indeed more sensitive than initially estimated and that other salts, particularly the sulfate and mesylate exhibited a better safety profile (370). Thus it was originally decided to use ISA sulfate in the present study synthesized according to the protocol of Potter et al. (379). The precipitation of ISA sulfate however failed in two attempts. Thus, ISA HCl was prepared instead by precipitation with 4 M HCl in dioxane. To enhance its shelf life, ISA HCl was stored under argon at -20 °C and part of it aliquoted in portions of several milligrams to limit freeze-thawing. Despite its volatile properties, no problems in its handling occurred in the approximately two years of its use. Compared to diazotransfer used in chemical synthesis, diazotransfer to OMVs has the advantage that only very small amounts of ISA are needed per reaction and thus the risk in handling is reduced. Indeed, the yield of 355 mg ISA HCl would be sufficient to perform over 4000 diazotransfer reactions at a scale of 500 µl per reaction.

Already before the synthesis of ISA the diazotransfer conditions described by van Dongen et al. were applied to SBCy050 OMVs to make sure that the presence of $CuSO_4$ and base would

not affect them (371). A particle-recovery of approx. 80% was deemed acceptable and the issue of precipitation was successfully tackled by replacing K_2CO_3 with NaOH (Figure 32).

After successful synthesis of ISA HCl, assessment of diazotransfer started. Assuming that diazotransfer would lead to a similar density of azide groups on the vesicle surface as modification with sulfo-cyanine 7 NHS ester – approx. 200 per particle – and assuming a concentration of approx. $2*10^{11}$ particle per ml, the azide concentration would be at around 66 pmol/ml after diazotransfer. Quantifying azide groups by FTIR at this low concentration in complex OMV samples would be very difficult and unreliable. Thus, the effectiveness of the diazotransfer process was evaluated by derivatization of the vesicles by SPAAC with a fluorescent dye. Due to its high fluorescence and good solubility, the alexafluor derivative DBCO AF594 was chosen. It had the additional advantage of allowing the visualization of modified particles using the 532 nm laser of the nanosight instrument. DBCO AF594 was used at 4.9 µM, the concentration determined as optimal for surface modification of OMVs with sulfo-cyanine 7 NHS ester.

To determine the concentration of ISA HCl used in the assay, some assumptions based on the protocol of van Dongen et al. were made (371). In their diazotransfer to horseradish peroxidase, they used an excess of 1.75 equivalents of ISA HCl compared to the amount of amines available in the enzyme. Assuming that the density of amino groups in the proteins encountered in the OMV-pellet would be similar to horseradish peroxidase and based on a protein-concentration of approx. 400 µg/ml in the pellet as indicated by BCA assay, the ISA HCl concentration was calculated. To account to the potentially less ideal conditions in the OMV pellet compared to an isolated protein in water, the amount of ISA was increased to "10 equivalents" instead of "1.75 equivalents". As diazotransfer to SBCy050 OMVs was quite successful after the optimization of the reaction pH and the incubation time, the initial ISA concentration was used throughout all experiments and was not further optimized. In his master thesis, Philipp Lapuhs tested diazotransfer on OMVs derived from another strain of Myxobacteria. There he also began evaluating the effect of varying the ISA HCl concentration between 0.08 mM and 1.62 mM compared to the standard concentration of 0.81 mM. He found a decrease to 56% for 0.08 mM and an increase to 142 % for 1.62 mM, suggesting that further optimization might be possible (Supp. figure 52 D).

As conditions of diazotransfer might negatively affect vesicle stability, its effect was measured in two ways. NTA was employed to assess the effect diazotransfer had on particle-recovery and the AUC of OMV-samples on the ÄKTA instrument measured at 280 nm gave a general approximation of the intactness of the vesicle surface-proteins and their cargo.

As the mechanism for diazotransfer involves the nucleophilic attack of the amine on the terminal nitrogen of ISA (364), increasing the nucleophilicity of amino groups through deprotonation at a high pH was likely beneficial. Consequently, the pH was the first parameter to be optimized. Initial experiments using the original protocol by van Dongen et al. showed only a low modification. Due to the presence of buffer-salts and soluble impurities, the OMV-pellet was buffered and would require the addition of considerably more base than in the original protocol (371). Increasing the pH increased the modification efficiency greatly. This finding was in accordance to the work of Schoffelen et al., who investigated diazotransfer at pH 11 and 8.5 (388). However, as to be expected, the increased pH also led to a decrease in vesicle-stability, visible in NTA- and ÄKTA-analysis. In most cases, vesicle-stability as indicated by NTA was higher than measured by ÄKTA AUC. This could indicate that while the increased pH and copper-ions could lead to the alteration and loss of surface-proteins of the vesicles, they would have less of an effect on the overall integrity of the vesicles as a particle.

To balance both modification efficiency and vesicle-stability, a pH of 9.5 was chosen for subsequent modification of SBCy050 OMVs. In his master thesis Philipp Lapuhs observed the same increase in modification efficiency with increasing pH, however the *Stigmatella aurantiaca*-dervied OMVs he used in his experiments better tolerated high pH-environments, as no decrease in recovery rate was found between pH 9.5 and pH 11.0 (Supp. figure 52 A-C). This indicates that diazotransfer can be transferred to OMVs from other bacterial strains, however they might differ in their susceptibility to the diazotransfer-conditions.

At the same time as the pH, the incubation time for diazotransfer was optimized. A shorter incubation time was desired, to speed up the process of OMV modification and to reduce the strain of incubation at increased pH. The incubation time was gradually reduced from 20 h – employed by van Dongen et al. (371) – to 2 h and then 30 minutes. Interestingly, the step from 20 h to the two shorter incubation times led to an increase in modification efficiency (Figure 35), hinting that the degradation of OMVs under longer incubation would outweigh the potentially higher amount of installed azides. The recovery rate at 30 min was only slightly increased by the change in incubation time, indicating that the incubation pH had a greater impact on OMV-stability than the incubation time.

As a further parameter to show the mild effect of diazotransfer on SBCy050 OMVs, the autofluorescence of treated and untreated OMVs was compared (Figure 36). The autofluorescence of the OMVs, discovered by Eilien Heinrich in her master thesis, is based on protoporphyrin IX, which due to its lipophilicity is likely associated with the membrane of the vesicles. The observed reduction to 85% of the control was well in line with the vesicle recovery measured by NTA and ÄKTA.

The actual association of the DBCO AF594 with the vesicles as opposed to the co-elution of dye-particles formed during incubation with the vesicles was confirmed using the fluorescence mode of the NTA instrument (Figure 34). The fluorescence mode showed that AF594 was generally associated with particles in the same size-range as the vesicles and that the fluorescence of the particles varied depending on the diazotransfer conditions, confirming the bulk fluorescence measured by plater reader.

To confirm the suitability of diazotransfer as a method to introduce azide groups to the surface of OMVs, the optimized protocol was compared to surface modification using sulfo-cyanine 7 NHS ester (Figure 39). While diazotransfer unsurprisingly led to a lower modification than application of the NHS ester to purified OMVs, it performed significantly better than both 4.9 µM and 49 µM sulfo-cyanine 7 NHS ester applied to the OMV pellet. These results assume that the SPAAC reaction performed as a second step for diazotransfer would be as effective in addressing azides as the NHS ester is at addressing amines. This is likely not the case, thus the effectiveness of diazotransfer was underestimated in this assay. Still, these results clearly indicate that at least for the modification of OMV-samples containing soluble impurities from the conditioned medium diazotransfer is superior in terms of vesicle surface engineering compared to NHS esters. While azidoacetic acid NHS ester and similar molecules are more widely commercially available than ISA, the lower consumption of material as well as the cheap and easy synthesis of ISA outweigh this disadvantage. This makes diazotransfer the more economical variant, which is an important consideration for industrial application. Additionally the application of ISA sulfate or mesylate would reduce problems associated with the volatile nature of ISA HCl.

In conclusion, it was demonstrated that OMVs can be effectively modified by diazotransfer and their integrity can be conserved through optimization of the experimental parameters. NHS esters, while effective for the modification of purified OMVs are very sensitive to soluble impurities. Cholesterol-insertion was shown to be not suitable for OMVs derived from SBCy050 myxobacteria, while it worked as expected with EVs derived from mammalian cells. Compared to modification with an NHS ester and diazotransfer, cholesterol-insertion however only showed a low modification efficiency.

5.3.   Introduction of targeting moieties to OMVs

5.3.1.   Design rationale of the linker and targeting moiety construct

After the successful optimization of diazotransfer, the next aim was the introduction of bacteria-specific targeting moieties to SBCy050 OMVs using a modular linker molecule (Box 2). As the

surface engineering of bacterial vesicles and chemical surface modification of EVs in general have not been explored in much detail yet, it was deemed worthwhile to design a molecule that would not only be applicable in this specific case of targeting SBCy050 OMVs to bacteria but that could find general applicability in the EV-field. To achieve this, the desired properties of the linker molecule were:

1) Sufficient solubility, so that non-reacted linker could be removed by SEC. This property is crucial, as co-eluting unbound molecules would interfere with the assessment of EV-targeting

2) A very fast and bioorthogonal linkage between linker and targeting moiety that would allow for the modular introduction of different targeting moieties, reaching from small molecules to antibodies. Ideally, it should be possible to generate the conjugate *in situ* by mixing an aliquot of linker and targeting moiety each and after their reaction applying them to AzideOMVs without further purification.

3) Incorporation of a fluorescent dye. As with the optimization of the diazotransfer protocol, fluorescence measurement would be a convenient read-out, both for the modification efficiency and the targeting ability. Knowing the effectiveness of the labeling, one can determine if unsuccessful targeting is caused by an insufficient amount of targeting moieties on the vesicle-surface or the general inactivity of the chosen targeting moiety. Fluorescent labeling of OMVs would also allow following their fate in future *in vivo* experiments.

Derivatives of cyanine 5 were chosen as the fluorescent dye. They show high fluorescence paired with relatively high photostability while being considerably cheaper than alexafluor dyes such as AF594 that were used in the initial experiments. Cyanine 5 in particular was chosen, because its excitation and emission wavelengths were compatible both with common fluorophores such as fluorescein and GFP that could be used to label bacteria in targeting experiments and the confocal microscope and FACS instrument available at the institute.

To both increase solubility and flexibility of the linker, short monodisperse PEG-chains were included into the molecule. While for the PEGylation of nanoparticles usually PEGs in the size range of 1000 Da or more are used (270), a shorter chain-length was chosen, to make synthetic handling of the linker easier and to reduce the shielding-effect, longer PEGs might have. The rationale behind this was that the natural ability of myxobacterial OMVs to interact with their prey might be beneficial for antibacterial drug-delivery.

An ideal fast and bioorthogonal reaction to link targeting moiety and linker is IEDDA. To make it orthogonal also to SPAAC and CuAAC, TCO would be used as the dienophile in IEDDA and DBCO as the strained alkyne in SPAAC (349). Both show no cross-reactivity towards azides

and tetrazines respectively. Tetrazine was chosen to be anchored on the targeting moiety due to the broader catalogue of commercially available tetrazine-derivatives with different functional groups.
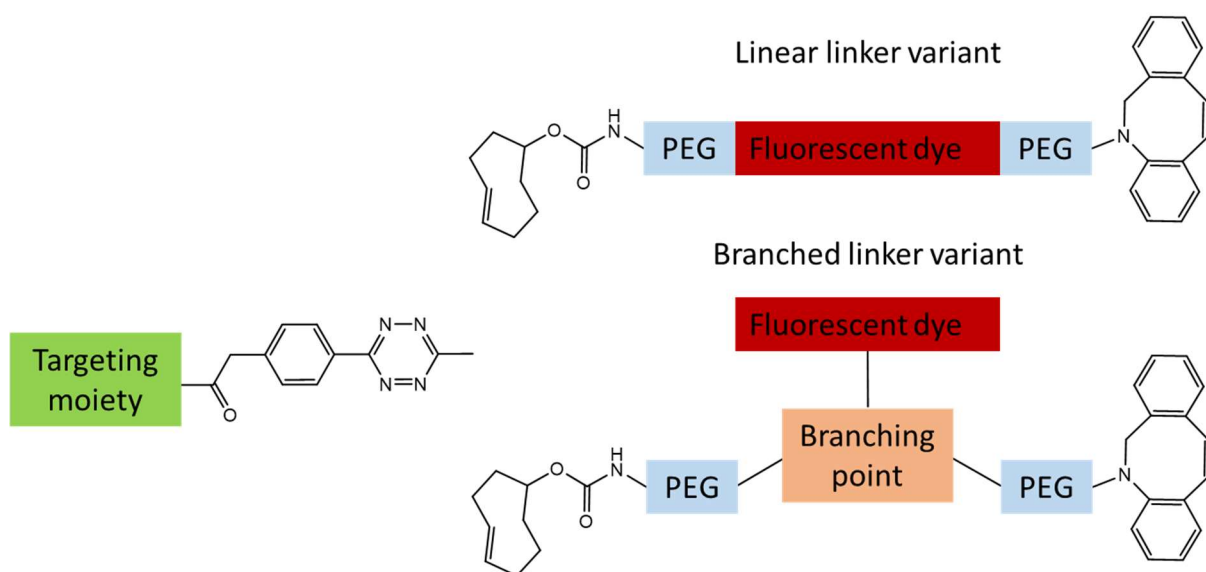
Figure 56: Schematic structures of the linear and branched linker molecule. For the surface modification of AzideOMVs, first, the linker would be reacted with the methyltetrazine-labeled targeting moiety via IEDDA, then the resulting molecule would react with the vesicles via SPAAC.

With all its parts determined only the overall make-up of the linker was left to be determined. With the alkyne and TCO to be located on opposite ends of the molecule either a linear molecule that incorporates the dye in its backbone or a branched molecule with three branches holding the alkyne, TCO and dye could be synthesized (Figure 56). The linear variant would rely on a bifunctional fluorescent dye forming a bridge between TCO and alkyne, while in the branched variant a trifunctional molecule would take over this duty.

5.3.2. Synthesis methyltetrazine-vancomycin

Parallel to the synthesis of the first linker molecule, methyltetrazine-vancomycin was synthesized as a model targeting moiety. Its wide application for the targeting of antibacterial nanoparticles and the possibility to precisely control its modification made it an ideal starting point and potential "positive control" to other targeting moieties employed later. Two distinct architectures of vancomycin are possible by addressing either its amino or carboxylic acid function (see 1.7.1). While attachment at the carboxylic acid is more widely applied, both variants showed bacterial binding in literature and attachment to the amine led to a higher specificity towards gram-negative bacteria. Thus, this variant was synthesized first to determine its applicability for OMV-targeting. While the yield of the reaction was quite low,

sufficient quantities of methyltetrazine-vancomycin were obtained for a first evaluation of its applicability as a targeting moiety for OMVs.

5.3.3.   Synthesis of the SPAAC-based linker

The SPAAC-based linker, the first linker molecule that was synthesized, was based on the linear linker-variant (Figure 56). The main reason for this was to reduce the amount of steps of the synthesis. As no suitable molecules incorporating both DBCO and two other functionalities to attach TCO and fluorescent dye are commercially available (or vice versa for TCO), the synthesis was based on azide-PEG$_3$-cyanine5-PEG$_4$-amine. While this allowed for reaching the desired linker-molecule in two steps, it greatly limited the reaction, as due to its exceedingly high price, the synthesis had to be carried out on a scale of just 2 mg. While the desired product was obtained, the yield obtained was very low.

This low yield was probably at least partially caused by the degradation of the product during HPLC. The ions observed in LC/MS can be assigned to the molecule lacking the DBCO group (see 4.5.2 and Figure 40), which is supported by the participation of the degradation product in the IEDDA reaction with methyltetrazine vancomycin. Apparently, the degradation of the linker was increased by longer dwelling-time on the column as the ratio of intact linker to degradation product strongly decreased, when the HPLC-method was made longer. This on-column degradation would also explain why the degradation product was found in all fractions of the prepHPLC – the observed degradation product was generated *in situ* during the analysis of the fractions.
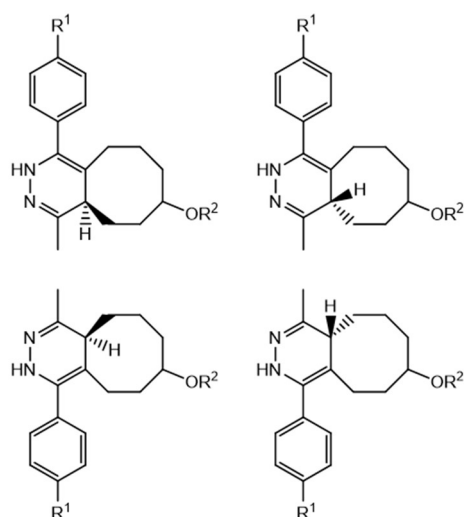
Figure 57: Possible products of the IEDDA reaction between methyltetrazine and TCO. R^1 represents the targeting moiety, R^2 represents the linker molecule.

Besides its low yield, the SPAAC-based linker demonstrated that the generation of the linker-targeting moiety-conjugate directly before the vesicle modification was indeed possible by simple mixing of 1 μl aliquots of the reaction partners for 1 h. LC/MS showed the generation of three peaks each for the SPAAC-based linker and its degradation product (Supp. figure 9). Multiple peaks with the mass corresponding to the product were indeed visible in all IEDDA reactions (Supp. figure 23, Supp. figure 45 & Supp. figure 47). Based on the possibilities for association between tetrazine and TCO, the reaction can lead to four diastereomeric products (Figure 57). The formation of different IEDDA-products was also observed by other researchers, who used norbornene instead of TCO as

the dienophile (389, 390). Due to the high amounts of compound needed to isolate and assign the respective isomer to the different peaks, no further analysis was performed in this regard.

It seems clear however, that depending on the educts the formation of some variants seem to be favored under the reaction-conditions employed. Generally, only three major peaks of the product were observed. This might however also be an issue of the resolution of the LC/MS-method employed for analysis. While different isomers might differentially impact the targeting ability of targeting moieties attached to vesicle surface, this effect should be greatly mitigated by the flexibility of the PEG-chains incorporated into the linker.

Test-experiments for the modification of AzideOMVs demonstrated the insufficient solubility of the SPAAC-based linker. From the early elution of linker molecules in the absence of OMVs, it can be inferred that the linker formed particles when mixed with PBS at 4.9 µM. Even though there was a higher fluorescence measured for AzideOMVs compared to the control OMVs and the PBS control (Figure 41), which would indicate a preferred interaction through SPAAC, the presence of unbound linker would lead to artifacts and wrong assumptions during the evaluation of OMV-targeting. The conjugation of vancomycin, which was supposed to increase the hydrophilicity of the linker, did not sufficiently improve the situation (Figure 42). Thus, a new, more soluble linker-molecule was needed.

5.3.4. Considerations for a more soluble linker molecule

The low solubility of the SPAAC-based linker indicated that short PEG-chains alone would not be enough to get a sufficiently soluble molecule. An easy way to increase the solubility of the molecule would be replacing the cyanine 5 dye with its water-soluble sulfonated version that would carry out the dual function of increasing solubility and providing fluorescence. This change meant also the transition from a linear to a branched linker-design, as no suitable heterobifunctional sulfo-cyanine derivatives are available and their de-novo-synthesis seemed too laborious to be worthwhile. A convenient branching point for the linker would be amino acid derivatives, as they contain three different branches and are widely available.

Another possible culprit for the low solubility of the SPAAC-based linker was the DBCO group. An alternative, less bulky cyclooctyne derivative would likely be less reactive and show cross-reactivity towards tetrazine and thus could not replace it (349). Thus, the only alternative would be changing from SPAAC to CuAAC and using a much less bulky alkyne to perform the linkage between linker and OMV. While this course of action entailed evaluating, if CuAAC would work with OMVs, the prospect of ensuring the sufficient solubility of the new linker made this a worthwhile endeavor. Moreover, as opposed to DBCO, where its introduction to the linker would require an extra step in the synthesis, propargyl glycine could be used as convenient,

alkyne-containing starting material. To extent the targeting moiety from the vesicle surface, a TCO-PEG-derivative would be used to introduce the TCO-group. Of the commercially available molecules, TCO-PEG$_8$-amine offered the best ratio of price and PEG-length.

5.3.5. Optimization of CuAAC

Before the CuAAC-based linker molecule was to be synthesized, first CuAAC for OMV modification needed evaluation.

CuAAC has been successfully performed with EVs before by Smyth and coworkers (333), but neither was their protocol very optimized, nor did they evaluate EV-stability beyond the size-distribution of treated and untreated EVs. The biggest concern in CuAAC is oxidative damage to biomolecules through copper and ascorbic acid, thus their concentrations should be as low as possible. Compared to the protocol of Hong et al., who recommend the usage of 0.1 mM CuSO4 and a five-times excess of the copper-ligand (340), Smyth et al. used a 100 times higher copper-concentration with only two times excess of bathophenantroline, which acted as the copper-ligand in their protocol.

Initial CuAAC-experiments directly followed the protocol of Hong et al. (340), but even after increasing the alkyne-concentration by a factor of four, only about 30% of the modification efficiency of the SPAAC reaction were reached. Two factors most likely greatly influenced the completion of the CuAAC reaction: The very low azide-concentration and the complexity of the OMV-sample. To counteract these issues, a modified protocol was devised. Cu(I) ions were generated directly and after complexation with THPTA were mixed with the concentrated alkyne, to effectively generate the active complex of copper and alkyne that would be able to directly react with the azides in the OMV sample. This measure increased the modification efficiency to approx. 50% of SPAAC, which was not deemed sufficient. Thus, further optimization was desired.

During the activation of the alkyne, its proton is replaced with a copper ion. It seemed likely that by making the solution of alkyne, THPTA, Cu(I) and ascorbate alkaline, the acidity of the alkyne would lead to the more effective generation of the alkyne-copper complex. As visible in Figure 43, this was indeed the case and using this approach, the same modification efficiency as with SPAAC was reached. While alkaline conditions lead to an increased oxidation of sodium ascorbate visible by an increasing yellow discoloration of the solution, sufficient amounts of ascorbate for the reduction of Cu(II) were evidently present.

The increase in pH was accompanied by a reduction in OMV-stability compared to SPAAC and CuAAC performed in the absence of NaOH. While this instability could be partially circumvented by decreasing the incubation time to 2 h, this also led to a decrease in

modification efficiency. Thus, the CuAAC-protocol with 4 h incubation and the inclusion of NaOH was adopted as the standard protocol.

Unfortunately, the effect of CuAAC on the autofluorescence of SBCy050 OMVs became apparent only later, during the evaluation of the PEG$_6$-linker. Compared to SPAAC, the autofluorescence of the vesicles was lost almost completely. As the recovery rate measured by ÄKTA AUC indicated that there was not a pronounced loss of vesicle-contents, the reduced autofluorescence suggests that the generation of reactive oxygen species during CuAAC could have led to its degradation. Omitting NaOH during CuAAC only slightly increased the recovered autofluorescence, indicating that indeed the presence of copper and ascorbate seemed to cause the loss in fluorescence. It is likely that CuAAC also caused oxidative damage to the vesicles beyond this easily assessable parameter. Thus, while unfortunate, this finding at least circumvented the laborious evaluation of modified OMVs for oxidative damage and clearly indicated that CuAAC is not suitable for the surface modification of EVs beyond prove-of-concept experiments.

5.3.6. Synthesis of linkers for CuAAC

Based on the initial positive assessment of CuAAC and the considerations for the design of a branched linker molecule, two attempts for the synthesis of a suitable CuAAC-linker were made, with the first unsuccessful iteration giving important insights for the second one.

Initially the synthesis was performed using TCO-PEG$_8$-amine and Boc-propargyl glycine. The Boc protection group, compared to using an Fmoc group to protect the amine, has the advantage that the byproducts generated during deprotection can be readily removed through evaporation on a rotavapor. However, the effect the deprotection-conditions would have on the carbamate ester, which attached the TCO group to the molecule, was underestimated. This led to the significant production of the diamine byproduct that, not being removed prior to the attachment of the dye, resulted in the formation of byproducts (Figure 44). While these were successfully removed and the pure PEG$_8$-linker acquired, the high acid-concentration during deprotection likely also had a more profound effect on the molecule, by most likely changing the cyclooctene from its reactive *trans*-isomer to the unreactive *cis*-isomer. No reactivity whatsoever in IEDDA reactions was found for the finished linker molecule, while the Boc-protected intermediate was still active (Supp. figure 22 & Supp. figure 23). NMR-analysis of both compounds revealed a change of the two protons associated with the double bond (Figure 45). The observed change in the NMR-spectrum conformed to the change observed by Nikić et al. who evaluated the effect thiols had on the isomerization of *trans*-cyclooctene to its *cis*-isomer (391).

Besides the Boc deprotection conditions, light exposure was deemed another potential corroborator of the isomerization of TCO. TCO is typically prepared from *cis*-cyclooctene through UV-irradiation at 254 nm (392). In the same way, light-exposure might lead the molecule to isomerize back to the inactive form.

Thus, for the second synthesis attempt, Fmoc-propargyl glycine was chosen as the branching point, after test-experiments with the Boc-protected intermediate showed no loss of IEDDA-reactivity upon incubation under Fmoc-deprotection conditions. In addition, all reaction-steps were carried out protected from light as far as possible. As no TCO-PEG$_8$-amine was available at the time of the second linker-synthesis, it was carried out using TCO-PEG$_6$-amine instead, assuming similar properties of the finished linker molecule.

Despite the precautions taken, NMR-analysis of the intermediates before and after Fmoc-deprotection and purification again showed a change in the protons associated with the double bond, suggesting the partial isomerization of TCO during these synthesis steps (Supp. figure 30). The presence of both isomers was confirmed by LC/MS of the crude PEG$_6$-linker after the attachment of sulfo-cyanine 5. There, the UV-channel showed the presence of two peaks, both corresponding with the mass of the linker (Supp. figure 31). The identity of the *cis*- and *trans*-isomer were confirmed by derivatization of a prepHPLC-fraction obtained from a test-purification that contained both molecules (Supp. figure 32). While the earlier eluting peak would react with methyltetrazine-vancomycin, the later-eluting peak remained. Thus, the prepHPLC-method was optimized to obtain an acceptable separation of both compounds.

NMR-analysis of the active and inactive PEG$_6$-linker showed the same picture as before (Figure 46). Both compounds were further analyzed by 2D-NMR to confirm the differences found in the cyclooctene ring (Table 2). There carbons and hydrogens making up the ring could be identified and revealed differences that would indicate a change in the conformation of the ring.

In total, the synthesis of the CuAAC-linkers revealed a very high sensitivity of the TCO-group, which complicated the whole process and made the synthesis less efficient. For future linker-molecules, thus a solution to the issue of TCO-isomerization during synthesis is desired. TCO in general is prone to inactivation by isomerization, as observed in the experiments presented here, but also by other researchers (391, 393). The isomerization-problem has been addressed by Darko and coworkers, who synthesized a dioxolane-fused *trans*-cyclooctene with enhanced chemical stability (350). However, the issue of light-sensitivity seems not to be resolved by this measure, as irradiation-based isomerization is still part of the synthetic procedure. Moreover, their molecule is not commercially available. Thus, two main solutions remain to limit the generation of inactive byproducts.

1. TCO and methyltetrazine could be exchanged. Attachment of TCO to the respective targeting moiety can be achieved in one step, thus limiting the exposure to potentially unfavorable conditions. At the same time, methyltetrazine has demonstrated a very high chemical stability (351) and in our hands no inactivation due to light-exposure was observed during the synthesis of methyltetrazine-vancomycin, neither are there descriptions of it in literature. Thus, using a methyltetrazine-PEG-derivative in the linker synthesis might lead to better results.

2. TCO could be replaced with another functional group. There are multiple possible dienophiles that could replace TCO (349). One of these, norbornene is commercially available, chemically stable and seems not to be as light sensitive as TCO. While the rate of the tetrazine-norbornene IEDDA reaction would be considerably slower than reactions using TCO, the reaction rate still would reach similar or faster kinetics than typical SPAAC-reactions (349). Norbornene has been successfully employed by multiple groups (389, 390) and is cheaply commercially available.

Both variants should be considered for future linker-molecules and also could be combined, by preparing a norbornene-labeled targeting moiety and a tetrazine-labeled linker.

5.3.7. Implementation of CuAAC-linkers

Despite its unreactivity in IEDDA reactions, the PEG_8-linker still was useful in preliminary experiments to demonstrate the sufficient solubility of the branched linker-design and its ability to react with AzideOMVs via CuAAC. Unspecific labeling of control OMVs was of a similar proportion as labeling with DBCO AF594, while only very little early elution of the linker in the absence of OMVs was found (Supp. figure 21). The amount of bound molecules using AzideOMVs was much higher than for both DBCO and alkyne AF594. The overall positive evaluation of the molecule was an important base for the synthesis of the subsequent PEG_6-linker.

With the IEDDA reactivity preserved, the PEG_6-linker was reacted with OMVs both in its native state and after IEDDA reaction with methyltetrazine-PEG_4-biotin and methyltetrazine-vancomycin. On its own, modification per particle was about 20% lower than for the PEG_8-linker, while the unspecific labeling stayed in the same range. However, compared to the linker incorporating the slightly longer PEG, the early elution in the absence of OMVs was approx. four times higher (Supp. figure 21). This would suggest that the small change from PEG_6 to PEG_8 actually had a greater than anticipated impact on the linker's solubility in aqueous media.

The issue of early elution was abolished completely by reacting the PEG_6-linker with methyltetrazine-PEG_4-biotin (Supp. figure 21). Modification with the resulting biotinlinker led to

a significantly higher degree of modification than the plain PEG$_6$-linker. However, unspecific labeling for the biotinlinker was also much higher than for all other molecules employed in OMV-labeling so far. This unspecific labeling could be either based on an unspecific interaction of the untreated vesicles with biotin or be related to the copper ions and ascorbic acid added during the CuAAC-reaction. No further evaluation was conducted on this yet.

Biotinylated OMVs were employed for a proof-of-concept experiment to provide evidence of the covalent attachment of active and accessible biotin to their surface. OMVs modified with the biotinlinker or various controls were incubated with FITC-labeled streptavidin and after SEC-purification to remove unbound or unspecifically attached streptavidin, FITC-fluorescence of OMV-containing samples was measured. AzideOMVs modified with the biotinlinker showed significantly higher fluorescence than all the controls, albeit also control OMVs treated with the biotinlinker showed an increased fluorescence compared to other controls, indicating that unspecific labeling also led to the presence of intact biotin on the vesicle-surface.

As leftover TCO-PEG$_4$-DBCO was available from the synthesis of the SPAAC-based linker, it was used to generate an alternative "SPAAC-biotinlinker" through reaction with methyltetrazine-PEG$_4$-biotin, with which AzideOMVs were modified using the optimized SPAAC-protocol. Due to the absence of a fluorescent dye in this molecule, no direct information could be inferred about the density of biotin on the surface of these OMVs. Their ability to bind labeled streptavidin however was much greater than for OMVs modified with the CuAAC-based linker, even after taking into account the slightly lower particle recovery rates of the CuAAC-reaction compared to SPAAC (Figure 43 B). From this, it can be concluded that either modification by SPAAC was much more effective than CuAAC or that the CuAAC-conditions led to structural changes of the biotin, reducing the amount of streptavidin-binding moieties.

During the conjugation of the reaction product of the PEG$_6$-linker and methyltetrazine-vancomycin (vancomycinlinker), more problems were encountered. While the reaction product was formed as indicated by LC/MS and HRMS, its application in CuAAC led to a very high unspecific labeling of control OMVs. Thus, it was evaluated, whether this finding was based on surface features of the OMVs that would interact with vancomycin or if the CuAAC-conditions were the cause for it. Compared to control OMVs treated with the native PEG$_6$-linker or the biotinlinker, incubation with the vancomycinlinker in the absence of CuAAC-excipients did not show an increase in unspecific labeling. Conversely, employing CuAAC-conditions with or without NaOH led to a significant increase in unspecific labeling. Taken together with the findings for modification with the biotinlinker mentioned above, these data suggest that the

conditions during CuAAC can lead to the unspecific labeling of OMVs, which is another indicator of the unsuitability of CuAAC for OMV-modification.

Unfortunately, the unspecific labeling of OMVs prevented the implementation of vancomycin-modified vesicles in experiments evaluating bacterial targeting.

5.3.8. Conclusions from the synthesis and attachment of targeting moieties

From the syntheses of various different linker-molecules and their implementation for OMV-labeling, multiple conclusions can be drawn for the future synthesis of optimized linker molecules:

- Due to its harsh conditions, CuAAC is not suitable for the modification of OMVs and should be replaced with SPAAC.

- The branched design of the CuAAC-based linkers and the inclusion of the sulfonated cyanine dye were important steps to obtain a linker with sufficient solubility in PBS. As the comparison of the elution-profiles of the pure PEG_6- and PEG_8-linker revealed the solubility of the linker seems to be nonetheless in a very delicate balance, thus, subsequent molecules should include a longer PEG-chain, to outweigh the replacement of the alkyne with a DBCO-group.

- TCO is very sensitive and prone to isomerization, while methyltetrazine showed no obvious instability. Thus, changing from TCO to another less sensitive dienophile, such as norbornene could improve yields and stability of the final product. To reduce exposure of the dienophile during synthesis, it could be attached to the targeting moiety instead of the linker, as the former attachment should generally be achievable in less steps. Suitable norbonene-derivatives containing amines or activated esters are available.

Based on these conclusions, an alternative linker synthesis can be proposed (Figure 58).
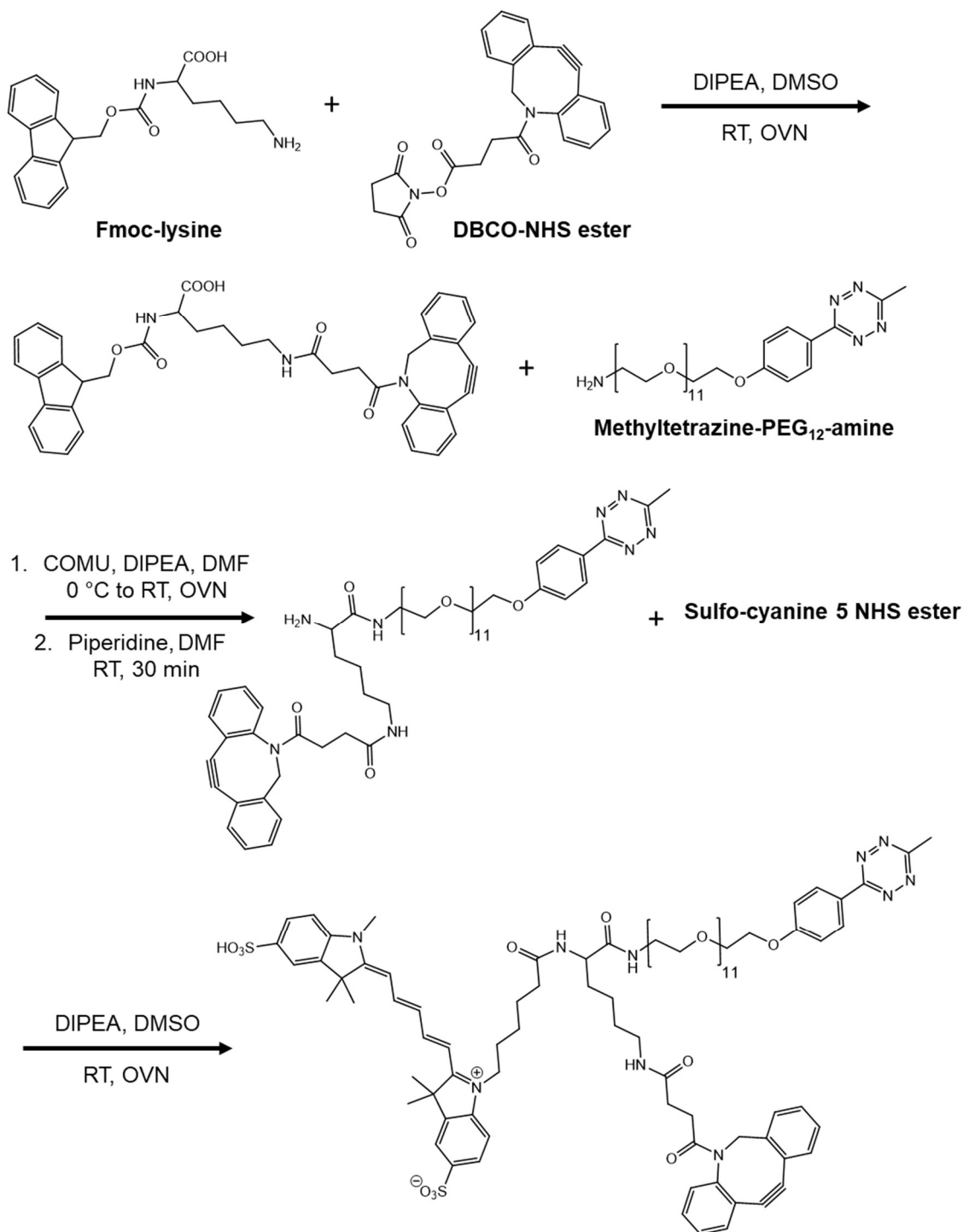
Figure 58: Proposed alternative synthesis pathway for a branched SPAAC-based linker.

5.4.   Glucuronidase encapsulation into EVs and evaluation of their storage stability

The third part of this thesis was concerned with the evaluation of the effect different storage conditions had on the stability of EVs, with the final aim of developing an optimized protocol for the lyophilisation of EVs for long-term storage (Box 2). As discussed above, keeping EVs stable during storage is an important factor for their future therapeutic application (1.6.1).

To assess the overall stability of EVs during storage, not only their colloidal stability needs to be measured, but also the stability of their cargos needs to be evaluated. As relevant cargos can greatly vary between EVs from different sources, β-glucuronidase was instead employed as a sensitive model-molecule that could be encapsulated into mammalian EVs using saponin incubation, as described in previous publications ((223, 224)). Enzyme activity was evaluated using the conversion of non-fluorescent fluorescein di-β-D-glucuronide to fluorescent fluorescein.

First, mammalian EVs from different sources were evaluated regarding their stability upon storage under different conditions and the stability of encapsulated enzyme, which was published in Frank, Richter et al. (377), with a detailed description of a protocol to evaluate the general storage-stability of EVs being published in Journal of Visualized Experiments (378).

Based on the findings obtained in these works, the conditions for lyophilisation were further optimized in cooperation with the group of Prof. Frieß at LMU Munich. The resulting manuscript by Trenkenschuh, Richter et al. is currently under review.

5.4.1.　　Storage stability of A549- and HUVEC-EVs

The effect of different storage conditions on the stability of mammalian EVs was evaluated using A549- and HUVE-EVs. These experiments were conducted as part of the publication of Frank, Richter et al., were besides A549 and HUVEC EVs also EVs derived from MSC-cells and liposomes were compared (377). Preliminary experiments using A549-EVs stored for only 48 h already revealed a central finding of this study that lyophilisation of EVs without the addition of a cryo- and lyoprotectant puts the vesicles under great strain and leads to particle-loss and an increase in particle size, which was also reflected in the size-distribution of EVs before and after storage (Figure 51). Similar results were obtained for HUVEC-EVs stored for 14 d (Figure 52). Here the physicochemical changes of EVs were even more profound, with only RT-storage showing no increase in mean particle size and especially frozen storage and lyophilisation showing a high loss of particles. These findings were in line with the experiments conducted by Julia Frank using liposomes and MSC-EVs. The latter however generally showed a higher stability than HUVEC- and A549-EVs. Importantly, not only lyophilisation, but practically all storage conditions evaluated led to particle loss. This indicates the general need for a better understanding of how EV-storage can be optimized. Based on these results, the effect of formulating EVs with the cryo- and lyoprotector trehalose was tested (Figure 53 & Figure 54). For 7 d storage of HUVEC-EVs, trehalose prevented an increase in vesicles-size, but it could not stop the loss of particles compared to storage at 4 °C. As with the other types of EVs evaluated by Julia Frank, the addition of trehalose led to an improved preservation of β-glucuronidase activity in lyophilized HUVEC-EVs.

Based on these results it was concluded that while lyophilisation exhibited some drawbacks regarding colloidal stability, other methods of storage also were not without problems and especially regarding the stability of encapsulated enzyme, lyophilisation seemed like the best alternative. Further optimization of lyophilisation-conditions would be nonetheless needed to make it a viable method that could replace the current gold standard, storage at -80 °C. Parameters to be optimized included the choice of cryoprotectants and their amounts, as well as an evaluation of the parameters of the lyophilisation-process. In the study by Frank et al. only trehalose, mannitol and PEG400 were evaluated. Other sugars, but also polymers such as PVP and mild detergents such as P188 and PS20, which were shown to stabilize liposome membranes (394, 395), potentially could improve EV-stability upon lyophilisation. Regarding the lyophilisation process, the basic protocol for the freezing and lyophilisation of the EV-samples could be optimized further to reflect the more intricate and controlled protocols used in industrial settings.

After the work of Frank Richter et al., more research was published on the lyophilisation of EVs (263, 264). These works confirmed the positive effect on trehalose on vesicle-stability. While Charoenviriyakul et al. did not evaluate the effect lyophilisation had on the particle-number (263), El Baradie et al. found a reduction in particle-concentration compared to samples before storage similar to our findings (264). They moreover evaluated PVP as an additional cryoprotective agent, which improved the recovery rate compared to trehalose alone.

5.4.2. Glucuronidase encapsulation into SBCy050 OMVs and Ro EVs

Based on the positive assessment of lyophilisation described in the previous chapter, a cooperation with the group of Prof. Frieß at LMU Munich was started to conduct a deeper evaluation of all factors that could be optimized to obtain lyophilisation conditions that would produce EV-formulations with long-term stability. RO-EVs were chosen as the vesicle-model, because their culture in suspension allowed an easier cultivation of the high amount of cells required for a large-scale long-term evaluation of different storage conditions.

Based on preliminary freeze-thaw and lyophilisation experiments conducted in Munich that demonstrated that a buffer exchange from PBS to 10 mM phosphate was crucial for obtaining stabilized vesicles and that the addition of P188 would further improve colloidal stability, four formulations were chosen for long-term storage:

1. 10 mM Na-phosphate with 5% sucrose and 0.02% P188

2. 10 mM K-phosphate with 5% sucrose and 0.02% P188

3. 10 mM Na-phosphate with 5% sucrose and 0.02% PVP

4. 10 mM Na-phosphate with 5% PVP and 0.02% P188

Na- and K-phosphate were differentiated, as they behave differently upon freezing, with Na-phosphate leading to an acidic pH-shift not found for K-phosphate (396). PVP was employed either as an adjuvant to sucrose, which replaced trehalose as a cheaper alternative with similar cryo- and lyoprotective properties, or PVP in combination with P188 was used as the main protective agent, in the same way as in the publication of El Baradie et al. (264). To obtain an assessment of the intactness and retention of EV-cargos, again β-glucuronidase was encapsulated in the vesicles.

Samples were stored up to six months at 2-8 °C and under stress-conditions at 25 and 40 °C. Colloidal integrity and enzyme stability were evaluated before and directly after lyophilisation and after one and six months of storage.

The evaluation of enzyme-activity before lyophilisation revealed much higher values for PVP-containing samples that for formulations 1 and 2 (Figure 55). This could indicate that PVP somehow had a protective effect during processing of samples before lyophilisation. Directly after lyophilisation however, the relation between the samples was reversed. While enzyme activity was reduced for formulations 1 and 2, no enzyme activity whatsoever was recovered for formulations 3 and 4, suggesting that PVP offered less protection during the freeze-drying process.

After one month of storage, enzyme activity increased for all samples compared to directly after lyophilisation, with formulation 1 at 4 °C showing the best recovery, revealing the same enzyme activity as before lyophilisation. The general propensity of the samples to recover their enzyme-activity could indicate that at least some of the changes introduced to the enzyme during lyophilisation were reversible under the conditions inside the EVs and the active conformation of the enzyme was partially recovered during the first month of storage through slow structural changes (261, 262). Compared to before lyophilisation, condition 1 performed best across all storage-temperatures, conditions 2 and 3 showed a similar reduction in enzyme activity and condition 4 lost the biggest fraction of its initial activity.

After six months of storage, enzyme activity was strongly reduced in all formulations. While some activity remained in formulations 1 and 2, 3 and 4 showed almost no recovery of active enzyme in their mean values with the individual results showing a broad spread around zero fluorescence. This high variance could be linked to the interaction of PVP with the β-glucuronidase-assay indicated by the values obtained with EV-free placebo samples, which showed a higher background than the controls for formulations 1 and 2. Overall, condition 1 afforded the best enzyme-stability.
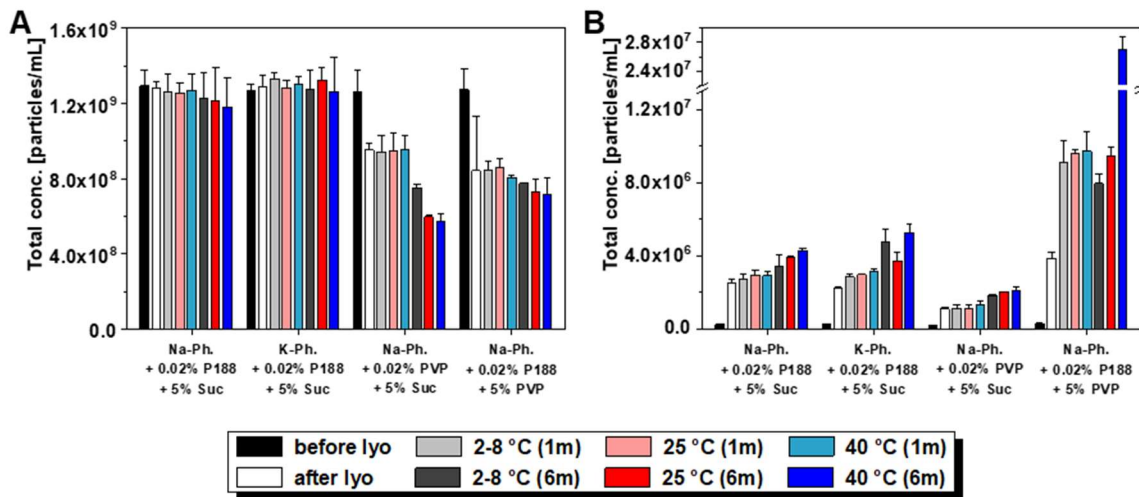
Figure 59: Assessment of the colloidal stability of RO-EVs. Vesicle-concentration was measured using TRPS. Panel A displays results obtained using the NP100 nanopore, which shows particles in the size-range from 50-330 nm. These correspond with intact EVs. Panel B shows results obtained using the NP600 nanopore, which corresponds to particles from 275-1570 nm and corresponds with vesicle-aggregates. This figure was adapted from Trenkenschuh E., Richter, M. et al. (2020). "Formulation development of lyophilized extracellular vesicles with long-term stability", manuscript submitted to Advanced Healthcare Materials.

The negative assessment of formulations 3 and 4 was also reflected in the data on the colloidal stability of the formulations obtained by Eduard Trenkenschuh in Munich. Both PVP-containing formulations showed a loss of particles, which got more pronounced with longer storage (Figure 59 A). While for formulation 4 it led to a high formation of aggregates, aggregate-formation was the lowest in formulation 3, which would indicate that here small particles were predominantly lost by vesicle-disintegration as opposed to aggregation (Figure 59 B). Formulation 1 and 2 showed an excellent colloidal stability throughout all time points and conditions (Figure 59).

The discrepancy between high colloidal stability and decreasing enzyme-activity could be based on either the loss or the inactivation of β-glucuronidase during freezing, lyophilisation or rehydration or it could be caused by slow degradation of the enzyme over time. As high enzyme-activity was recovered after one month of storage at least for some formulations, a general loss of enzyme through leakage from the vesicles seems unlikely. Thus it can be speculated that encapsulated enzyme degraded over time (397). With the high requirements of enzymes regarding their tertiary and quaternary structure, it is likely that small changes happening over time in the lyophilized state could accumulate and cause a reduction in enzyme-stability after six months of storage (261, 262). Enzyme-degradation could potentially be mitigated by the co-encapsulation of sufficient amounts of cryo- and lyoprotective agents,

as indicated by the study of Kannan et al. who showed that luminal sucrose increased the stability of liposomes during lyophilisation (398).

Due to its sensitivity to conformational changes, β-glucuronidase could potentially overestimate the effect lyophilisation has on less sensitive cargos of EVs such as RNA and DNA, where hydrolysis would be the main driver of their degradation. However, in this way, β-glucuronidase enabled a clear indication of potentially unfavorable storage conditions and compared to natural EV-cargos it allowed for a sensitive and easily performed assay for its quantification.

In conclusion, in this cooperative effort, optimized conditions for the lyophilisation and storage of mammalian EVs were obtained, to produce formulations with long-term stability. Importantly, the conditions of formulation 1, also led to a high colloidal stability of SBCy050-OMVs upon freeze-thawing and lyophilisation (Trenkenschuh E., Richter, M. et al. (2020). "Formulation development of lyophilized extracellular vesicles with long-term stability", manuscript submitted to Advanced Healthcare Materials), which suggests that the optimized conditions derived from this study could have general applicability to EVs regardless of their parent-cells. Still, further evaluation is needed in this regard. The next step will be the application of the knowledge gained on EVs with native biological activity, such as MSC EVs (399) or antibacterial OMVs derived from myxobacteria (21).

6. Conclusions and outlook

EVs hold many promises for future medicine and healthcare. Their successful translation from the lab to an approved medicinal product however has been lacking so far, despite numerous clinical trials. In this work, three main objectives were pursued (Box 2), development of a method for the surface modification of myxobacterial OMVs, introduction of bacteria-specific targeting moieties to the surface of said OMVs and evaluation of lyophilisation for long-term storage of mammalian EVs. While the first two targets mainly aimed at improving the pharmaceutical activity of OMVs by endowing them with targeting moieties, the third target is concerned with EV-storage as an important factor for their clinical translation.

After evaluation of cholesterol-insertion and NHS ester based chemical surface modification, diazotransfer was introduced to the vesicle-field as a new method for the generation of azide-labelled OMVs. Diazotransfer showed high efficiency in labeling and left only a low impact on vesicle integrity. Combined with SPAAC, it compared favorably to the established method of active ester based modification. These results demonstrated the high potential diazotransfer has as a fast and low-cost alternative to generate azide-labeled OMVs for subsequent surface modification using SPAAC, CuAAC or Staudinger ligation.

The introduction of bacteria-specific targeting moieties to AzideOMVs generated by diazotransfer was hindered by problems in the development of a suitable linker-molecule to tether the targeting moiety to the vesicle surface. While initial solubility-problems were successfully addressed, by changes in the linker design and the replacement of SPAAC with CuAAC, more problems were encountered subsequently. CuAAC, which after optimization showed similar efficiency to SPAAC, was shown to be unfavorable to EV-modification due to the reactive excipients used in the reaction. These led to changes in the OMVs indicated by a loss of autofluorescence and caused unspecific labeling of the vesicles when using vancomycin as a targeting moiety. Despite a successful proof of concept experiment using biotin as a targeting moiety, more work is needed to reach the goal of surface modification with bacteria specific targeting moieties.

Lyophilisation of EVs was first tested in two mammalian cell-lines, where the stress induced by lyophilisation became apparent through changes in vesicle-size and low particle recovery. Addition of trehalose as a cryoprotectant afforded some improvement and led to an improved preservation of the activity of encapsulated β-glucuronidase. Founded on these findings, in cooperation with the group of Prof. Frieß at LMU Munich, the conditions and excipients for lyophilisation were successfully optimized to obtain lyophilized EVs with very high colloidal stability and good preservation of the encapsulated enzyme. These results mark an important

step in the evaluation of lyophilisation for EV-storage, as for the first time mammalian EVs were lyophilized and stored without the loss of a substantial amount of particles.

Taken together, two of the original three main objectives of this work were reached successfully. For the second objective, despite not achieving the introduction of vancomycin as a targeting moiety to OMVs, nonetheless substantial advances were made towards the realization of this aim, as crucial requirements for future linker molecules have been elucidated.

6.1.   Outlook

For diazotransfer, the next steps will be the synthesis and implementation of another ISA-salt, either the sulfate or mesylate, to circumvent the volatile properties of the HCl salt employed in this study. Then, based on the work of Philipp Lapuhs, the ISA concentration employed during diazotransfer could be studied more closely to further optimize the method. Finally, the most important question for diazotransfer is whether it is applicable to mammalian EVs and other bacterial EVs, especially ones with innate antibacterial activity, which potentially could be further increased by the introduction of targeting moieties. Successful application of diazotransfer in mammalian EVs will moreover greatly increase its potential as a method of wide application in the vesicle-field.

Based on the findings presented here, a new linker molecule, potentially based on the example described in 5.3.8, needs to be synthesized. Once a linker molecule suitable for the reaction with targeting moieties and vesicles has been obtained, the applicability of vancomycin and other targeting moieties can be evaluated. The application of the modular linker could moreover be expanded beyond targeting bacteria, for example to target cells that might harbor bacteria in their cytoplasm.

The optimized protocol for the lyophilisation of EVs obtained in this work now can be applied to EVs with pharmaceutical activity. Additionally its ability to generate dry EV-formulations for inhalation or embedding in microparticles could be tested.

7. Supplementary data and figures
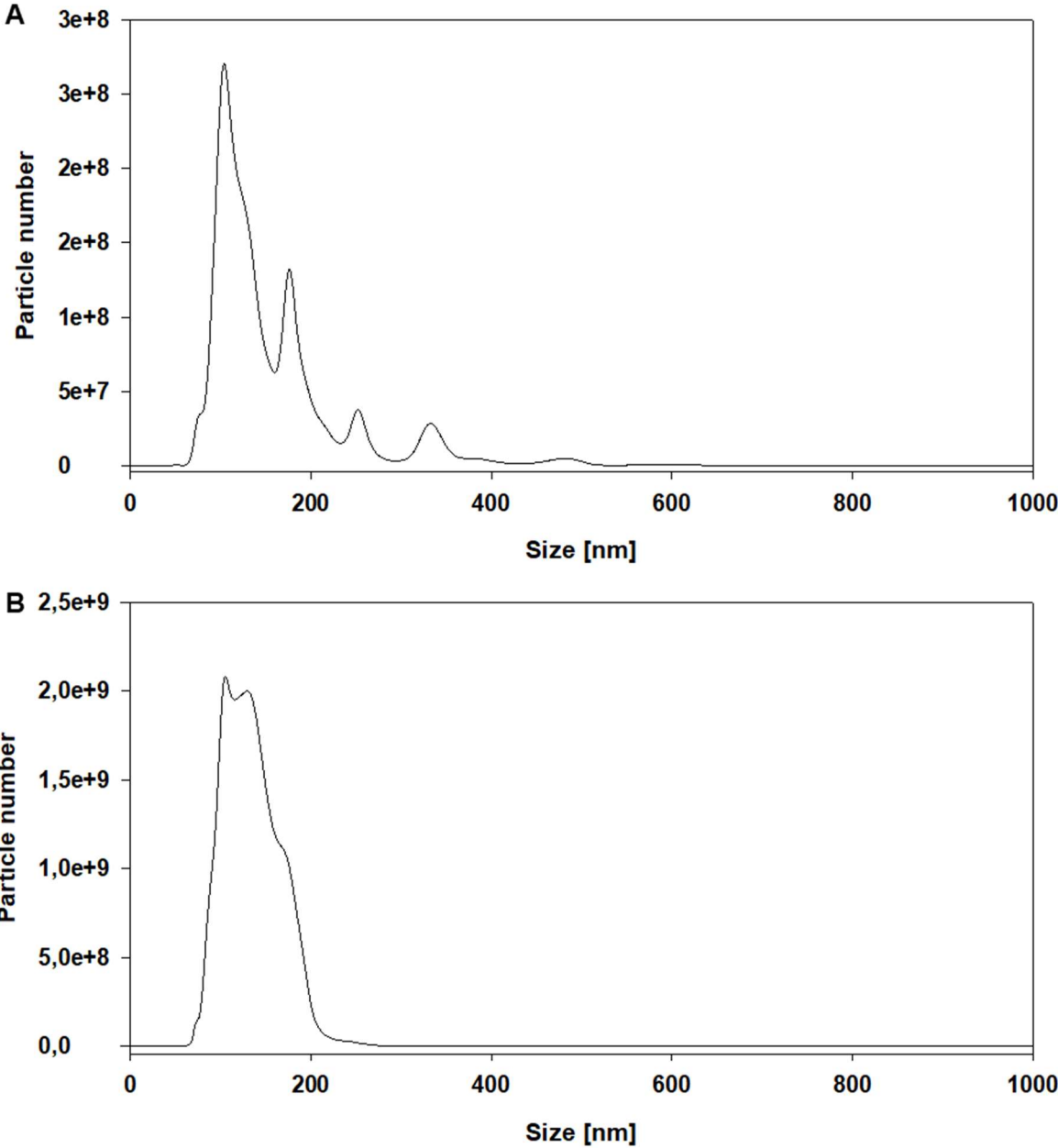
Supp. figure 1: Size distribution measured by NTA of A549 EVs (A) and liposomes (B). Curves represent mean values of three experiments.
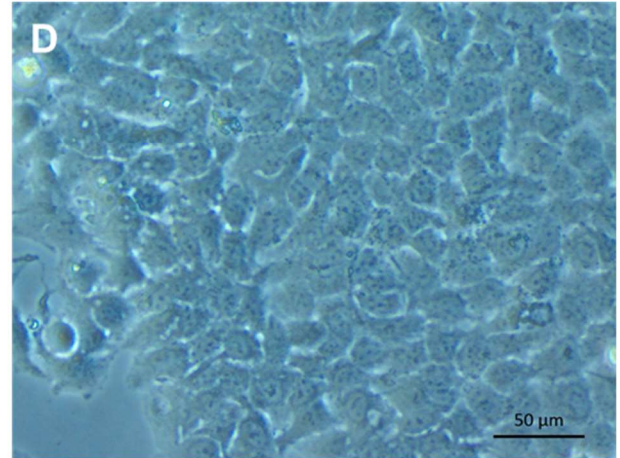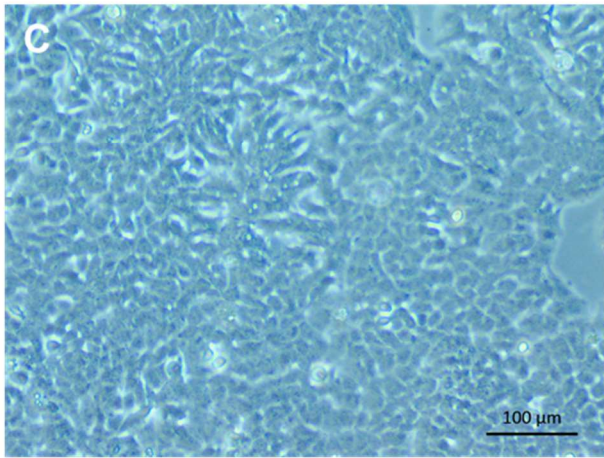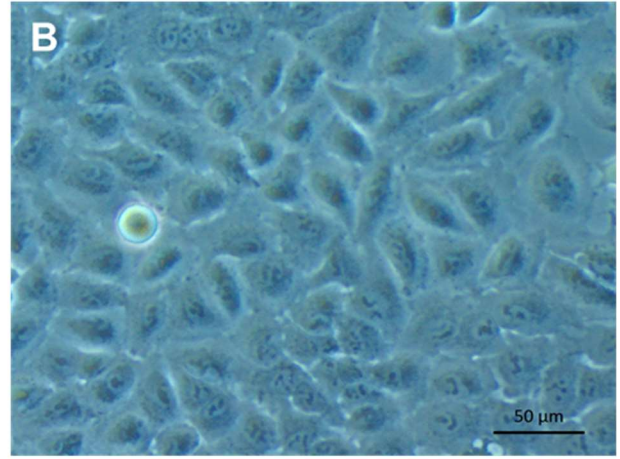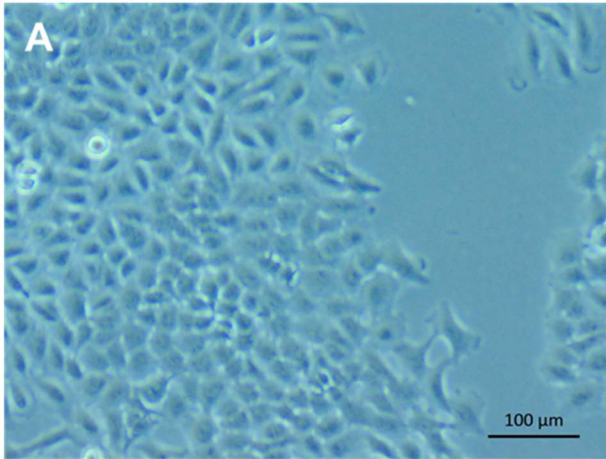
Supp. figure 2: Light microscopy of A549 cells. A&B show the cells after 120 h in culture, before the exchange to serum-free conditions. C&D show cells after another 48 h in serum-free conditions, just before EV-isolation.
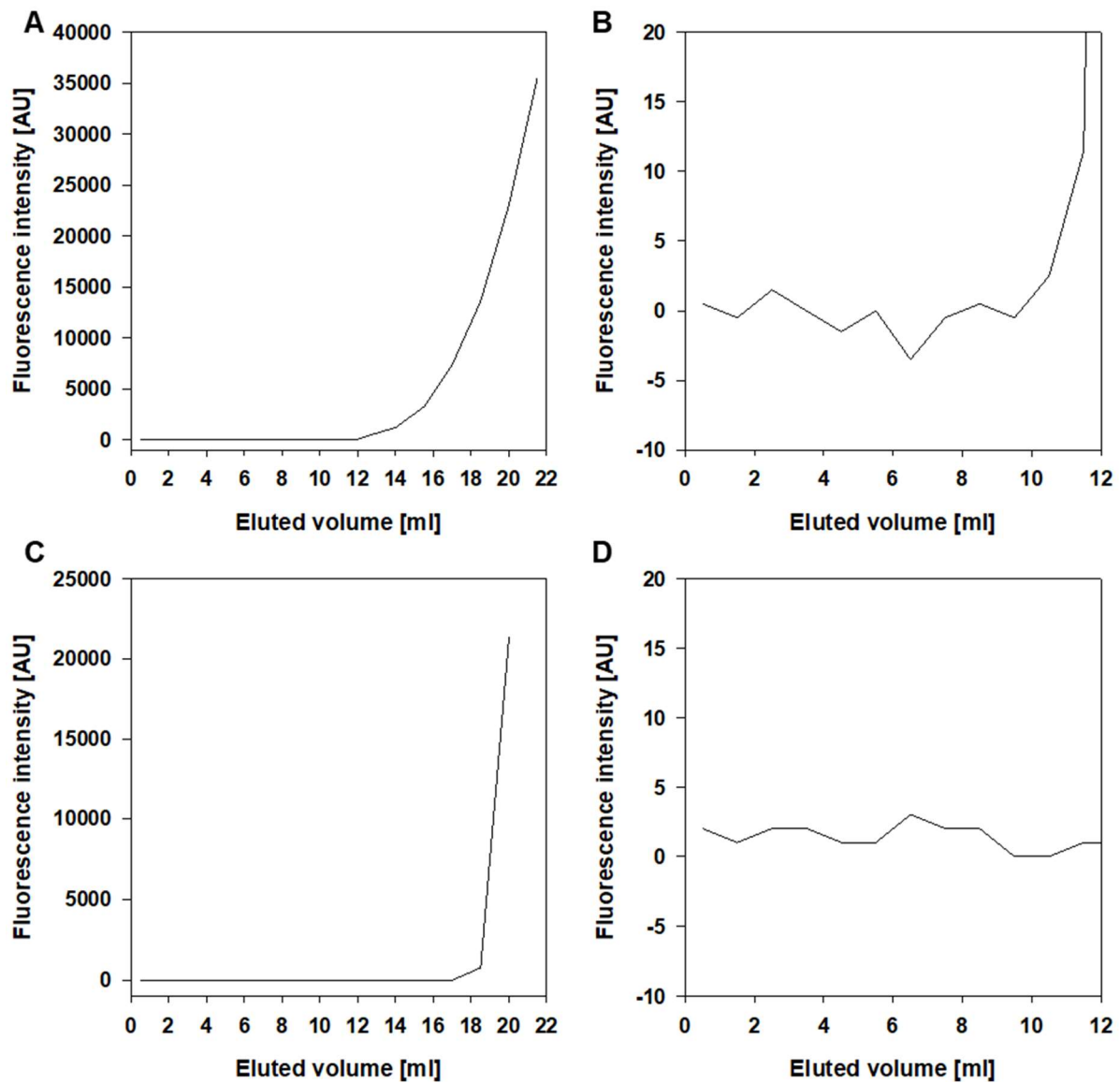
Supp. figure 3: SEC elution profile of injections of the DBCO Af549 (A&B) and alkyne AF594 (C&D). All samples were dissolved in PBS in the absence of EVs, DBCO AF594 at 4.9 µM, alkyne AF549 at 19.6 µM. Plots in the right column show a zoomed view of the region, were EVs would normally elute.
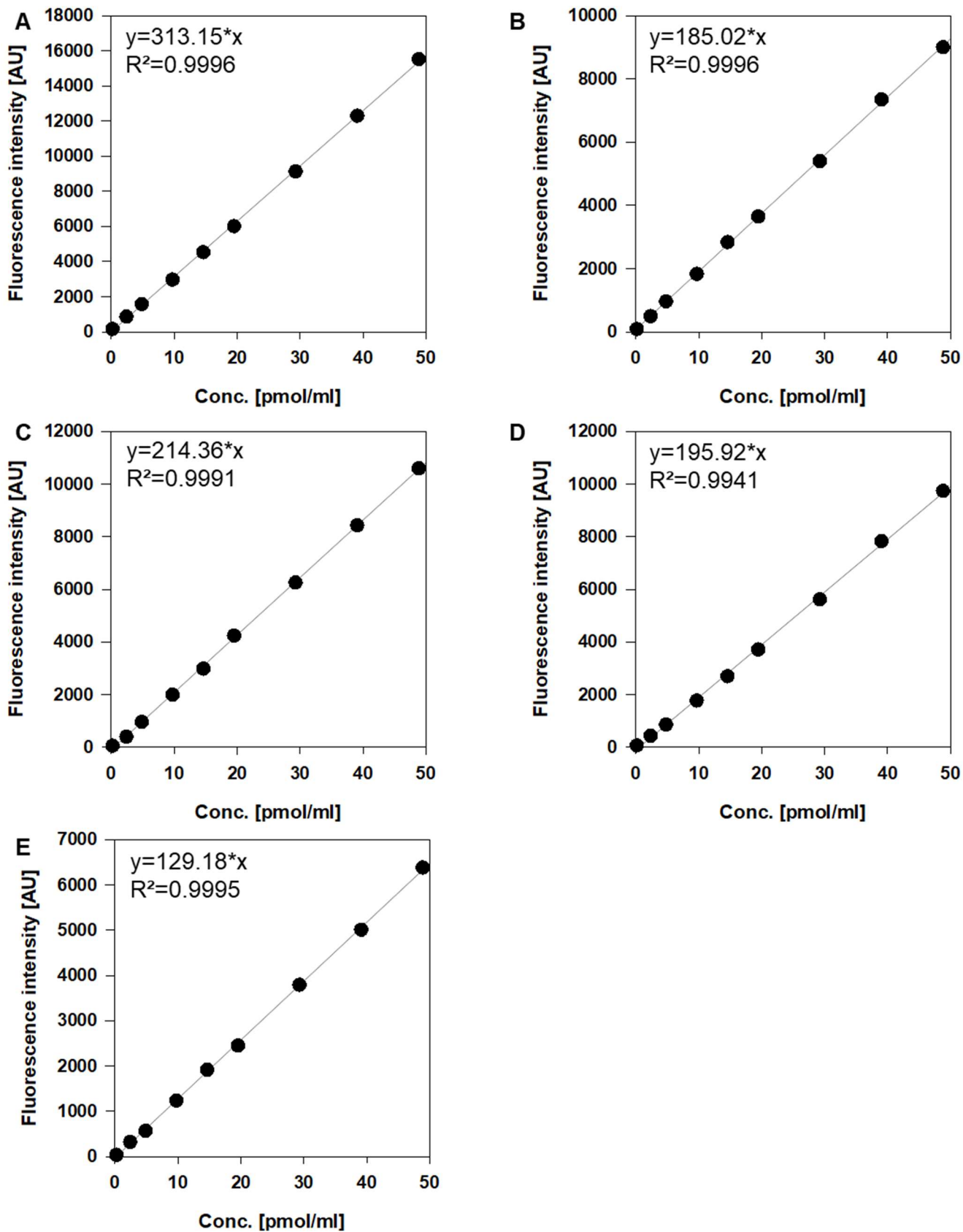
Supp. figure 4: Calibration curves for DBCO AF594 (A, n=4), alkyne Af549 (B, n=5), the PEG_8-linker (C, n=1), the PEG_6-linker (D, n=3) and the product of the IEDDA reaction of the PEG_6-linker and methyltetrazine-PEG_4-biotin (E, n=3). All calibration curves were prepared in fresh, filtered PBS. R^2-values were calculated using Excel 2016.
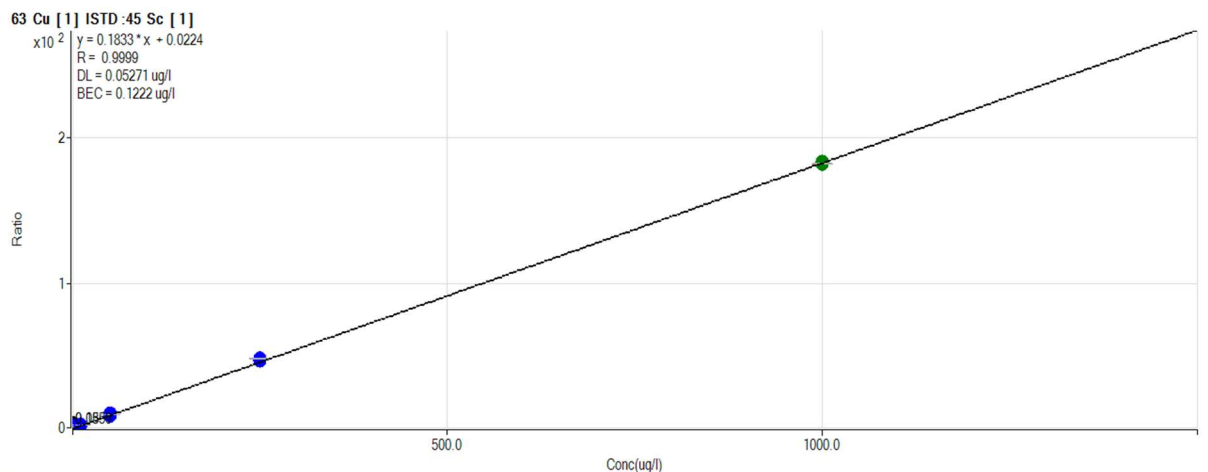
Supp. figure 5: Calibration curve for the quantification of residual copper in EV-samples. Prepared and measured by Kristina Brix.
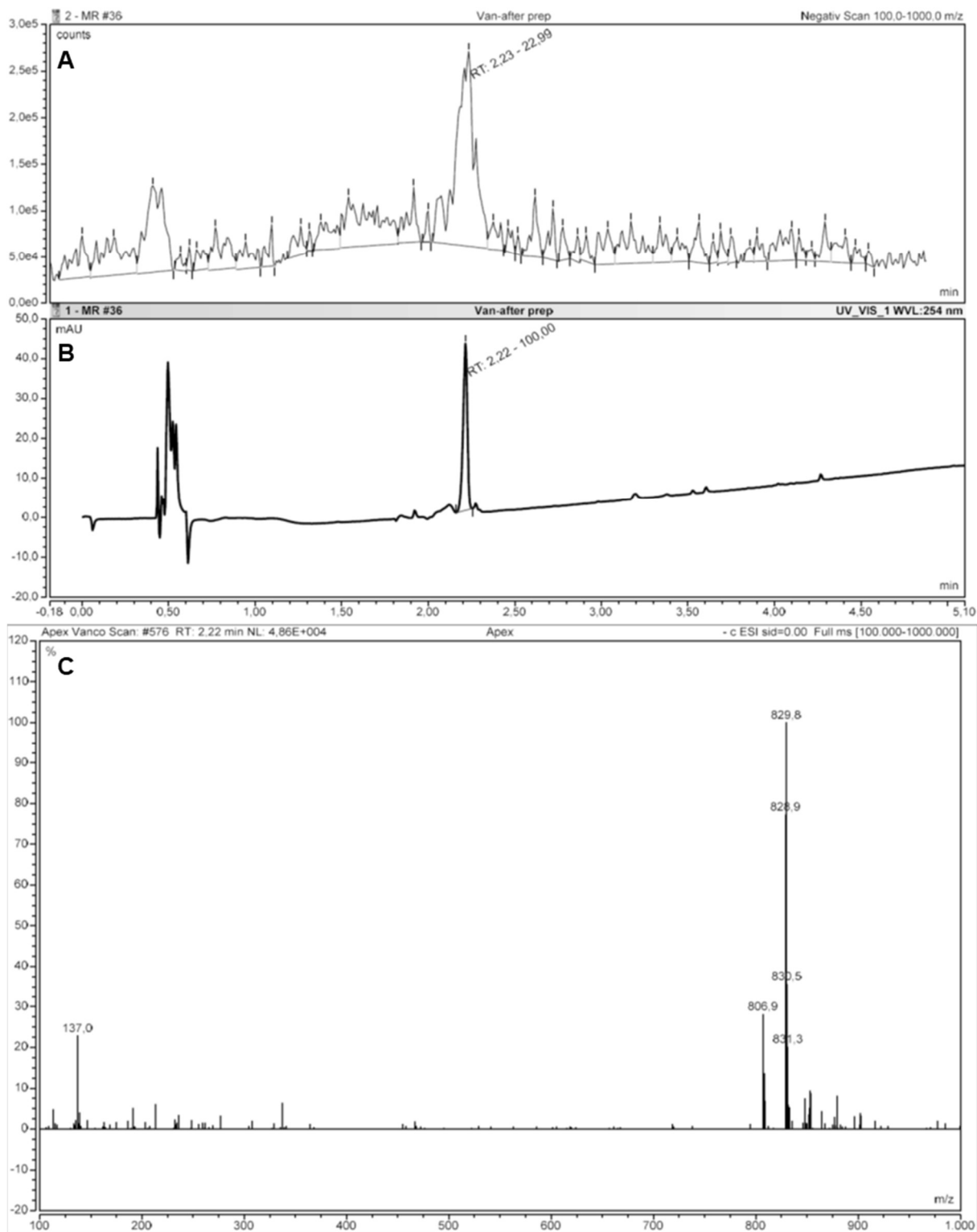
Supp. figure 6: Mass peak (A) and UV absorption at 254 nm (B) of purified methyltetrazine-vancomycin eluting at 2.2 min. Panel C shows the corresponding mass spectrum that shows the $[M-2H]^{2-}$ ion at 829.8 m/z.
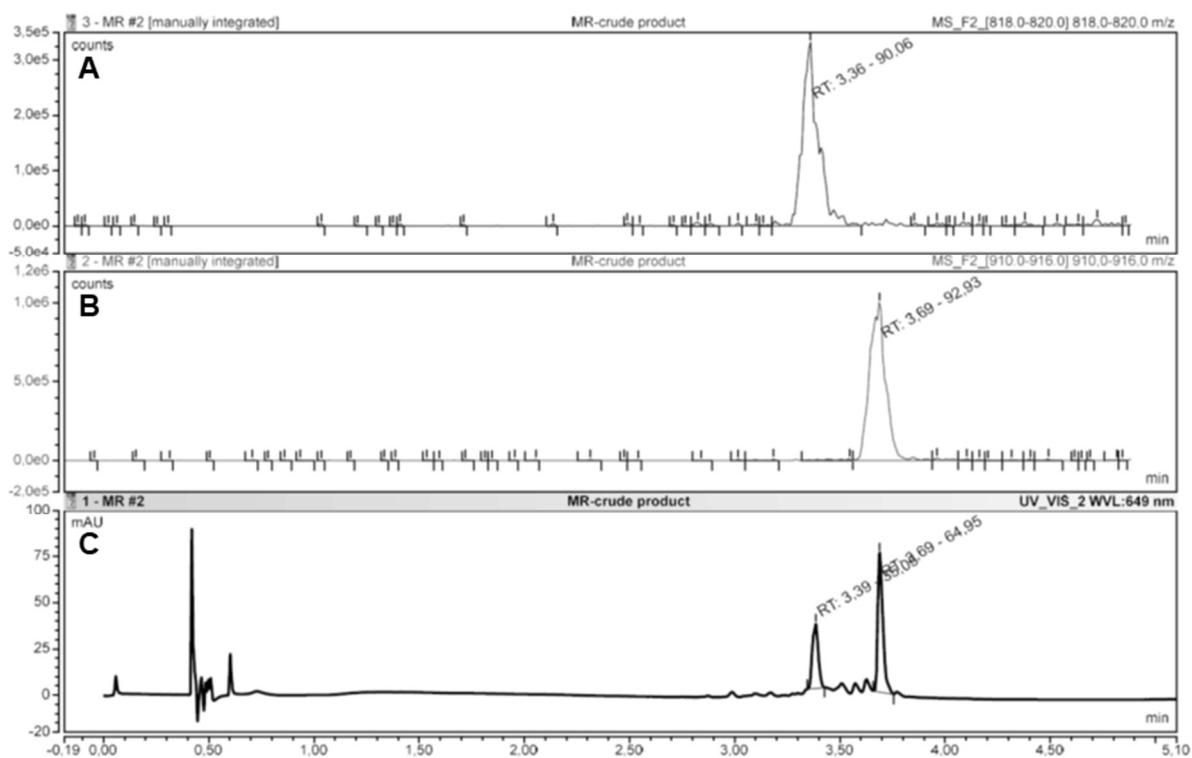
Supp. figure 7: Crude SPAAC-based linker. Panel A shows the peak corresponding to the mass of the degradation product eluting at 3.36 min. Panel B shows the peak corresponding to the SPAAC-based linker eluting at 3.69 min. Panel C shows the UV-absorption at 649 nm corresponding to the cyanine 5 dye incorporated into the linker and the degradation product.
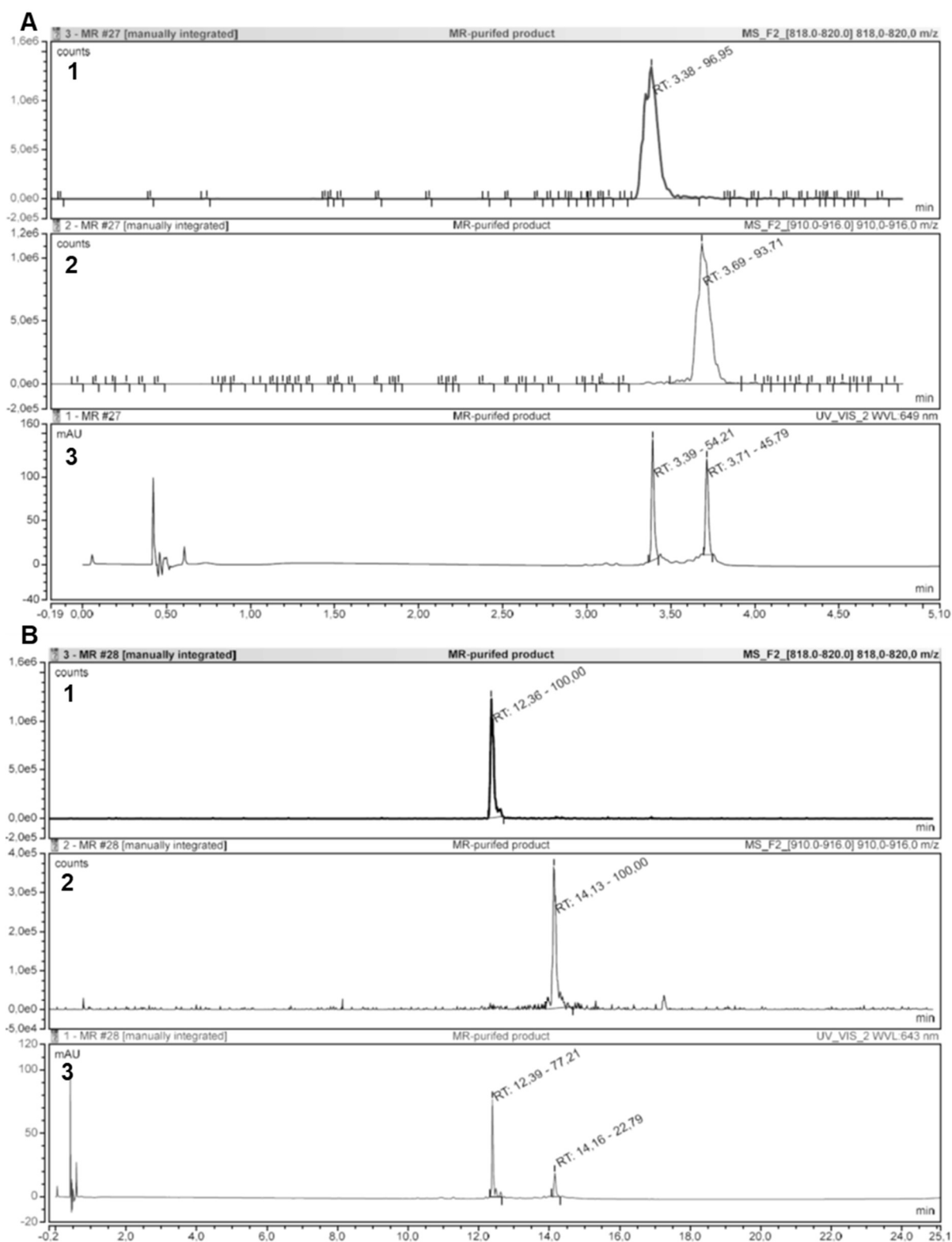
Supp. figure 8: Effect of different HPLC-methods on the stability of the SPAAC-based linker. A: 5 min HPLC-method. Peaks corresponding to the masses of degradation product (3.38 min; 1) and intact linker (3.69 min; 2), UV absorption at 649 nm (3). B: 25 min HPLC-method. Peaks corresponding to the masses of degradation product (12.36 min; 1) and intact linker (14.13 min; 2), UV absorption at 649 nm (3).
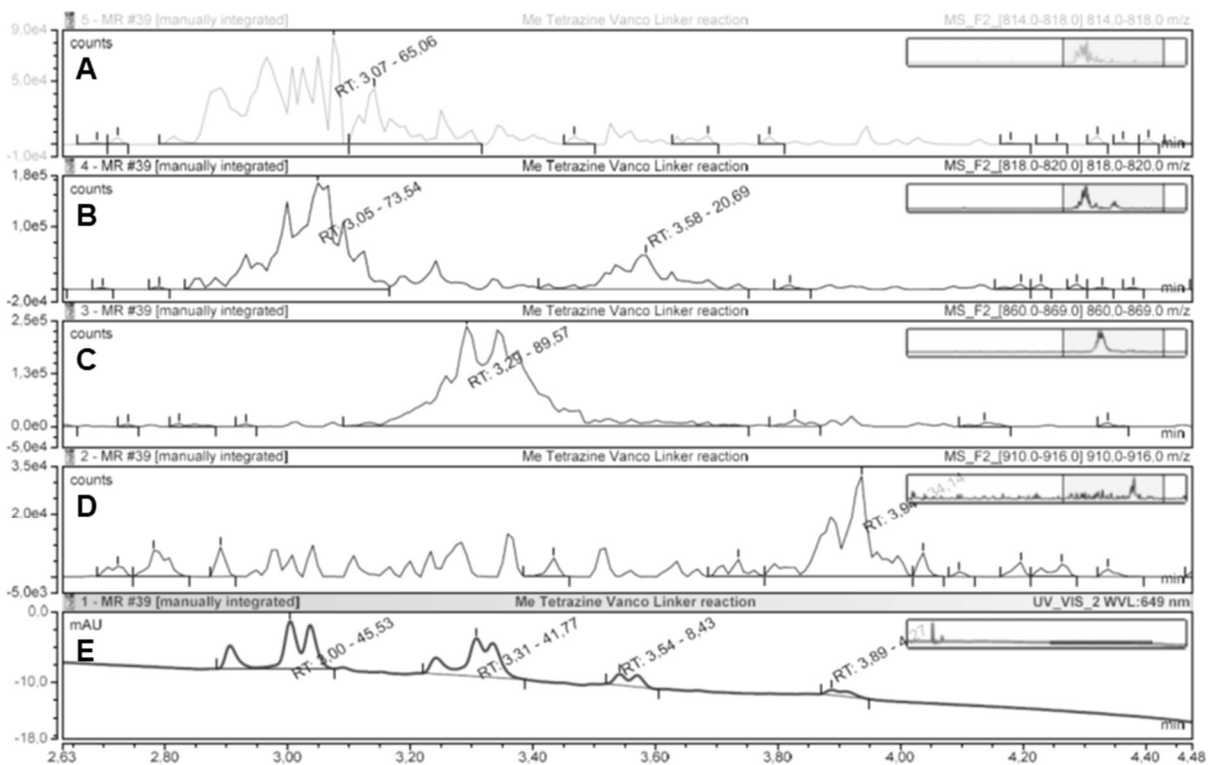
Supp. figure 9: IEDDA reaction of the SPAAC-based linker with methyltetrazine vancomycin zoomed in to the relevant peaks. A: Mass peak of the product of degradation product and methyltetrazine vancomycin (3.07 min). B: Mass peak of unreacted degradation product (3.58 min, ions with this mass were also measured for the product of the degradation product and methyltetrazine vancomycin). C: Mass peak of the product of SPAAC-based linker and methyltetrazine vancomycin (3.29 min). D: Mass peak of unreacted SPAAC-based linker (3.91 min). E: UV absorption at 649 nm of the reaction products of the degraded linker (3.00 min, three peaks), the intact SPAAC-based linker (3.37 min, three peaks), unreacted degradation product (3.54 min) and unreacted SPAAC-based linker (3.89).
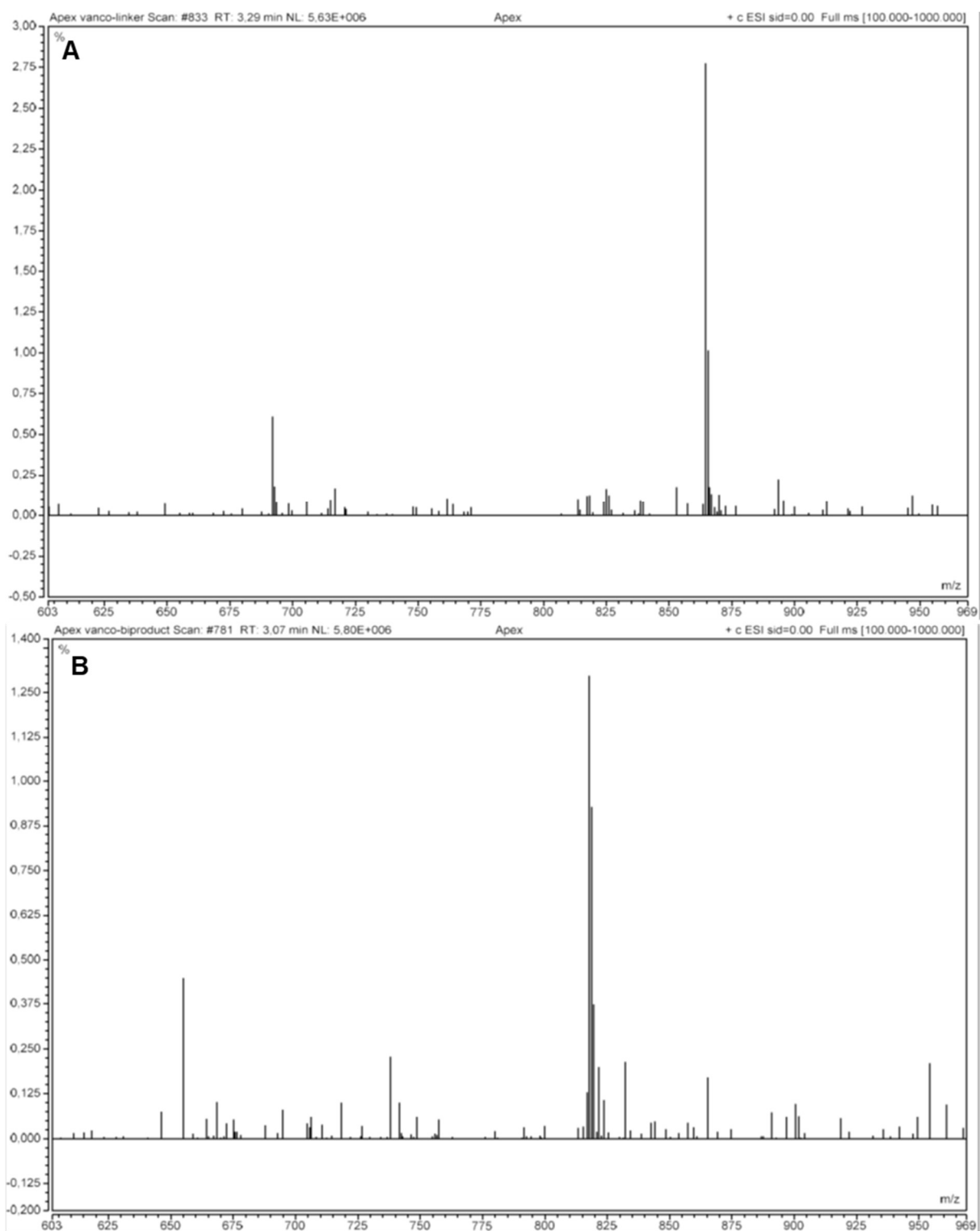
Supp. figure 10: Mass spectrum of the reaction-product of the IEDDA reaction with methyltetrazine vancomycin of the SPAAC-based linker (A, $[M+3H]^{4+}$ detected at 861.3 m/z) and the degradation product (B, $[M+3H]^{4+}$ detected at 817.8 m/z).
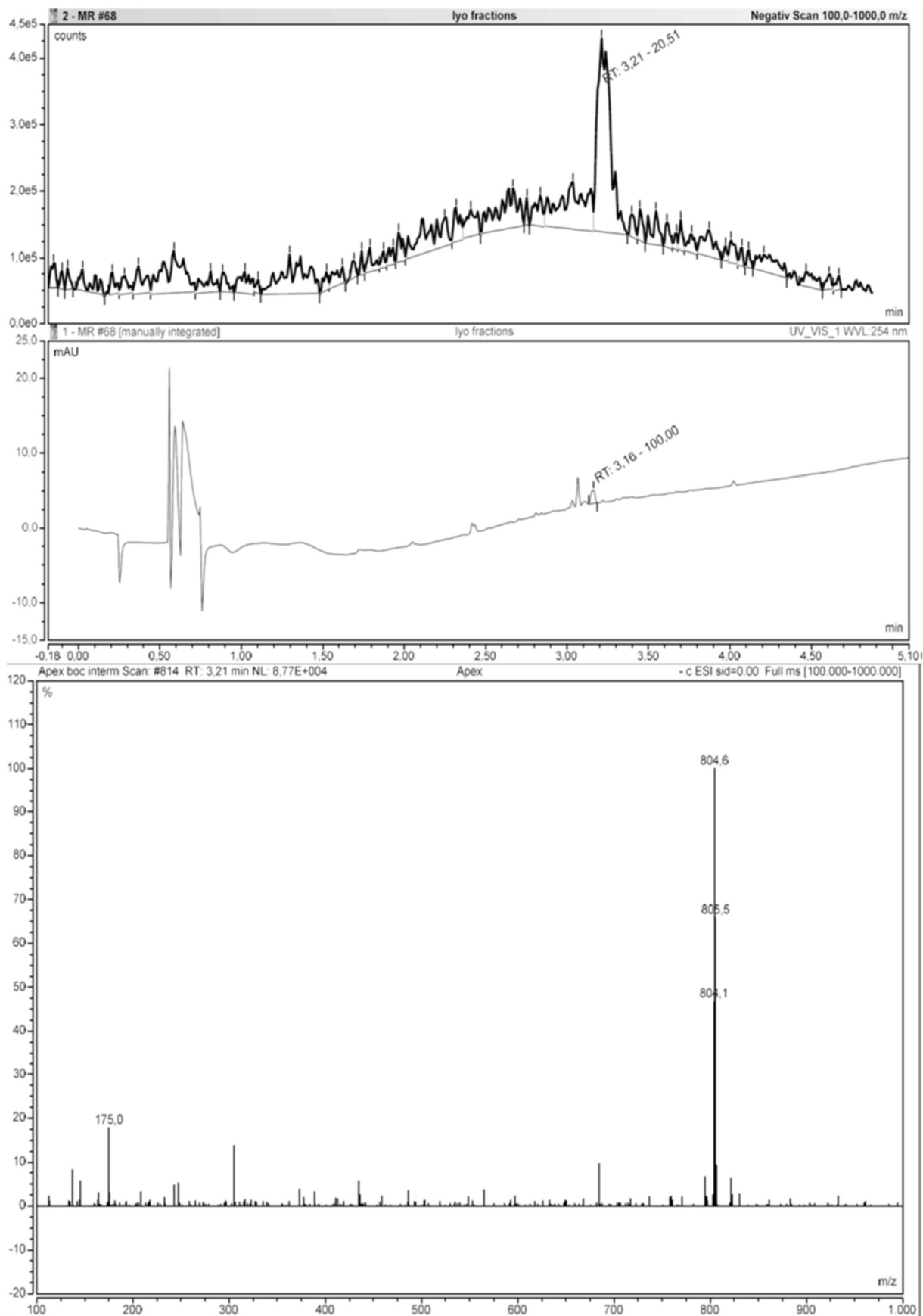
Supp. figure 11: Mass peak (A) and UV absorption at 254 nm (B) of the purified Boc-protected intermediate eluting at ~3.2 min. Panel C shows the corresponding mass spectrum that shows the [M+FA-H]⁻ ion at 804.6 m/z.
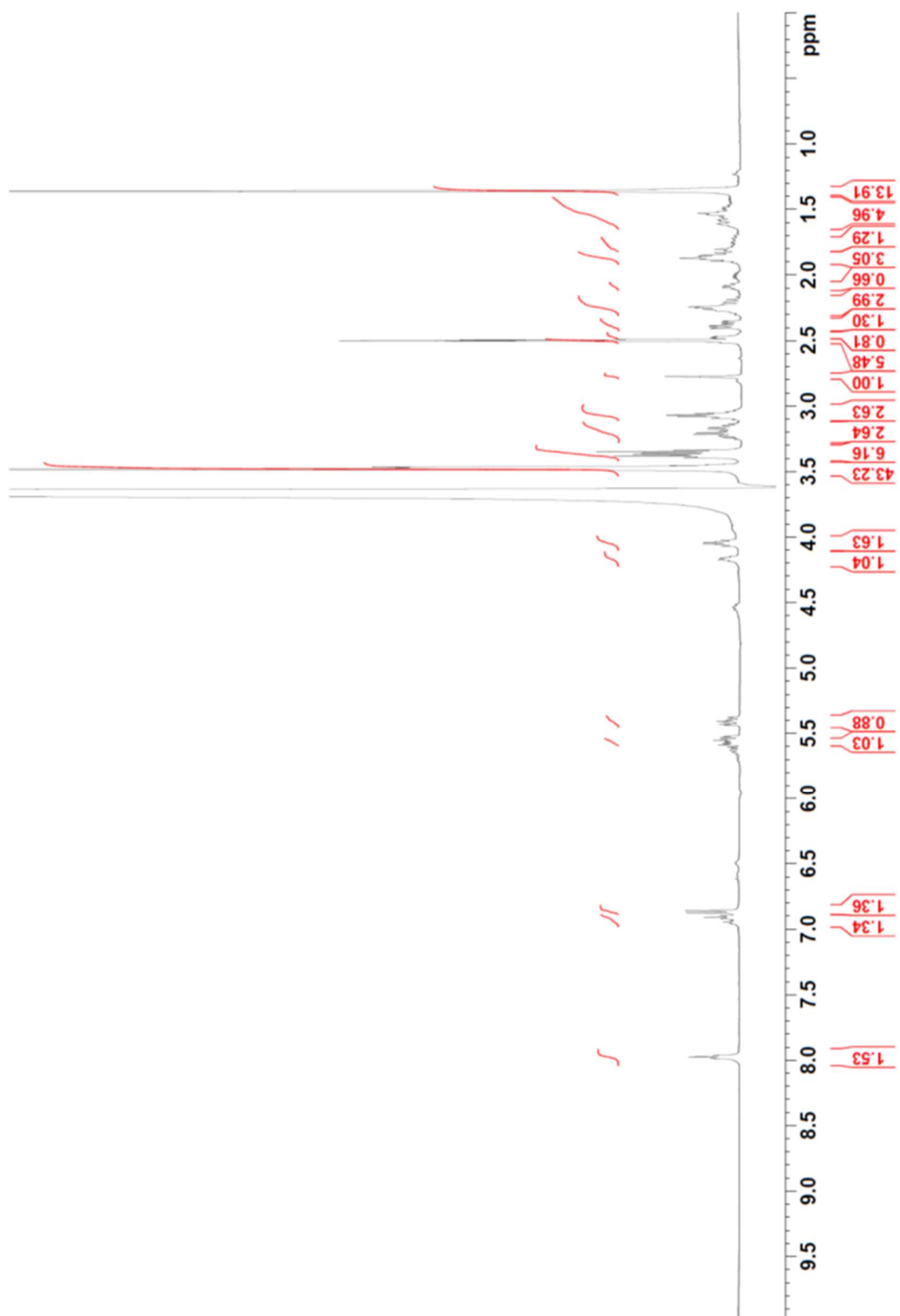
Supp. figure 12: ^{1}H-NMR spectrum of the Boc-protected intermediate acquired at 500 MHz in DMSO-d$_6$.
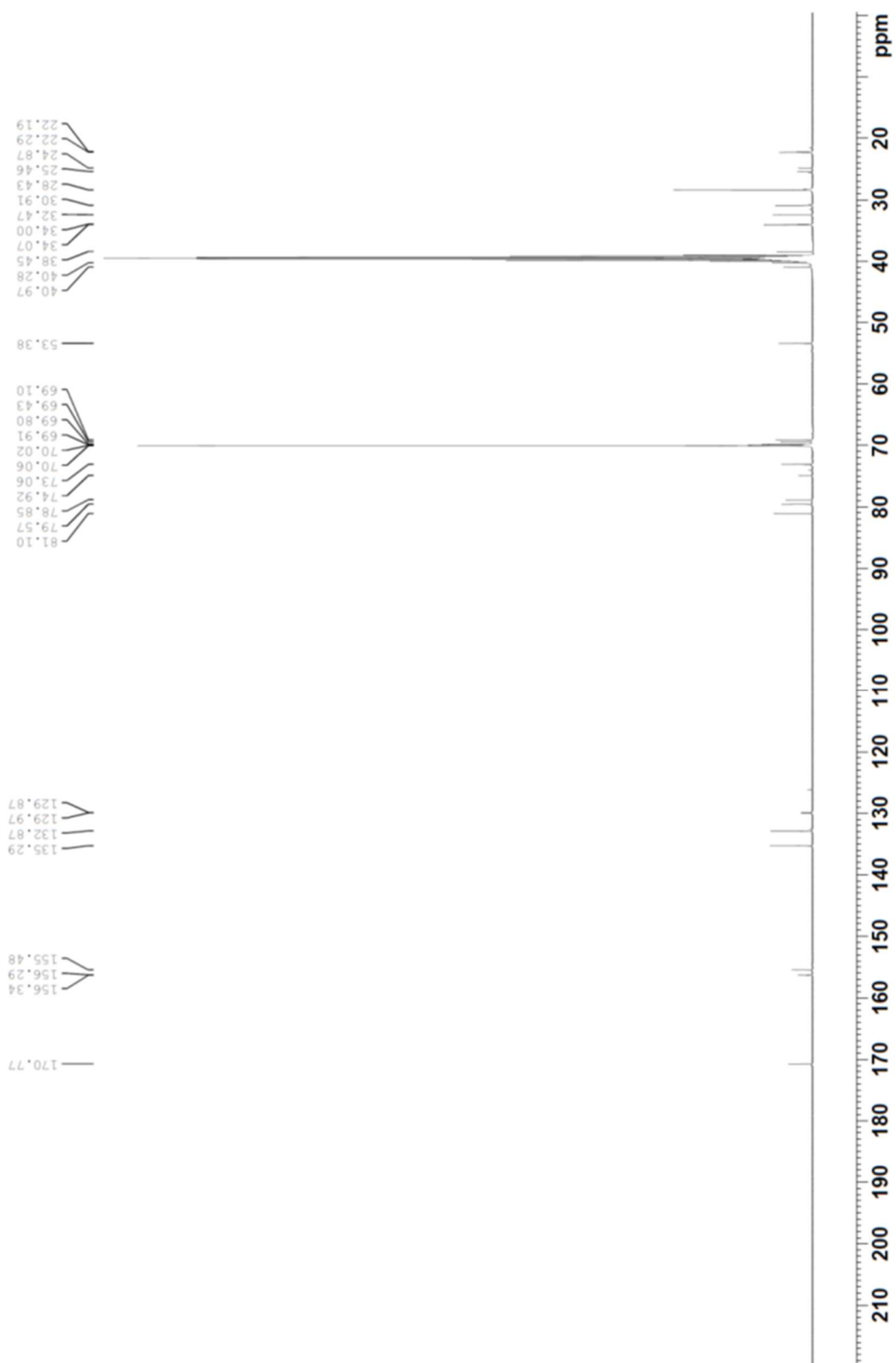
Supp. figure 13: ^{13}C-NMR spectrum of the Boc-protected intermediate acquired at 126 MHz in DMSO-d_6.
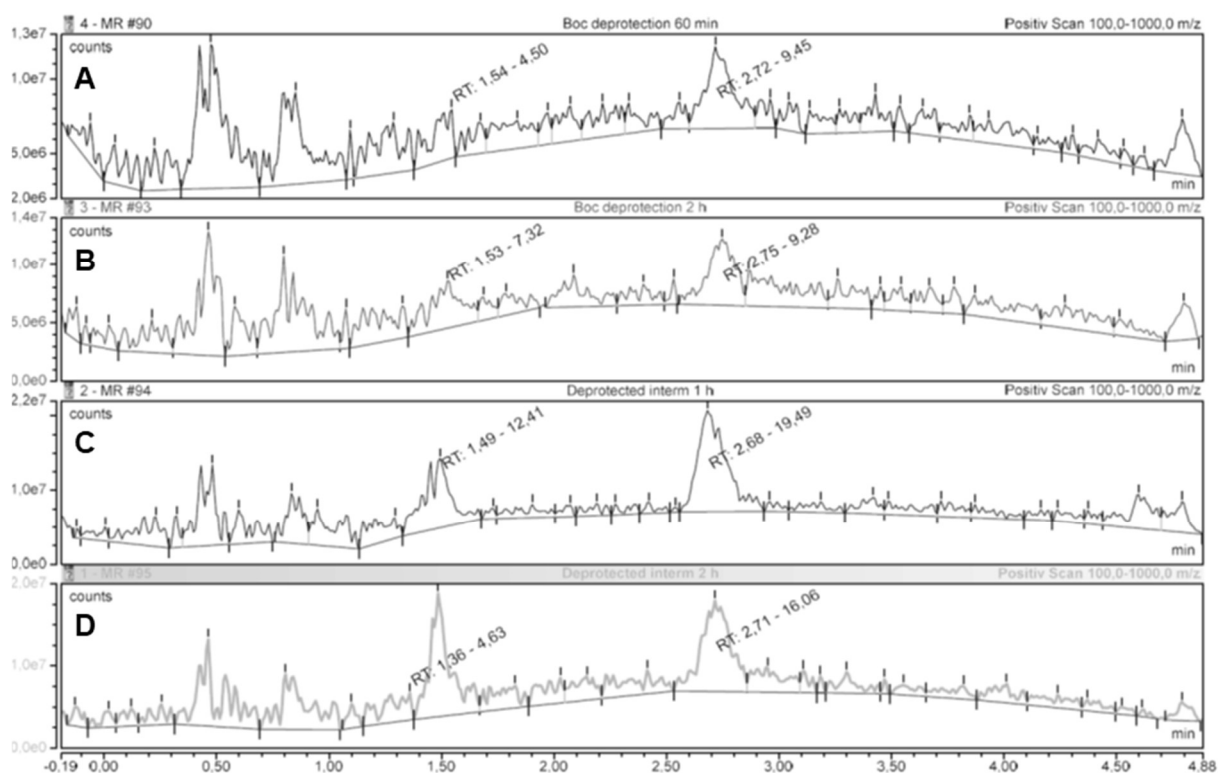
Supp. figure 14: LC/MS analysis of the Boc-deprotection test-experiment (A&B) and the bulk deprotection of the Boc-protected PEG₈-linker (C&D) after 1 and 2 h of deprotection. The deprotected product eluted at ~2.7 min. The putative byproduct eluted at ~1.5 min.

144
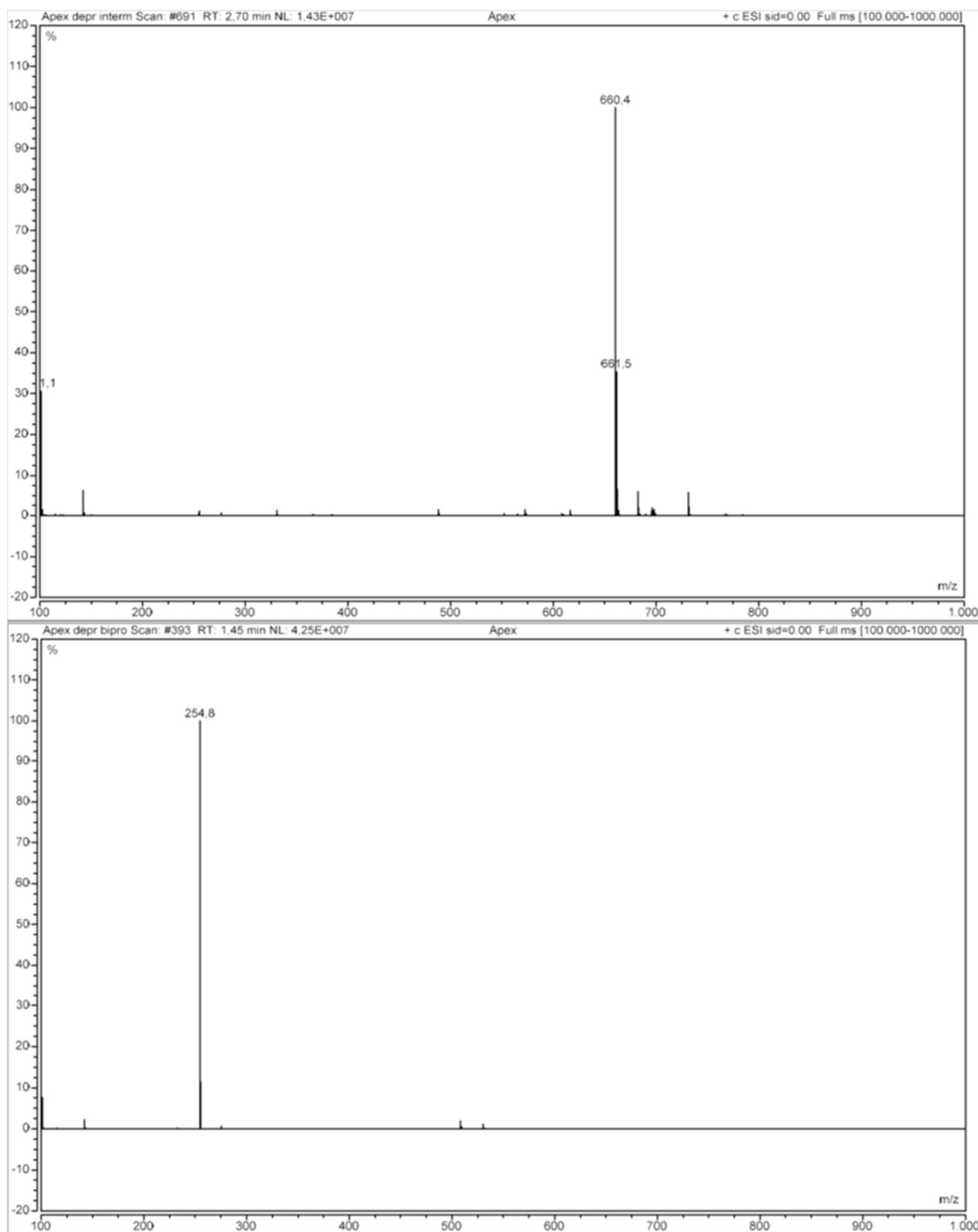
Supp. figure 15: Mass spectrum of the deprotected PEG$_8$-linker-intermediate (A, [M+H]$^+$ at 660.4 m/z) and the putative byproduct (B, [M+2H]$^{2+}$ at 254.8 m/z).
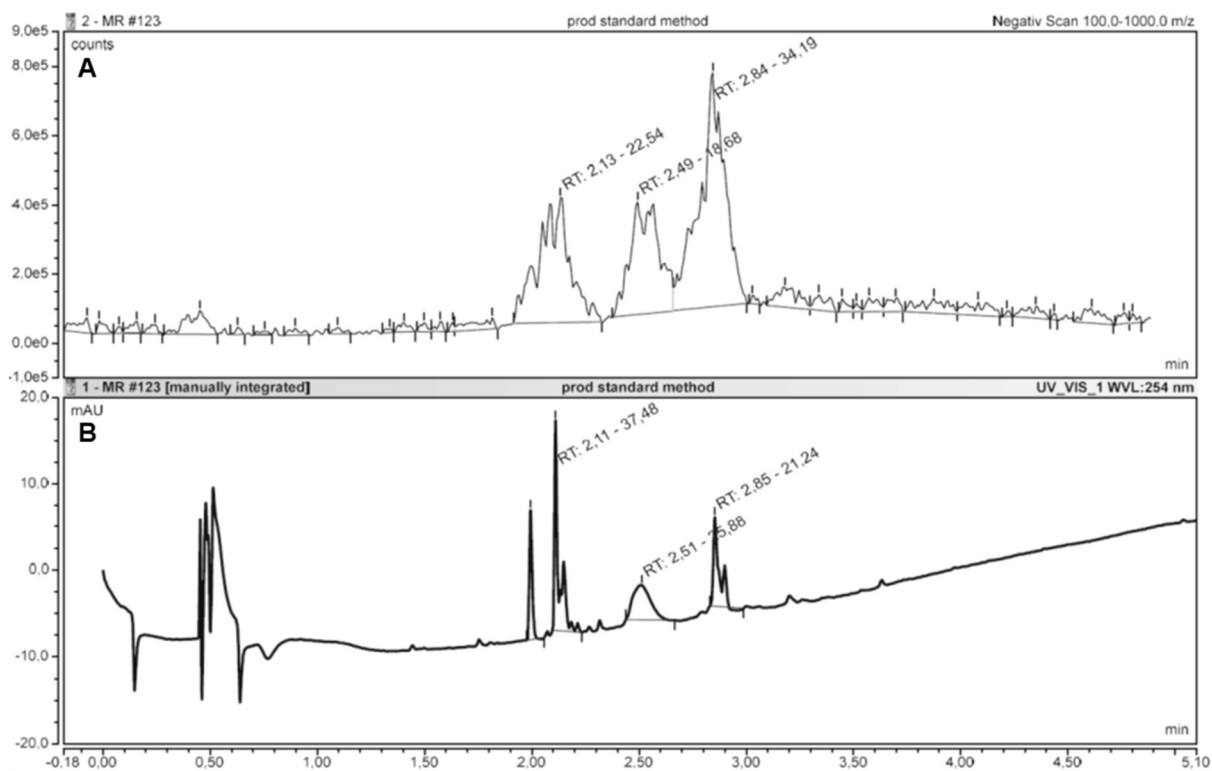
Supp. figure 16: Crude PEG₈-linker after reaction of sulfo-cyanine 5 NHS with the deprotected intermediate. Negative scan (A) and UV-absorption at 254 nm (B) revealed the intact PEG₈-linker at 2.85 min and two side-products eluting at 2.1 and 2.5 min respectively.
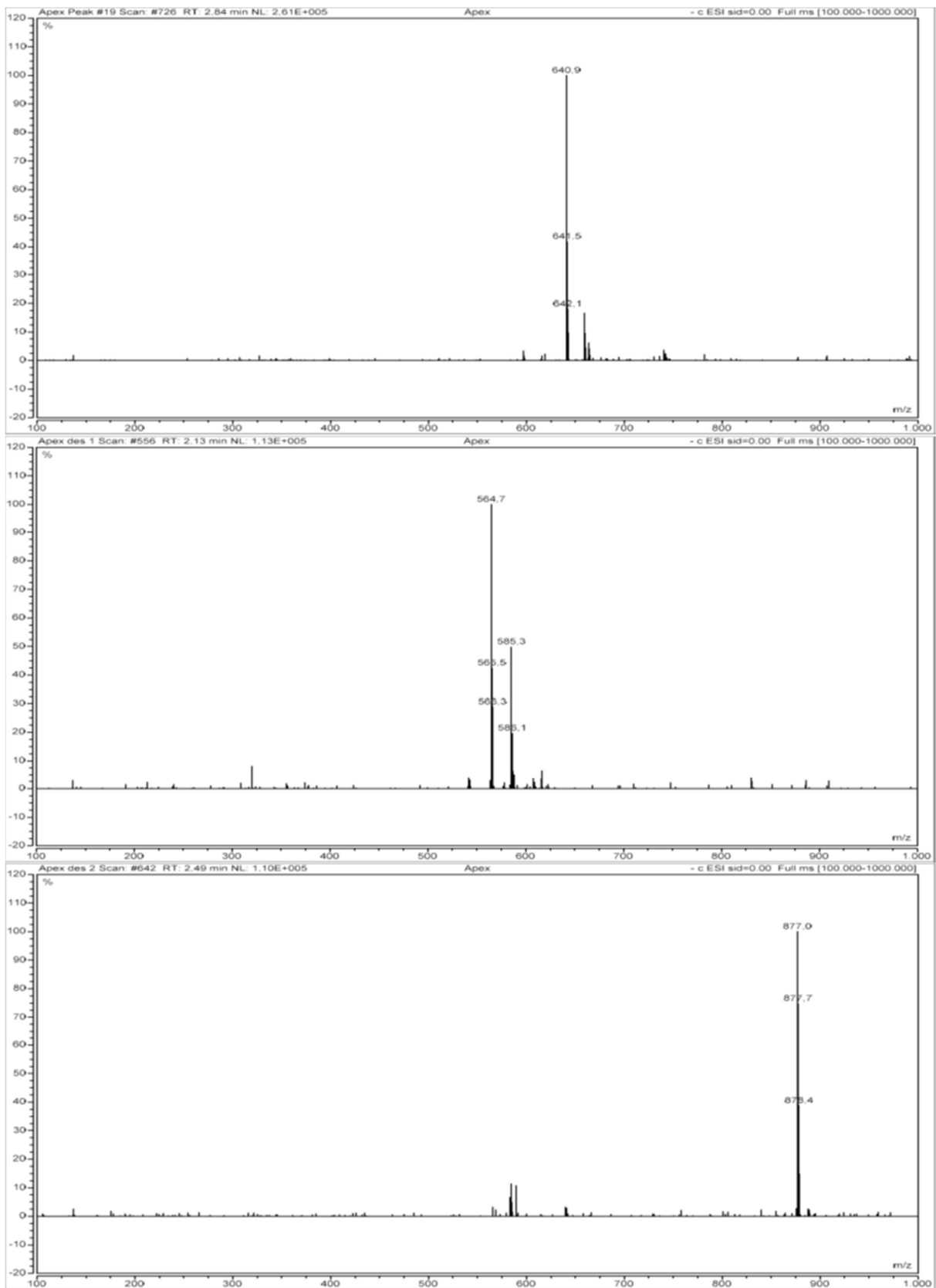
Supp. figure 17: Mass spectra of the PEG$_8$-linker (A, [M+ACN-2H]$^{2-}$ at 640.9 m/z) and the putative byproducts 2.1 (B, [M-2H]$^{2-}$ at 564.7 m/z) and 2.2 (C, [M-2H]$^{2-}$ at 877.0 m/z).
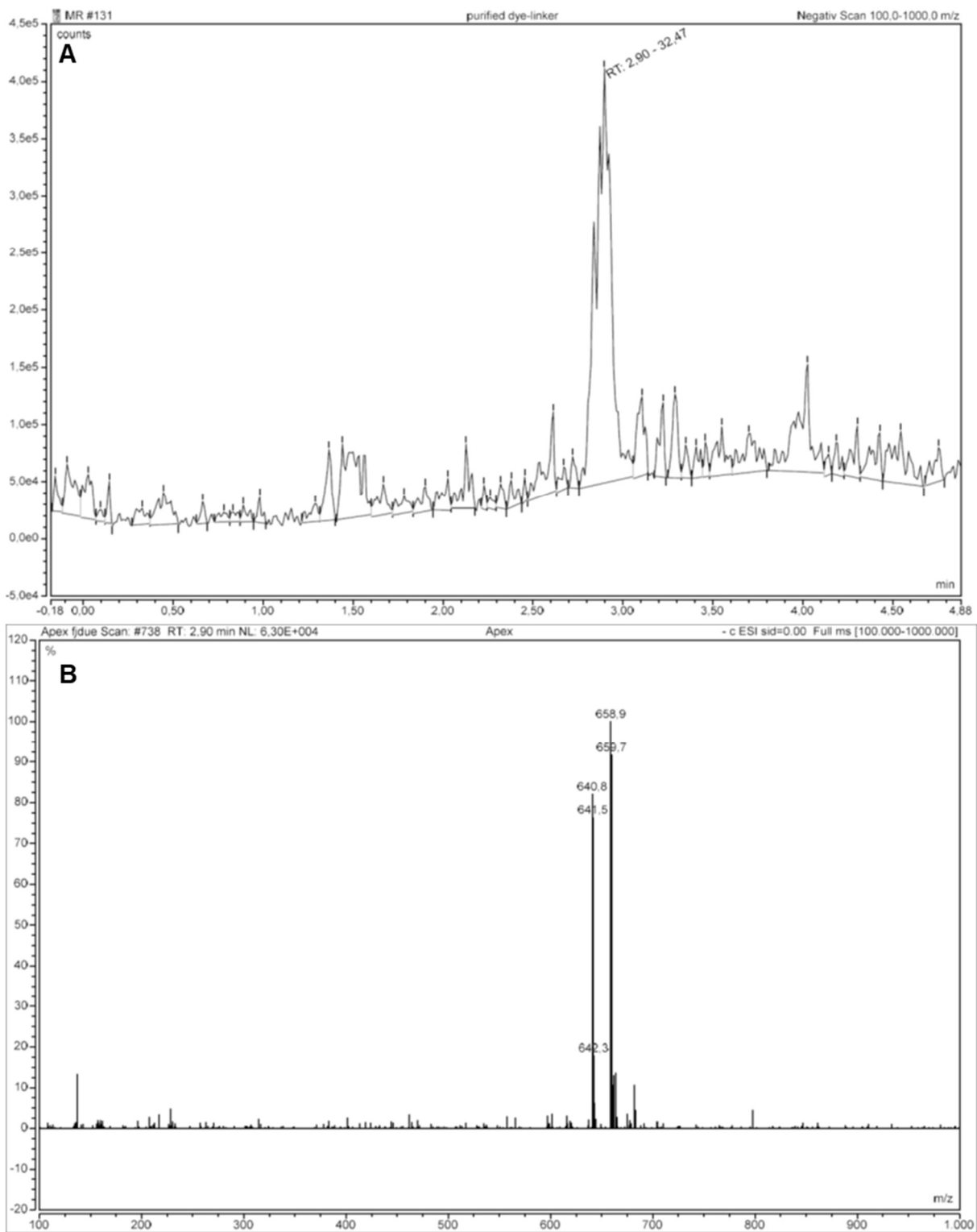
Supp. figure 18: Mass peak (A, 2.90 min) and corresponding mass spectrum of the purified PEG$_8$-linker (B, [M+ACN-2H]$^{2-}$ at 640.9 m/z).
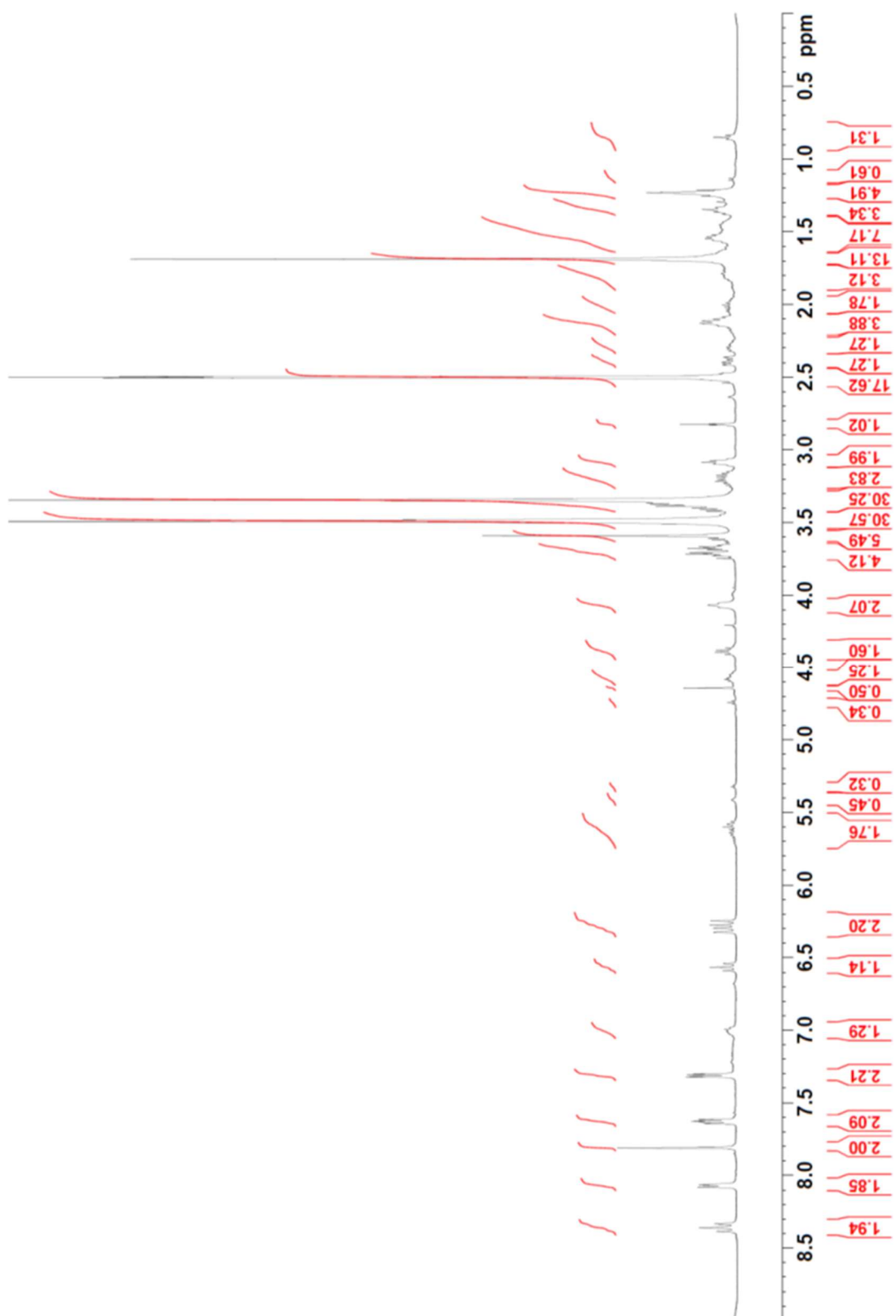
Supp. figure 19: ^{1}H-NMR spectrum of the PEG$_8$-linker acquired at 500 MHz in DMSO-d$_6$.
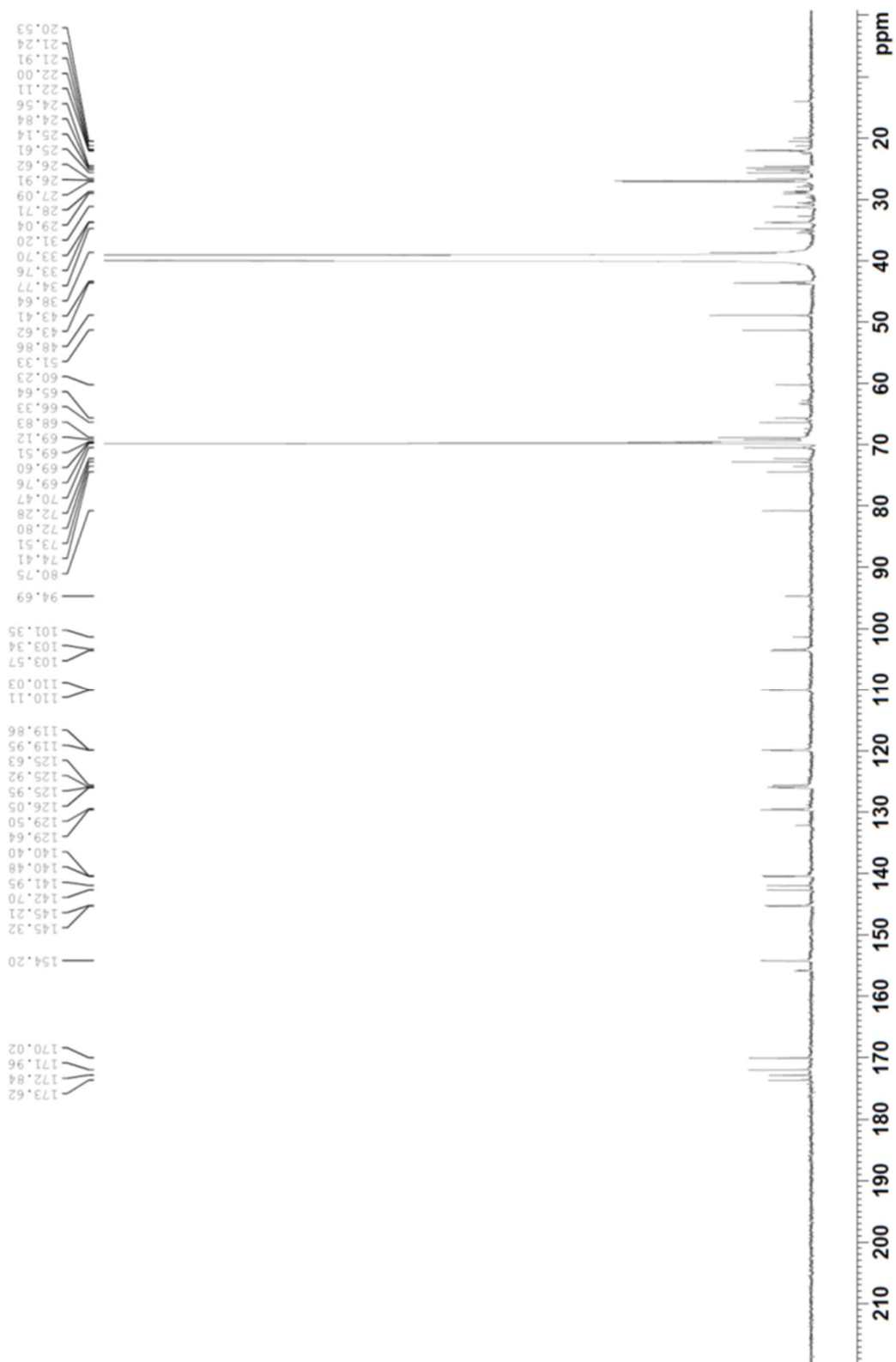
Supp. figure 20: ^{13}C-NMR spectrum of the PEG$_8$-linker acquired at 126 MHz in DMSO-d6.
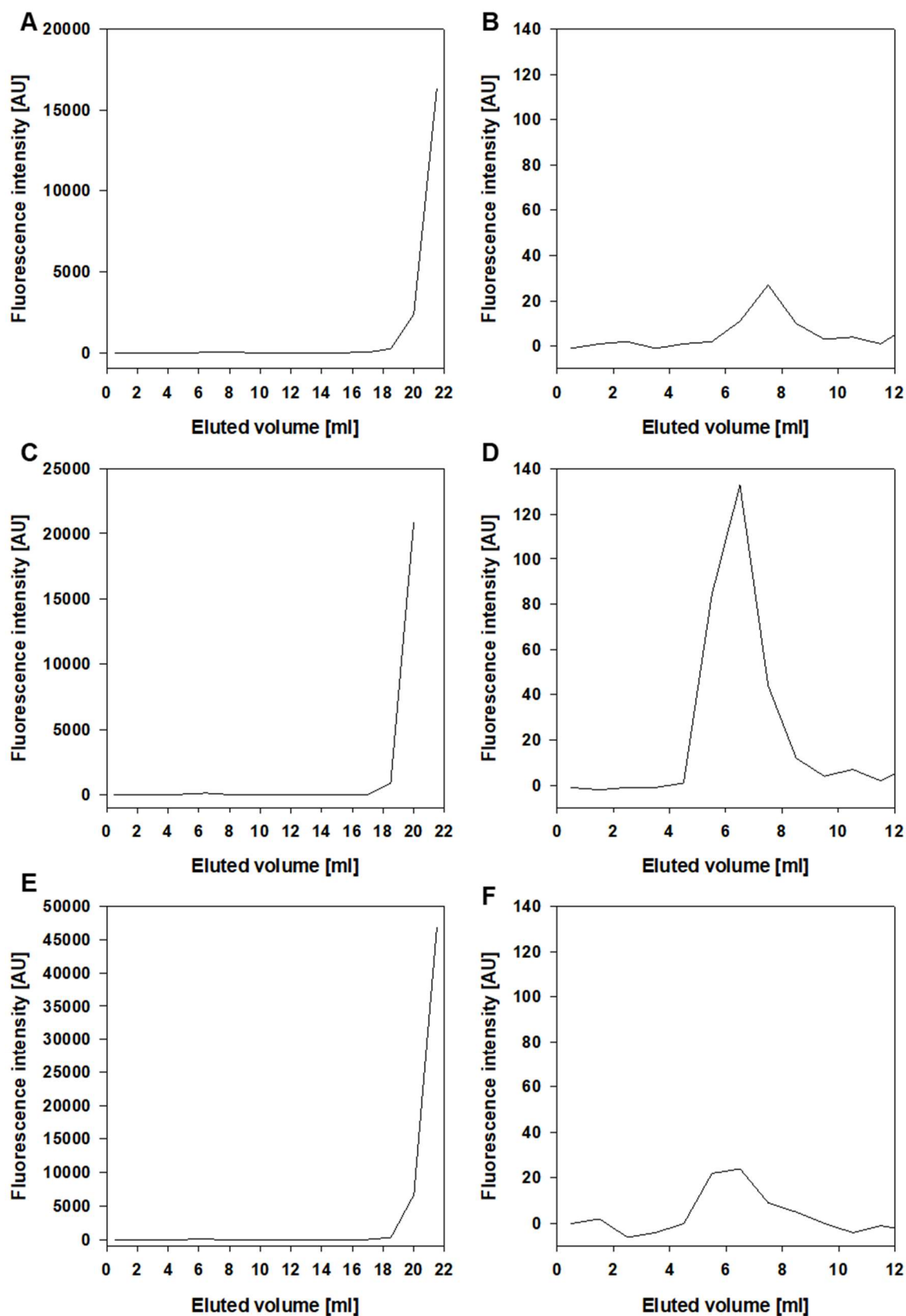
Supp. figure 21: SEC elution profile of injections of the PEG$_8$-linker (A&B), PEG$_6$-linker (C&D) and the reaction product of the PEG$_6$-linker and methyltetrazine-PEG$_4$-biotin (E&F). All samples were dissolved in PBS at 19.6 µM in the absence of EVs. Plots in the right column show a zoomed view of the region, were EVs would normally elute.

151
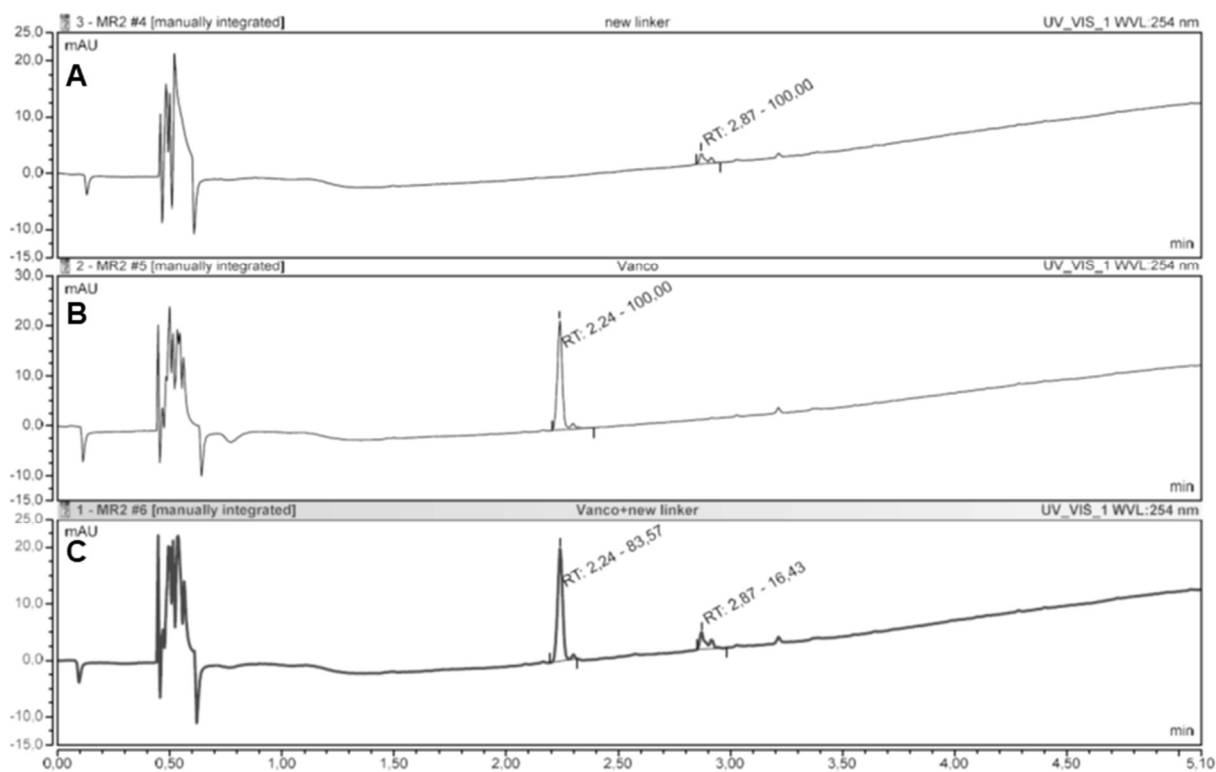
Supp. figure 22: Analysis of the IEDDA reaction of methyltetrazine-vancomycin and the PEG$_8$-linker. Panels A and B contain the UV-absorption at 254 nm of the PEG$_8$-linker (A, 2.87 min) and methyltetrazine-vancomycin (B, 2.24 min) respectively. Panel C shows the chromatogram after the IEDDA reaction. Besides the peaks at 2.24 and 2.87 min derived from the educts, no other peaks corresponding with the products of the reaction were visible.
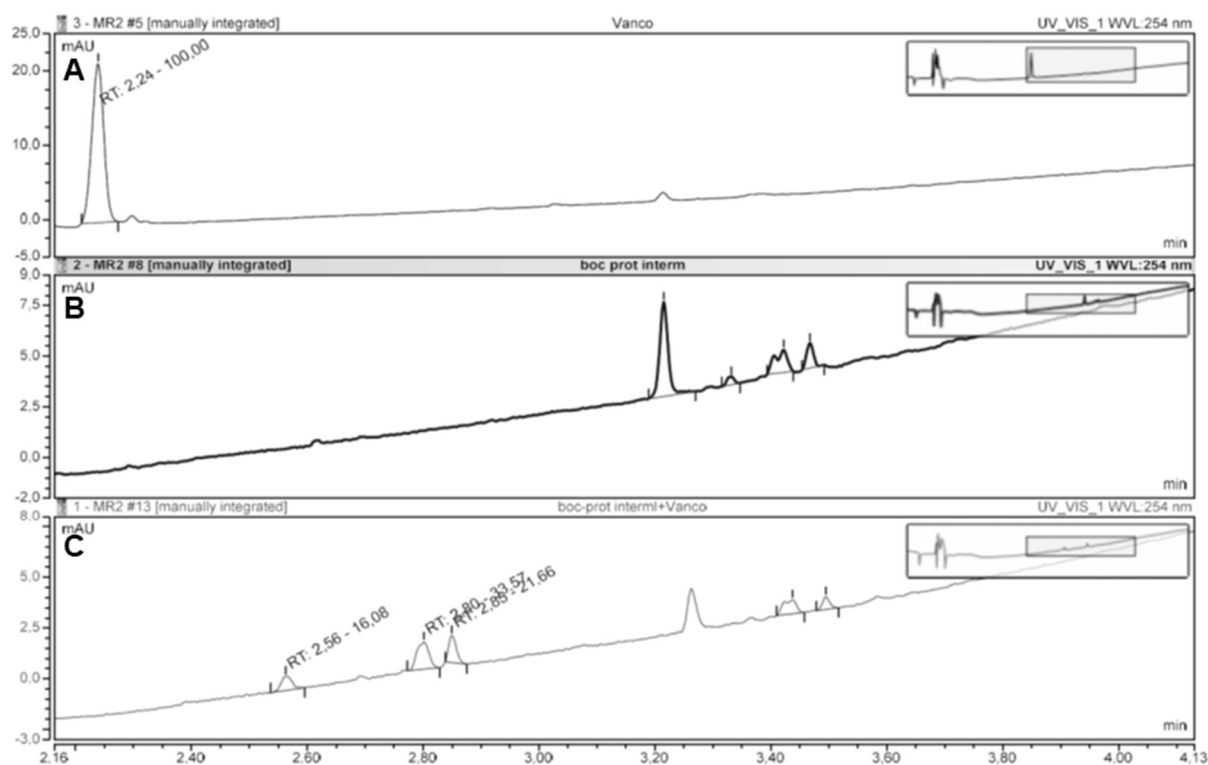
Supp. figure 23: Analysis of the IEDDA reaction of methyltetrazine-vancomycin and the Boc-protected intermediate. Panels A and B contain the UV-absorption at 254 nm of methyltetrazine-vancomycin (A, 2.24 min) and the Boc-protected intermediate (B) respectively. Panel C shows the chromatogram after the IEDDA reaction. Three peaks belonging to the product of the reaction were visible (2.56, 2.80 and 2.85 min).
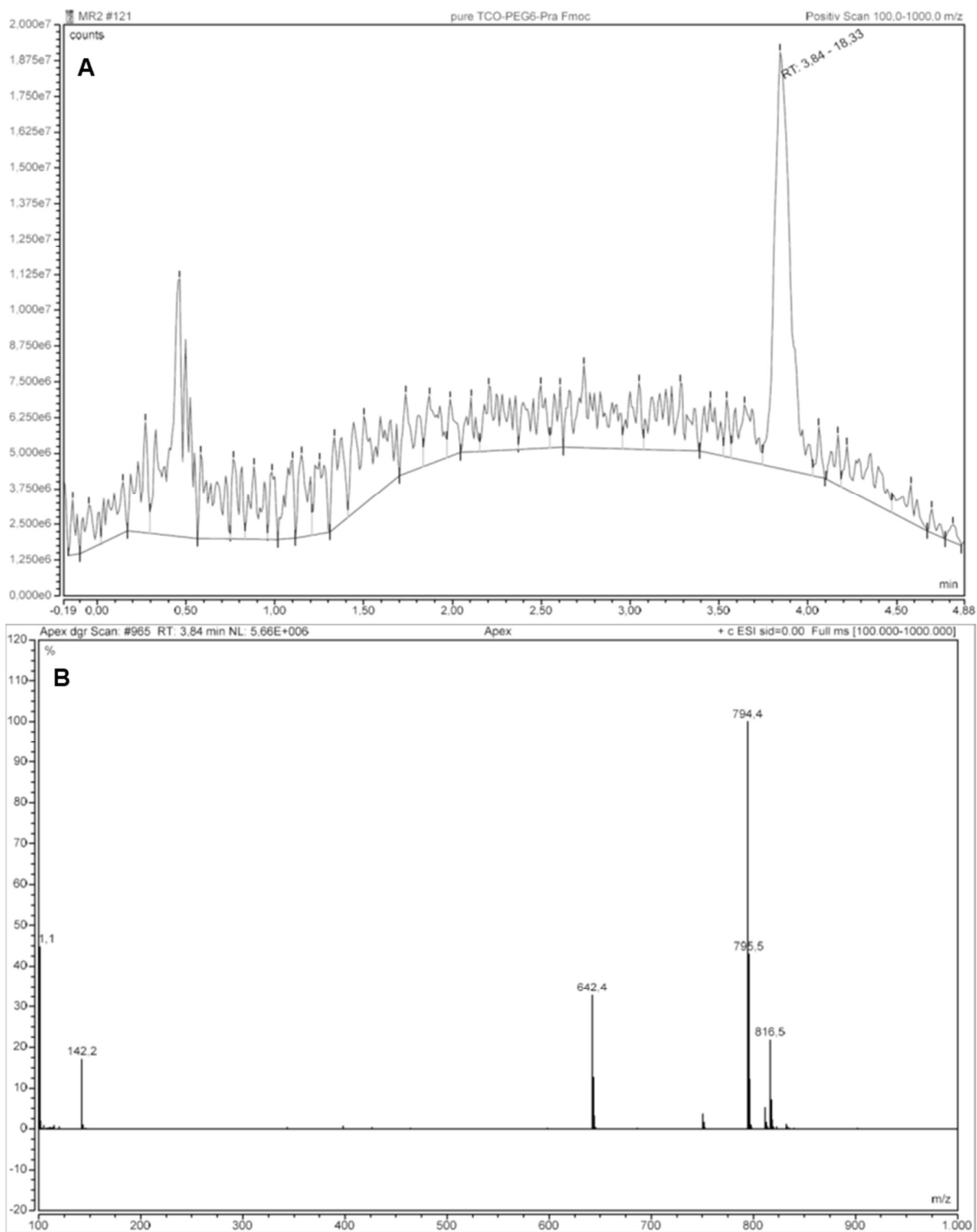
Supp. figure 24: Mass peak (A, 3.84 min) and corresponding mass spectrum of the purified Fmoc-protected intermediate (B, [M+H]⁺at 794.4 m/z).
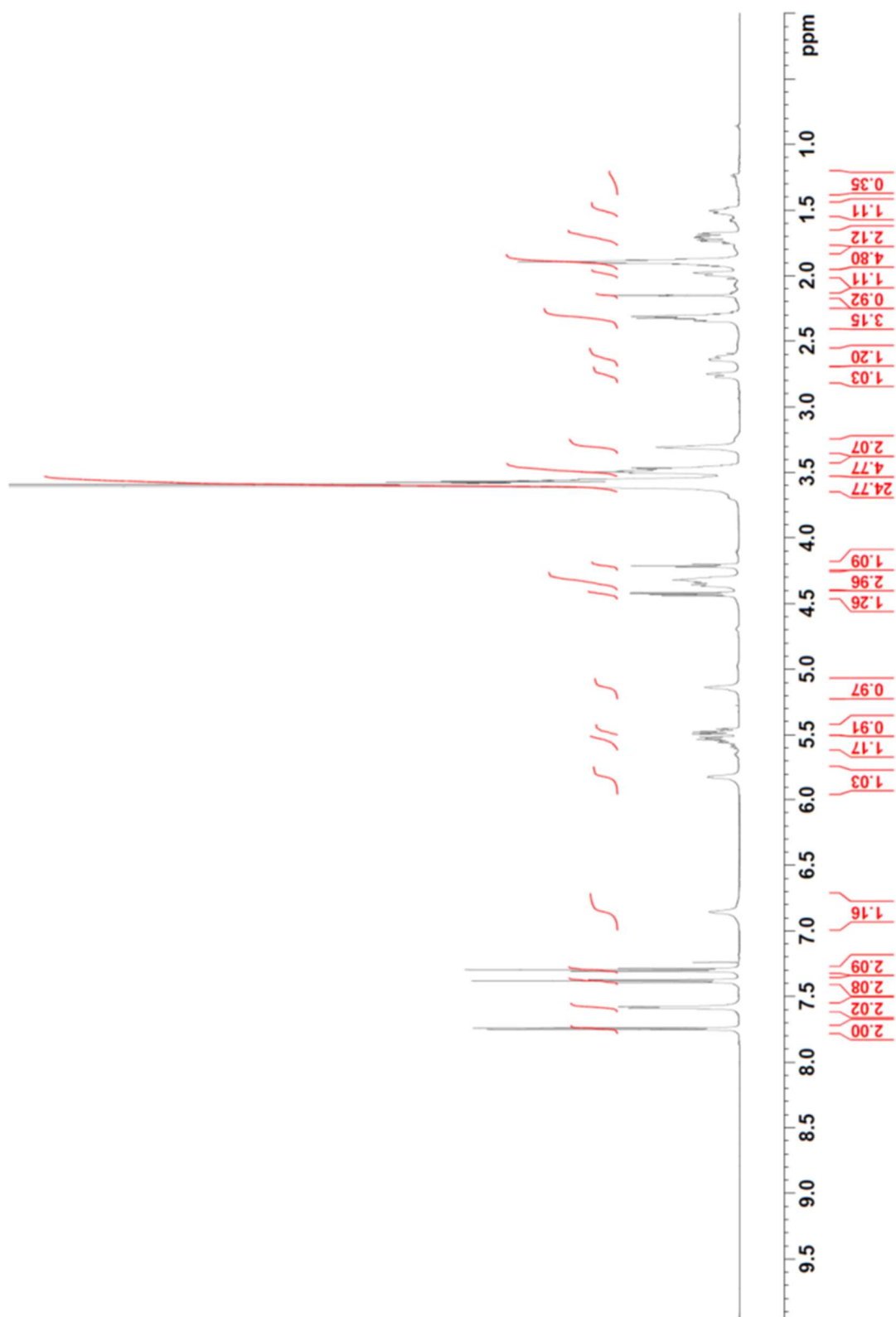
Supp. figure 25: ^{1}H-NMR spectrum of the Fmoc-protected intermediate acquired at 700 MHz in CDCl$_3$.
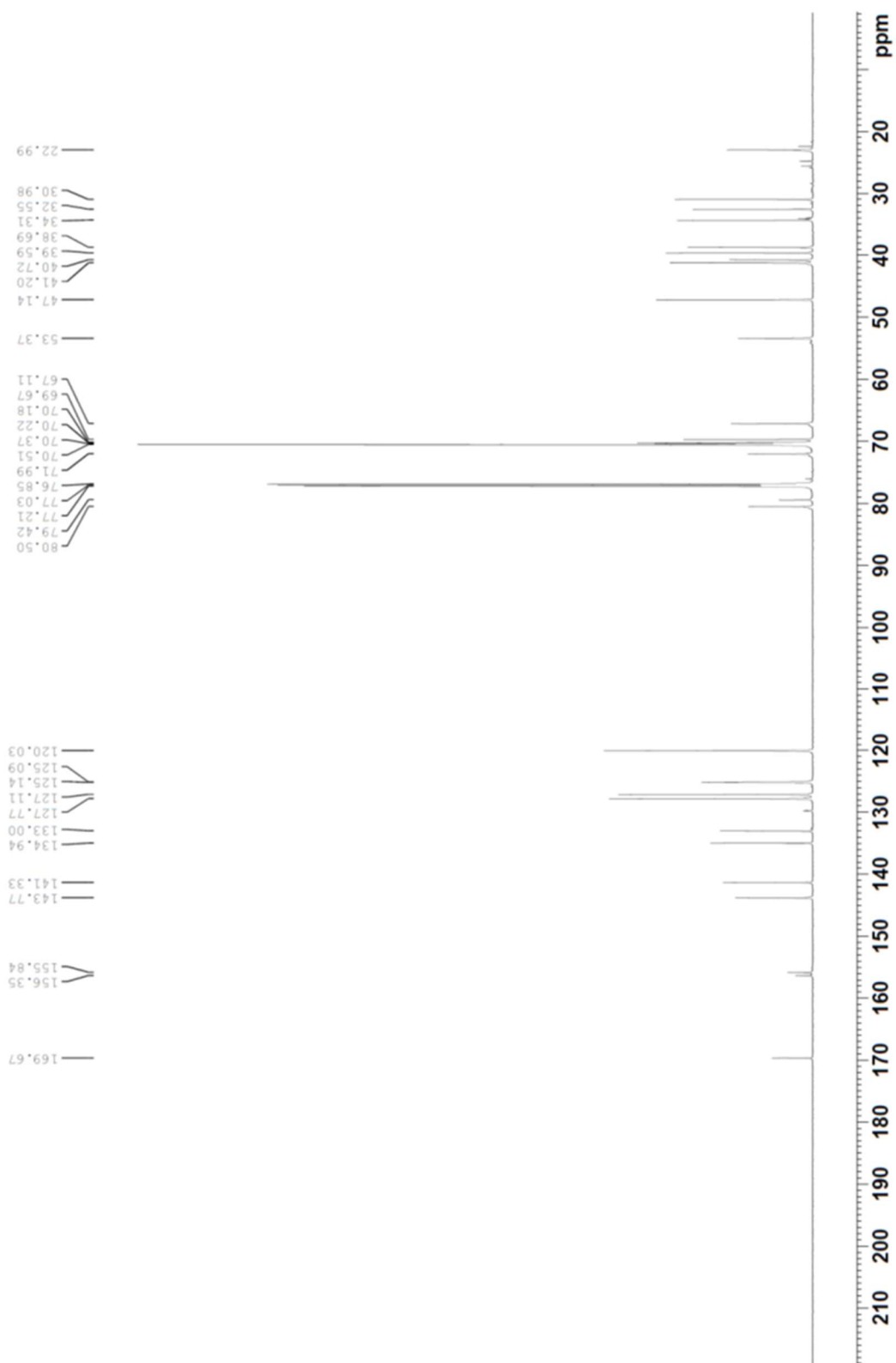
Supp. figure 26: ^{13}C-NMR spectrum of the Fmoc-protected intermediate acquired at 176 MHz in CDCl₃.
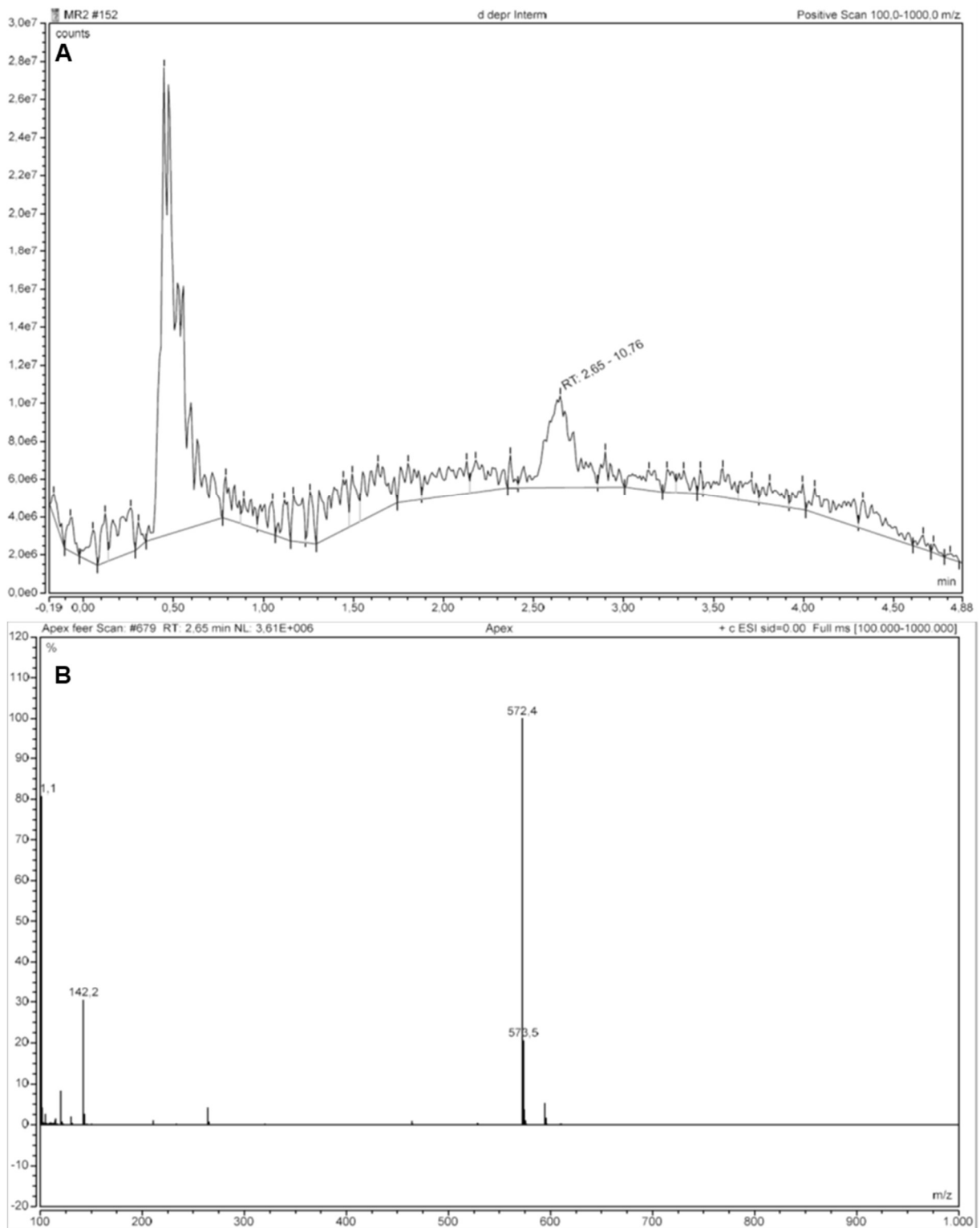
Supp. figure 27: Mass peak (A, 2.65 min) and corresponding mass spectrum of the purified deprotected intermediate (B, [M+H]$^+$at 572.4 m/z).
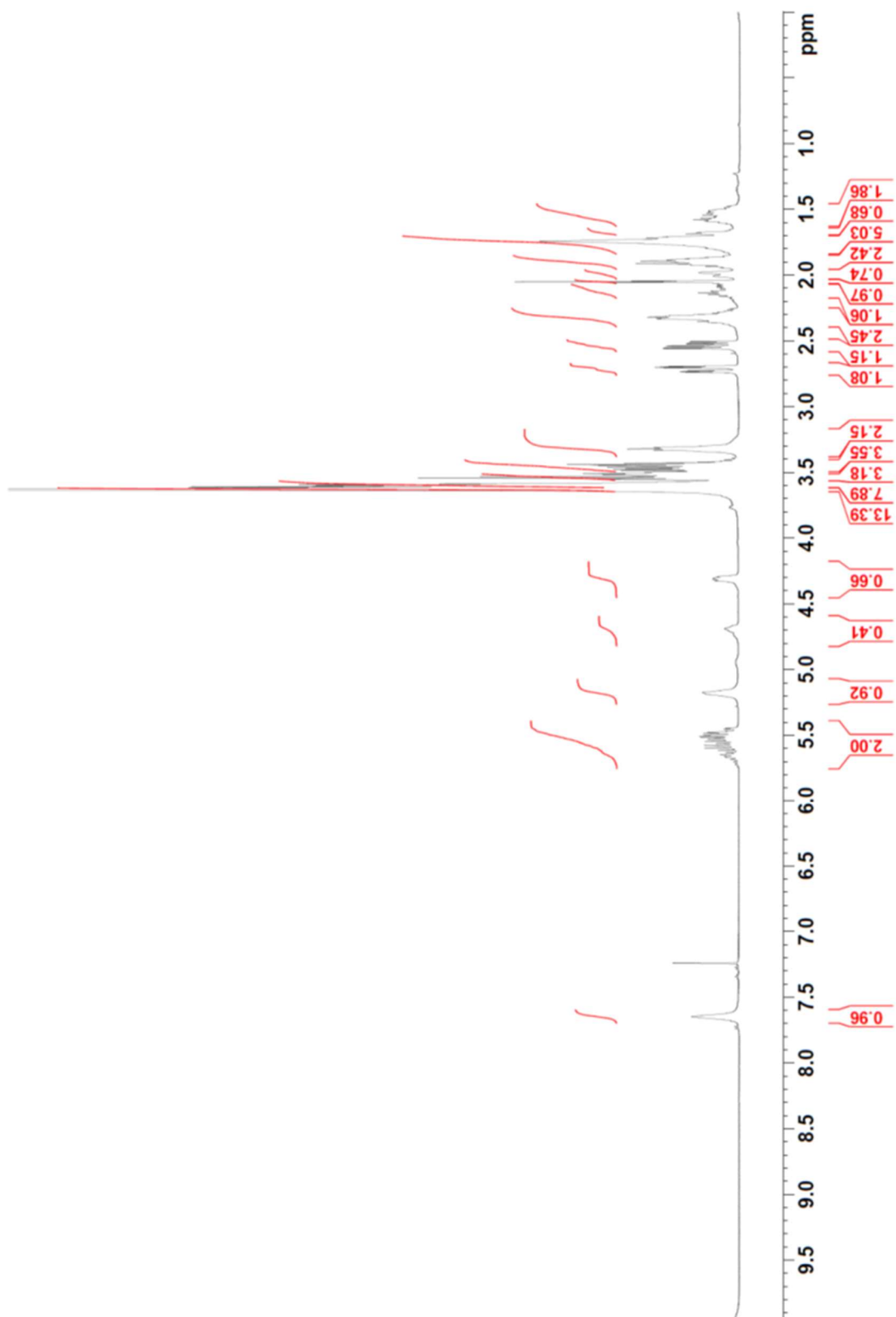
Supp. figure 28: ^{1}H-NMR spectrum of the deprotected intermediate acquired at 500 MHz in CDCl$_3$.
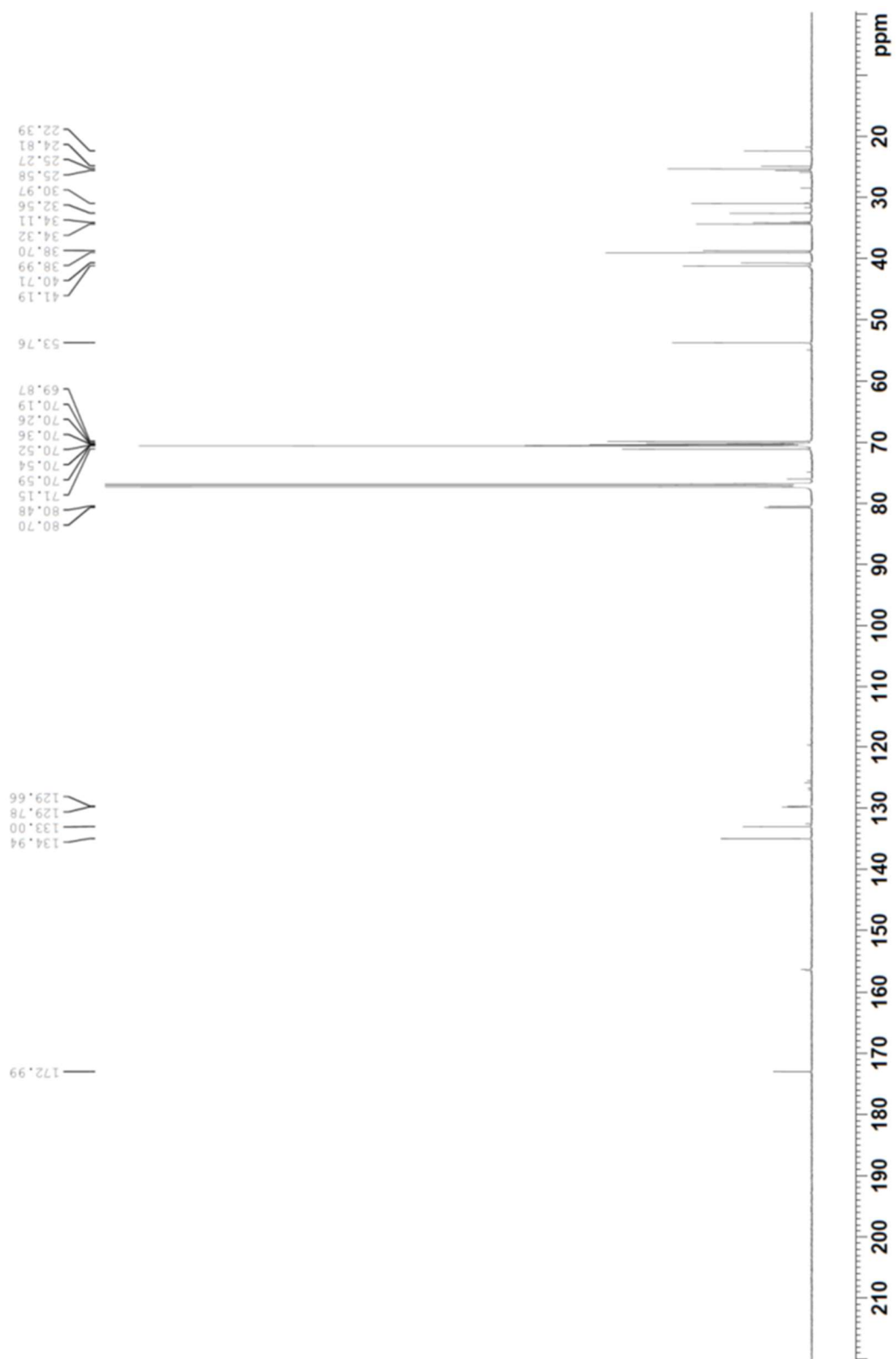
Supp. figure 29: ^{13}C-NMR spectrum of the deprotected intermediate acquired at 126 MHz in CDCl$_3$.
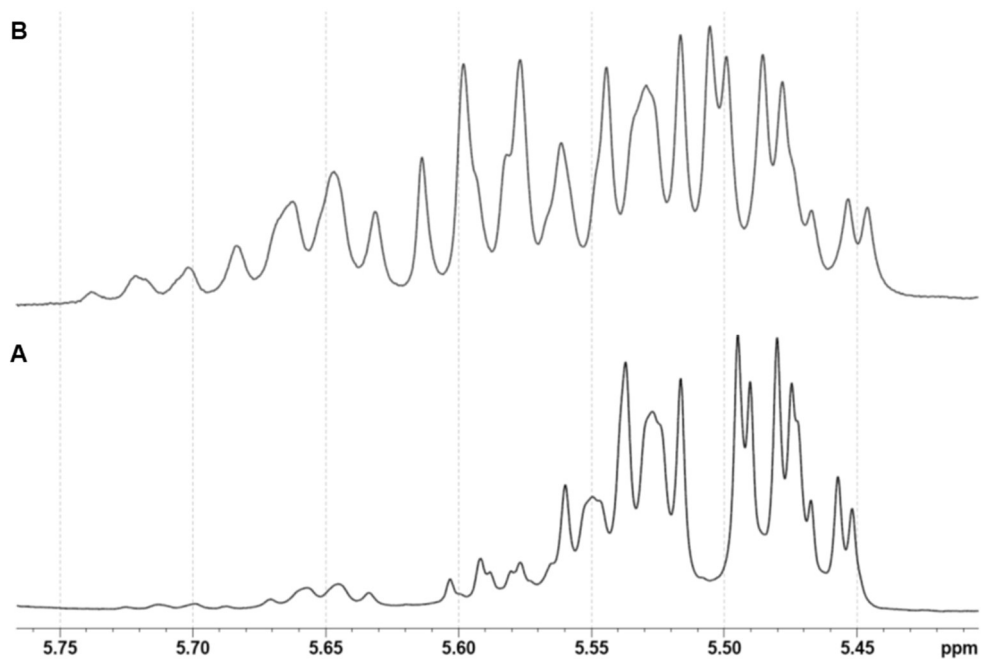
Supp. figure 30: Zoomed view of the ^{1}H-NMR spectra containing the signals of the protons belonging to the alkene-group of cyclooctene. Fmoc-intermediate (A) and deprotected intermediate (B) of the PEG$_6$-linker synthesis.
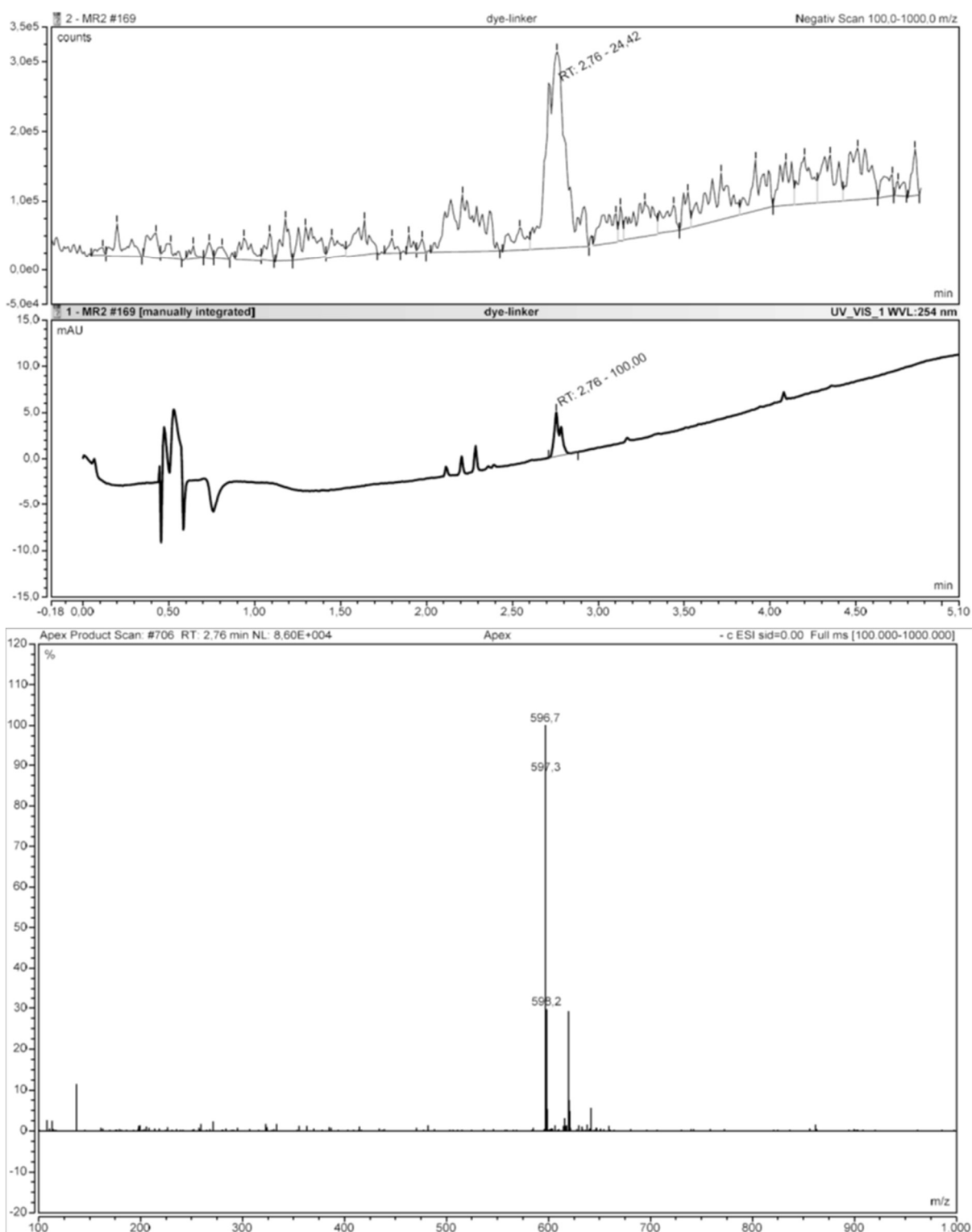
Supp. figure 31: Mass peak (A, 2.76 min) and UV-absorption at 254 nm (B) of the crude PEG$_6$-linker. The UV-spectrum shows two compound eluting at almost the same time, which is not visible in the negative scan. Panel C contains the corresponding mass spectrum ([M-2H]$^{2-}$at 596.7 m/z).
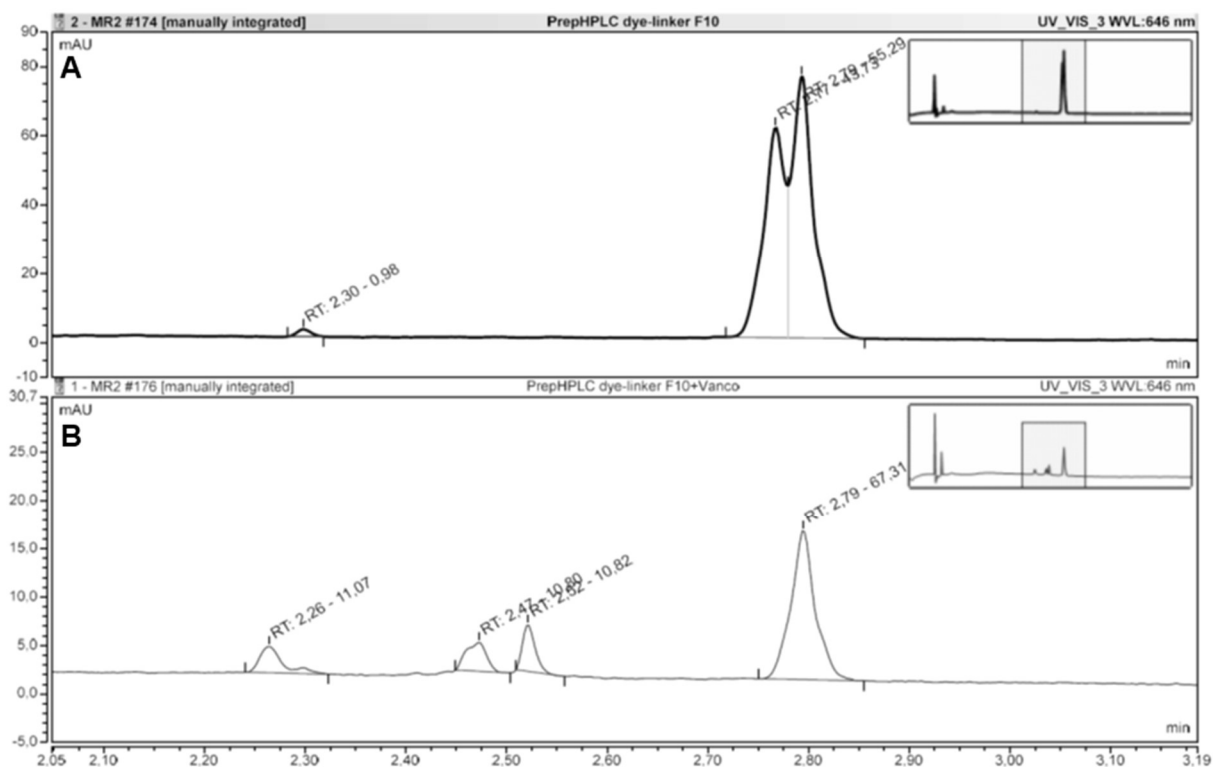
Supp. figure 32: Zoomed view of the UV-absorption at 646 nm of a prepHPLC fraction of the PEG$_6$-linker before (A) and after reaction with methyltetrazine-vancomycin (B). Panel A shows two peaks corresponding with the linker at 2.77 and 2.79 min. Only the peak at 2.79 min remained after the IEDDA reaction, while three new peaks emerged at 2.26, 2.47 and 2.52 min.
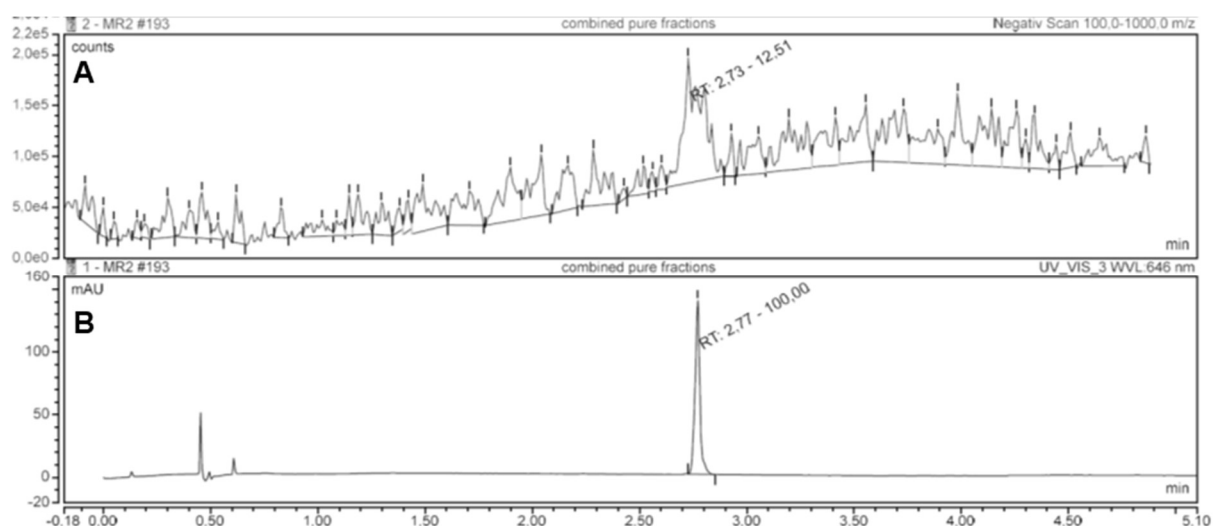
Supp. figure 33: Mass peak (A) and UV-absorption (B) of the purified PEG$_6$-linker before lyophilisation.
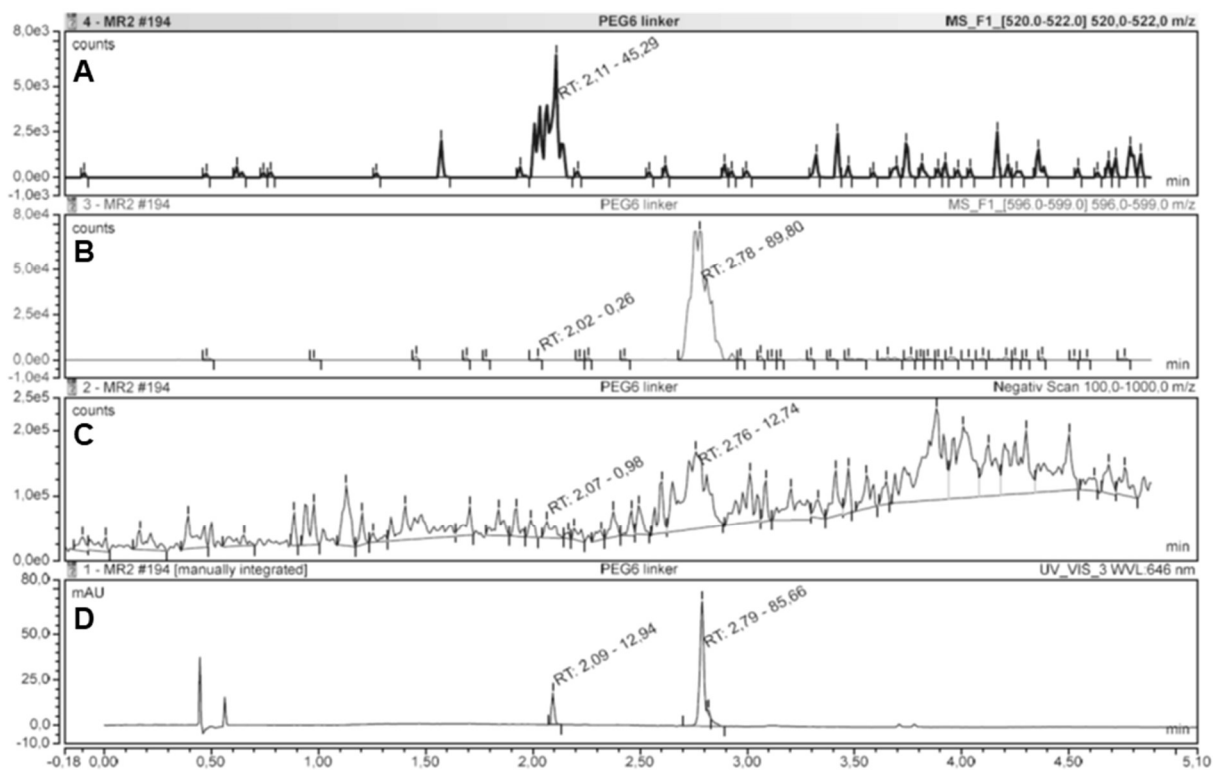
Supp. figure 34: LC/MS-analysis of the PEG$_6$-linker after lyophilisation. A degradation product with a signal at 520 m/z appeared (A, ~2.10 min). The intact linker eluted at 2.78 min as visible in panel B and C. Both molecules exhibited an absorption at 646 nm corresponding to the sulfo-cyanine 5 group (D).
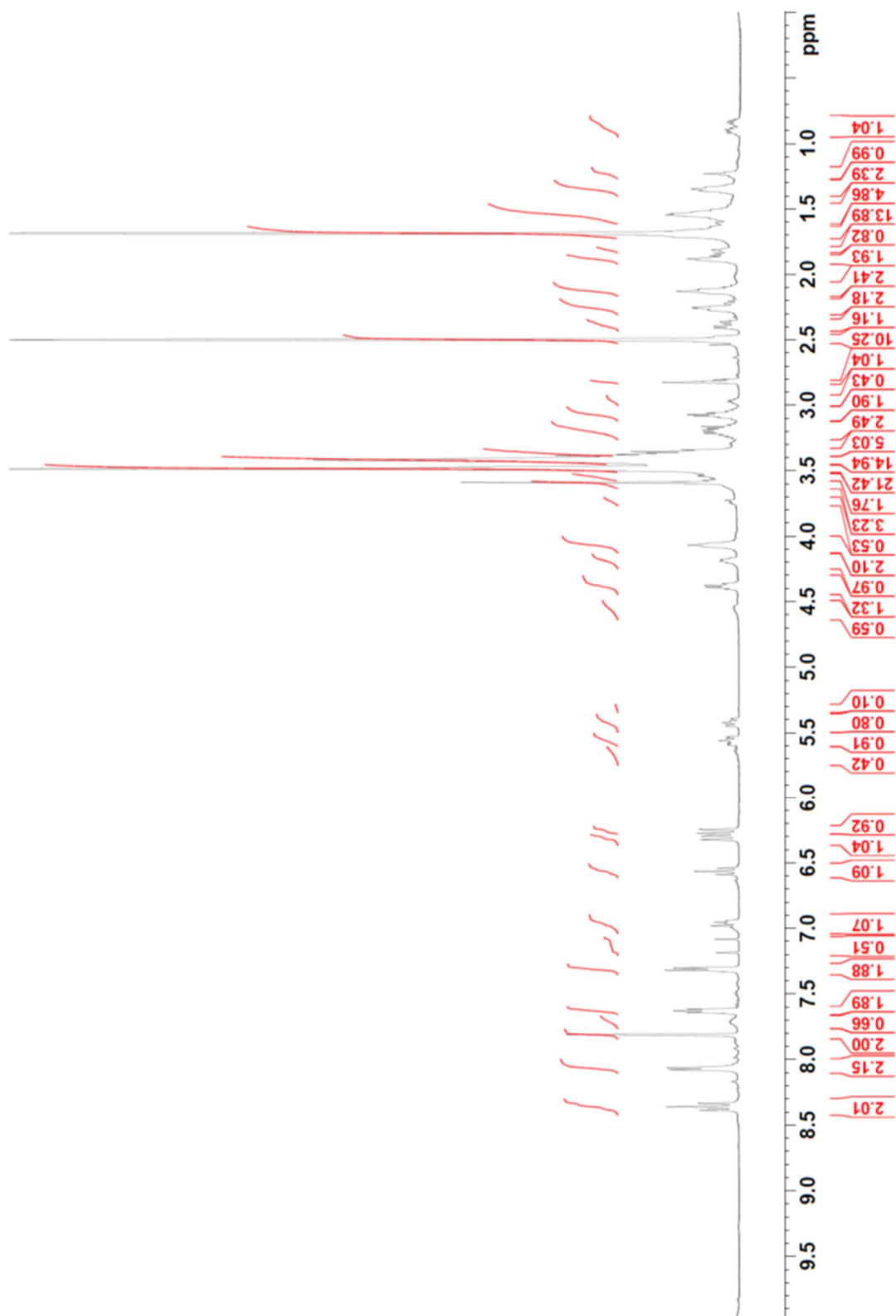
Supp. figure 35: ^{1}H-NMR spectrum of the active PEG$_6$-linker acquired at 500 MHz in DMSO-d$_6$.
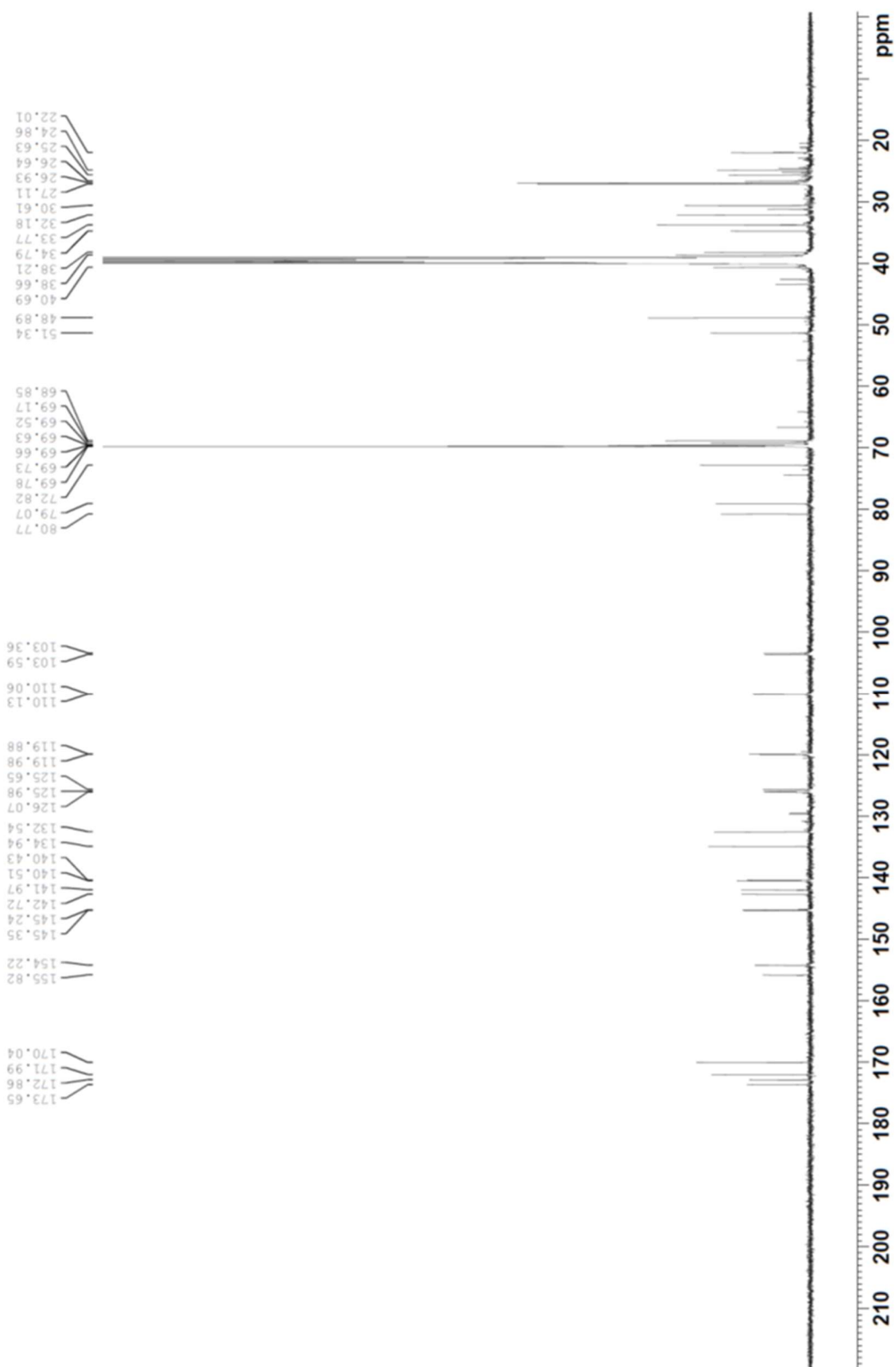
Supp. figure 36: ^{13}*C-NMR spectrum of the active PEG$_6$-linker acquired at 126 MHz in DMSO-d$_6$.*
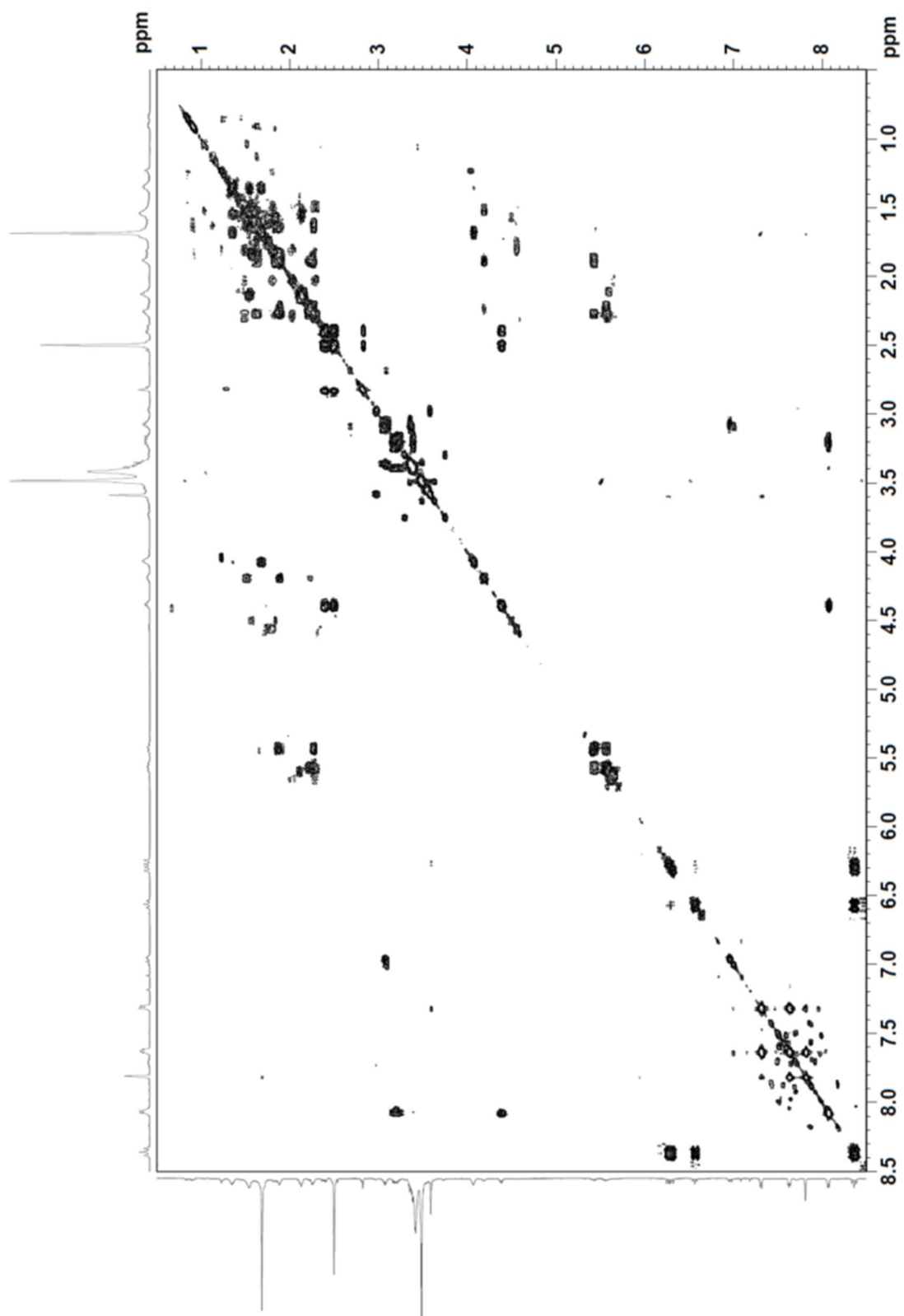
Supp. figure 37: COSY spectrum of the active PEG$_6$-linker acquired at 500 MHz in DMSO-d$_6$.
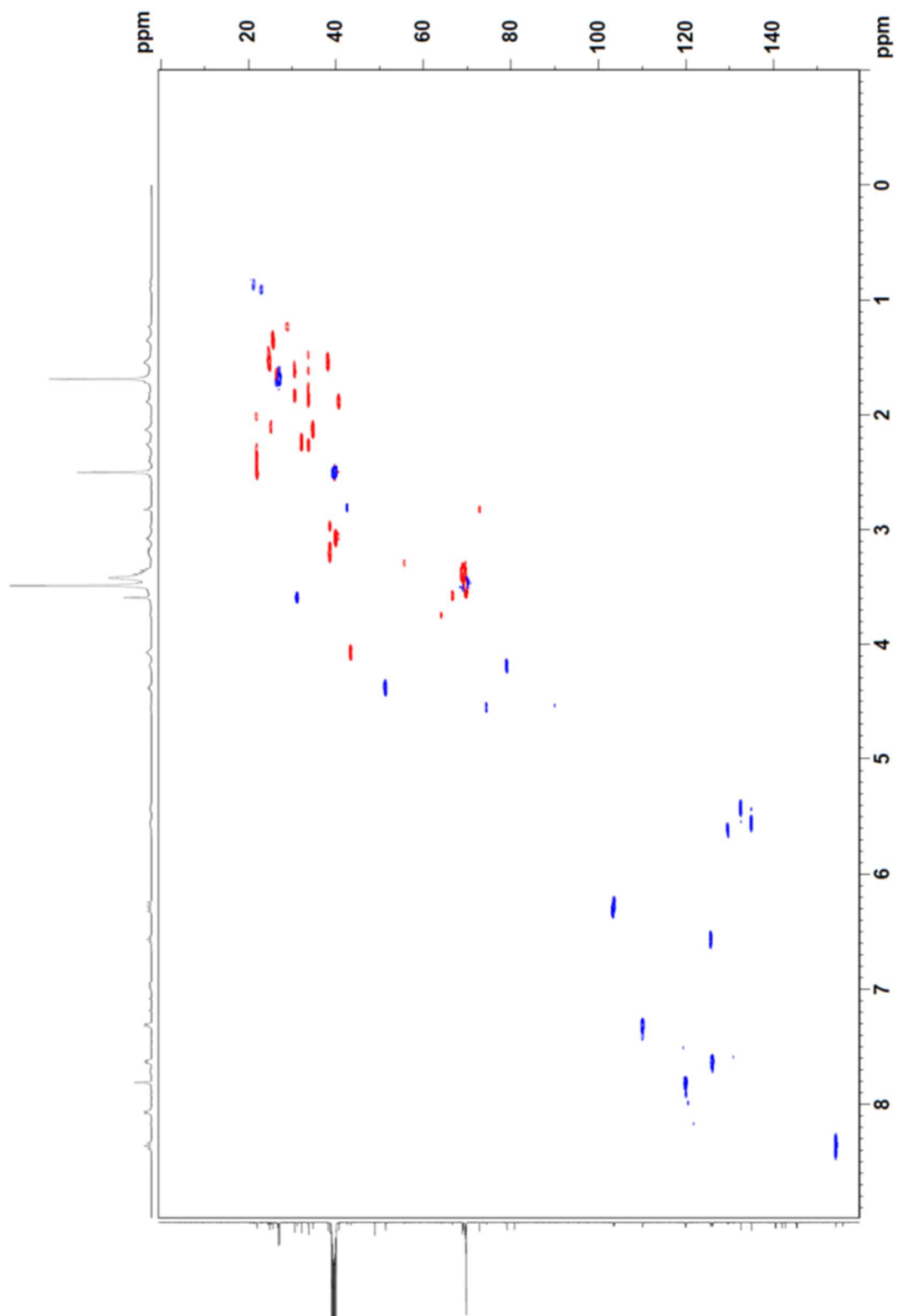
Supp. figure 38: HSQC spectrum of the active PEG$_6$-linker acquired at 500 MHz (^{1}H) and 126 MHz (^{13}C) in DMSO-d$_6$.
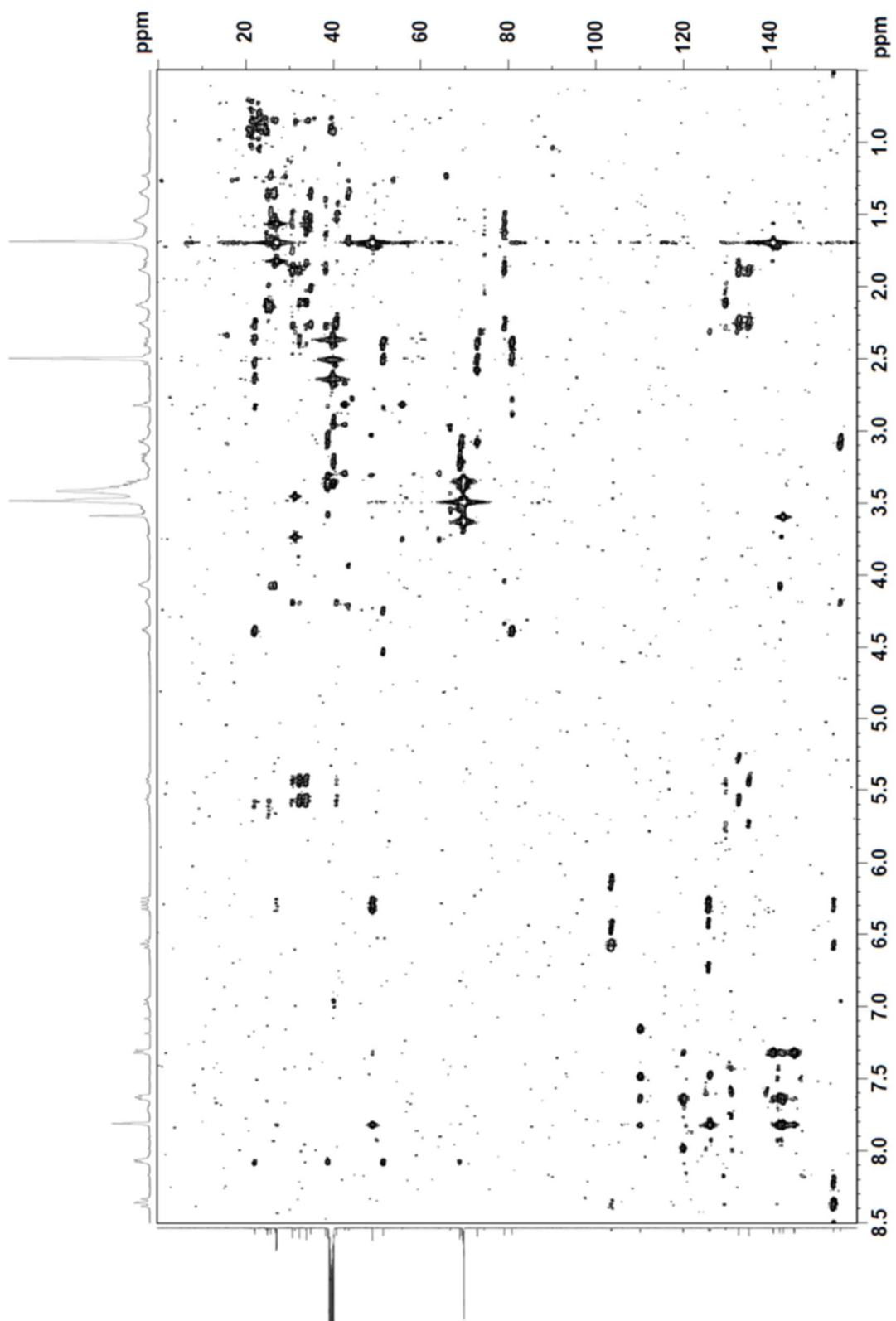
Supp. figure 39: HMBC spectrum of the active PEG$_6$-linker acquired at 500 MHz (^{1}H) and 126 MHz (^{13}C) in DMSO-d$_6$.
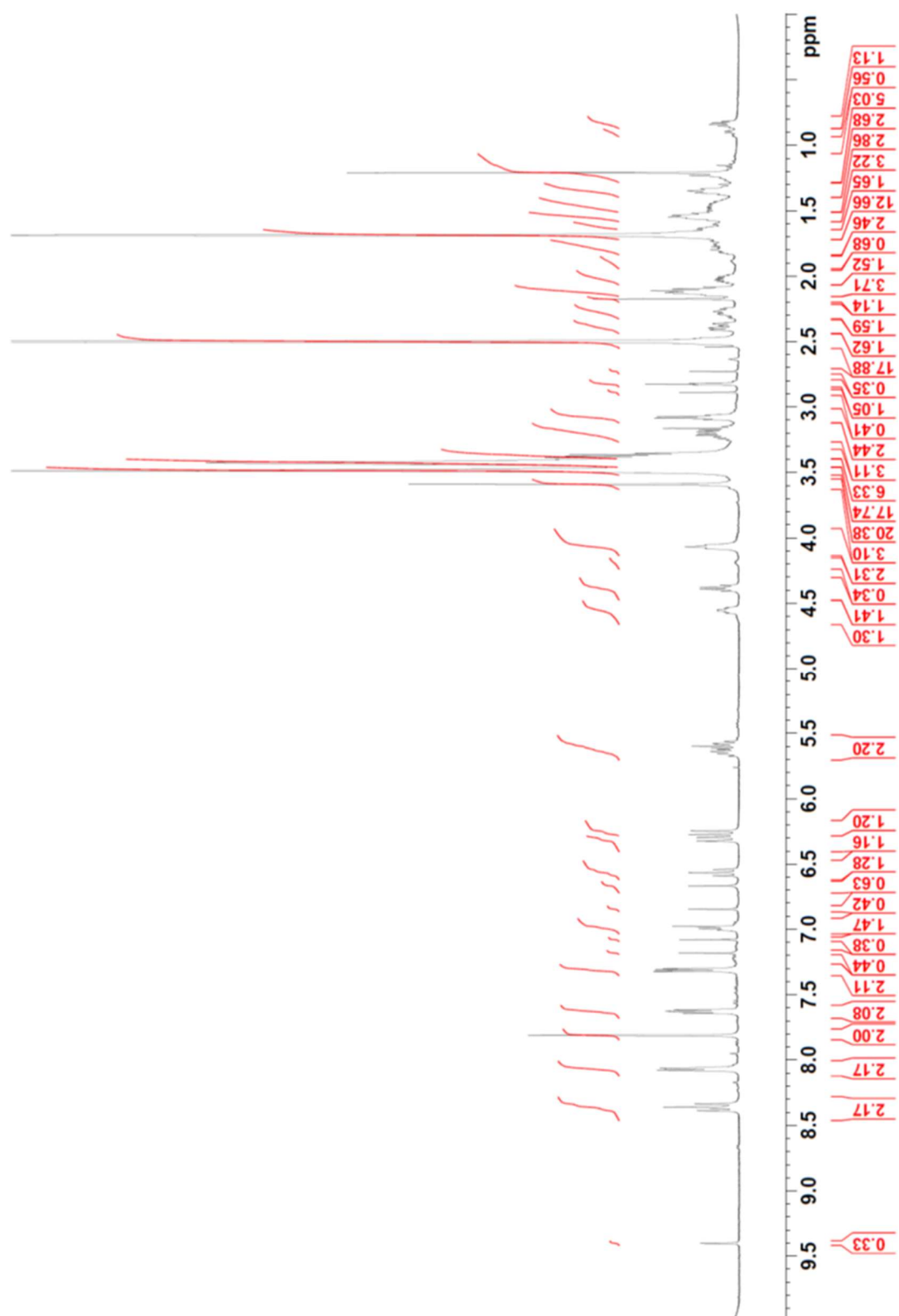
Supp. figure 40: ^{1}H-NMR spectrum of the inactive PEG$_{6}$-linker acquired at 500 MHz in DMSO-d$_{6}$.
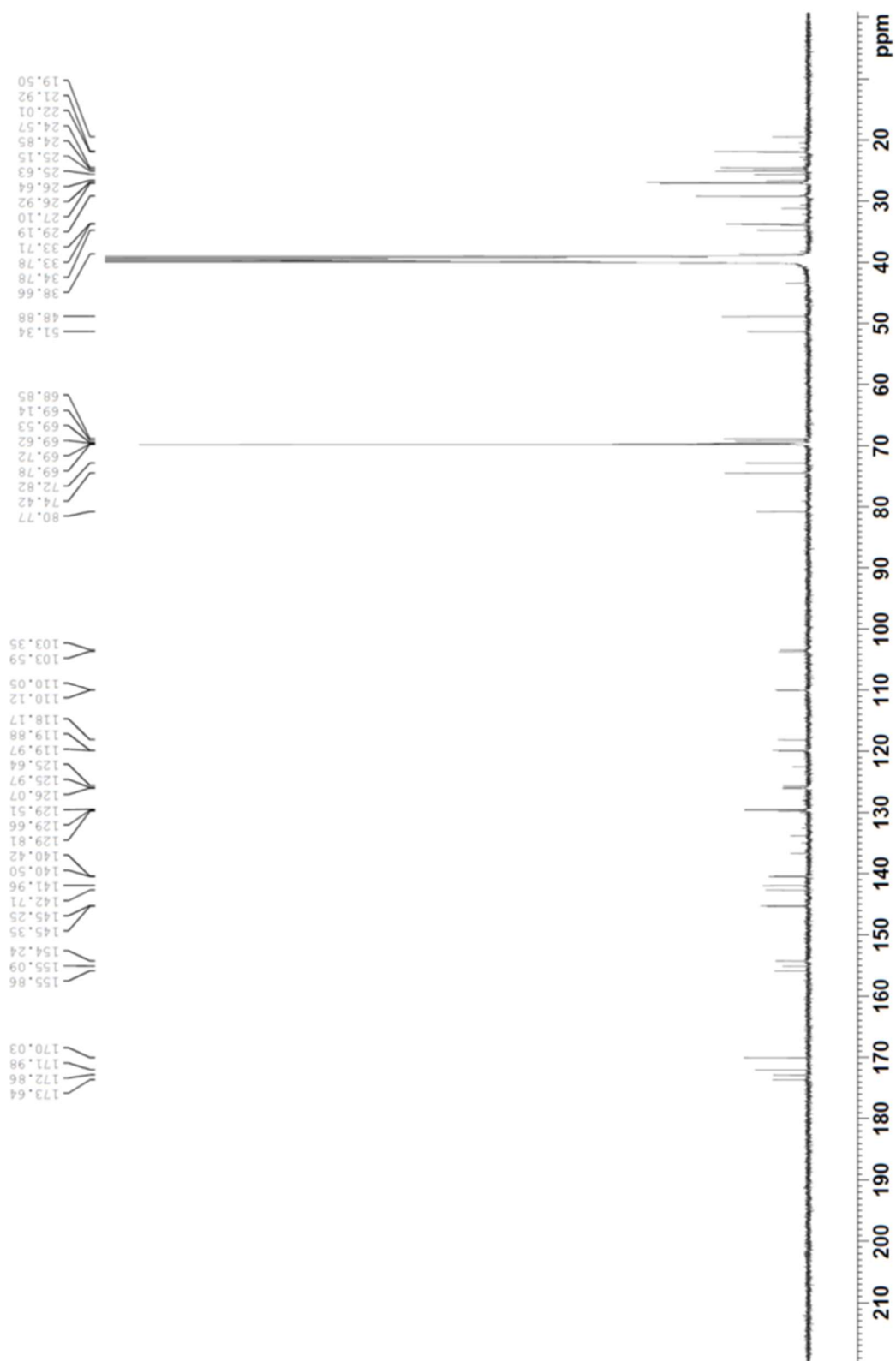
Supp. figure 41: ^{13}C-NMR spectrum of the inactive PEG$_6$-linker acquired at 126 MHz in DMSO-d$_6$.
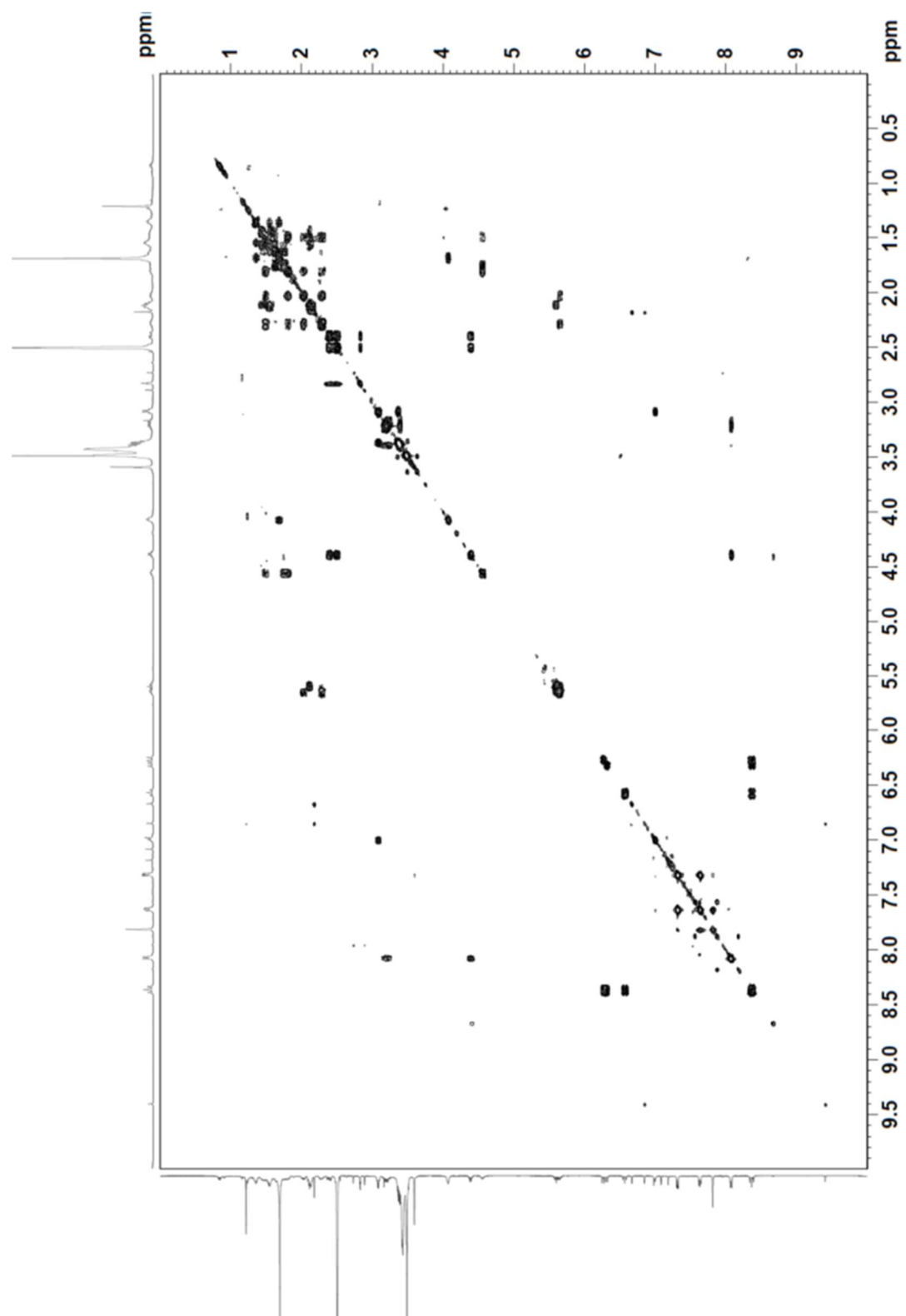
Supp. figure 42: COSY spectrum of the inactive PEG$_6$-linker acquired at 500 MHz in DMSO-d$_6$.
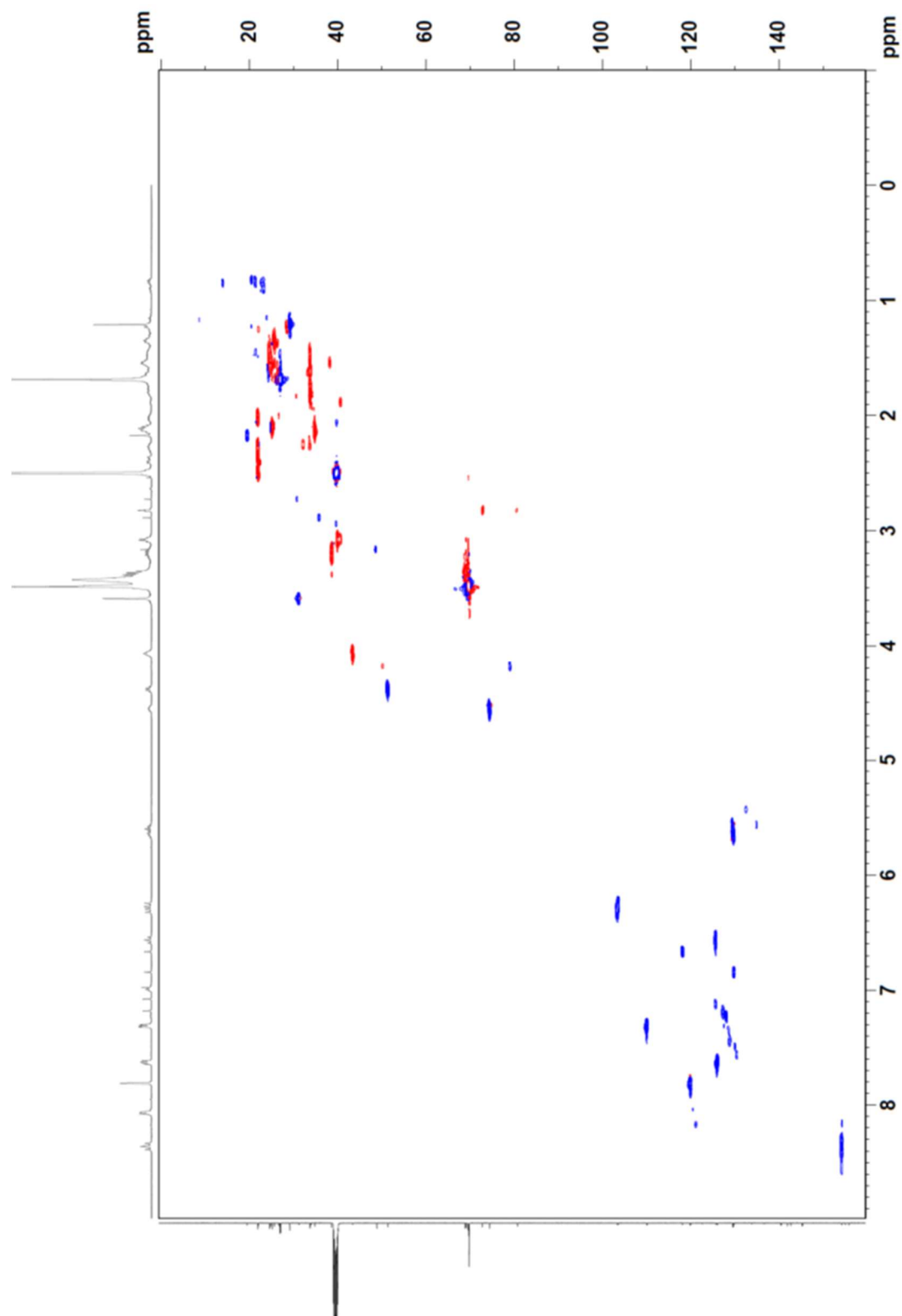
Supp. figure 43: HSQC spectrum of the inactive PEG₆-linker acquired at 500 MHz (^{1}H) and 126 MHz (^{13}C) in DMSO-d₆.
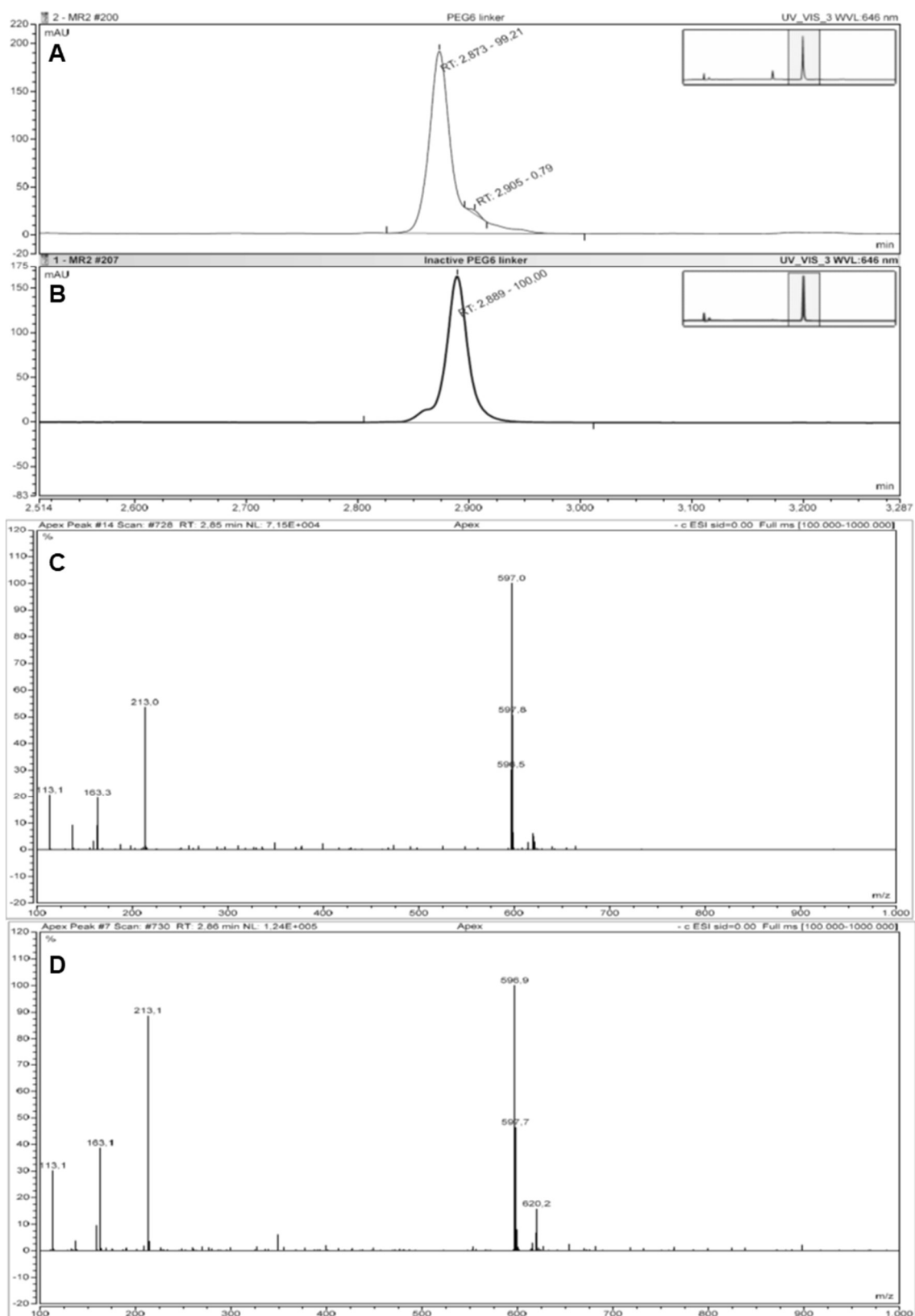
Supp. figure 44: Zoomed picture of the UV-absorption of the active PEG$_6$-linker (A, 2.873 min) and its inactive variant (B, 2.889 min). The mass spectra of both compounds (C&D) show the same signal of 597 m/z, corresponding to the [M-2H]$^{2-}$ ion.
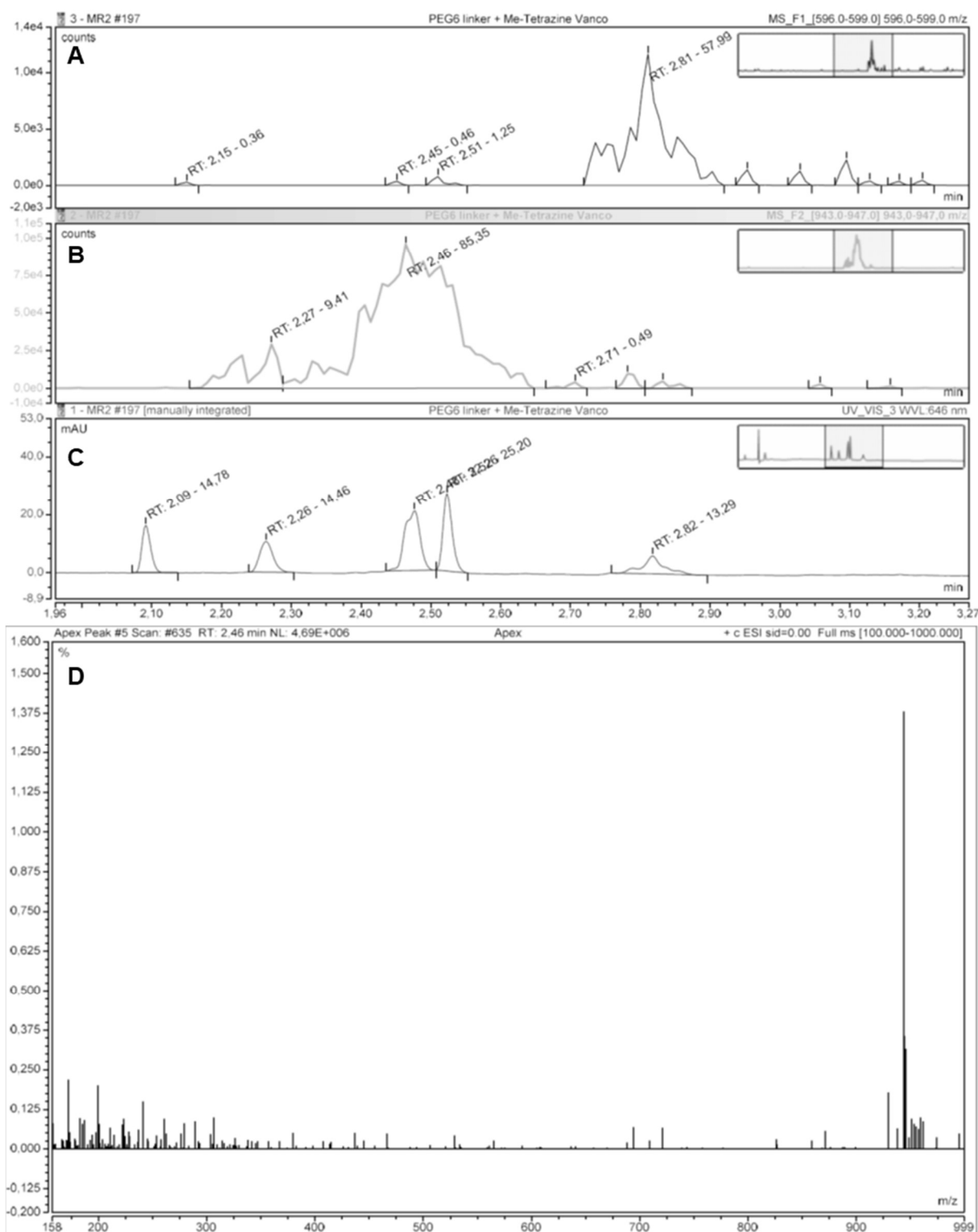
Supp. figure 45: LC/MS analysis of the IEDDA reaction of the PEG$_6$-linker and methyltetrazine-vancomycin. Panel A shows the peak corresponding with the [M-2H]$^{2-}$ ion of remaining PEG$_6$-linker at 2.81 min. Panel B shows the peaks corresponding with the IEDDA-product that was detected as the [M+3H]$^{3+}$ ion at 943 m/z (see also the corresponding mass spectrum D). The UV-absorption at 646 nm in panel C reveals that there were three peaks corresponding to the IEDDA-product eluting at 2.26, 2.46 and 2.52 min. Additionally the degradation product did not participate in the reaction and its peak eluted at 2.09 min.
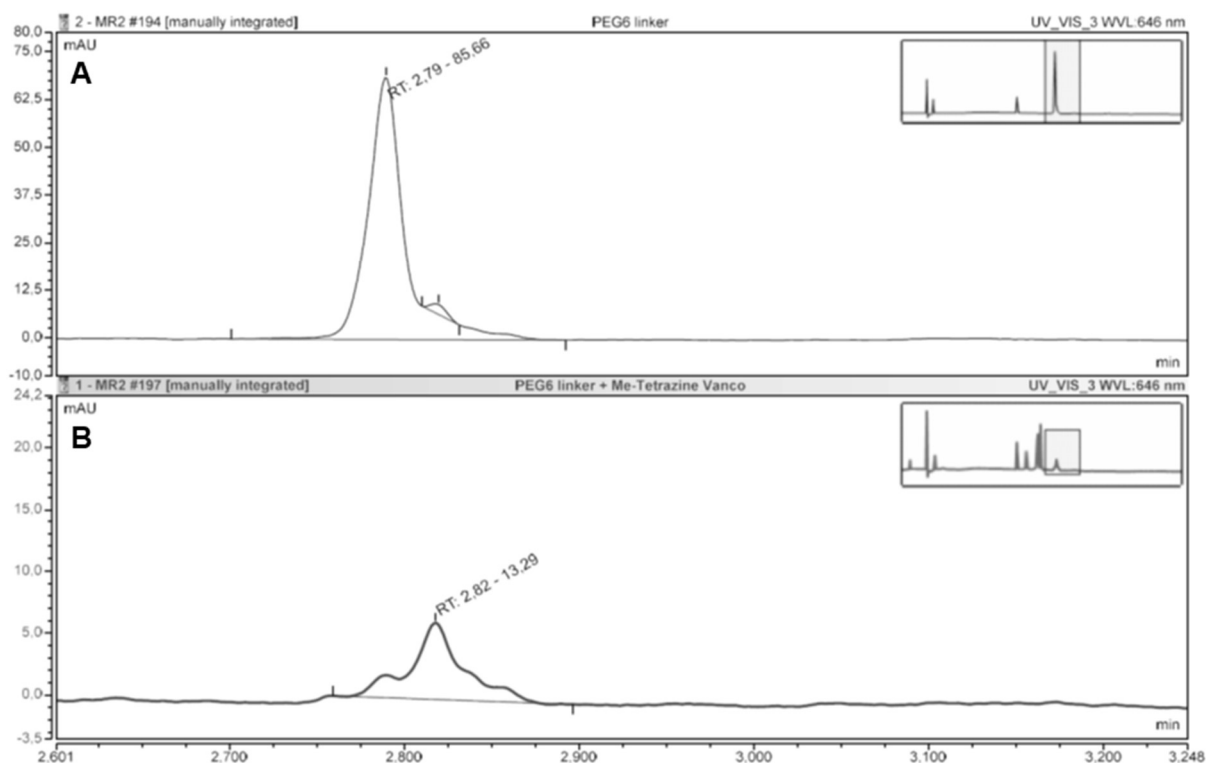
Supp. figure 46: Zoomed view of the UV-absorption peak at 646 nm corresponding with the PEG$_6$-linker. Before the IEDDA reaction (A), there is a main peak eluting at 2.79 min, with a shoulder that elutes later. After the IEDDA reaction (B), the main peak mostly disappeared and the shoulder remained (2.82 min).
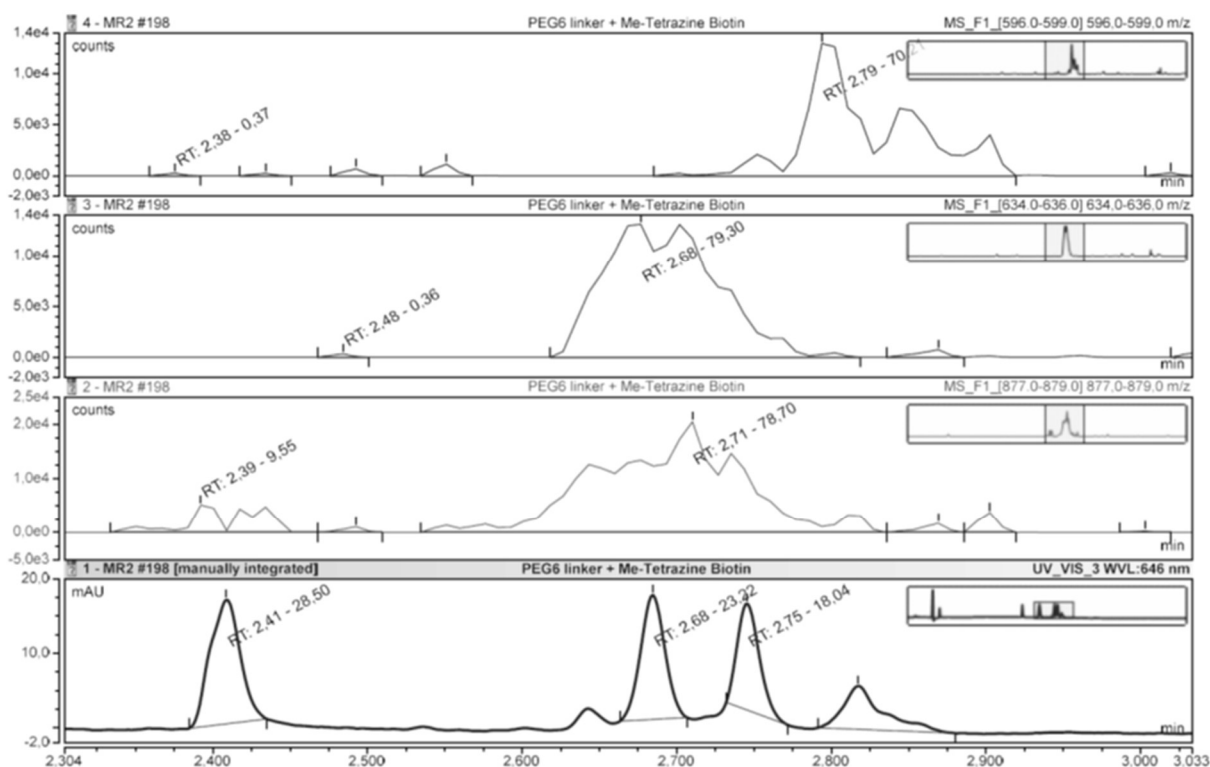
Supp. figure 47: LC/MS analysis of the IEDDA reaction of the PEG$_6$-linker and methyltetrazine-PEG$_4$-biotin zoomed to the relevant part of the spectrum. Panel A shows the peak corresponding with the [M-2H]$^{2-}$ ion of remaining PEG$_6$-linker at 2.79 min. Panel B shows the

175

peak corresponding with the [M+FA-H]⁻ ion of remaining methyltetrazine-PEG₄-biotin at 2.68 min (634 m/z). Panel C shows peaks at 2.39 and 2.71 min that corresponding with the [M-2H]²⁻ ion at 877 m/z. The UV-absorption at 646 nm in panel D revealed that there were three peaks corresponding to the IEDDA-product eluting at 2.41, 2.68 and 2.75 min.
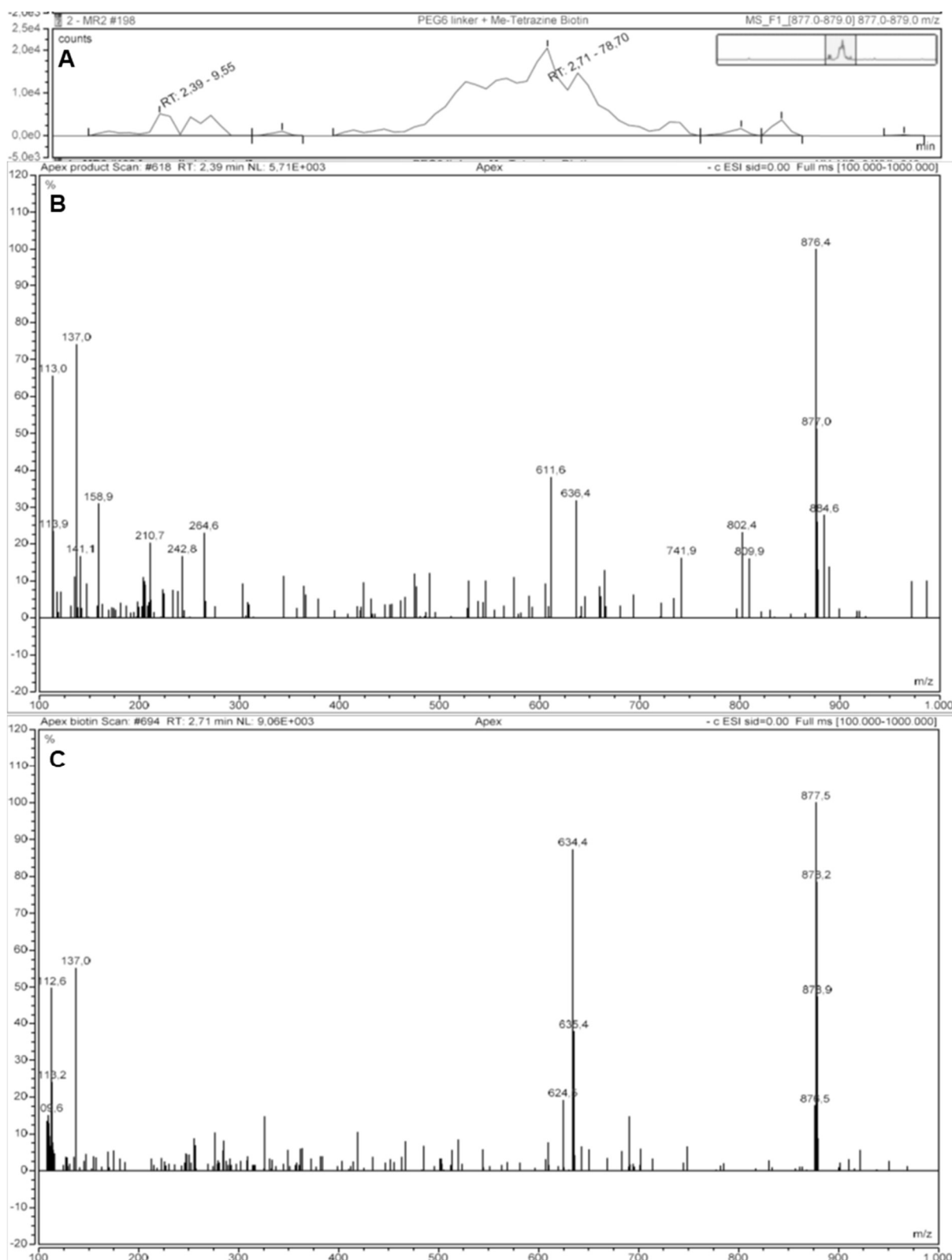
Supp. figure 48: LC/MS analysis of the IEDDA reaction of the PEG₆-linker and methyltetrazine-PEG₄-biotin zoomed to the relevant part of the spectrum. Panel A shows peaks at 2.39 and

176

2.71 min that corresponded with the [M-2H]²⁻ ion at 877 m/z. The mass spectra for the peak at 2.39 min (B) and 2.71 min (C) show that both peaks contained the IEDDA-product.
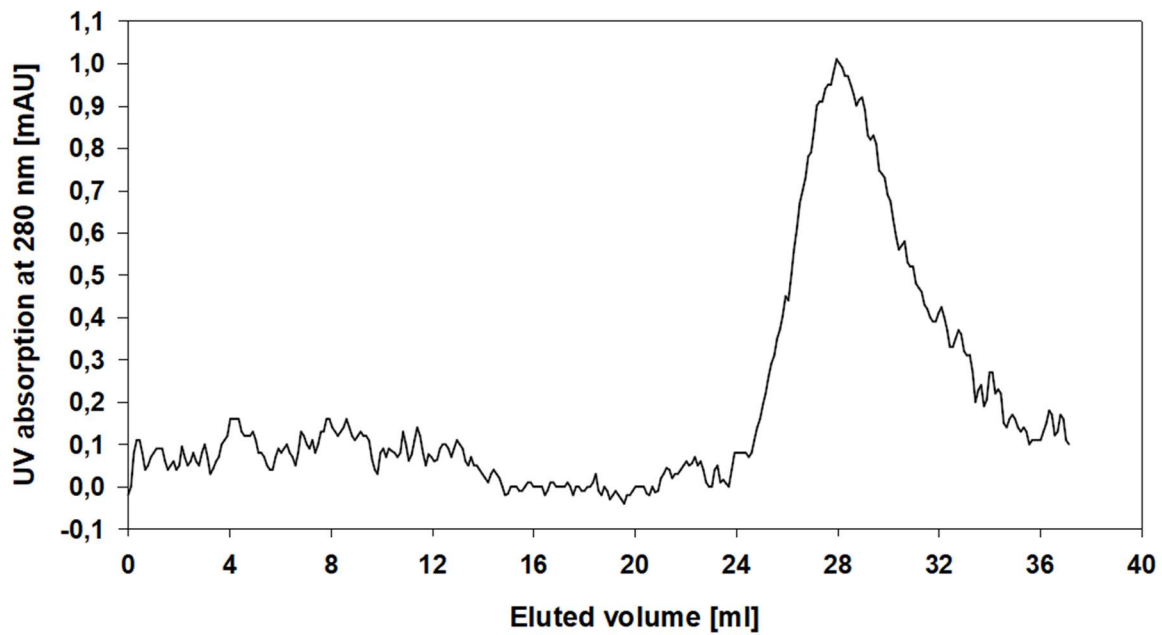
Supp. figure 49: Elution-profile of the IEDDA-product of TCO-PEG₄-DBCO and methyltetrazine-PEG₄-biotin. The molecule was dissolved at 4.9 µM in PBS and subjected to SEC-purification using the column generally employed for the purification of samples after CuAAC or SPAAC.
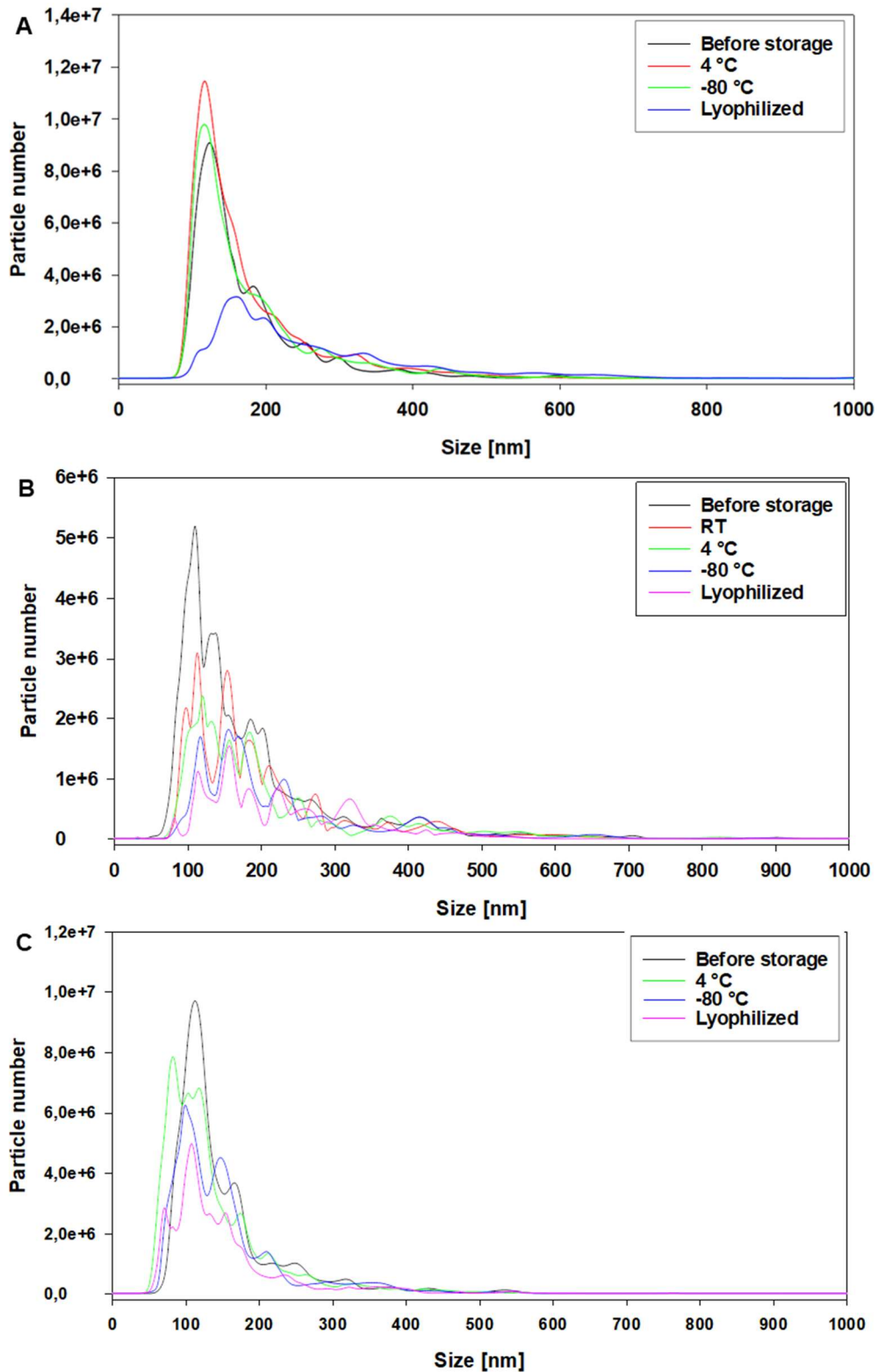
Supp. figure 50: Size distribution of EVs before and after storage. Panel A shows A549 EVs that were stored for 2 d at 4 °C, -80 °C or lyophilized without addition of trehalose. Panel B shows HUVEC EVs stored for 14 d at RT, 4 °C, -80 °C or lyophilized without addition of trehalose. Panel C shows HUVEC EVs stored for 7 d at 4 °C, -80 °C or lyophilized with addition of 4% trehalose.
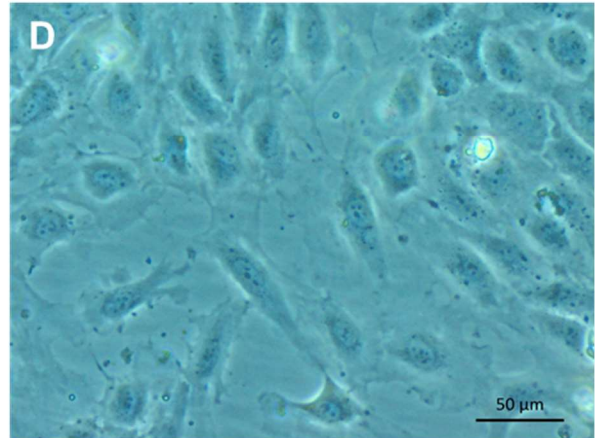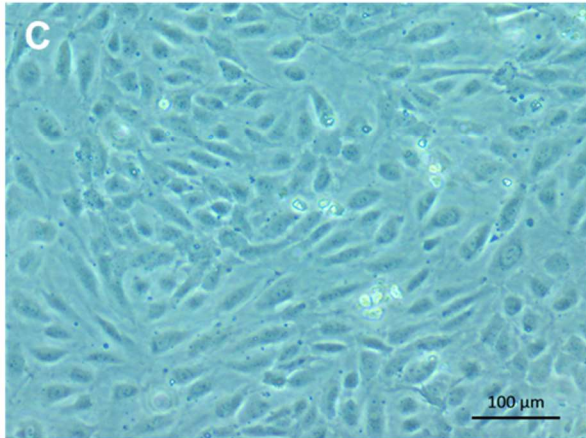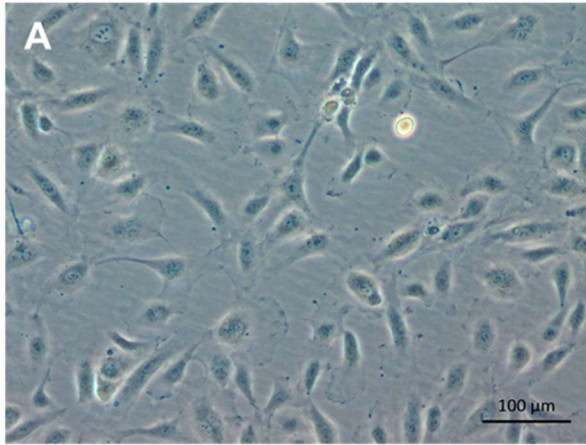
Supp. figure 51: Light microscopy of HUVEC cells. A&B show the cells after 120 h in culture, before the exchange to serum-free conditions. C&D show cells after another 48 h in serum-free conditions, just before EV-isolation.
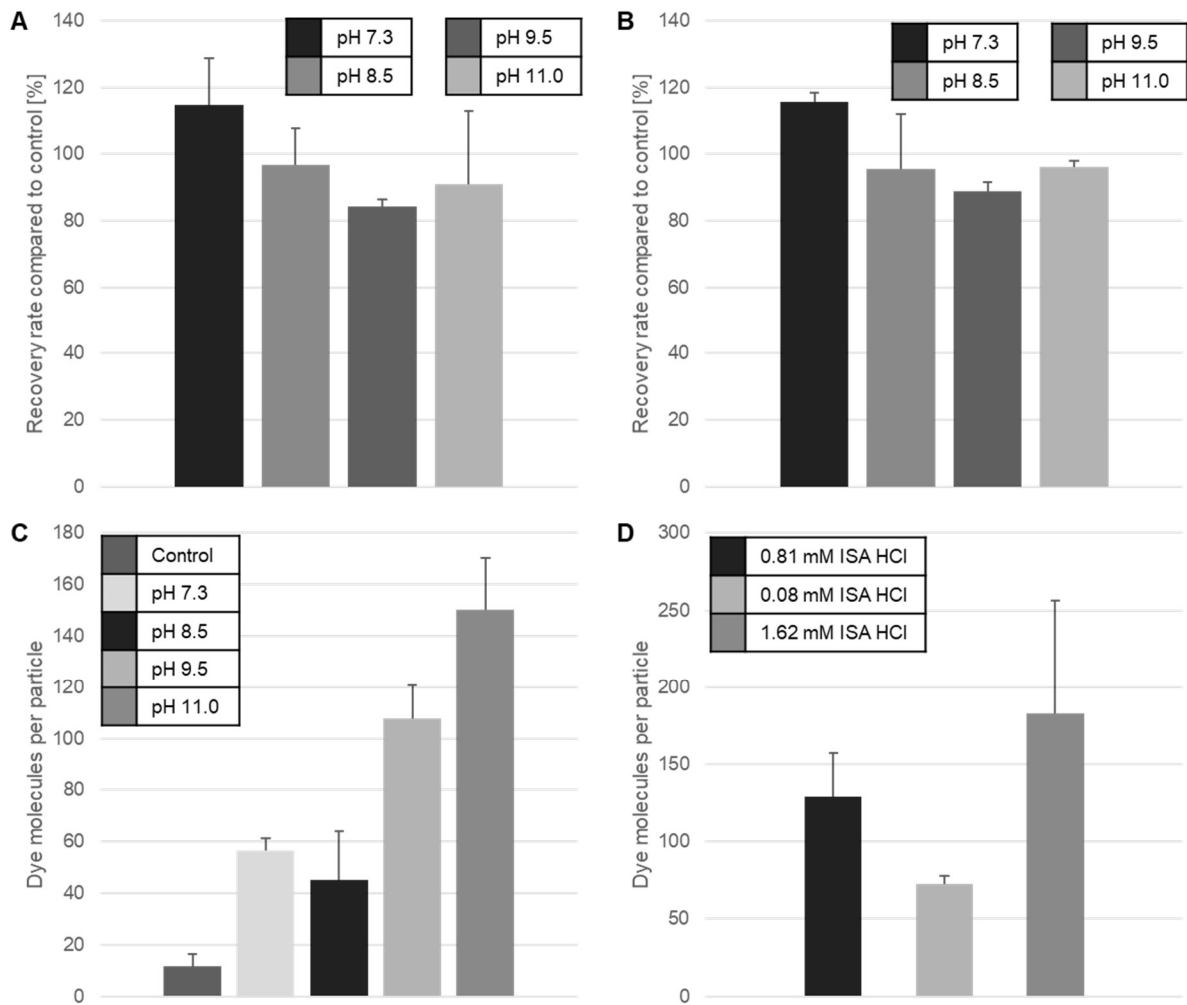
Supp. figure 52: Results of Philipp Lapuhs performing diazotransfer and SPAAC with OMVs derived from Stigmatella aurantiaca Sga15 myxobacteria. Panels A and B show the recovery rate measured by NTA (A) and ÄKTA (B) compared to the untreated control at different pH-values (n=3-6). Panel C shows the modification efficiency with DBCO AF594 depending on the pH (n=3-6). Panel D shows the modification efficiency depending on the ISA-concentration used for diazotransfer conducted at pH 9.5 (n=3). The figure was adapted from the master thesis of Philipp Lapuhs.

8. References

1. Sager R, Palade GE. Structure and development of the chloroplast in Chlamydomonas. I. The normal green cell. J Biophys Biochem Cytol. 1957;3(3):463-88.
2. Sotelo JR, Porter KR. An electron microscope study of the rat ovum. J Biophys Biochem Cytol. 1959;5(2):327-42.
3. De SN. Enterotoxicity of Bacteria-free Culture-filtrate of Vibrio cholerae. Nature. 1959;183(4674):1533-4.
4. Knox KW, Vesk M, Work E. Relation between excreted lipopolysaccharide complexes and surface structures of a lysine-limited culture of Escherichia coli. Journal of bacteriology. 1966;92(4):1206-17.
5. Johnstone RM, Adam M, Hammond JR, Orr L, Turbide C. Vesicle formation during reticulocyte maturation. Association of plasma membrane activities with released vesicles (exosomes). J Biol Chem. 1987;262(19):9412-20.
6. Lee E-Y, Choi D-Y, Kim D-K, Kim J-W, Park JO, Kim S, et al. Gram-positive bacteria produce membrane vesicles: Proteomics-based characterization of Staphylococcus aureus-derived membrane vesicles. PROTEOMICS. 2009;9(24):5425-36.
7. Regente M, Corti-Monzón G, Maldonado AM, Pinedo M, Jorrín J, de la Canal L. Vesicular fractions of sunflower apoplastic fluids are associated with potential exosome marker proteins. FEBS Letters. 2009;583(20):3363-6.
8. Prados-Rosales R, Baena A, Martinez LR, Luque-Garcia J, Kalscheuer R, Veeraraghavan U, et al. Mycobacteria release active membrane vesicles that modulate immune responses in a TLR2-dependent manner in mice. J Clin Invest. 2011;121(4):1471-83.
9. Ellen AF, Albers S-V, Huibers W, Pitcher A, Hobel CFV, Schwarz H, et al. Proteomic analysis of secreted membrane vesicles of archaeal Sulfolobus species reveals the presence of endosome sorting complex components. Extremophiles. 2008;13(1):67.
10. Rodrigues ML, Nimrichter L, Oliveira DL, Frases S, Miranda K, Zaragoza O, et al. Vesicular Polysaccharide Export in Cryptococcus neoformans Is a Eukaryotic Solution to the Problem of Fungal Trans-Cell Wall Transport. Eukaryotic Cell. 2007;6(1):48.
11. Woith E, Fuhrmann G, Melzig MF. Extracellular Vesicles-Connecting Kingdoms. International journal of molecular sciences. 2019;20(22):5695.
12. Kulp A, Kuehn MJ. Biological functions and biogenesis of secreted bacterial outer membrane vesicles. Annu Rev Microbiol. 2010;64(1):163-84.
13. Yáñez-Mó M, Siljander PRM, Andreu Z, Zavec AB, Borràs FE, Buzas EI, et al. Biological properties of extracellular vesicles and their physiological functions. Journal of Extracellular Vesicles. 2015;4:10.3402/jev.v4.27066.
14. Elhenawy W, Debelyy MO, Feldman MF. Preferential packing of acidic glycosidases and proteases into Bacteroides outer membrane vesicles. mBio. 2014;5(2):e00909-e914.
15. Mashburn LM, Whiteley M. Membrane vesicles traffic signals and facilitate group activities in a prokaryote. Nature. 2005;437(7057):422-5.
16. Cheng L, Sharples RA, Scicluna BJ, Hill AF. Exosomes provide a protective and enriched source of miRNA for biomarker profiling compared to intracellular and cell-free blood. Journal of Extracellular Vesicles. 2014;3(1):23743.
17. Stremersch S, De Smedt SC, Raemdonck K. Therapeutic and diagnostic applications of extracellular vesicles. Journal of Controlled Release. 2016;244, Part B:167-83.
18. Turnbull L, Toyofuku M, Hynen AL, Kurosawa M, Pessi G, Petty NK, et al. Explosive cell lysis as a mechanism for the biogenesis of bacterial membrane vesicles and biofilms. Nature Communications. 2016;7:11220.
19. Silver LL. Challenges of antibacterial discovery. Clin Microbiol Rev. 2011;24(1):71-109.
20. Boucher HW, Talbot GH, Bradley JS, Edwards JE, Gilbert D, Rice LB, et al. Bad Bugs, No Drugs: No ESKAPE! An Update from the Infectious Diseases Society of America. Clinical Infectious Diseases. 2009;48(1):1-12.

21.   Schulz E, Goes A, Garcia R, Panter F, Koch M, Müller R, et al. Biocompatible bacteria-derived vesicles show inherent antimicrobial activity. Journal of Controlled Release. 2018;290:46-55.

22.   Goes A, Lapuhs P, Kuhn T, Schulz E, Richter R, Panter F, et al. Myxobacteria-Derived Outer Membrane Vesicles: Potential Applicability Against Intracellular Infections. 2020;9(1):194.

23.   Théry C, Boussac M, Véron P, Ricciardi-Castagnoli P, Raposo G, Garin J, et al. Proteomic Analysis of Dendritic Cell-Derived Exosomes: A Secreted Subcellular Compartment Distinct from Apoptotic Vesicles. The Journal of Immunology. 2001;166(12):7309.

24.   Fuhrmann G, Herrmann IK, Stevens MM. Cell-derived vesicles for drug therapy and diagnostics: Opportunities and challenges. Nano Today. 2015;10(3):397-409.

25.   Zhang H, Freitas D, Kim HS, Fabijanic K, Li Z, Chen H, et al. Identification of distinct nanoparticles and subsets of extracellular vesicles by asymmetric flow field-flow fractionation. Nature Cell Biology. 2018;20(3):332-43.

26.   Nabhan JF, Hu R, Oh RS, Cohen SN, Lu Q. Formation and release of arrestin domain-containing protein 1-mediated microvesicles (ARMMs) at plasma membrane by recruitment of TSG101 protein. Proceedings of the National Academy of Sciences. 2012;109(11):4146.

27.   Steenbeek SC, Pham TV, de Ligt J, Zomer A, Knol JC, Piersma SR, et al. Cancer cells copy migratory behavior and exchange signaling networks via extracellular vesicles. The EMBO journal. 2018;37(15):e98357.

28.   de Jong OG, Murphy DE, Mäger I, Willms E, Garcia-Guerra A, Gitz-Francois JJ, et al. A CRISPR-Cas9-based reporter system for single-cell detection of extracellular vesicle-mediated functional transfer of RNA. Nature Communications. 2020;11(1):1113.

29.   Mulcahy LA, Pink RC, Carter DRF. Routes and mechanisms of extracellular vesicle uptake. Journal of Extracellular Vesicles. 2014;3(1):24641.

30.   Fitzner D, Schnaars M, van Rossum D, Krishnamoorthy G, Dibaj P, Bakhti M, et al. Selective transfer of exosomes from oligodendrocytes to microglia by macropinocytosis. Journal of Cell Science. 2011;124(3):447.

31.   Nazarenko I, Rana S, Baumann A, McAlear J, Hellwig A, Trendelenburg M, et al. Cell Surface Tetraspanin Tspan8 Contributes to Molecular Pathways of Exosome-Induced Endothelial Cell Activation. Cancer Research. 2010;70(4):1668.

32.   Chivet M, Javalet C, Laulagnier K, Blot B, Hemming FJ, Sadoul R. Exosomes secreted by cortical neurons upon glutamatergic synapse activation specifically interact with neurons. Journal of extracellular vesicles. 2014;3:24722-.

33.   Théry C, Witwer KW, Aikawa E, Alcaraz MJ, Anderson JD, Andriantsitohaina R, et al. Minimal information for studies of extracellular vesicles 2018 (MISEV2018): a position statement of the International Society for Extracellular Vesicles and update of the MISEV2014 guidelines. Journal of Extracellular Vesicles. 2018;7(1):1535750.

34.   van Niel G, D'Angelo G, Raposo G. Shedding light on the cell biology of extracellular vesicles. Nature Reviews Molecular Cell Biology. 2018;19(4):213-28.

35.   Mathieu M, Martin-Jaular L, Lavieu G, Théry C. Specificities of secretion and uptake of exosomes and other extracellular vesicles for cell-to-cell communication. Nature Cell Biology. 2019;21(1):9-17.

36.   Carayon K, Chaoui K, Ronzier E, Lazar I, Bertrand-Michel J, Roques V, et al. Proteolipidic composition of exosomes changes during reticulocyte maturation. The Journal of biological chemistry. 2011;286(39):34426-39.

37.   Colombo M, Moita C, van Niel G, Kowal J, Vigneron J, Benaroch P, et al. Analysis of ESCRT functions in exosome biogenesis, composition and secretion highlights the heterogeneity of extracellular vesicles. Journal of Cell Science. 2013;126(24):5553.

38.   Tamai K, Tanaka N, Nakano T, Kakazu E, Kondo Y, Inoue J, et al. Exosome secretion of dendritic cells is regulated by Hrs, an ESCRT-0 protein. Biochemical and Biophysical Research Communications. 2010;399(3):384-90.

39.   Smith VL, Jackson L, Schorey JS. Ubiquitination as a Mechanism To Transport Soluble Mycobacterial and Eukaryotic Proteins to Exosomes. The Journal of Immunology. 2015;195(6):2722.

40.   Wollert T, Wunder C, Lippincott-Schwartz J, Hurley JH. Membrane scission by the ESCRT-III complex. Nature. 2009;458(7235):172-7.

41.   Baietti MF, Zhang Z, Mortier E, Melchior A, Degeest G, Geeraerts A, et al. Syndecan–syntenin–ALIX regulates the biogenesis of exosomes. Nature Cell Biology. 2012;14(7):677-85.

42.   Friand V, David G, Zimmermann P. Syntenin and syndecan in the biogenesis of exosomes. Biology of the Cell. 2015;107(10):331-41.

43.   Stuffers S, Sem Wegner C, Stenmark H, Brech A. Multivesicular Endosome Biogenesis in the Absence of ESCRTs. Traffic. 2009;10(7):925-37.

44.   Trajkovic K, Hsu C, Chiantia S, Rajendran L, Wenzel D, Wieland F, et al. Ceramide Triggers Budding of Exosome Vesicles into Multivesicular Endosomes. Science. 2008;319(5867):1244.

45.   Hurley JH. ESCRTs are everywhere. The EMBO Journal. 2015;34(19):2398-407.

46.   del Conde I, Shrimpton CN, Thiagarajan P, López JA. Tissue-factor–bearing microvesicles arise from lipid rafts and fuse with activated platelets to initiate coagulation. Blood. 2005;106(5):1604-11.

47.   Beer KB, Rivas-Castillo J, Kuhn K, Fazeli G, Karmann B, Nance JF, et al. Extracellular vesicle budding is inhibited by redundant regulators of TAT-5 flippase localization and phospholipid asymmetry. Proceedings of the National Academy of Sciences. 2018;115(6):E1127.

48.   Taylor J, Azimi I, Monteith G, Bebawy M. Ca(2+) mediates extracellular vesicle biogenesis through alternate pathways in malignancy. Journal of extracellular vesicles. 2020;9(1):1734326-.

49.   Szabo G, Momen-Heravi F. Extracellular vesicles in liver disease and potential as biomarkers and therapeutic targets. Nature Reviews Gastroenterology & Hepatology. 2017;14(8):455-66.

50.   Charrin S, Jouannet S, Boucheix C, Rubinstein E. Tetraspanins at a glance. Journal of Cell Science. 2014;127(17):3641.

51.   Latysheva N, Muratov G, Rajesh S, Padgett M, Hotchin NA, Overduin M, et al. Syntenin-1 is a new component of tetraspanin-enriched microdomains: mechanisms and consequences of the interaction of syntenin-1 with CD63. Mol Cell Biol. 2006;26(20):7707-18.

52.   Charrin S, Manié S, Thiele C, Billard M, Gerlier D, Boucheix C, et al. A physical and functional link between cholesterol and tetraspanins. Eur J Immunol. 2003;33(9):2479-89.

53.   Andreu Z, Yáñez-Mó M. Tetraspanins in extracellular vesicle formation and function. Front Immunol. 2014;5:442-.

54.   Chairoungdua A, Smith DL, Pochard P, Hull M, Caplan MJ. Exosome release of β-catenin: a novel mechanism that antagonizes Wnt signaling. J Cell Biol. 2010;190(6):1079-91.

55.   Buschow SI, Nolte-'t Hoen ENM, Van Niel G, Pols MS, Ten Broeke T, Lauwen M, et al. MHC II in Dendritic Cells is Targeted to Lysosomes or T Cell-Induced Exosomes Via Distinct Multivesicular Body Pathways. Traffic. 2009;10(10):1528-42.

56.   van Niel G, Charrin S, Simoes S, Romao M, Rochin L, Saftig P, et al. The Tetraspanin CD63 Regulates ESCRT-Independent and -Dependent Endosomal Sorting during Melanogenesis. Developmental Cell. 2011;21(4):708-21.

57.   Villarroya-Beltri C, Gutiérrez-Vázquez C, Sánchez-Cabo F, Pérez-Hernández D, Vázquez J, Martin-Cofreces N, et al. Sumoylated hnRNPA2B1 controls the sorting of miRNAs into exosomes through binding to specific motifs. Nature communications. 2013;4:2980-.

58.   Bolukbasi MF, Mizrak A, Ozdener GB, Madlener S, Ströbel T, Erkan EP, et al. miR-1289 and "Zipcode"-like Sequence Enrich mRNAs in Microvesicles. Mol Ther Nucleic Acids. 2012;1(2):e10-e.

59.   Irion U, St Johnston D. bicoid RNA localization requires specific binding of an endosomal sorting complex. Nature. 2007;445(7127):554-8.

60.   Perez-Hernandez D, Gutiérrez-Vázquez C, Jorge I, López-Martín S, Ursa A, Sánchez-Madrid F, et al. The intracellular interactome of tetraspanin-enriched microdomains reveals their function as sorting machineries toward exosomes. The Journal of biological chemistry. 2013;288(17):11649-61.

61. Villarroya-Beltri C, Baixauli F, Mittelbrunn M, Fernández-Delgado I, Torralba D, Moreno-Gonzalo O, et al. ISGylation controls exosome secretion by promoting lysosomal degradation of MVB proteins. Nature Communications. 2016;7(1):13588.

62. Ostrowski M, Carmo NB, Krumeich S, Fanget I, Raposo G, Savina A, et al. Rab27a and Rab27b control different steps of the exosome secretion pathway. Nature Cell Biology. 2010;12(1):19-30.

63. Jahn R, Scheller RH. SNAREs — engines for membrane fusion. Nature Reviews Molecular Cell Biology. 2006;7(9):631-43.

64. Gross JC, Chaudhary V, Bartscherer K, Boutros M. Active Wnt proteins are secreted on exosomes. Nature Cell Biology. 2012;14(10):1036-45.

65. Fader CM, Sánchez DG, Mestre MB, Colombo MI. TI-VAMP/VAMP7 and VAMP3/cellubrevin: two v-SNARE proteins involved in specific steps of the autophagy/multivesicular body pathways. Biochim Biophys Acta. 2009;1793(12):1901-16.

66. Ruiz-Martinez M, Navarro A, Marrades RM, Viñolas N, Santasusagna S, Muñoz C, et al. YKT6 expression, exosome release, and survival in non-small cell lung cancer. Oncotarget. 2016;7(32).

67. Tkach M, Kowal J, Zucchetti AE, Enserink L, Jouve M, Lankar D, et al. Qualitative differences in T-cell activation by dendritic cell-derived extracellular vesicle subtypes. The EMBO journal. 2017;36(20):3012-28.

68. Morelli AE, Larregina AT, Shufesky WJ, Sullivan MLG, Stolz DB, Papworth GD, et al. Endocytosis, intracellular sorting, and processing of exosomes by dendritic cells. Blood. 2004;104(10):3257-66.

69. Miyanishi M, Tada K, Koike M, Uchiyama Y, Kitamura T, Nagata S. Identification of Tim4 as a phosphatidylserine receptor. Nature. 2007;450(7168):435-9.

70. Purushothaman A, Bandari SK, Liu J, Mobley JA, Brown EE, Sanderson RD. Fibronectin on the Surface of Myeloma Cell-derived Exosomes Mediates Exosome-Cell Interactions. The Journal of biological chemistry. 2016;291(4):1652-63.

71. Parolini I, Federici C, Raggi C, Lugini L, Palleschi S, De Milito A, et al. Microenvironmental pH is a key factor for exosome traffic in tumor cells. The Journal of biological chemistry. 2009;284(49):34211-22.

72. Montecalvo A, Larregina AT, Shufesky WJ, Stolz DB, Sullivan MLG, Karlsson JM, et al. Mechanism of transfer of functional microRNAs between mouse dendritic cells via exosomes. Blood. 2012;119(3):756-66.

73. Tian T, Zhu Y-L, Zhou Y-Y, Liang G-F, Wang Y-Y, Hu F-H, et al. Exosome uptake through clathrin-mediated endocytosis and macropinocytosis and mediating miR-21 delivery. The Journal of biological chemistry. 2014;289(32):22258-67.

74. Svensson KJ, Christianson HC, Wittrup A, Bourseau-Guilmain E, Lindqvist E, Svensson LM, et al. Exosome uptake depends on ERK1/2-heat shock protein 27 signaling and lipid Raft-mediated endocytosis negatively regulated by caveolin-1. The Journal of biological chemistry. 2013;288(24):17713-24.

75. Feng D, Zhao W-L, Ye Y-Y, Bai X-C, Liu R-Q, Chang L-F, et al. Cellular Internalization of Exosomes Occurs Through Phagocytosis. Traffic. 2010;11(5):675-87.

76. Joshi BS, de Beer MA, Giepmans BNG, Zuhorn IS. Endocytosis of Extracellular Vesicles and Release of Their Cargo from Endosomes. ACS Nano. 2020;14(4):4444-55.

77. Yuana Y, Sturk A, Nieuwland R. Extracellular vesicles in physiological and pathological conditions. Blood Reviews. 2013;27(1):31-9.

78. Suades R, Padró T, Vilahur G, Badimon L. Circulating and platelet-derived microparticles in human blood enhance thrombosis on atherosclerotic plaques. Thromb Haemost. 2012;108(6):1208-19.

79. Owens AP, 3rd, Mackman N. Microparticles in hemostasis and thrombosis. Circ Res. 2011;108(10):1284-97.

80. Brill A, Dashevsky O, Rivo J, Gozal Y, Varon D. Platelet-derived microparticles induce angiogenesis and stimulate post-ischemic revascularization. Cardiovascular Research. 2005;67(1):30-8.

81. Lindenbergh MFS, Stoorvogel W. Antigen Presentation by Extracellular Vesicles from Professional Antigen-Presenting Cells. Annual Review of Immunology. 2018;36(1):435-59.

82. Admyre C, Johansson SM, Qazi KR, Filén J-J, Lahesmaa R, Norman M, et al. Exosomes with Immune Modulatory Features Are Present in Human Breast Milk. The Journal of Immunology. 2007;179(3):1969.

83. Chivet M, Javalet C, Hemming F, Pernet-Gallay K, Laulagnier K, Fraboulet S, et al. Exosomes as a novel way of interneuronal communication. Biochem Soc Trans. 2013;41(1):241-4.

84. Korkut C, Li Y, Koles K, Brewer C, Ashley J, Yoshihara M, et al. Regulation of postsynaptic retrograde signaling by presynaptic exosome release. Neuron. 2013;77(6):1039-46.

85. Krämer-Albers EM, Bretz N, Tenzer S, Winterstein C, Möbius W, Berger H, et al. Oligodendrocytes secrete exosomes containing major myelin and stress-protective proteins: Trophic support for axons? Proteomics Clin Appl. 2007;1(11):1446-61.

86. Jiang N, Xiang L, He L, Yang G, Zheng J, Wang C, et al. Exosomes Mediate Epithelium-Mesenchyme Crosstalk in Organ Development. ACS nano. 2017;11(8):7736-46.

87. Timár CI, Lőrincz ÁM, Csépányi-Kömi R, Vályi-Nagy A, Nagy G, Buzás EI, et al. Antibacterial effect of microvesicles released from human neutrophilic granulocytes. Blood. 2013;121(3):510.

88. Shopova IA, Belyaev I, Dasari P, Jahreis S, Stroe MC, Cseresnyés Z, et al. Human Neutrophils Produce Antifungal Extracellular Vesicles against Aspergillus fumigatus. mBio. 2020;11(2):e00596-20.

89. Keller MD, Ching KL, Liang F-X, Dhabaria A, Tam K, Ueberheide BM, et al. Decoy exosomes provide protection against bacterial toxins. Nature. 2020;579(7798):260-4.

90. Wang T, Fang L, Zhao F, Wang D, Xiao S. Exosomes Mediate Intercellular Transmission of Porcine Reproductive and Respiratory Syndrome Virus. Journal of virology. 2018;92(4):e01734-17.

91. Wiley RD, Gummuluru S. Immature dendritic cell-derived exosomes can mediate HIV-1 trans infection. Proceedings of the National Academy of Sciences of the United States of America. 2006;103(3):738-43.

92. Kulkarni R, Prasad A. Exosomes Derived from HIV-1 Infected DCs Mediate Viral trans-Infection via Fibronectin and Galectin-3. Scientific Reports. 2017;7(1):14787.

93. Hill AF. Extracellular Vesicles and Neurodegenerative Diseases. The Journal of Neuroscience. 2019;39(47):9269.

94. Liu S, Hossinger A, Göbbels S, Vorberg IM. Prions on the run: How extracellular vesicles serve as delivery vehicles for self-templating protein aggregates. Prion. 2017;11(2):98-112.

95. Blackwell RH, Foreman KE, Gupta GN. The Role of Cancer-Derived Exosomes in Tumorigenicity & Epithelial-to-Mesenchymal Transition. Cancers (Basel). 2017;9(8):105.

96. Peinado H, Alečković M, Lavotshkin S, Matei I, Costa-Silva B, Moreno-Bueno G, et al. Melanoma exosomes educate bone marrow progenitor cells toward a pro-metastatic phenotype through MET. Nature Medicine. 2012;18(6):883-91.

97. Yue S, Mu W, Erb U, Zöller M. The tetraspanins CD151 and Tspan8 are essential exosome components for the crosstalk between cancer initiating cells and their surrounding. Oncotarget. 2014;6(4).

98. Wen SW, Sceneay J, Lima LG, Wong CSF, Becker M, Krumeich S, et al. The Biodistribution and Immune Suppressive Effects of Breast Cancer–Derived Exosomes. Cancer Research. 2016;76(23):6816.

99. Kaparakis-Liaskos M, Ferrero RL. Immune modulation by bacterial outer membrane vesicles. Nat Rev Immunol. 2015;15(6):375-87.

100. Bertani B, Ruiz N. Function and Biogenesis of Lipopolysaccharides. EcoSal Plus. 2018;8(1):10.1128/ecosalplus.ESP-0001-2018.

101. Raetz CRH, Whitfield C. Lipopolysaccharide endotoxins. Annu Rev Biochem. 2002;71:635-700.

102. Clifton LA, Skoda MWA, Le Brun AP, Ciesielski F, Kuzmenko I, Holt SA, et al. Effect of Divalent Cation Removal on the Structure of Gram-Negative Bacterial Outer Membrane Models. Langmuir. 2015;31(1):404-12.

103.   Copeland S, Warren HS, Lowry SF, Calvano SE, Remick D. Acute Inflammatory Response to Endotoxin in Mice and Humans. Clinical and Diagnostic Laboratory Immunology. 2005;12(1):60.

104.   Schwechheimer C, Kuehn MJ. Outer-membrane vesicles from Gram-negative bacteria: biogenesis and functions. Nature Reviews Microbiology. 2015;13(10):605-19.

105.   Yakhnina AA, Bernhardt TG. The Tol-Pal system is required for peptidoglycan-cleaving enzymes to complete bacterial cell division. Proceedings of the National Academy of Sciences. 2020;117(12):6777.

106.   Schwechheimer C, Rodriguez DL, Kuehn MJ. NlpI-mediated modulation of outer membrane vesicle production through peptidoglycan dynamics in Escherichia coli. Microbiologyopen. 2015;4(3):375-89.

107.   Murphy K, Park AJ, Hao Y, Brewer D, Lam JS, Khursigara CM. Influence of O polysaccharides on biofilm development and outer membrane vesicle biogenesis in Pseudomonas aeruginosa PAO1. Journal of bacteriology. 2014;196(7):1306-17.

108.   Elhenawy W, Bording-Jorgensen M, Valguarnera E, Haurat MF, Wine E, Feldman MF. LPS Remodeling Triggers Formation of Outer Membrane Vesicles in Salmonella. mBio. 2016;7(4):e00940-16.

109.   Kadurugamuwa JL, Beveridge TJ. Membrane vesicles derived from Pseudomonas aeruginosa and Shigella flexneri can be integrated into the surfaces of other Gram-negative bacteria. Microbiology. 1999;145(8):2051-60.

110.   Tashiro Y, Hasegawa Y, Shintani M, Takaki K, Ohkuma M, Kimbara K, et al. Interaction of Bacterial Membrane Vesicles with Specific Species and Their Potential for Delivery to Target Cells. Frontiers in microbiology. 2017;8:571-.

111.   Caruana JC, Walper SA. Bacterial Membrane Vesicles as Mediators of Microbe - Microbe and Microbe - Host Community Interactions. Frontiers in microbiology. 2020;11:432-.

112.   Kesty NC, Mason KM, Reedy M, Miller SE, Kuehn MJ. Enterotoxigenic Escherichia coli vesicles target toxin delivery into mammalian cells. The EMBO Journal. 2004;23(23):4538-49.

113.   Kouokam JC, Wai SN, Fällman M, Dobrindt U, Hacker J, Uhlin BE. Active cytotoxic necrotizing factor 1 associated with outer membrane vesicles from uropathogenic Escherichia coli. Infection and immunity. 2006;74(4):2022-30.

114.   Jin JS, Kwon S-O, Moon DC, Gurung M, Lee JH, Kim SI, et al. Acinetobacter baumannii secretes cytotoxic outer membrane protein A via outer membrane vesicles. PloS one. 2011;6(2):e17027-e.

115.   O'Donoghue EJ, Sirisaengtaksin N, Browning DF, Bielska E, Hadis M, Fernandez-Trillo F, et al. Lipopolysaccharide structure impacts the entry kinetics of bacterial outer membrane vesicles into host cells. PLOS Pathogens. 2017;13(11):e1006760.

116.   McBroom AJ, Kuehn MJ. Release of outer membrane vesicles by Gram-negative bacteria is a novel envelope stress response. Molecular Microbiology. 2007;63(2):545-58.

117.   Bonnington KE, Kuehn MJ. Outer Membrane Vesicle Production Facilitates LPS Remodeling and Outer Membrane Maintenance in Salmonella during Environmental Transitions. mBio. 2016;7(5):e01532-16.

118.   Lynch JB, Alegado RA. Spheres of Hope, Packets of Doom: the Good and Bad of Outer Membrane Vesicles in Interspecies and Ecological Dynamics. Journal of bacteriology. 2017;199(15):e00012-17.

119.   Bauman SJ, Kuehn MJ. Purification of outer membrane vesicles from Pseudomonas aeruginosa and their activation of an IL-8 response. Microbes Infect. 2006;8(9-10):2400-8.

120.   Lin J, Zhang W, Cheng J, Yang X, Zhu K, Wang Y, et al. A Pseudomonas T6SS effector recruits PQS-containing outer membrane vesicles for iron acquisition. Nature communications. 2017;8:14888-.

121.   Biller SJ, Schubotz F, Roggensack SE, Thompson AW, Summons RE, Chisholm SW. Bacterial Vesicles in Marine Ecosystems. Science. 2014;343(6167):183.

122.   Shen Y, Giardino Torchia ML, Lawson GW, Karp CL, Ashwell JD, Mazmanian SK. Outer membrane vesicles of a human commensal mediate immune regulation and disease protection. Cell Host Microbe. 2012;12(4):509-20.

123. Fábrega M-J, Rodríguez-Nogales A, Garrido-Mesa J, Algieri F, Badía J, Giménez R, et al. Intestinal Anti-inflammatory Effects of Outer Membrane Vesicles from Escherichia coli Nissle 1917 in DSS-Experimental Colitis in Mice. Frontiers in microbiology. 2017;8:1274-.

124. Kuhn T, Koch M, Fuhrmann G. Probiomimetics—Novel Lactobacillus-Mimicking Microparticles Show Anti-Inflammatory and Barrier-Protecting Effects in Gastrointestinal Models. Small. 2020;n/a(n/a):2003158.

125. Hold GL, Smith M, Grange C, Watt ER, El-Omar EM, Mukhopadhya I. Role of the gut microbiota in inflammatory bowel disease pathogenesis: what have we learnt in the past 10 years? World J Gastroenterol. 2014;20(5):1192-210.

126. Grenier D, Bertrand J, Mayrand D. Porphyromonas gingivalis outer membrane vesicles promote bacterial resistance to chlorhexidine. Oral Microbiol Immunol. 1995;10(5):319-20.

127. Manning AJ, Kuehn MJ. Contribution of bacterial outer membrane vesicles to innate bacterial defense. BMC Microbiol. 2011;11:258-.

128. Roszkowiak J, Jajor P, Guła G, Gubernator J, Żak A, Drulis-Kawa Z, et al. Interspecies Outer Membrane Vesicles (OMVs) Modulate the Sensitivity of Pathogenic Bacteria and Pathogenic Yeasts to Cationic Peptides and Serum Complement. International journal of molecular sciences. 2019;20(22):5577.

129. Stentz R, Horn N, Cross K, Salt L, Brearley C, Livermore DM, et al. Cephalosporinases associated with outer membrane vesicles released by Bacteroides spp. protect gut pathogens and commensals against β-lactam antibiotics. J Antimicrob Chemother. 2015;70(3):701-9.

130. Yaron S, Kolling GL, Simon L, Matthews KR. Vesicle-Mediated Transfer of Virulence Genes fromEscherichia coli O157:H7 to Other Enteric Bacteria. Applied and Environmental Microbiology. 2000;66(10):4414.

131. Fulsundar S, Harms K, Flaten GE, Johnsen PJ, Chopade BA, Nielsen KM. Gene Transfer Potential of Outer Membrane Vesicles of Acinetobacter baylyi and Effects of Stress on Vesiculation. Applied and Environmental Microbiology. 2014;80(11):3469.

132. Rumbo C, Fernández-Moreira E, Merino M, Poza M, Mendez JA, Soares NC, et al. Horizontal transfer of the OXA-24 carbapenemase gene via outer membrane vesicles: a new mechanism of dissemination of carbapenem resistance genes in Acinetobacter baumannii. Antimicrobial agents and chemotherapy. 2011;55(7):3084-90.

133. Chatterjee S, Mondal A, Mitra S, Basu S. Acinetobacter baumannii transfers the blaNDM-1 gene via outer membrane vesicles. Journal of Antimicrobial Chemotherapy. 2017;72(8):2201-7.

134. Baumgarten T, Sperling S, Seifert J, von Bergen M, Steiniger F, Wick LY, et al. Membrane Vesicle Formation as a Multiple-Stress Response Mechanism Enhances Pseudomonas putida DOT-T1E Cell Surface Hydrophobicity and Biofilm Formation. Applied and Environmental Microbiology. 2012;78(17):6217.

135. Yonezawa H, Osaki T, Woo T, Kurata S, Zaman C, Hojo F, et al. Analysis of outer membrane vesicle protein involved in biofilm formation of Helicobacter pylori. Anaerobe. 2011;17(6):388-90.

136. Schooling SR, Beveridge TJ. Membrane Vesicles: an Overlooked Component of the Matrices of Biofilms. Journal of Bacteriology. 2006;188(16):5945-57.

137. Wang W, Chanda W, Zhong M. The relationship between biofilm and outer membrane vesicles: a novel therapy overview. FEMS Microbiology Letters. 2015;362(15).

138. Kadurugamuwa JL, Beveridge TJ. Bacteriolytic effect of membrane vesicles from Pseudomonas aeruginosa on other bacteria including pathogens: conceptually new antibiotics. Journal of Bacteriology. 1996;178(10):2767-74.

139. Li Z, Clarke AJ, Beveridge TJ. Gram-Negative Bacteria Produce Membrane Vesicles Which Are Capable of Killing Other Bacteria. Journal of Bacteriology. 1998;180(20):5478-83.

140. Qin Z, Yang L, Qu D, Molin S, Tolker-Nielsen T. Pseudomonas aeruginosa extracellular products inhibit staphylococcal growth, and disrupt established biofilms produced by Staphylococcus epidermidis. Microbiology. 2009;155(7):2148-56.

141. Whitworth DE. Chapter 1 - Myxobacterial Vesicles: Death at a Distance? In: Laskin AI, Sariaslani S, Gadd GM, editors. Advances in Applied Microbiology. 75: Academic Press; 2011. p. 1-31.

142. Dawid W. Biology and global distribution of myxobacteria in soils. FEMS Microbiology Reviews. 2000;24(4):403-27.

143. Zhang L, Wang H, Fang X, Stackebrandt E, Ding Y. Improved methods of isolation and purification of myxobacteria and development of fruiting body formation of two strains. Journal of Microbiological Methods. 2003;54(1):21-7.

144. Berleman JE, Kirby JR. Deciphering the hunting strategy of a bacterial wolfpack. FEMS microbiology reviews. 2009;33(5):942-57.

145. Weissman KJ, Müller R. A brief tour of myxobacterial secondary metabolism. Bioorganic & Medicinal Chemistry. 2009;17(6):2121-36.

146. Herrmann J, Fayad AA, Müller R. Natural products from myxobacteria: novel metabolites and bioactivities. Natural Product Reports. 2017;34(2):135-60.

147. Baumann S, Herrmann J, Raju R, Steinmetz H, Mohr KI, Hüttel S, et al. Cystobactamids: Myxobacterial Topoisomerase Inhibitors Exhibiting Potent Antibacterial Activity. Angewandte Chemie International Edition. 2014;53(52):14605-9.

148. Evans AGL, Davey HM, Cookson A, Currinn H, Cooke-Fox G, Stanczyk PJ, et al. Predatory activity of Myxococcus xanthus outer-membrane vesicles and properties of their hydrolase cargo. Microbiology. 2012;158(11):2742-52.

149. Klimentová J, Stulík J. Methods of isolation and purification of outer membrane vesicles from gram-negative bacteria. Microbiological Research. 2015;170(Supplement C):1-9.

150. Gardiner C, Vizio DD, Sahoo S, Théry C, Witwer KW, Wauben M, et al. Techniques used for the isolation and characterization of extracellular vesicles: results of a worldwide survey. Journal of Extracellular Vesicles. 2016;5(1):32945.

151. Lobb RJ, Becker M, Wen SW, Wong CSF, Wiegmans AP, Leimgruber A, et al. Optimized exosome isolation protocol for cell culture supernatant and human plasma. Journal of extracellular vesicles. 2015;4:27031-.

152. Lee E-Y, Bang JY, Park GW, Choi D-S, Kang JS, Kim H-J, et al. Global proteomic profiling of native outer membrane vesicles derived from Escherichia coli. PROTEOMICS. 2007;7(17):3143-53.

153. Peterson BW, Sharma PK, van der Mei HC, Busscher HJ. Bacterial cell surface damage due to centrifugal compaction. Applied and environmental microbiology. 2012;78(1):120-5.

154. Théry C, Amigorena S, Raposo G, Clayton A. Isolation and Characterization of Exosomes from Cell Culture Supernatants and Biological Fluids. Current Protocols in Cell Biology: John Wiley & Sons, Inc.; 2001.

155. Auber M, Fröhlich D, Drechsel O, Karaulanov E, Krämer-Albers E-M. Serum-free media supplements carry miRNAs that co-purify with extracellular vesicles. Journal of extracellular vesicles. 2019;8(1):1656042-.

156. Linares R, Tan S, Gounou C, Arraud N, Brisson AR. High-speed centrifugation induces aggregation of extracellular vesicles. Journal of Extracellular Vesicles. 2015;4(1):29509.

157. Gupta S, Rawat S, Arora V, Kottarath SK, Dinda AK, Vaishnav PK, et al. An improvised one-step sucrose cushion ultracentrifugation method for exosome isolation from culture supernatants of mesenchymal stem cells. Stem Cell Res Ther. 2018;9(1):180-.

158. Heinemann ML, Ilmer M, Silva LP, Hawke DH, Recio A, Vorontsova MA, et al. Benchtop isolation and characterization of functional exosomes by sequential filtration. Journal of Chromatography A. 2014;1371:125-35.

159. Busatto S, Vilanilam G, Ticer T, Lin W-L, Dickson DW, Shapiro S, et al. Tangential Flow Filtration for Highly Efficient Concentration of Extracellular Vesicles from Large Volumes of Fluid. Cells. 2018;7(12):273.

160. Reiner AT, Witwer KW, van Balkom BWM, de Beer J, Brodie C, Corteling RL, et al. Concise Review: Developing Best-Practice Models for the Therapeutic Use of Extracellular Vesicles. STEM CELLS Translational Medicine. 2017;6(8):1730-9.

161. Ng KS, Smith JA, McAteer MP, Mead BE, Ware J, Jackson FO, et al. Bioprocess Decision Support Tool For Scalable Manufacture of Extracellular Vesicles. Biotechnology and Bioengineering. 2018;0(ja).

162. Gimona M, Pachler K, Laner-Plamberger S, Schallmoser K, Rohde E. Manufacturing of Human Extracellular Vesicle-Based Therapeutics for Clinical Use. International Journal of Molecular Sciences. 2017;18(6):1190.

163. Lobb RJ, Becker M, Wen Wen S, Wong CSF, Wiegmans AP, Leimgruber A, et al. Optimized exosome isolation protocol for cell culture supernatant and human plasma. Journal of Extracellular Vesicles. 2015;4:10.3402/jev.v4.27031.

164. Rider MA, Hurwitz SN, Meckes Jr DG. ExtraPEG: A Polyethylene Glycol-Based Method for Enrichment of Extracellular Vesicles. Scientific Reports. 2016;6:23978.

165. Van Deun J, Mestdagh P, Sormunen R, Cocquyt V, Vermaelen K, Vandesompele J, et al. The impact of disparate isolation methods for extracellular vesicles on downstream RNA profiling. Journal of Extracellular Vesicles. 2014;3:10.3402/jev.v3.24858.

166. Ludwig A-K, De Miroschedji K, Doeppner TR, Börger V, Ruesing J, Rebmann V, et al. Precipitation with polyethylene glycol followed by washing and pelleting by ultracentrifugation enriches extracellular vesicles from tissue culture supernatants in small and large scales. Journal of extracellular vesicles. 2018;7(1):1528109-.

167. Böing AN, van der Pol E, Grootemaat AE, Coumans FAW, Sturk A, Nieuwland R. Single-step isolation of extracellular vesicles by size-exclusion chromatography. Journal of Extracellular Vesicles. 2014;3:10.3402/jev.v3.23430.

168. Welton JL, Webber JP, Botos L-A, Jones M, Clayton A. Ready-made chromatography columns for extracellular vesicle isolation from plasma. Journal of Extracellular Vesicles. 2015;4:10.3402/jev.v4.27269.

169. Onódi Z, Pelyhe C, Terézia Nagy C, Brenner GB, Almási L, Kittel Á, et al. Isolation of High-Purity Extracellular Vesicles by the Combination of Iodixanol Density Gradient Ultracentrifugation and Bind-Elute Chromatography From Blood Plasma. Frontiers in physiology. 2018;9:1479-.

170. Karimi N, Cvjetkovic A, Jang SC, Crescitelli R, Hosseinpour Feizi MA, Nieuwland R, et al. Detailed analysis of the plasma extracellular vesicle proteome after separation from lipoproteins. Cell Mol Life Sci. 2018;75(15):2873-86.

171. Nakai W, Yoshida T, Diez D, Miyatake Y, Nishibu T, Imawaka N, et al. A novel affinity-based method for the isolation of highly purified extracellular vesicles. Scientific Reports. 2016;6:33935.

172. Ashcroft BA, de Sonneville J, Yuana Y, Osanto S, Bertina R, Kuil ME, et al. Determination of the size distribution of blood microparticles directly in plasma using atomic force microscopy and microfluidics. Biomedical Microdevices. 2012;14(4):641-9.

173. Wu M, Ouyang Y, Wang Z, Zhang R, Huang P-H, Chen C, et al. Isolation of exosomes from whole blood by integrating acoustics and microfluidics. Proceedings of the National Academy of Sciences. 2017;114(40):10584.

174. Liu C, Guo J, Tian F, Yang N, Yan F, Ding Y, et al. Field-Free Isolation of Exosomes from Extracellular Vesicles by Microfluidic Viscoelastic Flows. ACS Nano. 2017;11(7):6968-76.

175. He M, Zeng Y. Microfluidic Exosome Analysis toward Liquid Biopsy for Cancer. Journal of Laboratory Automation. 2016;21(4):599-608.

176. Kang D, Oh S, Ahn S-M, Lee B-H, Moon MH. Proteomic Analysis of Exosomes from Human Neural Stem Cells by Flow Field-Flow Fractionation and Nanoflow Liquid Chromatography−Tandem Mass Spectrometry. Journal of Proteome Research. 2008;7(8):3475-80.

177. Mourdikoudis S, Pallares RM, Thanh NTK. Characterization techniques for nanoparticles: comparison and complementarity upon studying nanoparticle properties. Nanoscale. 2018;10(27):12871-934.

178. Szatanek R, Baj-Krzyworzeka M, Zimoch J, Lekka M, Siedlar M, Baran J. The Methods of Choice for Extracellular Vesicles (EVs) Characterization. International journal of molecular sciences. 2017;18(6):1153.

179.   Gardiner C, Ferreira YJ, Dragovic RA, Redman CWG, Sargent IL. Extracellular vesicle sizing and enumeration by nanoparticle tracking analysis. Journal of Extracellular Vesicles. 2013;2(1):19671.

180.   Desgeorges A, Hollerweger J, Lassacher T, Rohde E, Helmbrecht C, Gimona M. Differential fluorescence nanoparticle tracking analysis for enumeration of the extracellular vesicle content in mixed particulate solutions. Methods. 2020;177:67-73.

181.   Hartjes TA, Mytnyk S, Jenster GW, van Steijn V, van Royen ME. Extracellular Vesicle Quantification and Characterization: Common Methods and Emerging Approaches. Bioengineering (Basel). 2019;6(1):7.

182.   Cizmar P, Yuana Y. Detection and Characterization of Extracellular Vesicles by Transmission and Cryo-Transmission Electron Microscopy. In: Kuo WP, Jia S, editors. Extracellular Vesicles: Methods and Protocols. New York, NY: Springer New York; 2017. p. 221-32.

183.   Sokolova V, Ludwig A-K, Hornung S, Rotan O, Horn PA, Epple M, et al. Characterisation of exosomes derived from human cells by nanoparticle tracking analysis and scanning electron microscopy. Colloids and Surfaces B: Biointerfaces. 2011;87(1):146-50.

184.   Vorselen D, van Dommelen SM, Sorkin R, Piontek MC, Schiller J, Döpp ST, et al. The fluid membrane determines mechanics of erythrocyte extracellular vesicles and is softened in hereditary spherocytosis. Nature communications. 2018;9(1):4960-.

185.   Maas SLN, Broekman MLD, de Vrij J. Tunable Resistive Pulse Sensing for the Characterization of Extracellular Vesicles. In: Hill AF, editor. Exosomes and Microvesicles: Methods and Protocols. New York, NY: Springer New York; 2017. p. 21-33.

186.   Vogel R, Pal AK, Jambhrunkar S, Patel P, Thakur SS, Reátegui E, et al. High-Resolution Single Particle Zeta Potential Characterisation of Biological Nanoparticles using Tunable Resistive Pulse Sensing. Scientific reports. 2017;7(1):17479-.

187.   Soares Martins T, Catita J, Martins Rosa I, A B da Cruz E Silva O, Henriques AG. Exosome isolation from distinct biofluids using precipitation and column-based approaches. PloS one. 2018;13(6):e0198820-e.

188.   Shu SL, Yang Y, Allen CL, Hurley E, Tung KH, Minderman H, et al. Purity and yield of melanoma exosomes are dependent on isolation method. Journal of Extracellular Vesicles. 2020;9(1):1692401.

189.   Görgens A, Bremer M, Ferrer-Tur R, Murke F, Tertel T, Horn PA, et al. Optimisation of imaging flow cytometry for the analysis of single extracellular vesicles by using fluorescence-tagged vesicles as biological reference material. Journal of Extracellular Vesicles. 2019;8(1):1587567.

190.   Larson MC, Luthi MR, Hogg N, Hillery CA. Calcium-phosphate microprecipitates mimic microparticles when examined with flow cytometry. Cytometry Part A. 2013;83A(2):242-50.

191.   Pospichalova V, Svoboda J, Dave Z, Kotrbova A, Kaiser K, Klemova D, et al. Simplified protocol for flow cytometry analysis of fluorescently labeled exosomes and microvesicles using dedicated flow cytometer. Journal of Extracellular Vesicles. 2015;4(1):25530.

192.   Hoppstädter J, Dembek A, Linnenberger R, Dahlem C, Barghash A, Fecher-Trost C, et al. Toll-Like Receptor 2 Release by Macrophages: An Anti-inflammatory Program Induced by Glucocorticoids and Lipopolysaccharide. Front Immunol. 2019;10:1634-.

193.   Sandfeld-Paulsen B, Jakobsen KR, Bæk R, Folkersen BH, Rasmussen TR, Meldgaard P, et al. Exosomal Proteins as Diagnostic Biomarkers in Lung Cancer. Journal of Thoracic Oncology. 2016;11(10):1701-10.

194.   Øverbye A, Skotland T, Koehler CJ, Thiede B, Seierstad T, Berge V, et al. Identification of prostate cancer biomarkers in urinary exosomes. Oncotarget. 2015;6(30):30357-76.

195.   Jia Y, Chen Y, Wang Q, Jayasinghe U, Luo X, Wei Q, et al. Exosome: emerging biomarker in breast cancer. Oncotarget. 2017;8(25):41717-33.

196.   Niu M, Li Y, Li G, Zhou L, Luo N, Yao M, et al. A longitudinal study on α-synuclein in plasma neuronal exosomes as a biomarker for Parkinson's disease development and progression. European Journal of Neurology. 2020;27(6):967-74.

197.   Cho Y-E, Im E-J, Moon P-G, Mezey E, Song B-J, Baek M-C. Increased liver-specific proteins in circulating extracellular vesicles as potential biomarkers for drug- and alcohol-induced liver injury. PLOS ONE. 2017;12(2):e0172463.

198.   Kolhe R, Hunter M, Liu S, Jadeja RN, Pundkar C, Mondal AK, et al. Gender-specific differential expression of exosomal miRNA in synovial fluid of patients with osteoarthritis. Scientific Reports. 2017;7(1):2029.
199.   Nilsson J, Skog J, Nordstrand A, Baranov V, Mincheva-Nilsson L, Breakefield XO, et al. Prostate cancer-derived urine exosomes: a novel approach to biomarkers for prostate cancer. Br J Cancer. 2009;100(10):1603-7.
200.   Sharma S, Gillespie BM, Palanisamy V, Gimzewski JK. Quantitative nanostructural and single-molecule force spectroscopy biomolecular analysis of human-saliva-derived exosomes. Langmuir : the ACS journal of surfaces and colloids. 2011;27(23):14394-400.
201.   Takeuchi T, Mori K, Sunayama H, Takano E, Kitayama Y, Shimizu T, et al. Antibody-Conjugated Signaling Nanocavities Fabricated by Dynamic Molding for Detecting Cancers Using Small Extracellular Vesicle Markers from Tears. Journal of the American Chemical Society. 2020;142(14):6617-24.
202.   Zhu X, Badawi M, Pomeroy S, Sutaria DS, Xie Z, Baek A, et al. Comprehensive toxicity and immunogenicity studies reveal minimal effects in mice following sustained dosing of extracellular vesicles derived from HEK293T cells. Journal of extracellular vesicles. 2017;6(1):1324730-.
203.   Saleh AF, Lázaro-Ibáñez E, Forsgard MAM, Shatnyeva O, Osteikoetxea X, Karlsson F, et al. Extracellular vesicles induce minimal hepatotoxicity and immunogenicity. Nanoscale. 2019;11(14):6990-7001.
204.   Bjørge IM, Kim SY, Mano JF, Kalionis B, Chrzanowski W. Extracellular vesicles, exosomes and shedding vesicles in regenerative medicine – a new paradigm for tissue repair. Biomaterials Science. 2018;6(1):60-78.
205.   Wiklander OPB, Brennan MÁ, Lötvall J, Breakefield XO, EL Andaloussi S. Advances in therapeutic applications of extracellular vesicles. Science Translational Medicine. 2019;11(492):eaav8521.
206.   Börger V, Bremer M, Ferrer-Tur R, Gockeln L, Stambouli O, Becic A, et al. Mesenchymal Stem/Stromal Cell-Derived Extracellular Vesicles and Their Potential as Novel Immunomodulatory Therapeutic Agents. International Journal of Molecular Sciences. 2017;18(7):1450.
207.   Romanelli P, Bieler L, Scharler C, Pachler K, Kreutzer C, Zaunmair P, et al. Extracellular Vesicles Can Deliver Anti-inflammatory and Anti-scarring Activities of Mesenchymal Stromal Cells After Spinal Cord Injury. Frontiers in Neurology. 2019;10(1225).
208.   Whittaker TE, Nagelkerke A, Nele V, Kauscher U, Stevens MM. Experimental artefacts can lead to misattribution of bioactivity from soluble mesenchymal stem cell paracrine factors to extracellular vesicles. Journal of Extracellular Vesicles. 2020;9(1):1807674.
209.   Gallet R, Dawkins J, Valle J, Simsolo E, de Couto G, Middleton R, et al. Exosomes secreted by cardiosphere-derived cells reduce scarring, attenuate adverse remodelling, and improve function in acute and chronic porcine myocardial infarction. Eur Heart J. 2017;38(3):201-11.
210.   Jiang L, Schinkel M, van Essen M, Schiffelers RM. Bacterial membrane vesicles as promising vaccine candidates. European Journal of Pharmaceutics and Biopharmaceutics. 2019;145:1-6.
211.   van der Pol L, Stork M, van der Ley P. Outer membrane vesicles as platform vaccine technology. Biotechnology journal. 2015;10(11):1689-706.
212.   Shim S-M, Song E-J, Song D, Lee T-Y, Kim D-J, Nam J-H, et al. Nontoxic outer membrane vesicles efficiently increase the efficacy of an influenza vaccine in mice and ferrets. Vaccine. 2017;35(30):3741-8.
213.   Chen DJ, Osterrieder N, Metzger SM, Buckles E, Doody AM, DeLisa MP, et al. Delivery of foreign antigens by engineered outer membrane vesicle vaccines. Proceedings of the National Academy of Sciences. 2010;107(7):3099.
214.   Rappuoli R, Pizza M, Masignani V, Vadivelu K. Meningococcal B vaccine (4CMenB): the journey from research to real world experience. Expert Review of Vaccines. 2018;17(12):1111-21.
215.   Launay O, Ndiaye AGW, Conti V, Loulergue P, Sciré AS, Landre AM, et al. Booster Vaccination With GVGH Shigella sonnei 1790GAHB GMMA Vaccine Compared to Single

Vaccination in Unvaccinated Healthy European Adults: Results From a Phase 1 Clinical Trial. Front Immunol. 2019;10(335).

216.   Mizrak A, Bolukbasi MF, Ozdener GB, Brenner GJ, Madlener S, Erkan EP, et al. Genetically engineered microvesicles carrying suicide mRNA/protein inhibit schwannoma tumor growth. Mol Ther. 2013;21(1):101-8.

217.   Sutaria DS, Badawi M, Phelps MA, Schmittgen TD. Achieving the Promise of Therapeutic Extracellular Vesicles: The Devil is in Details of Therapeutic Loading. Pharmaceutical research. 2017;34(5):1053-66.

218.   Sutaria DS, Jiang J, Elgamal OA, Pomeroy SM, Badawi M, Zhu X, et al. Low active loading of cargo into engineered extracellular vesicles results in inefficient miRNA mimic delivery. Journal of Extracellular Vesicles. 2017;6(1):1333882.

219.   Hung ME, Leonard JN. A platform for actively loading cargo RNA to elucidate limiting steps in EV-mediated delivery. Journal of extracellular vesicles. 2016;5:31027-.

220.   Kadurugamuwa JL, Beveridge TJ. Delivery of the Non-Membrane-Permeative Antibiotic Gentamicin into Mammalian Cells by Using Shigella flexneriMembrane Vesicles. Antimicrobial Agents and Chemotherapy. 1998;42(6):1476.

221.   Pascucci L, Coccè V, Bonomi A, Ami D, Ceccarelli P, Ciusani E, et al. Paclitaxel is incorporated by mesenchymal stromal cells and released in exosomes that inhibit in vitro tumor growth: A new approach for drug delivery. Journal of Controlled Release. 2014;192:262-70.

222.   Sun D, Zhuang X, Xiang X, Liu Y, Zhang S, Liu C, et al. A Novel Nanoparticle Drug Delivery System: The Anti-inflammatory Activity of Curcumin Is Enhanced When Encapsulated in Exosomes. Molecular Therapy. 2010;18(9):1606-14.

223.   Fuhrmann G, Serio A, Mazo M, Nair R, Stevens MM. Active loading into extracellular vesicles significantly improves the cellular uptake and photodynamic effect of porphyrins. Journal of Controlled Release. 2015;205:35-44.

224.   Haney MJ, Klyachko NL, Zhao Y, Gupta R, Plotnikova EG, He Z, et al. Exosomes as drug delivery vehicles for Parkinson's disease therapy. Journal of Controlled Release. 2015;207:18-30.

225.   Tian T, Zhang H-X, He C-P, Fan S, Zhu Y-L, Qi C, et al. Surface functionalized exosomes as targeted drug delivery vehicles for cerebral ischemia therapy. Biomaterials. 2018;150:137-49.

226.   Johnsen KB, Gudbergsson JM, Skov MN, Christiansen G, Gurevich L, Moos T, et al. Evaluation of electroporation-induced adverse effects on adipose-derived stem cell exosomes. Cytotechnology. 2016;68(5):2125-38.

227.   Kooijmans SAA, Stremersch S, Braeckmans K, de Smedt SC, Hendrix A, Wood MJA, et al. Electroporation-induced siRNA precipitation obscures the efficiency of siRNA loading into extracellular vesicles. Journal of Controlled Release. 2013;172(1):229-38.

228.   O'Loughlin AJ, Mäger I, de Jong OG, Varela MA, Schiffelers RM, El Andaloussi S, et al. Functional Delivery of Lipid-Conjugated siRNA by Extracellular Vesicles. Molecular Therapy. 2017.

229.   Didiot M-C, Hall LM, Coles AH, Haraszti RA, Godinho BMDC, Chase K, et al. Exosome-mediated Delivery of Hydrophobically Modified siRNA for Huntingtin mRNA Silencing. Molecular Therapy. 2016;24(10):1836-47.

230.   Stremersch S, Vandenbroucke RE, Van Wonterghem E, Hendrix A, De Smedt SC, Raemdonck K. Comparing exosome-like vesicles with liposomes for the functional cellular delivery of small RNAs. Journal of Controlled Release. 2016;232:51-61.

231.   Millard M, Yakavets I, Piffoux M, Brun A, Gazeau F, Guigner J-M, et al. mTHPC-loaded extracellular vesicles outperform liposomal and free mTHPC formulations by an increased stability, drug delivery efficiency and cytotoxic effect in tridimensional model of tumors. Drug Deliv. 2018;25(1):1790-801.

232.   Alvarez-Erviti L, Seow Y, Yin H, Betts C, Lakhal S, Wood MJA. Delivery of siRNA to the mouse brain by systemic injection of targeted exosomes. Nat Biotech. 2011;29(4):341-5.

233.   Lener T, Gimona M, Aigner L, Börger V, Buzas E, Camussi G, et al. Applying extracellular vesicles based therapeutics in clinical trials - an ISEV position paper. Journal of extracellular vesicles. 2015;4:30087-.

234.   Batrakova EV, Kim MS. Development and regulation of exosome-based therapy products. WIREs Nanomedicine and Nanobiotechnology. 2016;8(5):744-57.

235.   Willms E, Johansson HJ, Mäger I, Lee Y, Blomberg KEM, Sadik M, et al. Cells release subpopulations of exosomes with distinct molecular and biological properties. Scientific Reports. 2016;6(1):22519.

236.   Willis GR, Kourembanas S, Mitsialis SA. Toward Exosome-Based Therapeutics: Isolation, Heterogeneity, and Fit-for-Purpose Potency. Frontiers in Cardiovascular Medicine. 2017;4:63.

237.   EMA EMA. EMA/CHMP/BWP/534898/2008: Guideline on the requirements for quality documentation concerning biological investigational medicinal products in clinical trials. October 2020. 2018.

238.   Rohde E, Pachler K, Gimona M. Manufacturing and characterization of extracellular vesicles from umbilical cord–derived mesenchymal stromal cells for clinical testing. Cytotherapy. 2019;21(6):581-92.

239.   ICH ICfHoTRfPfHU. ICH Topic Q 6 B Specifications: Test Procedures and Acceptance Criteria for Biotechnological/Biological Products October 2020. 1999.

240.   Patel DB, Gray KM, Santharam Y, Lamichhane TN, Stroka KM, Jay SM. Impact of cell culture parameters on production and vascularization bioactivity of mesenchymal stem cell-derived extracellular vesicles. Bioengineering & Translational Medicine. 2017;2(2):170-9.

241.   Mol EA, Goumans M-J, Doevendans PA, Sluijter JPG, Vader P. Higher functionality of extracellular vesicles isolated using size-exclusion chromatography compared to ultracentrifugation. Nanomedicine: Nanotechnology, Biology and Medicine. 2017;13(6):2061-5.

242.   Huang R, Qin C, Wang J, Hu Y, Zheng G, Qiu G, et al. Differential effects of extracellular vesicles from aging and young mesenchymal stem cells in acute lung injury. Aging (Albany NY). 2019;11(18):7996-8014.

243.   Hoang DH, Nguyen TD, Nguyen H-P, Nguyen X-H, Do PTX, Dang VD, et al. Differential Wound Healing Capacity of Mesenchymal Stem Cell-Derived Exosomes Originated From Bone Marrow, Adipose Tissue and Umbilical Cord Under Serum- and Xeno-Free Condition. Frontiers in Molecular Biosciences. 2020;7(119).

244.   Baglio SR, Rooijers K, Koppers-Lalic D, Verweij FJ, Pérez Lanzón M, Zini N, et al. Human bone marrow- and adipose-mesenchymal stem cells secrete exosomes enriched in distinctive miRNA and tRNA species. Stem Cell Res Ther. 2015;6(1):127-.

245.   Welsh JA, Van Der Pol E, Arkesteijn GJA, Bremer M, Brisson A, Coumans F, et al. MIFlowCyt-EV: a framework for standardized reporting of extracellular vesicle flow cytometry experiments. Journal of Extracellular Vesicles. 2020;9(1):1713526.

246.   Welsh JA, van der Pol E, Bettin BA, Carter DRF, Hendrix A, Lenassi M, et al. Towards defining reference materials for measuring extracellular vesicle refractive index, epitope abundance, size and concentration. Journal of Extracellular Vesicles. 2020;9(1):1816641.

247.   Vulto AG, Jaquez OA. The process defines the product: what really matters in biosimilar design and production? Rheumatology (Oxford). 2017;56(suppl_4):iv14-iv29.

248.   van de Waterbeemd B, Zomer G, Kaaijk P, Ruiterkamp N, Wijffels RH, van den Dobbelsteen GPJM, et al. Improved Production Process for Native Outer Membrane Vesicle Vaccine against Neisseria meningitidis. PLOS ONE. 2013;8(5):e65157.

249.   Bari E, Perteghella S, Di Silvestre D, Sorlini M, Catenacci L, Sorrenti M, et al. Pilot Production of Mesenchymal Stem/Stromal Freeze-Dried Secretome for Cell-Free Regenerative Nanomedicine: A Validated GMP-Compliant Process. Cells. 2018;7(11):190.

250.   Pachler K, Ketterl N, Desgeorges A, Dunai ZA, Laner-Plamberger S, Streif D, et al. An In Vitro Potency Assay for Monitoring the Immunomodulatory Potential of Stromal Cell-Derived Extracellular Vesicles. International journal of molecular sciences. 2017;18(7):1413.

251.   Jeyaram A, Jay SM. Preservation and Storage Stability of Extracellular Vesicles for Therapeutic Applications. AAPS J. 2017;20(1):1.

252.   Lőrincz ÁM, Timár CI, Marosvári KA, Veres DS, Otrokocsi L, Kittel Á, et al. Effect of storage on physical and functional properties of extracellular vesicles derived from neutrophilic granulocytes. Journal of extracellular vesicles. 2014;3:25465-.

253.   Witwer KW, Buzás EI, Bemis LT, Bora A, Lässer C, Lötvall J, et al. Standardization of sample collection, isolation and analysis methods in extracellular vesicle research. Journal of Extracellular Vesicles. 2013;2(1):20360.

254.   Welch JL, Madison MN, Margolick JB, Galvin S, Gupta P, Martínez-Maza O, et al. Effect of prolonged freezing of semen on exosome recovery and biologic activity. Scientific reports. 2017;7:45034-.

255.   Bosch S, de Beaurepaire L, Allard M, Mosser M, Heichette C, Chrétien D, et al. Trehalose prevents aggregation of exosomes and cryodamage. Scientific Reports. 2016;6:36162.

256.   Kusuma GD, Barabadi M, Tan JL, Morton DAV, Frith JE, Lim R. To Protect and to Preserve: Novel Preservation Strategies for Extracellular Vesicles. Frontiers in Pharmacology. 2018;9(1199).

257.   Bauer K-H, Frömming K-H, Führer C, Lippold BC, Müller-Goymann C, Schubert R, et al. Bauer/Frömming/Führer Pharmazeutische Technologie : Mit Einführungen in Biopharmazie und Biotechnologie: Hirzel Verlag; 2016. Available from: https://elibrary.hirzel.de/book/99.105015/9783804734821.

258.   Kanojia G, Raeven RHM, van der Maas L, Bindels THE, van Riet E, Metz B, et al. Development of a thermostable spray dried outer membrane vesicle pertussis vaccine for pulmonary immunization. Journal of Controlled Release. 2018;286:167-78.

259.   Kawasaki H, Shimanouchi T, Kimura Y. Recent Development of Optimization of Lyophilization Process. Journal of Chemistry. 2019;2019:9502856.

260.   Carpenter JF, Pikal MJ, Chang BS, Randolph TW. Rational design of stable lyophilized protein formulations: some practical advice. Pharm Res. 1997;14(8):969-75.

261.   Chang L, Pikal MJ. Mechanisms of protein stabilization in the solid state. Journal of Pharmaceutical Sciences. 2009;98(9):2886-908.

262.   Cicerone MT, Pikal MJ, Qian KK. Stabilization of proteins in solid form. Advanced Drug Delivery Reviews. 2015;93:14-24.

263.   Charoenviriyakul C, Takahashi Y, Nishikawa M, Takakura Y. Preservation of exosomes at room temperature using lyophilization. International Journal of Pharmaceutics. 2018;553(1):1-7.

264.   El Baradie KBY, Nouh M, O'Brien III F, Liu Y, Fulzele S, Eroglu A, et al. Freeze-Dried Extracellular Vesicles From Adipose-Derived Stem Cells Prevent Hypoxia-Induced Muscle Cell Injury. 2020;8(181).

265.   Katsuda T, Tsuchiya R, Kosaka N, Yoshioka Y, Takagaki K, Oki K, et al. Human adipose tissue-derived mesenchymal stem cells secrete functional neprilysin-bound exosomes. Scientific reports. 2013;3:1197-.

266.   Wiklander OPB, Nordin JZ, O'Loughlin A, Gustafsson Y, Corso G, Mäger I, et al. Extracellular vesicle in vivo biodistribution is determined by cell source, route of administration and targeting. Journal of extracellular vesicles. 2015;4:26316-.

267.   Pužar Dominkuš P, Stenovec M, Sitar S, Lasič E, Zorec R, Plemenitaš A, et al. PKH26 labeling of extracellular vesicles: Characterization and cellular internalization of contaminating PKH26 nanoparticles. Biochimica et Biophysica Acta (BBA) - Biomembranes. 2018;1860(6):1350-61.

268.   Simonsen JB. Pitfalls associated with lipophilic fluorophore staining of extracellular vesicles for uptake studies. Journal of Extracellular Vesicles. 2019;8(1):1582237.

269.   Takov K, Yellon DM, Davidson SM. Confounding factors in vesicle uptake studies using fluorescent lipophilic membrane dyes. Journal of extracellular vesicles. 2017;6(1):1388731-.

270.   Suk JS, Xu Q, Kim N, Hanes J, Ensign LM. PEGylation as a strategy for improving nanoparticle-based drug and gene delivery. Advanced Drug Delivery Reviews. 2016;99, Part A:28-51.

271.   Verhoef JJF, Anchordoquy TJ. Questioning the Use of PEGylation for Drug Delivery. Drug Deliv Transl Res. 2013;3(6):499-503.

272.   Gudbergsson JM, Jønsson K, Simonsen JB, Johnsen KB. Systematic review of targeted extracellular vesicles for drug delivery - Considerations on methodological and biological heterogeneity. J Control Release. 2019;306:108-20.

273. Smyth T, Kullberg M, Malik N, Smith-Jones P, Graner MW, Anchordoquy TJ. Biodistribution and delivery efficiency of unmodified tumor-derived exosomes. Journal of controlled release : official journal of the Controlled Release Society. 2015;199:145-55.

274. Faruqu FN, Wang JT-W, Xu L, McNickle L, Chong EM-Y, Walters A, et al. Membrane Radiolabelling of Exosomes for Comparative Biodistribution Analysis in Immunocompetent and Immunodeficient Mice - A Novel and Universal Approach. Theranostics. 2019;9(6):1666-82.

275. Forge A, Schacht J. Aminoglycoside Antibiotics. Audiology and Neurotology. 2000;5(1):3-22.

276. Forouzesh A, Moise PA, Sakoulas G. Vancomycin Ototoxicity: a Reevaluation in an Era of Increasing Doses. Antimicrobial Agents and Chemotherapy. 2009;53(2):483.

277. Byrd AL, Belkaid Y, Segre JA. The human skin microbiome. Nature Reviews Microbiology. 2018;16(3):143-55.

278. Moffatt MF, Cookson WO. The lung microbiome in health and disease. Clin Med (Lond). 2017;17(6):525-9.

279. Huh AJ, Kwon YJ. "Nanoantibiotics": A new paradigm for treating infectious diseases using nanomaterials in the antibiotics resistant era. Journal of Controlled Release. 2011;156(2):128-45.

280. Raghunath A, Perumal E. Metal oxide nanoparticles as antimicrobial agents: a promise for the future. International Journal of Antimicrobial Agents. 2017;49(2):137-52.

281. Al-Sharqi A, Apun K, Vincent M, Kanakaraju D, Bilung LM, Sum MSH. Investigation of the antibacterial activity of Ag-NPs conjugated with a specific antibody against Staphylococcus aureus after photoactivation. Journal of Applied Microbiology. 2020;128(1):102-15.

282. Kang X-Q, Shu G-F, Jiang S-P, Xu X-L, Qi J, Jin F-Y, et al. Effective targeted therapy for drug-resistant infection by ICAM-1 antibody-conjugated TPGS modified β-Ga(2)O(3):Cr(3+) nanoparticles. Theranostics. 2019;9(10):2739-53.

283. Pootoolal J, Neu J, Wright GD. GLYCOPEPTIDE ANTIBIOTIC RESISTANCE. Annual Review of Pharmacology and Toxicology. 2002;42(1):381-408.

284. Gu H, Ho PL, Tong E, Wang L, Xu B. Presenting Vancomycin on Nanoparticles to Enhance Antimicrobial Activities. Nano Letters. 2003;3(9):1261-3.

285. Kell AJ, Stewart G, Ryan S, Peytavi R, Boissinot M, Huletsky A, et al. Vancomycin-Modified Nanoparticles for Efficient Targeting and Preconcentration of Gram-Positive and Gram-Negative Bacteria. ACS Nano. 2008;2(9):1777-88.

286. Kell AJ, Simard B. Vancomycin architecture dependence on the capture efficiency of antibody-modified microbeads by magnetic nanoparticles. Chemical Communications. 2007(12):1227-9.

287. Sundram UN, Griffin JH, Nicas TI. Novel Vancomycin Dimers with Activity against Vancomycin-Resistant Enterococci. Journal of the American Chemical Society. 1996;118(51):13107-8.

288. Peterson E, Joseph C, Peterson H, Bouwman R, Tang S, Cannon J, et al. Measuring the Adhesion Forces for the Multivalent Binding of Vancomycin-Conjugated Dendrimer to Bacterial Cell-Wall Peptide. Langmuir. 2018;34(24):7135-46.

289. Chen M, Xie S, Wei J, Song X, Ding Z, Li X. Antibacterial Micelles with Vancomycin-Mediated Targeting and pH/Lipase-Triggered Release of Antibiotics. ACS Applied Materials & Interfaces. 2018;10(43):36814-23.

290. Norouz Dizaji A, Ding D, Kutsal T, Turk M, Kong D, Piskin E. In vivo imaging/detection of MRSA bacterial infections in mice using fluorescence labelled polymeric nanoparticles carrying vancomycin as the targeting agent. Journal of Biomaterials Science, Polymer Edition. 2020;31(3):293-309.

291. Guo X, Cao B, Wang C, Lu S, Hu X. In vivo photothermal inhibition of methicillin-resistant Staphylococcus aureus infection by in situ templated formulation of pathogen-targeting phototheranostics. Nanoscale. 2020;12(14):7651-9.

292. Hussain S, Joo J, Kang J, Kim B, Braun GB, She Z-G, et al. Antibiotic-loaded nanoparticles targeted to the site of infection enhance antibacterial efficacy. Nature Biomedical Engineering. 2018;2(2):95-103.

293.   Azad AK, Rajaram MVS, Schlesinger LS. Exploitation of the Macrophage Mannose Receptor (CD206) in Infectious Disease Diagnostics and Therapeutics. Journal of cytology & molecular biology. 2014;1(1):1000003.

294.   Xiong M-H, Li Y-J, Bao Y, Yang X-Z, Hu B, Wang J. Bacteria-Responsive Multifunctional Nanogel for Targeted Antibiotic Delivery. Advanced Materials. 2012;24(46):6175-80.

295.   Choi ES, Song J, Kang YY, Mok H. Mannose-Modified Serum Exosomes for the Elevated Uptake to Murine Dendritic Cells and Lymphatic Accumulation. Macromolecular Bioscience. 2019;19(7):1900042.

296.   Kumar P, Wu H, McBride JL, Jung K-E, Hee Kim M, Davidson BL, et al. Transvascular delivery of small interfering RNA to the central nervous system. Nature. 2007;448(7149):39-43.

297.   Yang J, Zhang X, Chen X, Wang L, Yang G. Exosome Mediated Delivery of miR-124 Promotes Neurogenesis after Ischemia. Molecular Therapy - Nucleic Acids. 2017;7:278-87.

298.   Liu Y, Li D, Liu Z, Zhou Y, Chu D, Li X, et al. Targeted exosome-mediated delivery of opioid receptor Mu siRNA for the treatment of morphine relapse. Scientific Reports. 2015;5:17543.

299.   Stickney Z, Losacco J, McDevitt S, Zhang Z, Lu B. Development of exosome surface display technology in living human cells. Biochem Biophys Res Commun. 2016;472(1):53-9.

300.   Gujrati V, Kim S, Kim S-H, Min JJ, Choy HE, Kim SC, et al. Bioengineered Bacterial Outer Membrane Vesicles as Cell-Specific Drug-Delivery Vehicles for Cancer Therapy. ACS Nano. 2014;8(2):1525-37.

301.   Zeelenberg IS, Ostrowski M, Krumeich S, Bobrie A, Jancic C, Boissonnas A, et al. Targeting tumor antigens to secreted membrane vesicles in vivo induces efficient antitumor immune responses. Cancer Res. 2008;68(4):1228-35.

302.   Hartman ZC, Wei J, Glass OK, Guo H, Lei G, Yang X-Y, et al. Increasing vaccine potency through exosome antigen targeting. Vaccine. 2011;29(50):9361-7.

303.   Huang W, Wang S, Yao Y, Xia Y, Yang X, Li K, et al. Employing Escherichia coli-derived outer membrane vesicles as an antigen delivery platform elicits protective immunity against Acinetobacter baumannii infection. Scientific Reports. 2016;6(1):37242.

304.   Rappazzo CG, Watkins HC, Guarino CM, Chau A, Lopez JL, DeLisa MP, et al. Recombinant M2e outer membrane vesicle vaccines protect against lethal influenza A challenge in BALB/c mice. Vaccine. 2016;34(10):1252-8.

305.   Kim J-Y, Doody AM, Chen DJ, Cremona GH, Shuler ML, Putnam D, et al. Engineered Bacterial Outer Membrane Vesicles with Enhanced Functionality. Journal of Molecular Biology. 2008;380(1):51-66.

306.   Daleke-Schermerhorn MH, Felix T, Soprova Z, Ten Hagen-Jongman CM, Vikström D, Majlessi L, et al. Decoration of outer membrane vesicles with multiple antigens by using an autotransporter approach. Applied and environmental microbiology. 2014;80(18):5854-65.

307.   Gnopo YMD, Watkins HC, Stevenson TC, DeLisa MP, Putnam D. Designer outer membrane vesicles as immunomodulatory systems – Reprogramming bacteria for vaccine delivery. Advanced Drug Delivery Reviews.

308.   Gerritzen MJH, Martens DE, Wijffels RH, van der Pol L, Stork M. Bioengineering bacterial outer membrane vesicles as vaccine platform. Biotechnology Advances. 2017;35(5):565-74.

309.   Daleke-Schermerhorn MH, Felix T, Soprova Z, ten Hagen-Jongman CM, Vikström D, Majlessi L, et al. Decoration of Outer Membrane Vesicles with Multiple Antigens by Using an Autotransporter Approach. Applied and Environmental Microbiology. 2014;80(18):5854.

310.   Kuipers K, Daleke-Schermerhorn MH, Jong WSP, ten Hagen-Jongman CM, van Opzeeland F, Simonetti E, et al. Salmonella outer membrane vesicles displaying high densities of pneumococcal antigen at the surface offer protection against colonization. Vaccine. 2015;33(17):2022-9.

311.   Chen Q, Rozovsky S, Chen W. Engineering multi-functional bacterial outer membrane vesicles as modular nanodevices for biosensing and bioimaging. Chemical Communications. 2017;53(54):7569-72.

312. Lee TS, Kim Y, Zhang W, Song IH, Tung C-H. Facile metabolic glycan labeling strategy for exosome tracking. Biochim Biophys Acta Gen Subj. 2018;1862(5):1091-100.

313. Wang M, Altinoglu S, Takeda YS, Xu Q. Integrating Protein Engineering and Bioorthogonal Click Conjugation for Extracellular Vesicle Modulation and Intracellular Delivery. PLOS ONE. 2015;10(11):e0141860.

314. Lee J, Lee H, Goh U, Kim J, Jeong M, Lee J, et al. Cellular Engineering with Membrane Fusogenic Liposomes to Produce Functionalized Extracellular Vesicles. ACS Applied Materials & Interfaces. 2016;8(11):6790-5.

315. Zou J, Shi M, Liu X, Jin C, Xing X, Qiu L, et al. Aptamer-Functionalized Exosomes: Elucidating the Cellular Uptake Mechanism and the Potential for Cancer-Targeted Chemotherapy. Analytical chemistry. 2019;91(3):2425-30.

316. Wan Y, Wang L, Zhu C, Zheng Q, Wang G, Tong J, et al. Aptamer-Conjugated Extracellular Nanovesicles for Targeted Drug Delivery. Cancer research. 2018;78(3):798-808.

317. Zwarycz AS, Livingstone PG, Whitworth DE. Within-species variation in OMV cargo proteins: the Myxococcus xanthus OMV pan-proteome. Molecular Omics. 2020.

318. Scott BL, Van Komen JS, Liu S, Weber T, Melia TJ, McNew JA. Liposome Fusion Assay to Monitor Intracellular Membrane Fusion Machines. Methods in Enzymology. 372: Academic Press; 2003. p. 274-300.

319. Kweon D-H, Kong B, Shin Y-K. Hemifusion in Synaptic Vesicle Cycle. Front Mol Neurosci. 2017;10:65-.

320. Piffoux M, Silva AKA, Wilhelm C, Gazeau F, Tareste D. Modification of Extracellular Vesicles by Fusion with Liposomes for the Design of Personalized Biogenic Drug Delivery Systems. ACS Nano. 2018;12(7):6830-42.

321. Meers P, Mealy T, Pavlotsky N, Tauber AI. Annexin I-mediated vesicular aggregation: mechanism and role in human neutrophils. Biochemistry. 1992;31(28):6372-82.

322. Düzgüneş N. Fluorescence Assays for Liposome Fusion. Methods in Enzymology. 372: Academic Press; 2003. p. 260-74.

323. Sato YT, Umezaki K, Sawada S, Mukai S-a, Sasaki Y, Harada N, et al. Engineering hybrid exosomes by membrane fusion with liposomes. Scientific Reports. 2016;6:21933.

324. Uster PS, Allen TM, Daniel BE, Mendez CJ, Newman MS, Zhu GZ. Insertion of poly(ethylene glycol) derivatized phospholipid into pre-formed liposomes results in prolonged in vivo circulation time. FEBS Letters. 1996;386(2-3):243-6.

325. Steenpaß T, Lung A, Schubert R. Tresylated PEG-sterols for coupling of proteins to preformed plain or PEGylated liposomes. Biochimica et Biophysica Acta (BBA) - Biomembranes. 2006;1758(1):20-8.

326. Molnar D, Linders J, Mayer C, Schubert R. Insertion stability of poly(ethylene glycol)-cholesteryl-based lipid anchors in liposome membranes. European Journal of Pharmaceutics and Biopharmaceutics. 2016;103:51-61.

327. Kooijmans SAA, Fliervoet LAL, van der Meel R, Fens MHAM, Heijnen HFG, van Bergen en Henegouwen PMP, et al. PEGylated and targeted extracellular vesicles display enhanced cell specificity and circulation time. Journal of Controlled Release. 2016;224:77-85.

328. Parr MJ, Ansell SM, Choi LS, Cullis PR. Factors influencing the retention and chemical stability of poly(ethylene glycol)-lipid conjugates incorporated into large unilamellar vesicles. Biochimica et Biophysica Acta (BBA) - Biomembranes. 1994;1195(1):21-30.

329. Sawada SI, Sato YT, Kawasaki R, Yasuoka JI, Mizuta R, Sasaki Y, et al. Nanogel hybrid assembly for exosome intracellular delivery: effects on endocytosis and fusion by exosome surface polymer engineering. Biomater Sci. 2020;8(2):619-30.

330. Tamura R, Uemoto S, Tabata Y. Augmented liver targeting of exosomes by surface modification with cationized pullulan. Acta Biomaterialia. 2017;57:274-84.

331. Gao X, Ran N, Dong X, Zuo B, Yang R, Zhou Q, et al. Anchor peptide captures, targets, and loads exosomes of diverse origins for diagnostics and therapy. Science Translational Medicine. 2018;10(444):eaat0195.

332. McKay Craig S, Finn MG. Click Chemistry in Complex Mixtures: Bioorthogonal Bioconjugation. Chemistry & Biology. 2014;21(9):1075-101.

333.   Smyth T, Petrova K, Payton NM, Persaud I, Redzic JS, Graner MW, et al. Surface Functionalization of Exosomes Using Click Chemistry. Bioconjugate Chemistry. 2014;25(10):1777-84.

334.   Di H, Zeng E, Zhang P, Liu X, Zhang C, Yang J, et al. General Approach to Engineering Extracellular Vesicles for Biomedical Analysis. Analytical Chemistry. 2019;91(20):12752-9.

335.   Kolb HC, Finn MG, Sharpless KB. Click Chemistry: Diverse Chemical Function from a Few Good Reactions. Angewandte Chemie International Edition. 2001;40(11):2004-21.

336.   Rostovtsev VV, Green LG, Fokin VV, Sharpless KB. A Stepwise Huisgen Cycloaddition Process: Copper(I)-Catalyzed Regioselective "Ligation" of Azides and Terminal Alkynes. Angewandte Chemie International Edition. 2002;41(14):2596-9.

337.   Tornøe CW, Christensen C, Meldal M. Peptidotriazoles on Solid Phase: [1,2,3]-Triazoles by Regiospecific Copper(I)-Catalyzed 1,3-Dipolar Cycloadditions of Terminal Alkynes to Azides. The Journal of Organic Chemistry. 2002;67(9):3057-64.

338.   Worrell BT, Malik JA, Fokin VV. Direct Evidence of a Dinuclear Copper Intermediate in Cu(I)-Catalyzed Azide-Alkyne Cycloadditions. Science. 2013;340(6131):457.

339.   Hong V, Steinmetz NF, Manchester M, Finn MG. Labeling Live Cells by Copper-Catalyzed Alkyne−Azide Click Chemistry. Bioconjugate Chemistry. 2010;21(10):1912-6.

340.   Hong V, Presolski SI, Ma C, Finn MG. Analysis and Optimization of Copper-Catalyzed Azide–Alkyne Cycloaddition for Bioconjugation. Angewandte Chemie International Edition. 2009;48(52):9879-83.

341.   Agard NJ, Prescher JA, Bertozzi CR. A Strain-Promoted [3 + 2] Azide−Alkyne Cycloaddition for Covalent Modification of Biomolecules in Living Systems. Journal of the American Chemical Society. 2004;126(46):15046-7.

342.   Wittig G, Krebs A. Zur Existenz niedergliedriger Cycloalkine, I. Chemische Berichte. 1961;94(12):3260-75.

343.   Baskin JM, Prescher JA, Laughlin ST, Agard NJ, Chang PV, Miller IA, et al. Copper-free click chemistry for dynamic in vivo imaging. Proceedings of the National Academy of Sciences of the United States of America. 2007;104(43):16793-7.

344.   Jewett JC, Sletten EM, Bertozzi CR. Rapid Cu-Free Click Chemistry with Readily Synthesized Biarylazacyclooctynones. Journal of the American Chemical Society. 2010;132(11):3688-90.

345.   Kuzmin A, Poloukhtine A, Wolfert MA, Popik VV. Surface Functionalization Using Catalyst-Free Azide−Alkyne Cycloaddition. Bioconjugate Chemistry. 2010;21(11):2076-85.

346.   Lang K, Chin JW. Bioorthogonal Reactions for Labeling Proteins. ACS Chemical Biology. 2014;9(1):16-20.

347.   Thalhammer F, Wallfahrer U, Sauer J. Reaktivität einfacher offenkettiger und cyclischer dienophile bei Diels-Alder-reaktionen mit inversem elektronenbedarf. Tetrahedron Letters. 1990;31(47):6851-4.

348.   Blackman ML, Royzen M, Fox JM. Tetrazine ligation: fast bioconjugation based on inverse-electron-demand Diels-Alder reactivity. Journal of the American Chemical Society. 2008;130(41):13518-9.

349.   Oliveira BL, Guo Z, Bernardes GJL. Inverse electron demand Diels–Alder reactions in chemical biology. Chemical Society Reviews. 2017;46(16):4895-950.

350.   Darko A, Wallace S, Dmitrenko O, Machovina MM, Mehl RA, Chin JW, et al. Conformationally strained trans-cyclooctene with improved stability and excellent reactivity in tetrazine ligation. Chemical Science. 2014;5(10):3770-6.

351.   Karver MR, Weissleder R, Hilderbrand SA. Synthesis and evaluation of a series of 1,2,4,5-tetrazines for bioorthogonal conjugation. Bioconjugate chemistry. 2011;22(11):2263-70.

352.   Sletten EM, Bertozzi CR. Bioorthogonal Chemistry: Fishing for Selectivity in a Sea of Functionality. Angewandte Chemie International Edition. 2009;48(38):6974-98.

353.   Tom Dieck S, Müller A, Nehring A, Hinz FI, Bartnik I, Schuman EM, et al. Metabolic labeling with noncanonical amino acids and visualization by chemoselective fluorescent tagging. Current protocols in cell biology. 2012;Chapter 7:Unit7.11-Unit7.

354.   Chang PV, Prescher JA, Sletten EM, Baskin JM, Miller IA, Agard NJ, et al. Copper-free click chemistry in living animals. Proceedings of the National Academy of Sciences. 2010;107(5):1821.

355.   Saleh AM, Wilding KM, Calve S, Bundy BC, Kinzer-Ursem TL. Non-canonical amino acid labeling in proteomics and biotechnology. Journal of Biological Engineering. 2019;13(1):43.

356.   Amgarten B, Rajan R, Martínez-Sáez N, Oliveira BL, Albuquerque IS, Brooks RA, et al. Collagen labelling with an azide-proline chemical reporter in live cells. Chemical Communications. 2015;51(25):5250-2.

357.   Beatty KE, Fisk JD, Smart BP, Lu YY, Szychowski J, Hangauer MJ, et al. Live-cell imaging of cellular proteins by a strain-promoted azide-alkyne cycloaddition. Chembiochem : a European journal of chemical biology. 2010;11(15):2092-5.

358.   Uttamapinant C, Howe JD, Lang K, Beránek V, Davis L, Mahesh M, et al. Genetic code expansion enables live-cell and super-resolution imaging of site-specifically labeled cellular proteins. Journal of the American Chemical Society. 2015;137(14):4602-5.

359.   Rossin R, Renart Verkerk P, van den Bosch SM, Vulders RCM, Verel I, Lub J, et al. In Vivo Chemistry for Pretargeted Tumor Imaging in Live Mice. Angewandte Chemie International Edition. 2010;49(19):3375-8.

360.   Macias-Contreras M, He H, Little KN, Lee JP, Campbell RP, Royzen M, et al. SNAP/CLIP-Tags and Strain-Promoted Azide–Alkyne Cycloaddition (SPAAC)/Inverse Electron Demand Diels–Alder (IEDDA) for Intracellular Orthogonal/Bioorthogonal Labeling. Bioconjugate Chemistry. 2020;31(5):1370-81.

361.   Köhn M, Breinbauer R. The Staudinger Ligation—A Gift to Chemical Biology. Angewandte Chemie International Edition. 2004;43(24):3106-16.

362.   Scriven EFV, Turnbull K. Azides: their preparation and synthetic uses. Chemical Reviews. 1988;88(2):297-368.

363.   Brakel Rv, Vulders RCM, Bokdam RJ, Grüll H, Robillard MS. A Doxorubicin Prodrug Activated by the Staudinger Reaction. Bioconjugate Chemistry. 2008;19(3):714-8.

364.   Pandiakumar AK, Sarma SP, Samuelson AG. Mechanistic studies on the diazo transfer reaction. Tetrahedron Letters. 2014;55(18):2917-20.

365.   Goddard-Borger ED, Stick RV. An Efficient, Inexpensive, and Shelf-Stable Diazotransfer Reagent: Imidazole-1-sulfonyl Azide Hydrochloride. Organic Letters. 2007;9(19):3797-800.

366.   Titz A, Radic Z, Schwardt O, Ernst B. A safe and convenient method for the preparation of triflyl azide, and its use in diazo transfer reactions to primary amines. Tetrahedron Letters. 2006;47(14):2383-5.

367.   Nyffeler PT, Liang C-H, Koeller KM, Wong C-H. The Chemistry of Amine−Azide Interconversion: Catalytic Diazotransfer and Regioselective Azide Reduction. Journal of the American Chemical Society. 2002;124(36):10773-8.

368.   Castro V, Blanco-Canosa JB, Rodriguez H, Albericio F. Imidazole-1-sulfonyl Azide-Based Diazo-Transfer Reaction for the Preparation of Azido Solid Supports for Solid-Phase Synthesis. ACS Combinatorial Science. 2013;15(7):331-4.

369.   Stevens MY, Sawant RT, Odell LR. Synthesis of Sulfonyl Azides via Diazotransfer using an Imidazole-1-sulfonyl Azide Salt: Scope and 15N NMR Labeling Experiments. The Journal of Organic Chemistry. 2014;79(11):4826-31.

370.   Fischer N, Goddard-Borger ED, Greiner R, Klapötke TM, Skelton BW, Stierstorfer J. Sensitivities of Some Imidazole-1-sulfonyl Azide Salts. The Journal of Organic Chemistry. 2012;77(4):1760-4.

371.   van Dongen SFM, Teeuwen RLM, Nallani M, van Berkel SS, Cornelissen JJLM, Nolte RJM, et al. Single-Step Azide Introduction in Proteins via an Aqueous Diazo Transfer. Bioconjugate Chemistry. 2009;20(1):20-3.

372.   Lohse J, Swier LJYM, Oudshoorn RC, Médard G, Kuster B, Slotboom D-J, et al. Targeted Diazotransfer Reagents Enable Selective Modification of Proteins with Azides. Bioconjugate Chemistry. 2017;28(4):913-7.

373. Kooijmans SAA, Gitz-Francois JJJM, Schiffelers RM, Vader P. Recombinant phosphatidylserine-binding nanobodies for targeting of extracellular vesicles to tumor cells: a plug-and-play approach. Nanoscale. 2018;10(5):2413-26.

374. Schulz E, Karagianni A, Koch M, Fuhrmann G. Hot EVs – How temperature affects extracellular vesicles. European Journal of Pharmaceutics and Biopharmaceutics. 2020;146:55-63.

375. Zhang H. Thin-Film Hydration Followed by Extrusion Method for Liposome Preparation. Methods Mol Biol. 2017;1522:17-22.

376. Hoffmann J-E, Plass T, Nikić I, Aramburu IV, Koehler C, Gillandt H, et al. Highly Stable trans-Cyclooctene Amino Acids for Live-Cell Labeling. Chemistry – A European Journal. 2015;21(35):12266-70.

377. Frank J, Richter M, de Rossi C, Lehr C-M, Fuhrmann K, Fuhrmann G. Extracellular vesicles protect glucuronidase model enzymes during freeze-drying. Scientific Reports. 2018;8(1):12377.

378. Richter M, Fuhrmann K, Fuhrmann G. Evaluation of the Storage Stability of Extracellular Vesicles. JoVE. 2019(147):e59584.

379. Potter GT, Jayson GC, Miller GJ, Gardiner JM. An Updated Synthesis of the Diazo-Transfer Reagent Imidazole-1-sulfonyl Azide Hydrogen Sulfate. The Journal of Organic Chemistry. 2016;81(8):3443-6.

380. Mehanny M, Koch M, Lehr C-M, Fuhrmann G. Streptococcal Extracellular Membrane Vesicles Are Rapidly Internalized by Immune Cells and Alter Their Cytokine Release. Front Immunol. 2020;11(80).

381. Wei JH, Yin X, Welander PV. Sterol Synthesis in Diverse Bacteria. Frontiers in Microbiology. 2016;7:990.

382. Sáenz JP, Grosser D, Bradley AS, Lagny TJ, Lavrynenko O, Broda M, et al. Hopanoids as functional analogues of cholesterol in bacterial membranes. Proceedings of the National Academy of Sciences of the United States of America. 2015;112(38):11971-6.

383. Clifton LA, Skoda MWA, Le Brun AP, Ciesielski F, Kuzmenko I, Holt SA, et al. Effect of divalent cation removal on the structure of gram-negative bacterial outer membrane models. Langmuir : the ACS journal of surfaces and colloids. 2015;31(1):404-12.

384. Jun SH, Lee JH, Kim BR, Kim SI, Park TI, Lee JC, et al. Acinetobacter baumannii outer membrane vesicles elicit a potent innate immune response via membrane proteins. PloS one [Internet]. 2013 2013; 8(8):[e71751 p.]. Available from: http://europepmc.org/abstract/MED/23977136

https://www.ncbi.nlm.nih.gov/pmc/articles/pmid/23977136/pdf/?tool=EBI

https://www.ncbi.nlm.nih.gov/pmc/articles/pmid/23977136/?tool=EBI

https://doi.org/10.1371/journal.pone.0071751

https://europepmc.org/articles/PMC3743744

https://europepmc.org/articles/PMC3743744?pdf=render

https://www.ncbi.nlm.nih.gov/pmc/articles/PMC3743744/pdf/pone.0071751.pdf.

385. Jiang L, Luirink J, Kooijmans SAA, van Kessel KPM, Jong W, van Essen M, et al. A post-insertion strategy for surface functionalization of bacterial and mammalian cell-derived extracellular vesicles. Biochimica et Biophysica Acta (BBA) - General Subjects. 2020:129763.

386. Saxon E, Bertozzi CR. Cell Surface Engineering by a Modified Staudinger Reaction. Science. 2000;287(5460):2007.

387. Bräse S, Gil C, Knepper K, Zimmermann V. Organic Azides: An Exploding Diversity of a Unique Class of Compounds. Angewandte Chemie International Edition. 2005;44(33):5188-240.

388. Schoffelen S, van Eldijk MB, Rooijakkers B, Raijmakers R, Heck AJR, van Hest JCM. Metal-free and pH-controlled introduction of azides in proteins. Chemical Science. 2011;2(4):701-5.

389.   Lang K, Davis L, Torres-Kolbus J, Chou C, Deiters A, Chin JW. Genetically encoded norbornene directs site-specific cellular protein labelling via a rapid bioorthogonal reaction. Nature Chemistry. 2012;4(4):298-304.

390.   Devaraj NK, Weissleder R, Hilderbrand SA. Tetrazine-Based Cycloadditions: Application to Pretargeted Live Cell Imaging. Bioconjugate Chemistry. 2008;19(12):2297-9.

391.   Nikić I, Plass T, Schraidt O, Szymański J, Briggs JAG, Schultz C, et al. Minimal Tags for Rapid Dual-Color Live-Cell Labeling and Super-Resolution Microscopy. Angewandte Chemie International Edition. 2014;53(8):2245-9.

392.   Royzen M, Yap GPA, Fox JM. A Photochemical Synthesis of Functionalized trans-Cyclooctenes Driven by Metal Complexation. Journal of the American Chemical Society. 2008;130(12):3760-1.

393.   Davies S, Qiao L, Oliveira BL, Navo CD, Jiménez-Osés G, Bernardes GJL. Tetrazine-Triggered Release of Carboxylic-Acid-Containing Molecules for Activation of an Anti-inflammatory Drug. ChemBioChem. 2019;20(12):1541-6.

394.   Adhikari U, Goliaei A, Tsereteli L, Berkowitz ML. Properties of Poloxamer Molecules and Poloxamer Micelles Dissolved in Water and Next to Lipid Bilayers: Results from Computer Simulations. The Journal of Physical Chemistry B. 2016;120(26):5823-30.

395.   Law S-L, Chuang T-C, Kao M-C, Lin Y-S, Huang K-J. Gene Transfer Mediated by Sphingosine/ Dioleoylphosphatidylethanolamine Liposomes in the Presence of Poloxamer 188. Drug Deliv. 2006;13(1):61-7.

396.   Kolhe P, Amend E, Singh SK. Impact of freezing on pH of buffered solutions and consequences for monoclonal antibody aggregation. Biotechnol Prog. 2010;26(3):727-33.

397.   Montoya A, Castell J. Long-term storage of peroxidase-labelled immunoglobulins for use in enzyme immunoassay. Journal of Immunological Methods. 1987;99(1):13-20.

398.   Kannan V, Balabathula P, Thoma LA, Wood GC. Effect of sucrose as a lyoprotectant on the integrity of paclitaxel-loaded liposomes during lyophilization. Journal of Liposome Research. 2015;25(4):270-8.

399.   Giebel B, Kordelas L, Börger V. Clinical potential of mesenchymal stem/stromal cell-derived extracellular vesicles. Stem Cell Investig. 2017;4:84-.

9. List of publications, oral and poster presentations

Publications

Frank, Julia; **Richter, Maximilian**; de Rossi, Chiara; Lehr, Claus-Michael; Fuhrmann, Kathrin; Fuhrmann, Gregor (2018). "Extracellular vesicles protect glucuronidase model enzymes during freeze-drying." Scientific Reports 8(1): 12377.

Richter, Maximilian; Fuhrmann, Kathrin; Fuhrmann, Gregor (2019). "Evaluation of the Storage Stability of Extracellular Vesicles." JoVE(147): e59584.

Trenkenschuh, Eduard; **Richter, Maximilian**; Heinrich, Eilien; Koch, Marcus; Fuhrmann, Gregor; Friess, Wolfgang (2020). "Formulation development of lyophilized extracellular vesicles with long-term stability." Submitted to Advanced Healthcare Materials.

Richter, Maximilian; Vader, Pieter; Fuhrmann, Gregor (2020). "Approaches to surface engineering of extracellular vesicles". Submitted to Advanced drug delivery reviews.

Selected oral and poster presentations

Poster and short Talk at ISEV 2019: **Maximilian Richter**, Eleonora Diamanti, Markus Koch, Anna H. K. Hirsch, Gregor Fuhrmann: Exploration of the surface modification of outer membrane vesicles

Poster at Biobarriers 2018: **Maximilian Richter**, Gregor Fuhrmann: Surface modification of extracellular vesicles by cholesterol post-insertion

11.   Acknowledgements

Almost four years of new findings, dead ends, problems and their solutions, successes and failures, meeting new people that became friends and personal insights now come to an end. With an exciting research project and new impressions waiting behind every corner, time passed by faster than I would have ever imagined. And all the work throughout the years now resulted into this thesis, which however would never have been possible without all the people who helped me along the way from humble beginnings to the very end of my stay at HIPS.

I am very grateful for the financial support by Studienstiftung des Deutschen Volkes that made it possible to work on this thesis and for granting me the opportunity to partake in their retreats and seminars.

I would like to pay my special regards to my supervisor, Junior Prof. Dr. Gregor Fuhrmann, for the opportunity to work in his group on a very interesting project. Throughout my time in his group, I could always approach him with my ideas and problems. Granting me a lot of freedom to develop my own ideas he still made sure to keep me on track to reach the goals of our research-projects.

I am grateful to Prof. Dr. Anna Hirsch, for co-supervising my thesis, giving great input on the chemical side of my work and enabling the close cooperation with the DDOP-group. My thanks also go to Dr. Michael Ring for agreeing to be part of the committee.

I express my gratitude to the whole BION-team. I have many great memories of our group-activities and Christmas lunches and I will miss all of you a lot, particularly my PhD-colleagues Eilien Heinrich, Thomas Kuhn, Mina Mehanny, Adriely Goes and Cristina Zivko, with whom I spent a lot of time discussing scientific but also not so scientific things. You were definitely instrumental in making my stay at HIPS such a great and pleasant time. My special thanks go to Eilien Heinrich, who did a lot of work in the EV-lyophilisation project, Philipp Lapuhs, who worked on the application of diazotransfer during his master thesis and Dr. Kathrin Fuhrmann, who performed AF4-purification of EVs and took care of all our orders.

I also want to thank the members of the DDEL-group for their helpfulness and cooperativeness. In particular, I would like to mention Dr. Brigitta Loretz, for always having an open ear about any organizational questions, Olga Hartwig for helping me with all things FACS and the nice company in the DDEL-kitchen lunch-breaks, Robert Richter for sharing with me his detailed knowledge on the bacterial cell-envelope, discussions about our experimental approaches and providing each other with tips on obscure bands, Dr. Carlos Montefusco for banter and feijoada and Justus Horstmann for being a great conversation partner, especially over a beer at Ulanen Pavillion.

The people responsible for keeping everything running smoothly like well-maintained machinery of course also need to be mentioned. I would like to thank our technicians Jana Westhues and Petra König, who introduced me to the cell culture and were an integral part of the DDEL-kitchen lunch-breaks, Pascal Paul, who took care of all the instruments, introduced me to HPLC and renewed my interest in a long forgotten hobby and Dr. Annette Boese, who helped me with the FACS. My thanks also go to Karin Groß, Sarah Müller and Anette Herkströter, who took care of the secretariat and helped me with sending parcels and all other organizational stuff.

During my forays into organic synthesis, I received a lot of valuable input and practical help from many people in the DDOP-group, who gave me a warm welcome to the second floor. I am very grateful for the supervision of Dr. Eleonora Diamanti, who spent a lot of time introducing me to all the aspects of performing organic synthesis. I also want to acknowledge Dr. Martin Empting and Dr. Alexander Kiefer for their feedback and advice on my synthesis plans. Here also Prof. Dr. Alexander Titz has to be mentioned, as his lecture on chemical glycobiology was my original introduction to the concept of diazotransfer. Finally, I am thankful to Dr. Jelena Konstantinovic and Dr. Mostafa Hamed, who helped me with the operation and troubleshooting of HRMS and preparative HPLC. Appreciation is due also to Dr. Lena Keller from the MINS group, who performed NMR-measurements of my compounds and answered all my questions during the analysis of the results.

I would like to express my gratitude towards my external collaborators, Eduard Trenkenschuh and Prof. Dr. Wolfgang Frieß at LMU Munich for our fruitful collaboration in the EV-lyophilisation project, Dr. Markus Koch from INM for taking great Cryo-TEM pictures of our vesicles and PD Dr. Ralf Kautenburger from UdS for measuring the residual copper-content of my vesicles.

Finally, I am indebted to my family and Bahar for their unwavering support and continuous willingness to listen to the newest problem I encountered at work and just being there when I needed them. Without you, I would not have managed to come this far.